Towards a Better Understanding of Activated Carbon-Based Amendments for In Situ Treatment of Petroleum Hydrocarbons in Anaerobic Groundwater Systems

by

Andrea Lucienne Marrocco

A thesis
presented to the University of Waterloo
in fulfillment of the
thesis requirement for the degree of
Doctor of Philosophy
in
Civil Engineering (Water)

Waterloo, Ontario, Canada, 2023

Examining Committee Membership

The following served on the Examining Committee for this thesis. The decision of the Examining Committee is by a majority vote.

External Examiner	Paul Van Geel Carleton University
Supervisor(s)	Neil R Thomson Professor, University of Waterloo
	Laura A Hug Assistant Professor, University of Waterloo
Internal Member	Anh Pham Assistant Professor, University of Waterloo
Internal Member	Nandita Basu Professor, University of Waterloo
Internal-external Member	Steven Forsey Professor, University of Waterloo

Author's Declaration

This thesis consists of material all of which I authored or co-authored: see Statement of Contributions included in the thesis. This is a true copy of the thesis, including any required final revisions, as accepted by my examiners.

I understand that my thesis may be made electronically available to the public.

Statement of Contributions

The content in Chapter 2, 3 and 4 were prepared with the intent for submission to peer-reviewed journals although as presented they are not stand-alone chapters. The experimental designs in Chapter 2 were developed by me and Dr. Neil R Thomson and performed by myself. The experimental designs in Chapter 3 and 4 were developed by me, Dr. Neil R Thomson, Dr. Laura A Hug, Dr. Elizabeth A Edwards, Dr. Courtney R.A Toth, Marianne Vandergriendt and Adam E Schnieder, and the experiments were performed by myself and Adam E Schnieder (who will report on the KC, KC+PAC, SC, BA-PC and BA+PAC microcosms discussed in Chapter 3, and the KC+PACz columns discussed in Chapter 4 for his Master's research). I analyzed all data, and prepared all figures and content presented in Chapter 2, 3 and 4. Dr. Neil R Thomson, Dr. Laura A Hug, Dr. Elizabeth A Edwards, Dr. Courtney R.A Toth and Dr. Ramon Aravena provided guidance and support throughout all phases of the research, including experimental design, analyses, and interpretation of results. Dr. Neil R Thomson and Dr. Laura A Hug edited and reviewed all content presented in this thesis.

The experiments discussed in Chapter 2 and 4 were performed at the University of Waterloo in the Department of Civil and Environmental Engineering (in Dr. Neil R Thomson's Soil and Groundwater Remediation Engineering Laboratory). The experiments described in Chapter 3 were performed at the University of Waterloo in the Departments of Earth and Environmental Science (in the Ecohydrology Laboratory, managed and operated by Marianne Vandergriendt) and the Department of Biology (in Dr. Laura A Hug's Hug Research Laboratory). The aquifer material used in Chapter 3 and 4 was collected from Canadian Forces Base Borden, Ontario, Canada by Bob Ingleton, Paul Johnson and Aaron Vandenhoff from the University of Waterloo, Department of Earth and Environmental Sciences. Petroleum hydrocarbon sample analysis was completed at the University of Waterloo in the Soil and Groundwater Remediation Engineering Laboratory by Shirley Chatten. Molecular analysis was completed at the University of Toronto in the BioZone Center for Applied Bioscience and Bioengineering, and at McGill University in the Genome Quebec Innovation Centre. Isotope sample analysis was completed at the University of Waterloo in the Environmental Isotopes Laboratory primarily by Humam El Mugammar. Dissolved inorganic carbon sample analysis was completed at the University of Waterloo in the Environmental Geochemistry Laboratory by Richard Elgood. Methane and carbon dioxide sample analyses were completed at the University of Waterloo in the Ecohydrology Laboratory by Shirley Chatten. Sulfate sample analysis was completed at the University of Waterloo in the Department of Civil and Environmental Engineering Environmental and Water Resources (EWR) Laboratory primarily by Mark Merlau.

Abstract

Injected activated carbon (AC) particulate amendments for the *in situ* treatment of groundwater impacted by petroleum hydrocarbons (PHCs) is relatively new, and relies on a combination of AC sorption and biodegradation. Currently the performance of this technology remains unclear, primarily related to the long-term interplay between sorption and biodegradation and whether the presence of AC enhances the anaerobic biodegradation of PHCs. To address these uncertainties, this research investigated the sorption and anaerobic biodegradation (sulfate reducing and methanogenic) behaviour in microcosm experiments amended with AC and column experiments designed to mimic an AC permeable reactive barrier (PRB) over a period of 1 to 2 years.

The powdered AC (PAC) used in this research (WPC from Calgon Carbon Corporation) had a rough, irregular surface with potential macropore openings of 0.8 ± 0.3 μm, and variable particle sizes with an average diameter of 11.5 ± 4.4 μm. Sorption and desorption equilibrium experiments showed that the magnitude of single-solute (benzene [B], toluene [T], or *o*-xylene [X]) and multi-solute (BTX combined) sorption or desorption followed X > T > B and B > T > X, respectively. Due to competitive sorption, the magnitude of B, T, and X sorption in the multi-solute system was reduced relative to the single-solute systems. Sorption and desorption equilibrium conditions differed suggestive of hysteresis; however, this behaviour was not fully explored in this research. The best-fit single-solute Freundlich isotherm parameters for benzene, toluene and *o*-xylene were 36.1 ± 3.8, 0.484 ± 0.045, and 88.2 ± 7.7 for K_{f_i} ([mg/g][L/mg]^n) and 0.421 ± 0.044, 132 ± 20 and 0.371 ± 0.099 for n_{f_i} (-), respectively. The improved simplified ideal adsorption solution (ISIAS) model was fit to the multi-solute sorption data and the competition factors (a_i) were estimated for benzene, toluene and *o*-xylene as 1.42 ± 0.38, 1.43 ± 0.16 and 1.08 ± 0.08, respectively. Temporal sorption (up to 48 hours) and desorption (up to 720 hours) experiments showed that the time to reach sorption or desorption equilibrium for single-solute benzene and toluene was rapid (≤ 0.5 hours).

Single-solute (toluene-only) and multi-solute (BTX) abiotic and bioactive (including sulfate-limited [10-20 mg/L SO_4^{2-}]) or sulfate amended [138-275 mg/L SO_4^{2-}]) microcosms with and without PAC were constructed (in addition to starved controls without toluene, BTX or PAC). Aqueous and solid phase toluene or BTX concentrations from the single- and multi-solute PAC amended microcosms, respectively, were compared to the single- and multi-solute Freundlich or ISIAS model predictions. In general, both the single- and multi-solute sorption isotherm models were found to

overestimate the measured solid phase concentrations in the microcosms. This disparity is presumably due to differences in mixing conditions and solution matrix chemistry, or competitive sorption by metabolites and biofilm formation in the PAC amended microcosms. In the multi-solute microcosm systems, the observed *o*-xylene solid phase concentrations deviated the most from the ISIAS model predicted solid concentrations followed by toluene and then benzene.

In the subset of single- and multi-solute sulfate-limited bioactive microcosms, evidence of methanogenesis coupled to a background substrate (other than toluene or BTX) was evident from the geochemical (i.e., CH_4 production) and molecular (i.e., *Methanomethylovorans*, *Methanosaeta* and *Methanobacterium* enrichment) data. Methane production and methanogenic enrichment were consistently elevated in the bioactive microcosms with PAC, potentially supporting enhanced methanogenesis and archaeal growth in the presence of AC. Contrarily, in the subset of single- and multi-solute sulfate-amended bioactive microcosms, sulfate reduction was coupled to the oxidation of toluene or *o*-xylene (not benzene, which was recalcitrant) evidenced by the repetitive or preferential biodegradation of toluene followed by *o*-xylene in the multi-solute microcosm and supported by geochemical (i.e., SO_4^{2-} reduction, and HS^- and total inorganic carbon [TIC] formation) and molecular (i.e., enrichment of sulfate reducing bacteria, including *Desulfosporosinus*, *Desulfoprunum* and Desulfobacteraceae) data. In the single- and multi-solute sulfate-amended bioactive microcosms with PAC, the solid phase mass of toluene was repetitively reduced by ≥ 96% showing that PAC regeneration occurred during anaerobic biodegradation. Although anaerobic biodegradation of toluene and *o*-xylene were repetitively demonstrated, there was no substantial difference in the PHC, geochemical or molecular data collected between the single- or multi-solute sulfate amended bioactive microcosms with and without PAC indicating that the presence of PAC did not influence the anaerobic microbial activity. Additionally, the anaerobic biodegradation rate of toluene was not enhanced in the presence of PAC. Collectively, there were no discernible differences in the anaerobic biodegradation of toluene between the sulfate amended bioactive microcosms with and without PAC over the 1-year monitoring period.

Three types of single-solute (toluene-only) and multi-solute (BTX) columns (37 cm long, 3.75 cm inner diameter) were constructed to represent PAC sorption alone, bioactivity alone, and PAC sorption with bioactivity. The columns were operated for approximately 2 years, with Year-1 serving as an acclimation period, and Year-2 used for high-resolution temporal monitoring. For the columns containing PAC, a 6-cm long PAC zone (0.5% wt/wt) was located near the middle of the column to

mimic an AC PRB. During Year-2 for the multi-solute column with PAC sorption alone, the change in BTX concentration between the influent and effluent followed X > T > B given that *o*-xylene has the highest sorption capacity followed by toluene and then benzene. For the single-solute and multi-solute columns with PAC sorption alone the change in toluene concentration between the influent and effluent was greater for the single-solute column relative to the multi-solute column given that the sorption capacity of toluene was reduced in the multi-solute competitive system. For the multi-solute bioactive column without PAC sorption the change in concentration between the influent and effluent followed T > X > B due to the preferential biodegradation of toluene prior to *o*-xylene and the recalcitrance of benzene (as observed in the microcosm experiments). For the multi-solute bioactive column with PAC sorption the change in concentration between the influent and effluent followed T > X > B due to the preferential biodegradation of toluene and preferential sorption of *o*-xylene as toluene was biodegraded.

The solid phase concentration of toluene within the PAC zone of the single- and multi-solute bioactive columns was highest at the leading edge followed by a gradual reduction towards the end of the PAC zone. The gradient in the solid phase toluene concentration shows that toluene desorbed more due to biodegradation towards the end of the PAC zone, furthest from the influent where toluene was continually replenished. In the bioactive multi-solute column, the magnitude of solid phase BTX concentrations within the PAC zone followed X > T > B at the leading edge; however, directly downgradient the solid phase BTX concentrations within the PAC zone followed X > B > T due to the biodegradation of toluene which resulted in higher sorption of *o*-xylene and benzene.

Using the Year-2 data, an overall column mass balance was estimated by subtracting the cumulative effluent mass from the cumulative mass injected. The single- and multi-solute bioactive columns with PAC sorption yielded the largest removal of toluene mass compared to columns with either only PAC sorption or only bioactivity. For example, among the single-solute columns the mass removal of toluene was greatest for the bioactive column with PAC sorption (99.5% reduction), followed by the column with only PAC sorption (74.6% reduction) and the column with only bioactivity (44.4% reduction). The depletion in effluent toluene mass during Year-2 was consistent between the single- and multi-solute bioactive columns with PAC sorption; however, for the multi-solute column breakthrough of benzene and *o*-xylene occurred given the recalcitrance of benzene and the competitive inhibition of *o*-xylene during toluene biodegradation.

Anaerobic biodegradation within the single- and multi-solute bioactive columns with or without PAC sorption was supported by changes in geochemical parameters that would be expected

under sulfate reducing and methanogenic conditions (i.e., SO_4^{2-} reduction, and HS^-, TIC and CH_4 formation). Like the microcosm systems, there was no difference in the magnitude of change of the geochemical parameters between columns with or without PAC, suggesting that the PAC zone in the bioactive columns did not influence the microbial activity. However, the PAC zone did influence the spatial distribution of anaerobic microbes. For the columns with only bioactivity the relative abundance of *Methanosarcina* and *Methanomethylovorans* were highest at the influent ends relative to the effluent ends. Whereas, for the bioactive columns with PAC sorption the relative abundance of *Methanosaeta*, *Methanobacterium* and *Methanosarcina* were highest within the PAC zone relative to outside of the PAC zone, in addition to being higher in abundance relative to all bacteria detected within the PAC zone (primarily *Desulfosporosinus*, *Edwardsbacteria* and *Berkelbacteria*). In the multi-solute bioactive column with PAC sorption, the abundance of *Desulfosporosinus* was also notably elevated at the leading edge of the PAC zones (coinciding with the location of the highest solid phase toluene concentration sorbed to the PAC).

Compound specific isotope analysis (CSIA) revealed enrichment of ^{2}H-T in the single- and multi-solute columns with only bioactivity or PAC sorption, although the average value of δ^2H-T between the single- and multi-solute columns with only bioactivity was 36.1 ± 8‰ greater than the columns with only PAC sorption, as expected. The magnitude of hydrogen isotope fractionation of toluene associated with a combination of PAC sorption and biodegradation is unknown given toluene was depleted in the bioactive column with PAC sorption. Unlike toluene, a direct comparison of the hydrogen isotope fractionation of *o*-xylene between the multi-solute columns showed that the average value of δ^2H-X was 54‰ and 58‰ greater in the bioactive column with PAC sorption relative to the columns with only PAC sorption or only bioactivity, respectively. ^{2}H-X enrichment in the multi-solute bioactive column with PAC sorption was presumably due to a significant amount of *o*-xylene sorption to the PAC as toluene was biodegraded as opposed to substantial *o*-xylene biodegradation (supported by the solid phase data).

Collectively the compiled data sets provide comprehensive insight into how AC particulate amendments behave in anaerobic systems in contact with PHCs, and the interplay between BTX sorption and anaerobic biodegradation under sulfate reducing and methanogenic conditions. These data provide direct evidence that the presence of PAC particulate amendments does not enhance the biodegradation of BTX relative to systems with no PAC under sulfate reducing conditions. Instead, the presence of the PAC provides rapid reductions in contaminant concentrations relative to systems

without PAC and sustains reductions in the aqueous phase concentration of the most preferentially degraded solute under variable loading conditions as the PAC is regenerated. The PAC also influences microbial activity during PHC biodegradation by promoting microbial growth on the PAC, with notably high methanogenic enrichment. This research also provides evidence that ideal isotherms are not representative of the sorption behaviour in bioactive systems with AC and tend to overestimate sorption. Finally, PAC sorption, most notably for the most preferentially sorbed solute in the multi-solute system, generates substantial hydrogen isotope enrichment which may lead to overestimations in the fractionation presumed to be associated with biodegradation when integrating CSIA into monitoring approaches for bioactive systems with AC.

Acknowledgements

I would like to thank my main supervisor Dr. Neil R Thomson for the years of professional and personal guidance, support and encouragement you provided me. Your mentorship has been invaluable to me, allowing me to grow and broaden my perspective in this field of study and in life. Thank you for the years of constant input and direction with this research, and for playing such a pivotal role in shaping it into what it has evolved to be. I would also like to thank my co-supervisor Dr. Laura A Hug for your constant guidance and support throughout my graduate studies. Thank you for all the time and expertise you invested into this research, and your valued assistance in shaping the experimental designs and operations.

I would like to thank Dr. Elizabeth A Edwards and Dr. Courtney R.A Toth from the University of Toronto (BioZone Center for Applied Bioscience and Bioengineering) for the instrumental roles you played in shaping this research, and for your invaluable expertise on the subject matter. Thank you for the countless hours spent assisting with the interpretation of experimental results and providing suggestions on how to optimize experimental designs as this research was progressing. Thank you, Dr. Courtney R.A Toth for the comprehensive laboratory training you provided me over the years in running and maintaining microcosm experiments – I always looked forward to learning from you in all my trips to the BioZone and SiREM laboratories. Thank you, Dr. Ramon Aravena, for the many phone conversations and meetings where you provided pivotal input on the interpretation of all isotope data collected as part of this research.

I would like to thank the technical and research support staff at the University of Waterloo for all your assistance, guidance and invaluable technical expertise over the years - Shirley Chatten, Mark Merlau, Mark Sobon, Mark Hummel, Terry Ridgway, Felipe Sandor, Marianne Vandergriendt, Aaron Vandenhoff, Bob Ingleton, Paul Johnson, Humam Mugammar, William (Bill) Mark, Richard Elgood, Shuhuan Li and Emilie Spasov. Each of you helped shape this research through assistance with experimental designs, experimental set-up's, sample analyses (and sometimes collection) and addressing all the challenges that arose while carrying out this research. I would especially like to thank Shirley Chatten – the Laboratory Technician in Dr. Neil R Thomson's Soil and Groundwater Remediation Engineering Laboratory – for the many years of sample analyses in addition to providing input on experimental designs and being an extra hand in the laboratory when needed, helping with data collection and experimental maintenance.

I would like to thank my colleagues and research team who provided professional and personal support over the years - Adam Schneider, Bill McLaren, Iolanda Montagnese, Jacob Carlos, Yunxiao Wei, Seyfollah Gilak, Sina Golchi and Stuart Linley. I would especially like to thank Adam Schneider for the countless hours we spent designing and running our laboratory experiments – thank you for your patience, support and knowledge that you brought to everything we worked on together. I would also like to thank Najmeh Jaberi and Griselda Raquel Rocha Diaz de Leon, members of my research team, who also assisted with running and maintaining components of this research during their Postdoctoral Fellowship or Research Assistantship.

I would like to thank the many science and engineering co-op student's who assisted with this research - Zhenhuan Huang, Paula Vilcu, Dana Arends, Jenna Paik, Norman Ly and Iain Wright. Each of you went above and beyond while assisting with components of this research, and your work ethic and dedication to the project was unmistakable. You all made key contributions to the progression of this research, and without your hard work it would have not been possible.

I would like to thank all of the amazing friends I made throughout my graduate studies for your constant support and encouragement, and all of the laughs and cherished memories we made that I will take with me throughout the rest of my life. You all became some of my closest friends, and truly helped me through some of the toughest times of my life – Elli Papangelakis, Linda Li, Colin Van Niejenhuis, Takin Tadayon and Lilly Zheng.

I would like to thank my family – my parents, grandparents, brothers and Wade – for your constant love, support, and encouragement throughout my life and especially over the last several years to get here. Without the profound impact you have all had on my life I would not be the person I am today.

Funding for this research was provided by the Natural Sciences and Engineering Research Council of Canada (NSERC) Postgraduate Scholarship – Doctoral (PGS D); NSERC Discovery Grant, the American Petroleum Institute (API), and the Petroleum Environmental Research Forum (PERF) (PI: N.R. Thomson); and the Ontario Genomics Institute (OGI) and Ontario Research Fund – Genomic Applications Partnership Program (ORF-GAPP) (PI: E.A. Edwards).

Table of Contents

Examining Committee Membership ii
Author's Declaration iii
Statement of Contributions iv
Abstract v
Acknowledgements x
List of Figures xv
List of Tables xix
List of Acronyms xx
List of Symbols xxii
Chapter 1 1
1.1 General background 1
1.1.1 Sorption 1
1.1.2 Biodegradation 5
1.1.2.1 Compound specific isotope analysis 6
1.1.2.2 Quantitative polymerase chain reactions and next generation sequencing 7
1.1.3 AC particulate amendments for treatment of groundwater 8
1.2 Objective and research questions 10
1.3 Thesis scope 12
Chapter 2 13
Powdered activated carbon sorption and desorption of benzene, toluene and *o*-xylene 13
2.1 Introduction 13
2.2 Materials and methods 14
2.2.1 PAC characterization 15
2.2.2 Sorption and desorption equilibrium capacity 15
2.2.3 Sorption and desorption equilibrium time 19
2.2.4 Mass balance 20
2.3 Results and discussion 21

2.3.1 PAC characterization 21
2.3.2 Sorption and desorption 22
2.3.2.1 Single-solute sorption and desorption equilibrium capacities 22
2.3.2.2 Multi-solute sorption and desorption equilibrium capacities 25
2.3.2.3 Single-solute sorption and desorption equilibrium time 28
2.4 Conclusion 30
Chapter 3 33
Anaerobic biodegradation of benzene, toluene and *o*-xylene in the presence of powdered activated carbon particulate amendments – Microcosm study 33
3.1 Introduction 33
3.2 Materials and methods 34
3.2.1 Microcosm design 36
3.2.2 Sampling 38
3.2.3 Analyses 42
3.2.4 Mass balance estimates 44
3.3 Results and discussion 45
3.3.1 Isotherm comparison 48
3.3.2 Killed and starved controls 51
3.3.3 Bioactive systems (no electron acceptor amendment) 58
3.3.4 Bioactive electron acceptor amended systems 63
3.4 Conclusion 71
Chapter 4 74
Anaerobic biodegradation of benzene, toluene and *o*-xylene in powdered activated carbon particulate amended aquifer material – Column study 74
4.1 Introduction 74
4.2 Materials and methods 75
4.2.1 Column description 76

4.2.2 Operation 80
4.2.3 Sample collection and analyses 81
4.3 Results and discussion 84
4.3.1 Killed control columns 89
4.3.2 Toluene-only bioactive system 96
4.3.3 BTX bioactive system 103
4.4 Conclusion 112
Chapter 5 115
5.1 Conclusion 115
5.2 Recommendations for future work 121
References 123
Appendix A: Supplementary material for Chapter 2 141
Appendix B: Supplementary material for Chapter 3 150
Appendix C: Supplementary material for Chapter 4 175

List of Figures

Figure 2.1: Environmental scanning electron microscopy (ESEM) generated images of WPC powdered activated carbon (PAC) at (a) 500 nm (82 000 ×), (b) 1 µm (53 817 ×) and (c) 20 µm (2 000 ×) scales (magnifications). Location of potential pores openings on the PAC particle surfaces in (c) are identified with red outlines. 22

Figure 2.2: Sorption and single-step desorption equilibrium capacities for single-solute (a) benzene, (b) toluene and (c) *o*-xylene, and multi-solute (d) benzene, (e) toluene and (f) *o*-xylene in contact with WPC powdered activated carbon (PAC). C_e on the x axis represents the sorption or desorption equilibrium aqueous phase concentration (mg/L), and q_e on the y axis represents the sorption or desorption equilibrium solid phase concentration (mg/g). The multi-solute sorption data are numbered in order of increasing initial aqueous phase concentration for each solute (C_{o_i}), and the multi-solute sorption ($C_{e_i}^{s}$ and $q_{e_i}^{s}$) or desorption ($C_{e_i}^{d}$ and $q_{e_i}^{d}$) data for each solute are dependent on the sorption and desorption data of the other solutes, corresponding to the same C_{o_i}. Single- and multi-solute sorption equilibrium data are represented as filled (a, d) red triangles for benzene, (b, e) green squares for toluene, and (c, f) blue circles for *o*-xylene, and the single-step single- and multi-solute desorption equilibrium data are represented as filled diamonds with the same colours used to represent the sorption equilibrium data for each solute. Solid lines connect the single- or multi-solute sorption and desorption data, and arrows represent the direction of concentration change between processes. The standard deviation of triplicate measurements is represented as ± error bars on each data point. The single-solute Freundlich isotherms with 95% confidence envelopes (black solid bands) are represented as solid coloured lines, including (a) red for benzene, (b) green for toluene, and (c) blue for *o*-xylene. The multi-solute improved simplified ideal adsorption solution (ISIAS) model fit to the multi-solute $C_{e_i}^{s}$ and $q_{e_i}^{s}$ data for each solute, are represented as unfilled gradient symbols above or below each data point. 24

Figure 2.3: Temporal sorption and desorption data for single-solute (a) benzene and (b) toluene over 48 hours (2 days) and at 3 and 30 mg/L initial aqueous phase concentrations (C_{o_i}). The solid phase concentration for sorption and desorption and for both solutes is denoted as q_t (mg/g) versus time (hours). At the C_{o_i} of 30 mg/L the sorption data is represented as filled (a) red triangles for benzene and (b) green squares for toluene, and the desorption data is represented as the same unfilled shapes as the sorption data. At the C_{o_i} of 5 mg/L the sorption data is represented as filled (a) red diamonds for benzene and (b) green diamonds for toluene, and the desorption data is represented as unfilled diamonds. Desorption data from 72 hours (3 days) to 720 hours (30 days) is shown for (c) benzene and (d) toluene. The standard deviation of triplicate measurements is represented as ± error bars. 29

Figure 3.1: Repetitive and sacrificial sampling design for the single-solute (toluene-only) or multi-solute (benzene, toluene and *o*-xylene [BTX]) (a) KC, KC+PAC and SC; (b) BA-PC and BA+PAC; and (c) BA-PC+EA and BA+PAC+EA microcosms. Repetitive and sacrificial sampling intervals are represented as green and black hash marks, respectively, on the horizontal axes. The microcosm bottle locations on the horizontal axes represent when a new bottle or triplicate set was sampled following a prior sacrificial sampling event. 40

Figure 3.2: Measured solid phase concentrations within the KC+PAC (large sized symbols), BA+PAC+EA (medium sized symbols) and BA+PAC (small sized symbols) microcosms for (a)

single-solute toluene (filled green squares) against the measured aqueous phase concentrations at each sacrificial sampling time, and (b) multi-solute benzene (filled red triangles), toluene (filled green squares) and *o*-xylene (filled blue circles) (BTX) against the predicted solid phase concentration generated from the improved simplified ideal adsorption solution (ISIAS) model (using the single-solute Freundlich model parameters for each solute [K_{f_i} and n_{f_i}] and the multi-solute ISIAS competition factors for each solute [a_i] [listed in Table 2.2]). The single-solute Freundlich isotherm for toluene with a 95% confidence envelope (black solid band) is represented as a solid green line in (a), and a black solid 1:1 line is shown in (b). The standard deviation of triplicate measurements is represented as ± error bars on each data point. The red circles indicate data corresponding to sampling times (a) < 5 days following a toluene dosing event, or (b) between 6 and 64 days following a TX dosing event. 50

Figure 3.3: Abundance of total bacteria, total archaea and *Desulfosporosinus* detected using quantitative polymerase chain reaction (qPCR) analysis for all (a) single-solute (toluene-only) and (b) multi-solute (benzene, toluene and *o*-xylene [BTX]) microcosm types after 1-year relative to background conditions. Error bars represent ± 1 standard error. 53

Figure 3.4: Relative abundance (≥ 4%) of bacteria and archaea at the (a) phylum, (b) family and (c) genus taxonomic levels detected using 16S ribosomal ribonucleic acid (rRNA) next generation sequencing (NGS) for the SC, BA-PC, BA+PAC, BA-PC+EA and BA+PAC+EA single-solute (toluene-only) microcosms after 1-year relative to background conditions. The relative abundance of all replicate bottles (A, B and C) is shown for the SC, BA-PC and BA+PAC microcosms, whereas the relative abundance of a single replicate bottle (C) is shown for the BA-PC+EA and BA+PAC+EA microcosms. 56

Figure 3.5: Relative abundance (≥ 4%) of bacteria and archaea at the (a) phylum, (b) family and (c) genus taxonomic levels detected using 16S ribosomal ribonucleic acid (rRNA) next generation sequencing (NGS) for the SC, BA-PC, BA+PAC, BA-PC+EA and BA+PAC+EA multi-solute (benzene, toluene and *o*-xylene [BTX]) microcosms after 1-year relative to background conditions. The relative abundance of all replicate bottles (A, B and C) is shown for the SC, BA-PC and BA+PAC microcosms, whereas the relative abundance of a single replicate bottle (C) is shown for the BA-PC+EA and BA+PAC+EA microcosms. 57

Figure 3.6: Temporal changes in the (a, d) aqueous and solid phase toluene concentrations ($T_{(aq)}$ and $T_{(s)}$) (green and black filled squares, respectively), (b, e) aqueous sulfate ($SO_4^{2-}{}_{(aq)}$) (black filled gradient symbols) and sulfide ($HS^-_{(aq)}$) (yellow filled left triangles) concentrations, and (c, f) total inorganic carbon (TIC) (purple filled diamonds) and gaseous methane concentration ($CH_{4(g)}$) (orange filled right triangles) for the single-solute (toluene-only) (a-c) BA-PC and (d-f) BA+PAC microcosms. Each timepoint represents the average of three values and the error bars are ± 1 standard deviation. 60

Figure 3.7: Temporal changes in the (a, d) aqueous phase benzene, toluene and *o*-xylene (BTX) ($B,T,X_{(aq)}$) (red filled triangle [B], green filled squares [T] and blue filled circles [X]) and solid phase BTX ($B,T,X_{(s)}$) (black filled triangles [B], squares [T] and circles [X]) concentrations, (b, e) aqueous sulfate ($SO_4^{2-}{}_{(aq)}$) (black filled gradient symbols) and sulfide ($HS^-_{(aq)}$) (yellow filled left triangles) concentrations, and (c, f) total inorganic carbon (TIC) (purple filled diamonds) and gaseous methane concentration ($CH_{4(g)}$) (orange filled right triangles) for the multi-solute (BTX) (a-c) BA-PC and (d-f)

BA+PAC microcosms. Each timepoint represents the average of three values and the error bars are ± 1 standard deviation..... 61

Figure 3.8: Temporal changes in the (a, d) aqueous and solid phase toluene concentrations ($T_{(aq)}$ and $T_{(s)}$) (green and black filled squares, respectively), (b, e) aqueous sulfate ($SO_4^{2-}{}_{(aq)}$) (black filled gradient symbols) and sulfide ($HS^-_{(aq)}$) (yellow filled left triangles) concentrations, and (c, f) total inorganic carbon (TIC) (purple filled diamonds) and gaseous methane concentration ($CH_{4(g)}$) (orange filled right triangles) for the single-solute (toluene-only) (a-c) BA-PC+EA and (d-f) BA+PAC+EA microcosms. Empty symbols and dashed lines represent target (non-measured) concentrations or trends, respectively. Each timepoint represents the average of three values and the error bars are ± 1 standard deviation..... 68

Figure 3.9: Temporal changes in the (a, d) aqueous phase benzene, toluene and *o*-xylene (BTX) ($B,T,X_{(aq)}$) (red filled triangle [B], green filled squares [T] and blue filled circles [X]) and solid phase BTX ($B,T,X_{(s)}$) (black filled triangles [B], squares [T] and circles [X]) concentrations, (b, e) aqueous sulfate ($SO_4^{2-}{}_{(aq)}$) (black filled gradient symbols) and sulfide ($HS^-_{(aq)}$) (yellow filled left triangle**s**) concentrations, and (c, f) total inorganic carbon (TIC) (purple filled diamonds) and gaseous methane concentration ($CH_{4(g)}$) (orange filled right triangles) for the multi-solute (BTX) (a-c) BA-PC+EA and (d-f) BA+PAC+EA microcosms. Empty symbols and dashed lines represent target (non-measured) concentrations or trends, respectively. Each timepoint represents the average of three values and the error bars are ± 1 standard deviation. 69

Figure 4.1: Schematic of the column set-up in up-flow mode for a column with an installed powdered activated carbon (PAC) zone. 79

Figure 4.2: Influent (dashed lines with open symbols) and effluent (solid lines with closed symbols) aqueous concentrations of (a, d, g) toluene, (b, e, h) sulfate (SO_4^{2-}) and sulfide (HS^-), and (c, f, i) methane (CH_4) and dissolved inorganic carbon (DIC) from the single-solute (toluene-only) KC+PACz (left panel), BA-PC (middle panel) and BA+PACz (right panel) columns. The vertical solid lines represent an increase in influent concentration. 90

Figure 4.3: Influent (dashed lines with open symbols) and effluent (solid lines with closed symbols) aqueous concentration of (a, d, g) benzene, toluene and *o*-xylene (BTX), (b, e, h) sulfate (SO_4^{2-}) and sulfide (HS^-), and (c, f, i) methane (CH_4) and dissolved inorganic carbon (DIC) from the multi-solute (BTX) KC+PACz (left panel), BA-PC (middle panel) and BA+PACz (right panel) columns. The vertical solid lines represent an increase in influent concentration.. 91

Figure 4.4: Influent isotope source signature (open symbols) and effluent (a, d) δ^{13}C-toluene, (b, e) δ^2H-toluene and (c, f, g) δ^{13}C-DIC (dissolved inorganic carbon) isotopes (solid lines with closed symbols) for the single-solute (toluene-only) KC+PACz (left panel), BA-PC (middle panel) and BA+PACz (right panel) columns. Solid horizontal lines represent the average of the influent isotope source signatures and dashed horizontal lines and error bars on data represent the error, including ±0.3‰ (2σ) for δ^{13}C-T, ±5‰ (2σ) for δ^2H-T and ±0.2‰ (2σ) for δ^{13}C-DIC..... 94

Figure 4.5: Influent isotope source signature (open symbols) and effluent (a, d, g) δ^{13}C-benzene (B), toluene (T), and *o*-xylene (X), (b, e, h) δ^2H-B,T,X and (c, f, i) δ^{13}C-DIC (dissolved inorganic carbon) isotopes (solid lines with closed symbols) for the multi-solute (BTX) KC+PACz (left panel), BA-PC (middle panel) and BA+PACz (right panel) columns. Solid horizontal lines represent the average of

the influent isotope signatures and dashed horizontal lines and error bars on data represent the error, including ±0.3‰ (2σ) for δ^{13}C-B,T,X, ±5‰ (2σ) for δ^{2}H-B,T,X and ±0.2‰ (2σ) for δ^{13}C-DIC. 95

Figure 4.6: Solid phase (a, f) concentration of toluene (green filled squares); (b, g) abundance of *Desulfosporosinus* (light blue filled diamonds), total bacteria (grey filled circles) and total archaea (dark red filled squares) from quantitative polymerase chain reaction (qPCR) analysis; and relative abundance (≥ 4%) of bacteria and archaea detected at the (c, h) phylum, (d, i) family and (e, j) genus taxonomic levels using 16S ribosomal ribonucleic acid (rRNA) next generation sequencing (NGS) for the single-solute (toluene-only) BA-PC (top panel) and BA+PACz (bottom panel) columns after Year-2 of column operation. The grey region in the bottom panel represents the powdered activated carbon (PAC) zone. The vertical line in (a, f) represents the method detection limit of solid phase toluene (8.0×10^{-5} mg/g). The data in (b, g) represent the average of three measurements and the dashed vertical lines represent the background abundances. Error bars and solid vertical lines in (b, g) are ± 1 standard deviation. The phylum, family and genus legends correspond to (c, h), (d, i) and (e, j), respectively. Sample depths from the influent represent the median distance of incrementally collected samples that were homogenized..... 97

Figure 4.7: Solid phase (a, f) concentration of benzene (red filled triangles), toluene (green filled squares) and *o*-xylene (blue filled circles) (BTX); (b, g) abundance of *Desulfosporosinus* (light blue filled diamonds), total bacteria (grey filled circles) and total archaea (dark red filled squares) from quantitative polymerase chain reaction (qPCR) analysis; and relative abundance (≥ 4%) of bacteria and archaea detected at the (c, h) phylum, (d, i) family and (e, j) genus taxonomic levels using 16S ribosomal ribonucleic acid (rRNA) next generation sequencing (NGS) for the multi-solute (BTX) BA-PC (top panel) and BA+PACz (bottom panel) columns after Year-2 of column operation. The grey region in the bottom panel represents the powdered activated carbon (PAC) zone. The vertical line in (a, f) represents the method detection limit of solid phase BTX (8.0×10^{-5} mg/g). The data in (b, g) represent the average of three measurements and the dashed vertical lines represent the background abundances. Error bars and solid vertical lines in (b, g) are ± 1 standard deviation. The phylum, family and genus legends correspond to (c, h), (d, i) and (e, j), respectively. Sample depths from the influent represent the median distance of incrementally collected samples that were homogenized. 106

List of Tables

Table 1.1: Commonly used single-solute sorption isotherm models in AC amended systems in contact with BTEX. 4

Table 2.1: Physical and chemical properties of WPC powdered activated carbon (PAC). 14

Table 2.2: Single-solute Freundlich (K_{f_i} and n_{f_i}) model parameters for benzene, toluene and *o*-xylene (BTX) and multi-solute ISIAS competition factors (a_i) for BTX in contact with WPC powdered activated carbon (PAC) ± confidence intervals (CI), and the root mean square error (RMSE) of the regressions. 25

Table 3.1: Cumulative target mass and number of amendments of toluene-only, BTX or sulfate added to each single- and multi-solute microcosm type over a 1-year monitoring period. 47

List of Acronyms

AC	Activated carbon
AGW	Artificial groundwater
AKIE	Apparent kinetic isotope effect
ASV	Amplicon sequencing variant
BAC	Biological activated carbon
BA+PAC	Bioactive + powdered activated carbon
BA+PACz	Bioactive + powdered activated carbon zone
BA+PAC+EA	Bioactive + powdered activated carbon + electron acceptor
BA-PC	Bioactive-positive control
BA-PC+EA	Bioactive-positive control + electron acceptor
BB	Biobarrier
BET	Brunauer, Emmett and Teller
BETX	Benzene, ethylbenzene, toluene, and xylene
BGS	Below ground surface
BS	Borden sand
BTX	Benzene, toluene, and (*o*)-xylene
CFB	Canadian forces base
CSIA	Compound specific isotope analysis
DCM	Dichloromethane
DFT	Density functional theory
DIC	Dissolved inorganic carbon
DIET	Direct interspecies electron transfer
DNA	Deoxyribonucleic acid
DO	Dissolved oxygen
EA	Electron acceptor
ESEM	Environmental scanning electron microscopy
EPS	Extracellular polymeric substances
FID	Flame ionization detector
GAC	Granular activated carbon
GC	Gas chromatography
IC	Ion chromatography
ID	Inner diameter
IHT	Interspecies hydrogen transfer
ISIAS	Improved simplified ideal adsorption solution
KC	Killed control
KC+PAC	Killed control + powdered activated carbon
KC+PACz	Killed control + powdered activated carbon zone
KIA	Kinetic isotope effect
MDL	Method detection limit
NDIR	Non-dispersive infrared detector
NGS	Next generation sequencing
ORP	Oxidation reduction potential
PAC	Powdered activated carbon
PAH	Polycyclic aromatic hydrocarbon

PC	Positive control
PHC	Petroleum hydrocarbon
PRB	Permeable reactive barrier
PTFE	Polytetrafluoroethylene
PV	Pore volume
PVC	Polyvinyl chloride
PZC	Point of zero charge
QA/QC	Quality assurance and quality control
qPCR	Quantitative polymerase chain reaction
RMSE	Root mean square error
RNA	Ribonucleic acid
RPM	Rotations per minute
rRNA	Ribosomal ribonucleic acid
SC	Starved control
S-PAC	Super fine powdered activated carbon
SS	Stainless steel
SRB	Sulfate reducing bacteria
TCD	Thermal conductivity detector
TIC	Total inorganic carbon

List of Symbols

a_i	Improved simplified ideal adsorption solution competition factor of solute *i* (-)
$B_{(aq)}$	Aqueous phase concentration of benzene (mg/L)
B_{effluent}	Aqueous phase effluent concentration of benzene (mg/L)
B_{influent}	Aqueous phase influent concentration of benzene (mg/L)
$B_{(s)}$	Solid phase concentration of benzene (mg/g)
C_{aq_i}	Aqueous phase concentration of solute *i* (mg/L)
$C_{\mathrm{CO}_{2(g)}}$	Gas phase concentration of carbon dioxide (mg/L)
$C_{\mathrm{DIC}_{(aq)}}$	Concentration of dissolved inorganic carbon (mg/L)
C_{e_i}	Equilibrium aqueous phase concentration of solute *i* (mg/L)
$C_{\mathrm{e}_i}^{\mathrm{d}}$	Desorption equilibrium aqueous phase concentration of solute *i* (mg/L)
$C_{\mathrm{e}_i}^{\mathrm{s}}$	Sorption equilibrium aqueous phase concentration of solute *i* (mg/L)
$CH_{4\ \text{effluent}}$	Aqueous phase effluent concentration of methane (mg/L)
$CH_{4(g)}$	Gas phase concentration of methane (mg/L)
$CH_{4\ \text{influent}}$	Aqueous phase influent concentration of methane (mg/L)
C_{o_i}	Initial aqueous phase concentration of solute *i* (mg/L)
$\mathrm{DIC}_{\text{influent}}$	Influent concentration of dissolved inorganic carbon (mg/L)
$\mathrm{DIC}_{\text{effluent}}$	Effluent concentration of dissolved inorganic carbon (mg/L)
$HS^-_{(aq)}$	Aqueous phase concentration of sulfide (mg/L)
HS^-_{effluent}	Aqueous phase effluent concentration of sulfide (µg/L)
HS^-_{influent}	Aqueous phase influent concentration of sulfide (µg/L)
f_{oc}	Fraction of organic carbon (-)
f_{PAC}	Fraction of powdered activated carbon (-)
K_{d_i}	Soil-water partitioning coefficient for solute *i* (L/kg)
K_{f}'	Average value of K_{f_i}
K_{f_i}	Freundlich sorption capacity of solute *i* ([mg/g][L/mg]^n)
K_{h_i}	Henry's constant for solute *i* (-)
K_{oc_i}	Organic carbon partitioning coefficient for solute *i* (cm^3/g)
K_{ow_i}	Octanol water portioning coefficient for solute *i* (-)
M_{aq_i}	Mass of solute *i* in the aqueous phase (mg)
$M_{\mathrm{aq}_i}^{\mathrm{d}}$	Desorption equilibrium or temporal mass of solute *i* in the aqueous phase (mg)
$M_{\mathrm{aq}_i}^{\mathrm{s}}$	Sorption equilibrium or temporal mass of solute *i* in the aqueous phase (mg)
m_{BS}	Mass of Borden sand (g)
M_{BS_i}	Mass of solute *i* in the Borden sand (mg)
$M_{\mathrm{CO}_{2(g)}}$	Mass of a gas phase carbon dioxide (mg)
$M_{\mathrm{DIC}_{(aq)}}$	Mass of aqueous phase dissolved inorganic carbon (mg)
M_{err_i}	Absolute mass of solute *i* lost or gained (mg)
M_{g_i}	Mass of solute *i* in the gas phase (mg)
M_{o_i}	Initial mass of solute *i* (mg)
m_{PAC}	Mass of powdered activated carbon (g)
M_{PAC_i}	Mass of solute *i* in the powdered activated carbon (mg)

M_{s_i}	Mass of solute *i* in the solid phase (mg)
$M_{s_i}^{d}$	Desorption equilibrium or temporal mass of solute *i* in the solid phase (mg)
$M_{s_i}^{s}$	Sorption equilibrium or temporal mass of solute *i* in the solid phase (mg)
M_{T_i}	Total mass of solute *i* in all phases (mg)
M_{TIC} or TIC	Mass of total inorganic carbon (mg)
$MW._{C}$	Molecular weight of carbon (g/mol)
$MW._{CO_2}$	Molecular weight of carbon dioxide (g/mol)
N	Sample size
n_f'	Average value of n_{f_i}
n_{f_i}	Freundlich sorption intensity of solute *i* (-)
P	Number of parameters
q_{e_i}	Equilibrium mass of solute *i* per gram of powdered activated carbon (mg/g)
$q_{e_i}^{d}$	Desorption equilibrium mass of solute *i* per gram of powdered activated carbon (mg/g)
$q_{e_i}^{s}$	Sorption equilibrium mass of solute *i* per gram of powdered activated carbon (mg/g)
q_{model}	Model generated q_e estimate (mg/g)
q_{exp}	Experimental q_e estimate (mg/g)
Q	Flow rate (L/day)
$SO_4^{2-}{}_{(aq)}$	Aqueous phase concentration of sulfate (mg/L)
$SO_4^{2-}{}_{effluent}$	Aqueous phase effluent concentration of sulfate (mg/L)
$SO_4^{2-}{}_{influent}$	Aqueous phase influent concentration of sulfate (mg/L)
$T_{(aq)}$	Aqueous phase concentration of toluene (mg/L)
$T_{effluent}$	Aqueous phase effluent concentration of toluene (mg/L)
$T_{influent}$	Aqueous phase influent concentration of toluene (mg/L)
$T_{(s)}$	Solid phase concentration of toluene (mg/g)
$X_{(aq)}$	Aqueous phase concentration of *o*-xylene (mg/L)
$X_{effluent}$	Aqueous phase effluent concentration of *o*-xylene (mg/L)
$X_{influent}$	Aqueous phase influent concentration of *o*-xylene (mg/L)
$X_{(s)}$	Solid phase concentration of *o*-xylene (mg/g)
V or $V_{(aq)}$	Volume of aqueous phase (L)
$V_{(g)}$	Volume of gas phase (L)
V_p	Pure phase volume (µL)
V_{PAC_Z}	Volume of powdered activated carbon zone (cm^3)
$\delta^{13}C$	Ratio of heavy (^{13}C) to light (^{12}C) carbon isotopes (‰)
$\Delta\delta^{13}C$	Change in $\delta^{13}C$
$\delta^{2}H$	Ratio of heavy (^{2}H) to light (^{1}H) hydrogen isotopes (‰)
$\Delta\delta^{2}H$	Change in $\delta^{2}H$
Λ	Lambda
ρ	Density (mg/µL)
ρ_{BS}	Bulk density of Borden sand (g/cm^3)

Chapter 1

1.1 General background

Petroleum hydrocarbons (PHCs) are chemical compounds comprised solely of hydrogen and carbon (e.g., monoaromatic compounds, such as benzene, toluene, ethylbenzene and xylene isomers [BTEX]) which are globally produced and consumed as major constituents in gasoline. Due to their widespread use, PHCs are frequently released into groundwater as a result of improper disposal, industrial discharges, accidental spills or leaking underground storage tanks. PHC contaminated groundwater is of concern due to the known toxicity and carcinogenicity of many PHC compounds. Therefore, there is an increased demand for the development and optimization of mass reduction or removal technologies. Of the numerous *in situ* and *ex situ* remedial options available (e.g., pump and treat, biosparging, permeable reactive barrier [PRB], bioremediation) [1, 2, 3, 4], sorption and/or biodegradation are primary mass reduction and removal mechanisms commonly integrated into treatment designs.

1.1.1 Sorption

Activated carbon (AC) is often used as a sorbent material in sorption-based technologies due to the extensive pore volume which provides a larger internal surface area. The large internal surface area of AC allows for a high sorption capacity and improved contaminant partitioning from the groundwater compared to other sorbent materials. AC is manufactured from carbon rich raw source materials (e.g., coconut shells), and through chemical or physical (thermal) activation volatiles are removed which results in the high carbon content of AC. Following activation, the resulting AC is comprised of a carbon frame of void spaces that forms a randomly distributed pore network of irregular shapes and sizes [5, 6, 7, 8]. The pore walls of the AC (~0.002 to 0.01 μm thick) are highly disordered and unhomogenized, and made of graphite-like platelets of hexagonal or pentagonal carbon rings that are randomly oriented relative to one another (a *turbostratic* structure) [5, 9, 10, 11] and held in place by van der Waals forces [6, 12]. AC is classified as granular AC (GAC), powdered AC (PAC) or super fine PAC (S-PAC) when the particle diameter is within the range of 0.2 to 5 mm, 15 to 25 μm [13] or ≤ 1 μm [14, 15], respectively.

Prior to external AC surface sorption aqueous phase solute (sorbate) molecules are diffusively transported through the boundary layer surrounding an AC particle surface (i.e., film

diffusion) [16, 17]. Once the sorbate contacts the AC surface, the magnitude and type of AC surface sorption is largely affected by the presence of functional groups (e.g., carboxyl, lactone, phenol, chromene, pyrone [18, 6]) or heteroatoms which are bonded to free vacancies at the edge of the graphite-like platelets or sites of broken hexagonal or pentagonal carbon rings [5, 10]. Depending on the solution pH relative to the point of zero charge (pH_{Pzc}) of the AC, deprotonation ($pH > pH_{Pzc}$) or protonation ($pH < pH_{Pzc}$) of surface functional groups may occur resulting in a negative or positive surface charge, respectively [18, 6], and electrostatic attraction for a cationic or anionic sorbate [6, 19]. In the absence of functional groups, the characteristically non-polar AC particle preferentially sorbs neutral, non-polar hydrophobic organic compounds as compared to polar inorganic species [5]. AC surface sorption may occur through strong chemical bonding (i.e., ionic or covalent) or weaker physical bonds (i.e., van der Waals forces, including dipole-dipole interactions and hydrogen bonding) [20, 5]. For aromatic compounds such as BTEX AC sorption commonly occurs through electron donor-acceptor complex interactions between the aromatic ring of the sorbate (electron acceptor) and functional groups or free vacancies on the AC (electron donor), in addition to physical bonding [21, 17, 22, 23].

Although some external AC surface sorption occurs, most takes place internally which is initiated by concentration gradients causing the sorbate molecules to diffuse inside an AC particle when the internal sorbate concentration is lower relative to the surrounding external aqueous phase concentration. Internal transport of the sorbate begins in *macropores* which are pore openings connected to the external AC surface (≥ 50 nm in diameter). Macropores contribute the least to the internal surface area of the AC (< 5% surface area) and are connected to transitional pores referred to as *mesopores* (2 to 50 nm in diameter). Mesopores are connected to the smallest size range of pores, referred to as *micropores* (≤ 2 nm in diameter) which contribute the most to the internal surface area (≥ 95% surface area) [5, 24, 25] and sorption [5]. Micropores are classified as either *supermicropores* (1-2 nm) or *ultra micropores* (≤ 0.8 nm) [10, 25]. Intraparticle diffusion of the sorbate persists until equilibrium conditions are reached [20], provided the molecules are small enough to fit inside the pore spaces with limited diffusional resistance [22] and the pore space is not blocked by functional groups or cross links [26]. For smaller sorbate molecules, relative to larger molecules, the overall sorption rate may be reduced during intraparticle diffusion due to longer diffusion paths in micropores [5]. Once equilibrium conditions are reached, internal sorption occurs at sorption sites

with higher binding energy relative to surface sorption due to multiple internal contact points within the three-dimensional pore volume as opposed to the lower attractive forces associated with the two-dimensional particle surface [27].

In addition to properties of the AC sorbent material, properties of a sorbate which may heavily influence the magnitude or capacity of internal or external sorption relative to another sorbate include higher molecular weights and octanol water partitioning coefficients (K_{ow}) [28, 21, 16, 29]. In single-solute systems, differences in the magnitude of these properties leads to variable equilibrium aqueous and solid phase concentrations between sorbates. In multi-solute systems competition for sorption sites are introduced between sorbates due to the limited number of active sites on the AC relative to the single-solute systems. Therefore, the sorbate most preferentially sorbed in the multi-solute system (based on chemical properties) will occupy the greatest number of the sorption sites at equilibrium [29]. Various equilibria models are used to describe sorbate sorption to AC [30], including those listed in Table 1.1 for single-solute sorption. Of these models, the Freundlich [31, 32, 33], Langmuir [29, 34, 35] or Sips [33] are commonly found to fit isotherm data well in AC amended systems in contact with BTEX, and the Freundlich isotherm model is commonly used in more complex systems with bioactivity [36, 37, 38, 39].

Table 1.1: Commonly used single-solute sorption isotherm models in AC amended systems in contact with BTEX.

Isotherm model [1]		**Model parameters** [2]	**Model assumption(s), details, and application**
Henry's law	$q_e = K_H C_e$	K_H	Simplest sorption isotherm, limited to low C_e and/or surface coverage.
Langmuir	$q_e = \frac{q_{m,L} K_L C_e}{1 + K_L C_e}$	$q_{m,L}, K_L$	Homogeneous sorbent surfaces, monolayer sorption.
Freundlich	$q_e = K_F {C_e}^{n_F}$	K_F, n_F	Heterogeneous sorbent surfaces, variable energy at sorption sites, applicable for multilayer sorption.
Sips	$q_e = \frac{q_{m,SP} K_{SP} {C_e}^{n_{SP}}}{1 + K_{SP} {C_e}^{n_{SP}}}$	$q_{m,SP}, K_{SP}, n_{SP}$	Homogeneous and heterogeneous systems of sorption, monolayer sorption, combined Langmuir-Freundlich model (Freundlich at low concentrations and Langmuir at high concentrations).
Redlich-Peterson	$q_e = \frac{K_R C_e}{1 + a_R {C_e}^{\beta_R}}$	K_R, a_R, β_R	Homogeneous and heterogeneous systems of sorption, sorption over a wide range of concentrations.
Radke-Prausnitz	$q_e = \frac{q_{m,RP} K_{RP} C_e}{1 + K_{RP} {C_e}^{m_{RP}}}$	$q_{m,RP}, K_{RP}, m_{RP}$	Sorption over a wide range of concentrations.

Notes:
1. References: [40, 13, 30].
2. q_e is the solid phase concentration; C_e is the equilibrium aqueous phase concentration; q_{mi} is the maximum sorption capacity; K_i, n_F, and a_R are the sorption equilibrium constants; and n_{SP}, β_R, and m_{RP} are model exponents.

Just as internal AC sorption is initiated by concentration gradients between the bulk aqueous phase surrounding the AC particle and the internal sorbate concentration within pores, desorption is prompted by similar concentration gradients. Specifically, desorption occurs when the internal aqueous concentration of a sorbate is higher than the external concentration, and in response diffusion of sorbed mass from pores persists until new equilibrium conditions are reached [13]. Hysteresis occurs when some fraction of the sorbed mass does not readily desorb, resulting in a difference between the sorption and desorption pathways [41]. Hysteresis may be time dependent (reversible) or independent of time (irreversible) [41, 42]. Time dependent hysteresis may be caused by slow equilibrium times [32], or physical sorption of the sorbate by weaker van der Walls forces of attraction [38] or hydrogen bonding [43]. Whereas, hysteresis independent of time may be due to permanent chemical bonds at high energy

sorption sites [38] or with oxygen containing functional groups [20, 44], or pore deformation and collapse due to the pressure exerted on pore walls during sorption which may lead to solute entrapment during desorption [41, 42].

1.1.2 Biodegradation

Unlike sorption which reduces aqueous phase sorbate or contaminant concentrations, biodegradation may completely mineralize contaminants [45, 46]. Many organic contaminants are readily biodegraded aerobically by microorganisms, although these conditions are rapidly depleted due to the thermodynamic favourability of oxygen [47]. As a result, anaerobic conditions are generated that exhibit a redox gradient based on the presence and distribution of other electron acceptors (e.g., NO_3^-, Fe^{3+}, SO_4^{-2} or HCO_3^-). Reactions which yield the highest amount of energy are carried out first (i.e., $NO_3^- > Fe^{3+} > SO_4^{-2} > HCO_3^-$), and once a higher energy yielding condition is depleted due to the loss of an oxidizing agents, the next highest energy yielding reaction is initiated [48, 49, 50, 51, 52]. Redox reactions between electron donors (e.g., BTEX) and electron acceptors (e.g., SO_4^{-2} [53, 54, 55, 56, 57]) are initiated by microbes which are genetically capable of expressing enzymes required to break the chemical bonds of compounds involved in the reaction [58, 46]. Some microbes are enzymatically capable of continued metabolic function under different electron accepting conditions [59]. Once bonds are broken, electrons are transferred between the electron donor which become oxidized and loses electrons, and the electron acceptor which become reduced and gains electrons. As a result, biodegradation by-products or metabolites are generated (e.g., intermediates formed following fumarate addition to the methyl groups of TEX [60] such as benzoate or benzoyl-CoA which is a common intermediate shared between BTEX, and benzylsuccinate synthase is the active enzyme [61, 62, 63, 60, 46]), and energy is released which facilitates cell growth and maintenance. Competitive inhibition may result when the biodegradation of multiple compounds is involved in a single enzymatic pathway, such as the anaerobic biodegradation of BTEX to benzoate. Under these conditions differences in the chemical properties, reaction rates or concentrations between compounds often determine which substrate(s) are preferentially biodegraded first. Although, during metabolism of the primary substrate(s) co-metabolism of the other more recalcitrant compounds can indirectly occur. In lower pathway reactions of the primary substrate, enzymes typically become more specialized which may then result in the accumulation of dead-end products from the secondary substrate(s) [64].

In highly reduced, low energy yielding environments sulfate reducing bacteria (SRB) often outcompete acetogens or methanogens for common substrates (e.g., hydrogen and acetate) or inhibit methanogenesis due to the kinetic and thermodynamic advantages of SRB [65, 66, 67]. However, the coexistence or syntrophic relationships between SRB, methanogens and fermenters are common due to interspecies specialization [68, 69], where each microbe carries out certain biodegradation steps and the metabolite(s) produced can be utilized by other members in subsequent reactions [70, 46]. This is commonly observed during interspecies hydrogen transfer (IHT), where electron donating microbes (e.g., syntrophic, fermentative or acetate oxidizing bacteria) reduce simple substrates to products (i.e., H_2) that are shuttled to electron accepting microbes (e.g., hydrogenotrophic methanogens) for oxidation during the reduction of carbon compounds (e.g., CO_2) to methane (CH_4) [71, 72, 70]. Limitations to IHT arise when fast growing bacteria generate excessive substrates at toxic levels that can not be converted by slow growing methanogens (e.g., accumulation of $H_2 > 10^{-4}$ atm, resulting in thermodynamically unfavourable conditions [$\triangle G > 0$], making PHC biodegradation energetically unfeasible) or when the slow molecular diffusion of electron shuttles becomes rate limiting to biodegradation [73, 74]. Alternatively, electrons can be transferred from direct cell-to-cell contact through conductive pili and outer membrane c-type cytochromes or membrane-bound transport proteins by direct interspecies electron transfer (DIET). This process is less energy intensive given that the requirement for metabolite production and exchange through IHT is eliminated [75, 76, 77, 78].

1.1.2.1 Compound specific isotope analysis

Biodegradation, dilution, dispersion, and sorption are processes occurring during natural attenuation at contaminated sites and contribute to contaminant mass reduction. To assist in determining which mass reduction processes are responsible for reductions in contaminant concentrations, compound specific isotope analysis (CSIA) is an effective tool. CSIA is used assuming that most isotope fractionation occurs during biotic processes (i.e., biodegradation), while relatively little, if any, occurs during other attenuation processes (e.g., sorption, dilution, dispersion, volatilization) [79, 80, 81, 82]. Fractionation of PHCs occurs due to the elemental composition of these compounds which are comprised of carbon and hydrogen, with each element having two stable isotopes (i.e., $^{12}C/^{13}C$ for carbon and $^{1}H/^{2}H$ for hydrogen). During biodegradation, microbes often preferentially degrade the lighter isotope fraction of each element (with weaker molecular bonds and lower activation energies for the reaction) as compared to the heavier

isotope fraction (with stronger molecular bonds and higher activation energies for the reaction) which results in the non-degraded fraction of the contaminant mass becoming enriched in the heavier isotope [83, 84, 45, 85]. Fractionation due to other processes, such as sorption (i.e., of enrichment or depletion of the light isotopes during sorption or desorption, respectively) has also been reported [86, 87, 88, 89], although isotope shifts are less than for biodegradation [84, 45]. For CSIA to be an effective tool fractionation must be detectable, although this is sometimes constrained by variation in detection sensitivity between elements due to differences in relative mass between stable isotopes. For example, the magnitude of fractionation is often much larger and more detectable for hydrogen relative to carbon due to the larger mass difference between the heavy and light isotope fractions [83, 84].

To further discern which contaminant mass reduction processes or biodegradation pathways are occurring the slope (i.e., lambda [Λ]) between the $\Delta\delta^{2}H$ versus the $\Delta\delta^{13}C$, using dual isotope plots, can be compared to known ranges of Λ in the literature [90, 91, 92, 93, 94]. Dual isotope plots eliminate non- or slightly fractionating rate-limiting steps (e.g., substrate uptake into cells or binding to an enzyme during enzymatic reactions) that potentially occur prior to the isotope-sensitive bond change, generating an apparent kinetic isotope effect (AKIE). The elimination of the AKIE, which is generally smaller than the intrinsic kinetic isotope effect (KIE) (i.e., the difference in the reaction rates between heavy and light isotopes), occurs given that carbon and hydrogen are assumed to be equally affected by potential rate limitations. Once eliminated, Λ is considered representative of the various *in situ* processes (e.g., biodegradation, chemical oxidation, volatilization [95]). Specially, for biodegradation Λ indicates the initial carbon-hydrogen bond cleavage reaction associated with a specific catabolic pathway (e.g., fumarate addition by benzylsuccinate synthase), and a linear trend indicates a consistent reaction mechanism as biodegradation proceeds [90, 91, 92, 93].

1.1.2.2 Quantitative polymerase chain reactions and next generation sequencing

Quantitative polymerase chain reaction (qPCR) and next generation sequencing (NGS) are tools that provide enhanced monitoring of biodegradation. qPCR involves the detection and amplification of purified fragments of deoxyribonucleic acid (DNA) or ribonucleic acid (RNA) sequences within extracted samples. Specific gene of interest are first targeted by primers added to reaction mixtures, which allow for the detection of microbes known to participate in certain biodegradation processes. The copy number of replicated DNA is then quantified during successive amplification cycles which provides an estimate of the

abundance of the detected organisms [96]. Contrary to qPCR, NGS is a high throughput multiplexed amplicon sequencing approach which aligns amplified sequences to a known reference database of organisms, providing information related to the organisms' taxonomic positions, the abundance of taxonomic groups and community or inter-sample diversity [97, 98].

Commonly, the 16S ribosomal RNA (rRNA) gene is targeted by primers given it is universally present in all bacteria and archaea and has regions of high conservation amenable to primer design as well as regions of high variability that allow precise taxonomic differentiation between organisms [99]. Amplification of more specialized genes that are specific to organisms or certain catabolic pathways can also be used. For example, primers targeting the *bssA, bamAB* or *bcrA* genes can assess the diversity and prevalence of the enzyme benzylsuccinate synthase or benzoyl-CoA reductase, critical functions during BTEX biodegradation [58].

1.1.3 AC particulate amendments for treatment of groundwater

The combined use of AC and biodegradation is well documented, with successful application in biological AC (BAC) wastewater systems. BAC systems are predominantly operated under aerobic conditions in the presence of GAC and used for the treatment of a range of contaminants, including organic [36, 100, 101, 39] or chlorinated [38] compounds. Relative to bioactive systems without AC, BAC systems have been found to require less time prior to the initiation of biodegradation, and maintain lower effluent concentrations during operational periods of increased flow rates or contaminant loading due to AC sorption [36, 100, 101, 39]. The premise of BAC technology has gained commercial popularity for the *in situ* treatment of contaminated groundwater [102, 103], when installed similarly to permeable reactive barriers (PRB) or biobarriers (BB) [104, 105, 106]. Specifically, a slurry of AC (e.g., PAC) and potentially other additives (e.g., electron acceptors, cultured microbes, etc.) are strategically injected downgradient of a contaminant source zone to create an AC PRB capable of sequestering organic contaminants. The AC maximizes hydrophobic organic partitioning from the groundwater and accumulates the contaminants to several orders of magnitude higher relative to the surrounding aqueous phase. Following mass reduction by sorption, mass removal of some contaminants is often reliant on the growth of a biofilm layer on the AC surface. As the biofilm grows microbial cells secret extracellular polymeric substances (EPS) (e.g., nucleic acids, enzymes, proteins, polysaccharides and lipids) which strengthens cell attachment to the PAC surface. EPS are typically negatively charged due to the presence of functional groups, which contributes to the

surface charge and sorption properties of the PAC [107, 108]. The biofilm stimulates microbial biodegradation of the aqueous phase surrounding the AC particles, which in turn promotes the desorption of sorbed mass from the AC due to the concentration gradient within the aqueous phase. In mature AC PRB systems, continued desorption and aqueous phase biodegradation facilitates AC regeneration, and reduced aqueous phase contaminant concentrations are sustained due to continued partitioning [100, 109, 38].

In an AC PRB system initially the rate of sorption exceeds biodegradation and sorption is the dominant, short-term mass reduction mechanism, resulting in a depletion in the aqueous phase concentration prior to exhaustion of the AC sorption capacity. Once the sorption sites of the AC are saturated no further sorption occurs in a static system, while in a typical groundwater system an increase in the aqueous concentration downgradient of the PRB occurs (i.e., breakthrough). Once a microbial community has formed (i.e., biofilm) within the PRB, mass removal by biodegradation occurs with perhaps the rate of biodegradation approaching the rate of sorption or desorption. In a mature system biodegradation may become the dominant mass removal mechanism [36, 38, 107, 13]; however, the AC sorption capacity may diminish as a result of increased biofilm thickness causing diffusional resistance [37], or the alteration of AC surface properties due the EPS potentially filling pores [110, 13].

AC is a key component in an AC PRB given that the AC provides a protective surface for microbial growth during biofilm formation [36, 38, 111]. The AC may also reduce the lag time prior to biodegradation given that microbial growth rates on AC have been found to be faster as compared to other substrates [36]. Additionally, the AC extends the residence time between the biofilm and sorbed contaminants and metabolic intermediates due to continual desorption during biodegradation [102, 108]. DIET may also occur through electron exchange with the surface of the AC (e.g., AC acts as an electron acceptor or donor) and between microbes in the biofilm [112, 76, 78, 108], given that the AC is conductive. Relative to systems without AC, DIET is enhanced in AC systems as contact to the AC is the primary connection required and less metabolic energy is exerted to form conductive pili or cytochromes, as described in Section 1.1.2 [112, 73]. *Geobacter* is a representative electron-donating bacterium known to participate in AC-mediated DIET by transferring electrons to the AC [113, 112, 114, 77, 115, 116, 117]. Whereas, *Methanosaeta* [112, 118, 117] and *Methanosarcina* [76, 119, 117] are representative methanogens and receive electrons from the AC for accelerated substrate conversion to CH_4 [112, 114, 115, 108].

1.2 Objective and research questions

Although the combination of AC sorption and biodegradation is well documented for the treatment of wastewater [36, 100, 101, 38], application in *in situ* AC PRBs for the treatment of contaminated groundwater (e.g., with PHCs or chlorinated solvents) is relatively new [102, 103]. Given this, limited scientific evidence exists regarding process behaviour and performance of *in situ* AC PRBs. Uncertainties are primarily related to the interplay between AC sorption and biodegradation and the long-term behaviour of these processes in AC amended systems, and if the presence of AC enhances or influences biodegradation. To address these uncertainties specific research questions asked as part of this research include:

Q1. Are AC sorption isotherms generated under ideal conditions representative of sorption behaviour in bioactive AC systems?
Q2. Does AC influence microbial activity during PHC biodegradation?
Q3. Does biodegradation regenerate AC sorption capacity?
Q4. Does AC enhance the biodegradation rate of PHCs?
Q5. How do bioactive systems with AC respond to variable PHC loading?
Q6. Can CSIA distinguish biodegradation from AC sorption in bioactive systems?

To address Q1 to Q6 a series laboratory experiments were conducted, including isotherm, microcosm (1-year) and column (2-year) experiments. The isotherm experiments were first carried out to determine the sorption (and single step desorption) capacities and sorption isotherms for a PAC in contact with benzene, toluene and *o*-xylene (BTX), either alone (single-solute system) or combined (multi-solute system). Additionally, the PAC particle size and structure were characterized, and the sorption and desorption equilibrium times of single-solute benzene and toluene were approximated. The PAC was then used in microcosm and column experiments to investigate the long-term AC sorption and anaerobic biodegradation behaviour of toluene and BTX in single- or multi-solute systems, respectively, specifically under sulfate reducing and methanogenic conditions. Anaerobic microcosm experiments were performed to represent simplified stagnant system behaviour under ideal conditions, where AC dosing, PHC loading and contact time were controlled. Whereas anaerobic column experiments were conducted to provide a

more realistic representation of a dynamic field scenario, and to mimic an *in situ* groundwater system where an AC PRB was installed.

To address **Q1** single- and multi-solute sorption isotherm model parameters for BTX and the PAC were first developed under ideal conditions in the absence of bioactivity. The single- and multi-solute BTX isotherms were then directly compared to single- or multi-solute aqueous and solid phase BTX concentration data generated from the microcosm experiments to determine if the ideal isotherms are representative of the sorption behaviour in bioactive systems. **Q2** was addressed from both microcosm and column experimental data, by comparing changes in the PHC, geochemical (primarily sulfate, sulfide, CO_2 and CH_4) and molecular (i.e., qPCR and NGS) parameters monitored between bioactive (and abiotic) systems with and without PAC to determine if the presence of the PAC influence microbial activity during PHC biodegradation. **Q3** was addressed from the microcosm experimental data, where the single- and multi-solute solid phase concentrations of toluene or BTX were directly measured over the monitoring period to determine if the solid phase toluene or BTX concentrations are reduced or the PAC sorption capacities for each solute are regenerated with bioactivity. **Q4** was addressed from the microcosm experimental data, by comparing the zero-order rate constants for toluene oxidation coupled to sulfate reduction between bioactive systems with and without PAC to determine if the presence of the PAC enhances the rate of toluene biodegradation. **Q5** was addressed from the column experimental data, by comparing changes in the effluent toluene or BTX concentrations during sequentially increased influent concentrations between bioactive (and abiotic) systems with and without PAC to determine how the bioactive systems with AC respond to variable PHC loading relative to the others (i.e., abiotic with AC or bioactive without AC). **Q6** was addressed from the column experimental data, by comparing changes primarily in effluent δ^2H-B,T,X (in addition to δ^{12}C-B,T,X) between bioactive (and abiotic) systems with and without PAC to determine if CSIA can distinguish biodegradation from AC sorption in bioactive systems.

Collectively. the compiled data set addressing Q1 to Q6 can be used to help inform how AC particulate amendments behave in *in situ* anaerobic systems in contact with PHCs, and more specifically with regards to the interplay between toluene or BTX sorption and anaerobic biodegradation under sulfate reducing and methanogenic conditions. These data will also provide an enhanced understanding of the long-term behaviour and system performance of AC particulate amendments in bioactive systems, and how the addition of AC may enhance or influence biodegradation relative to systems without AC.

1.3 Thesis scope

The remainder of this thesis is comprised of four (4) additional chapters. Chapter 2 discusses the PAC particle characterization (size and surface structure), batch isotherm experiments (sorption and single step desorption) and the sorption and desorption equilibrium times. Chapter 3 describes the anaerobic microcosm experiments comparing bioactive microcosms with and without PAC, and with and without additional electron acceptors (EA) for a simple single-solute system (toluene only) and a more complex multi-solute system (BTX). Chapter 4 presents the anaerobic column experiments comparing columns with sorption or bioactivity alone relative to a combination of sorption and bioactivity for single-solute (toluene-only) and multi-solute (BTX) systems. The microcosm experiments ran for one year, and the column experiment ran for approximately two years with detailed monitoring conducted during Year-2. In Chapter 3, timeseries data for toluene and BTX and geochemical parameters (sulfate, sulfide, total inorganic carbon [TIC], CH_4, pH, the oxidation reduction potential [ORP] and dissolved oxygen [DO]) are discussed, and molecular data (qPCR and NGS) collected at the end of the 1-year monitoring period is presented. In Chapter 4, the same parameters as the microcosm experiments were monitored during Year-2 and are described, in addition to temporal CSIA results. Finally, Chapter 5 provides conclusions and recommendations pertaining to the research conducted.

Chapter 2

Powdered activated carbon sorption and desorption of benzene, toluene and *o*-xylene

2.1 Introduction

Of the many sorbent materials available (e.g., resins, activated carbon [AC], zeolites, etc. [120]), AC is favourable given the large internal surface area primarily due to the high proportion of small diameter pores (i.e., *micropores* that are ≤ 2 nm in diameter) that comprise 95% of the internal volume [24, 25]. The large internal surface area allows for solute sorption [5] which is initiated due to concentration gradients between the solute(s) in the area surrounding and within the AC. Similarly, desorption of the solute(s) back to the area surrounding the AC is also initiated by concentration gradients. For both the sorption and desorption processes solute diffusion will continue until new equilibrium conditions are reached [13]. The magnitude of sorption and desorption of the solute(s) to and from the AC are controlled by the physical and chemical properties of the sorbent (e.g., presence of functional groups [18, 5, 6]) and the solute(s) (e.g., molecular weights and octanol water partitioning coefficients (K_{ow}) [28, 21, 16, 29]) that are in contact.

Although the equilibrium sorption and desorption characteristics of benzene, toluene and *o*-xylene (BTX) in contact with activated carbon (AC) has been investigated by others [31, 37, 36, 34], this inquiry focused on defining these characteristics for a specific PAC. Initially, images of the PAC were generated using environmental scanning electron microscopy (ESEM) to characterize the particle surface structure and size. Then a series of single-solute (benzene, toluene or *o*-xylene) and multi-solute (BTX) sorption experiments were conducted to generate equilibrium isotherms and model parameters. The isotherms were then compared to more complex systems with bioactivity (discussed in Chapter 3) to determine if the single-solute (toluene-only) or multi-solute (BTX) sorption isotherms are representative of the sorption behaviour in bioactive AC systems (addressing Q1 [Section 1.2]). Additionally, single-step desorption equilibrium behaviour was assessed, and the sorption and desorption equilibrium times of single-solute benzene and toluene were investigated.

2.2 Materials and methods

WPC PAC (Calgon Carbon, Pittsburgh, PA, USA), a virgin coconut-based thermally activated product, was used as received (see Table 2.1 for typical physical and chemical properties).

Table 2.1: Physical and chemical properties of WPC powdered activated carbon (PAC).

Properties	Value	Reference(s)
Ash content	18 wt. % (max)	[121]
Moisture content	8 wt. % (max)	[121]
< 325 US mesh (0.045 mm)	90 wt. % (min)	[121]
< 100 US mesh (0.150 mm)	99 wt. % (min)	[121]
Iodine number	800 mg/g (max)	[121]
Point of zero charge (pH_{pzc}) [1]	10.1	[122]
Particle diameter [2]	13.1 μm	[123]
BET surface area [3]	801 m^2/g, 996 m^2/g	[124], [123]
DFT surface area [3]	853 m^2/g (slit-pore), 1355 m^2/g (cylindrical-pore)	[123]
DFT Micropore volume (< 0.8-2 nm) [4]	0.31 cm^3/g, 0.37 cm^3/g (slit-pore), 0.4 cm^3/g (cylindrical-pore)	[122], [123], [123]
DFT Mesopore volume (2-24 nm) [4]	0.04 cm^3/g	[122]
DFT Mesopore volume (2-35 nm) [4]	0.011 cm^3/g (slit-pore), 0.015 cm^3/g (cylindrical-pore)	[123], [123]
DFT Total pore volume [4]	0.32 cm^3/g, 0.35 cm^3/g, 0.38 cm^3/g (slit-pore), 0.42 cm^3/g (cylindrical-pore)	[124], [122], [123], [123]
% of micropore volume	89%, 90.5%	[122], [124]

Notes:

1. At neutral aqueous phase pH (7) the net surface charge of the PAC is positive due to protonation ($pH < pH_{pzc}$) [125, 23, 19].
2. Particle size was measured by laser diffraction using a Horiba LA-960 laser particle size analyzer.
3. The Brunauer, Emmett and Teller (BET) theory or density functional theory (DFT) were used to determine the surface area of internal pores from gas phase sorption equilibria data.
4. The DFT was used to determine the internal pore volume and pore size distribution from gas phase sorption equilibria data.

Analytical grade benzene (EMD Millipore, China), toluene (EMD Millipore, Darmstadt, DE) and *o*-xylene (BDH Limited, Poole, EN) (≥ 99% purity for all compounds) were used as the aqueous phase solutes.

The artificial groundwater (AGW) consisted of: ammonium chloride, sodium chloride (VWR, BDH Chemicals, Padnor, PA, USA), magnesium chloride, manganese (II) chloride, potassium dihydrogen phosphate, sodium sulfate (Sigma Aldrich, St. Louis, MO, USA), calcium chloride (EMD

Millipore Corporation, Darmstadt, HE, DE) and monosodium phosphate (Fisher Scientific, Waltman, MA, USA) (see Table A.1 for details).

Dichloromethane (DCM) (Sigma-Aldrich, St. Louis, MO, USA), *m*-fluorotoluene (Sigma-Aldrich, St. Louis, MO, USA) and 2-fluorobiphenyl (Chem Service, West Chester, PA, USA) (25 mg/L) were used for sample analysis. Sodium azide (EMD Millipore Corporation, Darmstadt, HE, DE) was used as a biocide during the desorption experiments.

2.2.1 PAC characterization

ESEM was carried out using a Quanta Feg 250 environmental scanning electron microscope (Field Electron and Ion Company, Hillsboro, OR, USA). The PAC sample was prepared by homogeneously spreading ~1 mg of dry PAC onto a sterilized metal mount affixed with conductive double sided carbon tape and removing any excess unadhered particles from the adhesive surface. The mount was then loaded onto a sample holder and transferred into the microscope chamber for imaging. Image analysis of a scale calibrated ESEM image was performed in ImageJ (Fiji 1.53) using the Measure and Label macro to measure features within the two-dimensional image frame.

2.2.2 Sorption and desorption equilibrium capacity

A series of sorption and single-step desorption experiments were conducted to determine the equilibrium capacity between PAC and BTX in both single-solute (benzene, toluene or *o*-xylene) and multi-solute (BTX) systems. Stock solutions of benzene, toluene and/or *o*-xylene were prepared by adding the required volume of each pure phase compound into vigorously mixing AGW, representative of a simplified groundwater solution (see Table A.1 for the AGW recipe) (the volume of single- or multi-solute BTX added to the AGW was variable, dependent on the total solution volume and final concentration). After the pure phase addition of BTX, the stock solutions were sealed with Teflon-lined rubber stoppers (Themo Fischer Scientific, Waltham, MA, USA) and mixed on a C-MAG HS 7 magnetic stirrer (IKA, Staufen im Breisgau, DE) for at least 12 hours. Following mixing, the stock solutions were used to immediately fill a subset of clear glass 160 mL serum bottles prepared in triplicate (Pierce Chemical Company, Rockford, IL, USA) with either the single-solute or the multi-solute (1:1:1 concentration ratio of the single-solute concentrations) solution prepared to the highest aqueous phase concentration of 25 mg/L (normal value) (see Table A.2 for the experimental design).

Once the subset of triplicate sets of serum bottles were filled with the highest solution concentrations, the BTX stock solutions were diluted to 12 mg/L (nominal value) with fresh AGW, and the next subset of serum bottles prepared in triplicate were filled. Dilutions of the BTX stock solutions were repeated several times to successively lower concentrations (10, 6, 3 and then 0.5 mg/L [nominal values]) (see Table A.2 for the experimental design) and serum bottle filling continued until all subsets of bottles, designated to be filled with each successively lower aqueous concentration, were filled. The serum bottles were preloaded with either 10 mg of PAC or without PAC (control). The PAC and control serum bottles were filled without headspace and capped with crimp caps fit with 24 mm Teflon-lined silicon septa (Restek, Bellefonte, PA, USA). All serum bottles were then loaded on a platform rotary shaker (Barnstead Thermolyne, Dubuque, IA, USA) at 100 to 150 rotations per minute (RPM) for 24 hours to ensure continuous mixing. Following shaking, the serum bottles were left to stand for an additional 24 hours (48 hours total) to allow any suspended PAC to settle from the aqueous phase. In a supplemental investigation to ensure that the PAC settled from solution following the settling period, 12 mL of supernatant was removed from several serum bottles and ultracentrifuged which confirmed no PAC was present in the solution phase.

To determine sorption equilibrium aqueous concentrations, 19 mL samples of the aqueous phase were transferred from the 160 mL serum bottles to 20 mL glass screw top vials (Sci Spec, Hanover, MD, USA) preloaded with 1 mL of DCM containing internal standards of *m*-fluorotoluene and 2-fluorobiphenyl (25 mg/L). Aqueous samples were transferred from the 160 mL serum bottles to the 20 mL sample vials using a 20 mL glass syringe with a luer-lock fitting attached to an 18-gauge stainless steel needle (Ace Glass, Vineland, NJ, USA). The sample vials were then sealed with Teflon lined silicon septa screw caps (Chromspec, Brockville, ON) and horizontally loaded on a platform rotary shaker at 350 RPM for 15 minutes. Following shaking, the vials were left to stand for 10 to 30 minutes to allow the DCM and water phases to separate. Using a dedicated glass microliter syringe (Hamilton, Reno, NV, USA) 0.7 mL of the DCM phase was removed from the sample vials and transferred to 2 mL glass autosampler vials (VWR, Padnor, PA, USA) sealed with Teflon-lined screw caps in preparation for analysis by gas chromatography (GC).

To generate aqueous data representative of a single desorption step, the remaining aqueous phase in the serum bottles (~140 mL) was decanted using a 20 mL glass syringe with a luer-lock fitting attached to an 18-gauge stainless steel needle, while ensuring minimal disturbance of the settled PAC.

Fresh stock AGW was then added to the serum bottles by filling without headspace (160 mL), and the bottles were crimp capped. The serum bottles were shaken, sampled for the aqueous phase, and extracted similarly as described above for the estimation of sorption equilibrium aqueous phase concentrations.

To estimate the sorption equilibrium solid phase sorbed concentration of benzene, toluene and/or *o*-xylene on the PAC a replicated set of all serum bottles with PAC were prepared, shaken, and fully decanted identically as for the set constructed for aqueous phase sorption and desorption (the aqueous phase was not measured prior to decanting). The remaining PAC was then saturated by the addition of 1 mL of DCM (containing *m*-fluorotoluene and 2-fluorobiphenyl [25 mg/L]), and the serum bottles were resealed with crimp caps and vertically loaded on a platform rotary shaker to agitate the PAC and DCM at ≤ 10 RPM for at least 1 day (typically 3-5 days). Following shaking, 0.7 mL of the DCM was transferred to 2 mL autosampler vials, following the same procedure described above for the estimation of sorption and desorption equilibrium aqueous phase concentrations.

The equilibrium solid phase sorbed concentration of benzene, toluene and/or *o*-xylene remaining on the PAC following the single desorption step was estimated from the same serum bottles used for aqueous phase sorption and desorption sampling. The serum bottles were fully decanted and extracted similarly as described above for the estimation of sorption equilibrium solid phase sorbed concentrations.

All aqueous and solid samples were analysed on an Agilent 7890A gas chromatograph system equipped with a flame ionization detector (FID) and an Agilent Sampler 80 autosampler. Three microliters (3 μL) of the sample extract were injected in splitless mode onto a 0.25 mm × 30 m DB5 capillary column with a stationary phase film thickness of 0.25 μm. The chromatographic conditions were: 275ºC injection port temperature, 35ºC initial column temperature (held for 0.5 min), 15ºC/min heating rate, 300ºC final temperature (held for 2 min), 325ºC detector temperature, and 1 mL/min column flow rate with helium as the gas carrier. Reagent water blanks were analysed for quality assurance and quality control (QA/QC), and calibration standards were prepared in triplicate and extracted in the same manner as described for the aqueous samples [126, 127]. Data integration was performed with a Chemstation chromatography data system. Aqueous phase method detection limits (MDLs) were 108 μg/L, 49 μg/L and 45 μg/L for benzene, toluene and *o*-xylene, respectively, and the solid phase MDL was 0.08 μg/g for benzene, toluene and *o*-xylene.

The sorption equilibrium mass of benzene, toluene and/or *o*-xylene per gram of PAC, $q_{e_i}^{s}$ (mg/g), was indirectly estimated from the difference between the aqueous phase concentration in the control and PAC serum bottles, as given by

$$q_{e_i}^{s} = (C_{o_i} - C_{e_i}^{s})V/m_{PAC} \quad (2.1)$$

where C_{o_i} is the initial or aqueous phase concentration of solute *i* in the control bottle (mg/L), $C_{e_i}^{s}$ is the sorption equilibrium aqueous phase concentration of solute *i* in the PAC bottle (mg/L), m_{PAC} is the mass of PAC (g) and the *V* is the aqueous phase volume (L).

The desorption equilibrium solid phase concentration of solute *i*, $q_{e_i}^{d}$ (mg/g), was estimated, as give by

$$q_{e_i}^{d} = \left(\left[C_{o_i} - C_{e_i}^{s}\right] - C_{e_i}^{d}\right) V/m_{PAC} \quad (2.2)$$

where $\left[C_{o_i} - C_{e_i}^{s}\right]$ represents the solid phase concentration of solute *i* on the PAC at sorption equilibrium, and $C_{e_i}^{d}$ is the desorption equilibrium aqueous phase concentration of solute *i* in the PAC bottle (mg/L).

The nonlinear Freundlich isotherm model, which describes multilayer sorption on heterogeneous surfaces with a limited number of sorption sites of non-uniform, variable distributions of energy, was assumed to represent the $q_{e_i}^{s}$ and $C_{e_i}^{s}$ data of each solute *i* as given by

$$q_{e_i}^{s} = K_{f_i}(C_{e_i}^{s})^{n_{f_i}} \quad (2.3)$$

where K_{f_i} ([mg/g][L/mg]^{n}) and n_{f_i} (dimensionless) are the sorption capacity and intensity, respectively [128], for a solute *i*, and were determined by fitting Equation (2.3) to the $q_{e_i}^{s}$ and $C_{e_i}^{s}$ data by nonlinear regression.

For multi-solute BTX sorption, the improved simplified ideal adsorption solution (ISIAS) model [129, 128] was assumed to provide representative $q_{e_i}^{s}$ when using the $C_{e_i}^{s}$ data of each solute *i* in the multi-solute system as given by

$$q_{e_i}^{s} = [K_f'^{\left(\frac{n_f'-1}{n_f'}\right)}\left[\frac{K_{f_i}}{a_i}C_{e_i}^{s\,n_{f_i}}\right]^{\frac{1}{n_f'}}[\sum_i^3(\frac{\frac{K_{f_i}}{a_i}}{K_f'}C_{e_i}^{s\,n_{f_i}})^{\frac{1}{n_f'}}]^{n_f'-1)}] \quad (2.4)$$

where K_{f_i} and n_{f_i} are the single-solute model parameters (from Equation (2.3)) for each solute *i*, $K_f' = \frac{\sum(\frac{K_{f_i}}{a_i})}{3}$ and $n_f' = \frac{\sum n_{f_i}}{3}$ are the average values of K_{f_i} and n_{f_i}, respectively, and a_i is the competition factor (dimensionless) for each solute *i* that are incorporated into the model and accounts for non-ideal competition between solutes for heterogeneous sorption sites. The a_i values were determined by fitting Equation (2.4) to the multi-solute $q_{e_i}^{s}$ and $C_{e_i}^{s}$ data by non-linear regression.

To determine the error associated with the Freundlich or ISIAS model fits the root mean square error (RMSE) were estimated for each non-linear regression, as given by

$$\text{RMSE} = \sqrt{\frac{\sum_{i=1}^{N}(q_{exp}-q_{model})^2}{N-P}} \quad (2.5)$$

where q_{exp} and q_{model} are the experimental (from Equation (2.1)) and model (from Equation (2.3) or Equation (2.4)) generated estimates of $q_{e_i}^{s}$, respectively, N is the sample size and P is the number of parameters fit by the regression. Smaller, relative to larger values, of the RMSE indicate the model better represents the data [130, 33].

2.2.3 Sorption and desorption equilibrium time

To evaluate the time to sorption equilibrium for benzene and toluene in single-solute systems, multiple triplicate sets of control and PAC serum bottles were prepared and filled with stock solutions of each solute at a low and high concentration (i.e., nominally 3 and 30 mg/L) so that each triplicate set could be sequentially sacrificially sub-sampled at successive timepoints (i.e., 0.5, 2, 4, 8, 24 and 48 hrs) (see Table A.2 for the experimental design). The serum bottles were then shaken, sub-sampled, extracted and analyzed as described above for the bottles prepared to estimate the sorption equilibrium aqueous phase concentrations of BTX (Section 2.2.2). The solid phase sorbed mass of benzene or toluene on the PAC were also estimated from the same serum bottle by decanting the remaining aqueous phase, adding 1 mL of DCM, and shaking the serum bottles as described above for those prepared to estimate the desorption equilibrium solid phase concentrations of BTX (Section

2.2.2). The DCM phase was then transferred to an autosampler vial and analyzed by GC as described in Section 2.2.2.

To estimate the time to desorption equilibrium for benzene and toluene in single-solute systems, a replicated set of serum bottles were prepared for aqueous and solid phase sub-sampling with two additional triplicate sets of bottles added. The serum bottles were prepared identically as described above for the sorption equilibrium times for benzene and toluene, although these serum bottles were left on the platform rotary shaker for 24 hours then left to stand for an additional 24 hours (48 hours total). The bottles were then decanted and refilled with fresh AGW (160 mL) and 0.5 mL of a 10% solution of sodium azide to prevent microbial growth and potential aerobic biodegradation. Serum bottles were then shaken, left to stand, sub-sampled, decanted, extracted and analyzed like the bottles prepared to estimate the sorption equilibrium times for benzene and toluene, although aqueous phase sacrificial sub-sampling took place over a longer total duration (i.e., 0.5, 2, 4, 8, 24, 72, 216 and 720 hrs) (see Table A.2 for the experimental design). The solid phase sorbed mass of benzene or toluene were then estimated from the same serum bottles and following the same methodology as described for the bottles prepared to estimate the sorption equilibrium times.

The mass of benzene or toluene per gram of PAC at each sorption sampling time, $q^{\mathrm{s}}_{\mathrm{t}_i}$ (mg/g), were indirectly estimated from Equation (2.1), where $q^{\mathrm{s}}_{\mathrm{e}_i}$ and $C^{\mathrm{s}}_{\mathrm{e}_i}$ were replaced with $q^{\mathrm{s}}_{\mathrm{t}_i}$ and $C^{\mathrm{s}}_{\mathrm{t}_i}$, respectively, representing the temporal sorption data. The mass of benzene or toluene per gram of PAC at each desorption sampling time, $q^{\mathrm{d}}_{\mathrm{t}_i}$ (mg/g), were indirectly estimated from Equation (2.2), where $q^{\mathrm{d}}_{\mathrm{e}_i}$, $C^{\mathrm{s}}_{\mathrm{e}_i}$ and $C^{\mathrm{d}}_{\mathrm{e}_i}$ were replaced with $q^{\mathrm{d}}_{\mathrm{t}_i}$, $C^{\mathrm{s}}_{\mathrm{t}_i}$ and $C^{\mathrm{d}}_{\mathrm{t}_i}$, respectively, representing the temporal desorption data.

2.2.4 Mass balance

Mass balance between the measured aqueous and solid phases was considered to account for changes in mass potentially resulting from (1) PAC removal during repeated aqueous phase decanting steps from the same serum bottle [41], (2) BTX volatilization from the aqueous phase during decanting or sampling or (3) inter bottle variations in C_{o_i} (between control and PAC bottles) or m_{PAC} (between replicated aqueous and solid phase bottles [pertaining to equilibrium capacity experiments] or sorption

and desorption bottles [pertaining to the equilibrium time experiments]). For sorption, the absolute mass lost or gained, $M^{\mathrm{s}}_{\mathrm{err}_i}$ (mg), was estimated for each solute *i* as given by

$$M^{\mathrm{s}}_{\mathrm{err}_i} = \left| \frac{M_{\mathrm{o}_i} - \left(M^{\mathrm{s}}_{\mathrm{aq}_i} + M^{\mathrm{s}}_{\mathrm{s}_i}\right)}{M_{\mathrm{o}_i}} \right| \times 100 \tag{2.6}$$

where $M^{\mathrm{s}}_{\mathrm{err}_i}$ was found from the difference between the mass of solute *i* in the aqueous, $M^{\mathrm{s}}_{\mathrm{aq}_i}$ (mg), and solid, $M^{\mathrm{s}}_{\mathrm{s}_i}$ (mg), phases relative to the total initial mass of solute *i* in the control bottle, M_{o_i} (mg), and averaged across all samples (of varying M_{o_i}, or time at constant M_{o_i}). For desorption, the absolute mass lost or gained, $M^{\mathrm{d}}_{\mathrm{err}_i}$ (mg), was estimated for each solute *i* as given by

$$M^{\mathrm{d}}_{\mathrm{err}_i} = \left| \frac{\left(M_{\mathrm{o}_i} - M^{\mathrm{s}}_{\mathrm{aq}_i}\right) - \left(M^{\mathrm{d}}_{\mathrm{aq}_i} + M^{\mathrm{s}}_{\mathrm{s}_i}\right)}{\left(M_{\mathrm{o}_i} - M^{\mathrm{s}}_{\mathrm{aq}_i}\right)} \right| \times 100 \tag{2.7}$$

where $M^{\mathrm{d}}_{\mathrm{err}_i}$ was found from the difference between the mass of solute *i* in the aqueous, $M^{\mathrm{d}}_{\mathrm{aq}_i}$ (mg), and solid, $M^{\mathrm{d}}_{\mathrm{s}_i}$ (mg), phases relative to the total initial mass of solute *i* sorbed to the PAC, $(M_{\mathrm{o}_i} - M^{\mathrm{s}}_{\mathrm{aq}_i})$ (mg), and averaged across all samples (of varying $(M_{\mathrm{o}_i} - M^{\mathrm{s}}_{\mathrm{aq}_i})$, or time at a constant $(M_{\mathrm{o}_i} - M^{\mathrm{s}}_{\mathrm{aq}_i})$).

2.3 Results and discussion

2.3.1 PAC characterization

Greyscale ESEM images of PAC are shown in Figure 2.1. Figure 2.1(a, b) shows a rough, irregular particle surface which is characteristic of thermally activated amorphous PAC [24], and Figure 2.1(c) shows a heterogeneous particle size distribution. On the surface of the particles shown in Figure 2.1(c), nine potential external pore openings were identified (locations indicted by red outlines), and the mean diameter was measured to be 0.8 ± 0.3 μm (i.e., *macropores* [≥ 0.05 μm]) [24, 25]. The mean particle diameter of 17 particles with clearly defined edges in Figure 2.1(c) were also measured and found to be 11.5 ± 4.4 μm (measurements shown in Figure A.1). The mean particle diameter is similar to the value determined by S. Hakimabadi (2023) using laser diffraction (Table 2.1) [123] and within the range of commercial PAC (i.e., between 15 to 25 μm [6]).

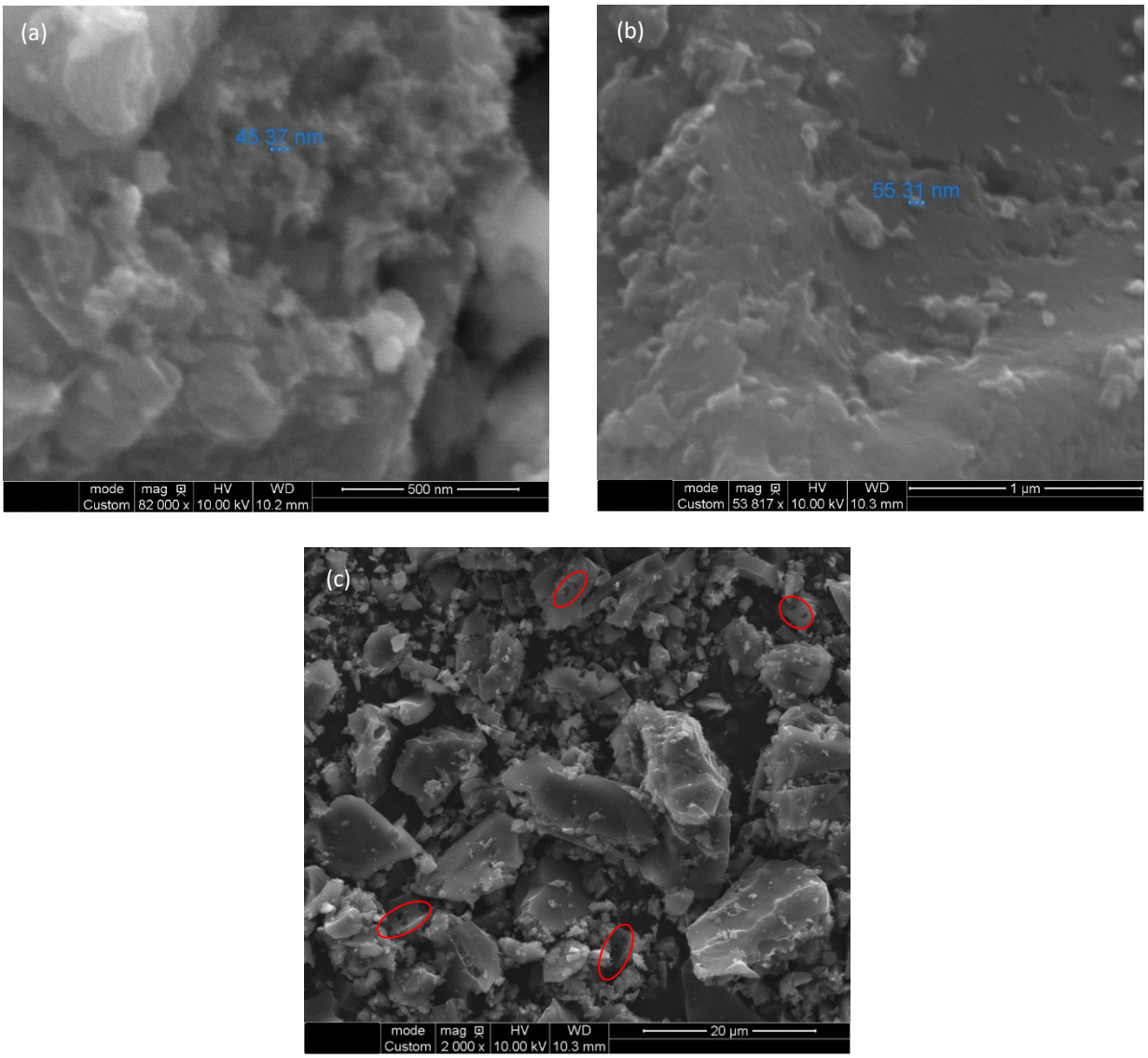

Figure 2.1: Environmental scanning electron microscopy (ESEM) generated images of WPC powdered activated carbon (PAC) at (a) 500 nm (82 000 ×), (b) 1 µm (53 817 ×) and (c) 20 µm (2 000 ×) scales (magnifications). Location of potential pores openings on the PAC particle surfaces in (c) are identified with red outlines.

2.3.2 Sorption and desorption

2.3.2.1 Single-solute sorption and desorption equilibrium capacities

The sorption and desorption equilibrium capacities of benzene, toluene and *o*-xylene in single-solute systems are shown on Figure 2.2(a-c) for six initial aqueous concentrations (C_{o_i}) (i.e., 0.4 ± 0.1, 2.6 ± 0.4, 5.8 ± 0.6, 8.8 ± 1.3, 11.6 ± 0.7 and 24.7 ± 2.2 mg/L [average between solutes]). For each solute, at low C_{o_i} sorption is dominated by non-linear partitioning to the solid phase ($q_{e_i}^{s}$). As C_{o_i} increases for a

constant PAC mass the change in $q_{e_i}^{s}$ decreases while the aqueous phase equilibrium concentration ($C_{e_i}^{s}$) increases due to the lower availability of sorption sites on the PAC [40, 131]. The Freundlich isotherm model, assuming multilayer sorption on the energetically heterogeneous PAC surface, was used to represent the sorption data (see Figure 2.2(a-c) for the Freundlich model fits to the single-solute data, and Table 2.2 for the best-fit K_{f_i} and n_{f_i} estimates of each solute and the RMSE of the regression). From Table 2.2, the magnitude of the K_{f_i} ([mg/g][L/mg]^{n}) decreased following X > T > B, whereas n_{f_i} (dimensionless) decreased in reverse order following B > T > X. The difference in the magnitude of the Freundlich model parameters for each solute suggest that *o*-xylene was sorbed the most and occupied the largest fraction of sorption sites at equilibrium, followed by toluene then benzene in the single-solute systems. The difference in sorption between solutes is attributed to the difference in the magnitude of chemical properties (e.g., high molecular weight and hydrophobicity generally yields higher sorption and lower aqueous phase concentrations at equilibrium) [28, 21, 16, 29] (see Table A.3 for the chemical properties of BTX).

For each solute, the single-solute desorption results for BTX (Figure 2.2(a-c)) show that desorption is concentration dependent, with more mass transfer occurring during single-step desorption for data corresponding to higher $q_{e_i}^{s}$ for a given C_{o_i} relative to lower $q_{e_i}^{s}$. Between solutes, less change in q_{e_i} occurred between sorption ($q_{e_i}^{s}$) and desorption ($q_{e_i}^{d}$) for *o*-xylene (Figure 2.2(c)) relative to toluene (Figure 2.2(b)) followed by benzene (Figure 2.2(a)). The smaller change in q_{e_i} for *o*-xylene indicates that a larger fraction of this solute did not readily desorb off the PAC and back into the aqueous phase after a single desorption step. Comparatively, benzene shows the largest change in q_{e_i} between the sorption and desorption processes for a given C_{o_i} which is attributed to the lower affinity of this solute to the PAC. As described for single-solute sorption, differences in the magnitude of desorption between solutes is due to the difference in chemical properties between solutes [28, 21, 16, 29] (see Table A.3 for the chemical properties of BTX).

For all solutes, the single-solute desorption data lie outside of the 95% confidence envelopes surrounding the single-solute sorption isotherms which suggests the desorption process may differ relative to sorption, indicative of hysteresis [32, 41, 132]. However, given the limited nature of the desorption data, representing only one desorption step as shown in Figure 2.2(a-c) (indicated by solid lines adjoining the sorption and corresponding desorption data for a given C_{o_i}, with arrows representing the direction of concentration change between processes), hysteresis has not been fully explored.

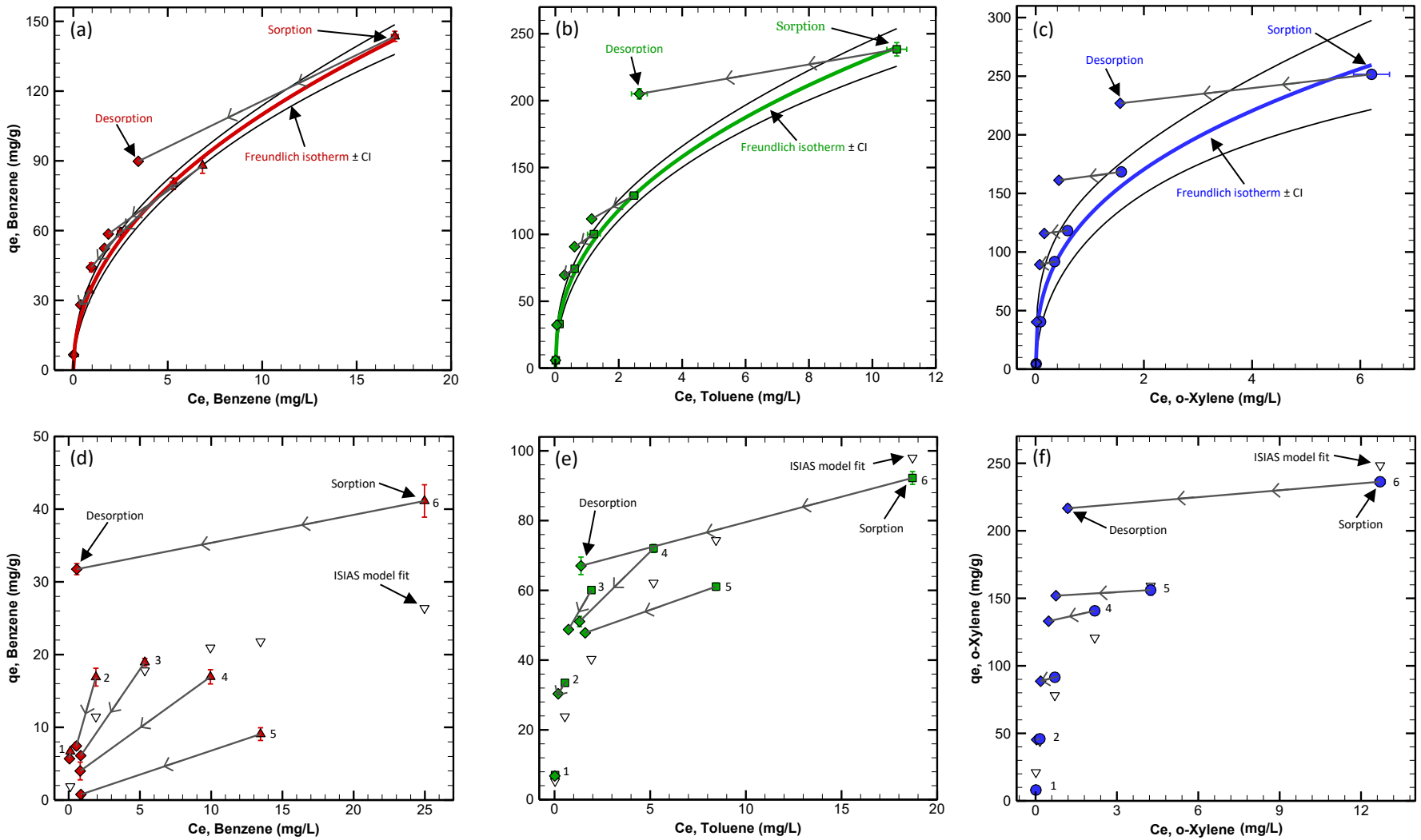

Figure 2.2: Sorption and single-step desorption equilibrium capacities for single-solute (a) benzene, (b) toluene and (c) *o*-xylene, and multi-solute (d) benzene, (e) toluene and (f) *o*-xylene in contact with WPC powdered activated carbon (PAC). C_e on the x axis represents the sorption or desorption equilibrium aqueous phase concentration (mg/L), and q_e on the y axis represents the sorption or desorption equilibrium solid phase concentration (mg/g). The multi-solute sorption data are numbered in order of increasing initial aqueous phase concentration for each solute (C_{o_i}), and the multi-solute sorption ($C_{e_i}^s$ and $q_{e_i}^s$) or desorption ($C_{e_i}^d$ and $q_{e_i}^d$) data for each solute are dependent on the sorption and desorption data of the other solutes, corresponding to the same C_{o_i}. Single- and multi-solute sorption equilibrium data are represented as filled (a, d) red triangles for benzene, (b, e) green squares for toluene, and (c, f) blue circles for *o*-xylene, and the single-step single- and multi-solute desorption equilibrium data are represented as filled diamonds with the same colours used to represent the sorption equilibrium data for each solute. Solid lines connect the single- or multi-solute sorption and desorption data, and arrows represent the direction of concentration change between processes. The standard deviation of triplicate measurements is represented as ± error bars on each data point. The single-solute Freundlich isotherms with 95% confidence envelopes (black solid bands) are represented as solid coloured lines, including (a) red for benzene, (b) green for toluene, and (c) blue for *o*-xylene. The multi-solute improved simplified ideal adsorption solution (ISIAS) model fit to the multi-solute $C_{e_i}^s$ and $q_{e_i}^s$ data for each solute, are represented as unfilled gradient symbols above or below each data point.

Table 2.2: Single-solute Freundlich (K_{f_i} and n_{f_i}) model parameters for benzene, toluene and *o*-xylene (BTX) and multi-solute ISIAS competition factors (a_i) for BTX in contact with WPC powdered activated carbon (PAC) ± confidence intervals (CI), and the root mean square error (RMSE) of the regressions.

	Benzene ± CI	**Toluene ± CI**	***o*-Xylene ± CI**
Single-solute			
K_{f_i} ([mg/g][L/mg]^n)	36.1 ± 3.8	88.2 ± 7.7	132 ± 20
n_{f_i}(-)	0.484 ± 0.045	0.421 ± 0.044	0.371 ± 0.099
RMSE	2.49	5.26	14.5
Multi-solute			
a_i (-)	1.42 ± 0.38	1.43 ± 0.16	1.08 ± 0.078
RMSE	12	12	12

The $M^{s}_{err_i}$ for single-solute benzene, toluene and *o*-xylene were 1.2 ± 1%, 9.6 ± 5.6% and 5.5 ± 3.3%, respectively, for sorption (Figure A.2(a)) and the $M^{d}_{err_i}$ for single-solute benzene, toluene and *o*-xylene were 5.5 ± 6.6%, 7.3 ± 5.4% and 2.6 ± 1.9%, respectively, for desorption (Figure A.2(b)), indicating minimal mass was lost or gained (see Table A.4 for the $M^{s}_{err_i}$ and $M^{d}_{err_i}$ estimates corresponding to each C_{o_i}). Additionally, the $q^{s}_{e_i}$ and $q^{d}_{e_i}$ indirectly estimated from Equation (2.1) and (2.2), respectively, using aqueous phase data versus the direct measurements from solid phase data are shown in a scatterplot in Figure A.3 (in addition to all data generated from the experiments described in Sections 2.2.2 and 2.2.3). The similarity between the indirect and direct estimates of $q^{s}_{e_i}$ and $q^{d}_{e_i}$ in Figure A.3 relative to a 1:1 line indicates that the indirect estimates are representative of the observed solid phase concentrations and are therefore considered reliable when used in determining the Freundlich model parameters.

2.3.2.2 Multi-solute sorption and desorption equilibrium capacities

The sorption and desorption equilibrium capacities of BTX in contact with WPC PAC in the multi-solute system are shown on Figure 2.2(d-f) for six C_{o_i} (i.e., 0.5 ± 0.03, 2.9 ± 0.2, 6.3 ± 0.5, 10.6 ± 0.8, 13.4 ± 1 and 26.2 ± 1.7 mg/L [average between solutes]). In Figure 2.2(d-f), the equilibrium concentrations ($C^{s}_{e_i}$ and $q^{s}_{e_i}$) for each solute are dependent on those of the other solutes in the multi-solute system. Like single-solute sorption (Figure 2.2(a-c)), Figure 2.2(d-f) shows that the magnitude of multi-solute sorption between the aqueous and solid phases followed X > T > B. Therefore, given that *o*-xylene occupied the largest fraction of sorption sites on the PAC this solute was preferentially

sorbed in the presence of toluene and benzene, and thereby limited the availability of sorption sites for the other less preferentially sorbed solutes (toluene, then benzene) [27, 128, 29]. The ISIAS equilibria model, assuming competitive sorption and accounting for non-ideal competition between solutes for heterogeneous sorption sites on the PAC, was used to represent the sorption data (see Figure 2.2(d-f) for the ISIAS model fits to the multi-solute data, and Table 2.2 for the best-fit a_i estimates of each solute and the RMSE of the regression). The ISIAS estimates of a_i confirm competitive sorption was more ideal for *o*-xylene (1.08 ± 0.078), relative to toluene (1.43 ± 0.16) and benzene (1.42 ± 0.38), as the value of a_i for *o*-xylene was closer to unity. For toluene and benzene, although sorption sites on the PAC were equally accessible to these solutes the values of a_i (i.e., more distant from 1) indicate multi-solute sorption was more distant from ideal competition when toluene and benzene were in the presence of *o*-xylene [129, 128]. Relative to the single-solute systems, less sorption occurred for each solute in the multi-solute system with the difference in the magnitude of sorption between systems and solutes following B > T > X. Therefore, the sorption capacity of all solutes was reduced in the multi-solute system when other competing solutes were present (at equivalent C_{o_i} [1:1:1]), and a greater number of sorption sites were unavailable to the solutes of lower single-solute sorption capacities (i.e., benzene then toluene) relative to those of greater single-solute sorption capacity (i.e., *o*-xylene) [29, 33]. Similar to the single-solute systems (Section 2.3.2.1), variation in chemical properties between solutes controls the multi-solute competitive sorption dynamics [28, 21, 16, 29] (see Table A.3 for the chemical properties of BTX).

The multi-solute desorption results for BTX are also shown on Figure 2.2(d-f), which represent a single desorption step (indicated by solid lines adjoining the sorption and corresponding desorption data for a given C_{o_i}, with arrows representing the direction of concentration change between processes). Similar to the single-solute systems (Figure 2.2(a-c)) described in Section 2.3.2.1, the magnitude of multi-solute desorption followed B > T > X due to the differences in chemical properties between solutes [28, 21, 16, 29] (see Table A.3 for the chemical properties of BTX). Additionally, as was described for the single-solute desorption data (Section 2.3.2.1), the multi-solute desorption data are dissimilar relative to multi-solute sorption data for each solute (i.e., q_{e_i} and C_{e_i}, for sorption and the corresponding desorption data for a given C_{o_i}, differ between processes) which is indicative of hysteresis. Although, given the multi-solute desorption data represent a single desorption step hysteresis has not been fully explored.

The $M_{\mathrm{err}_i}^{\mathrm{s}}$ for benzene, toluene and *o*-xylene were 4.1 ± 2%, 8.3 ± 2.2% and 8.7 ± 4.5%, respectively, for sorption (Figure A.2(c)) and the $M_{\mathrm{err}_i}^{\mathrm{d}}$ for benzene, toluene and *o*-xylene were 29.6 ± 37.7%, 12.2 ± 14.6% and 7.1 ± 5.5%, respectively, for desorption (Figure A.2(d)) (see Table A.4 for the $M_{\mathrm{err}_i}^{\mathrm{s}}$ and $M_{\mathrm{err}_i}^{\mathrm{d}}$ estimates corresponding to each C_{o_i}). Like the single-solute system (Section 2.3.2.1), these data show minimal mass was lost or gained for all solutes during multi-solute sorption. Although, during multi-solute desorption the $M_{\mathrm{err}_i}^{\mathrm{d}}$ increased for benzene and toluene, with the greatest increase for benzene. At the lower C_{o_i} for benzene (0.5, 3, 6.6 and 11 mg/L) and toluene (0.5, 2.6, 5.8 and 9.7 mg/L) the average $M_{\mathrm{err}_i}^{\mathrm{d}}$ for benzene (5.6 ± 6.9%) and toluene (5.3 ± 2.1%) were low. However, at the higher C_{o_i} for benzene (14 and 27.5 mg/L) and toluene (12.2 and 24.3 mg/L) the average $M_{\mathrm{err}_i}^{\mathrm{d}}$ for benzene (77.5 ± 7.9%) and toluene (26.1 ± 21.8%) increased considerably (see Table A.4 for the stepwise M_{err_i} estimates) which resulted in the elevated average $M_{\mathrm{err}_i}^{\mathrm{d}}$ for benzene and toluene and high standard deviations. Given that more desorption to the aqueous phase occurs at higher C_{o_i} for all solutes, combined with the higher volatilities (Table A.3) and the lower fractions of benzene and toluene sorbed to the PAC at equilibrium relative to *o*-xylene in the multi-solute system, the higher average values of $M_{\mathrm{err}_i}^{\mathrm{d}}$ for benzene and toluene during desorption may be attributed to losses from volatilization (during sampling and multiple decanting steps, as described in Sections 2.2.2). The $q_{\mathrm{e}_i}^{\mathrm{s}}$ and $q_{\mathrm{e}_i}^{\mathrm{d}}$ indirectly estimated from Equation (2.1) and (2.2), respectively, using aqueous phase data versus the direct measurements from solid phase data are shown on the same scatterplot as the single-solute data described in Section 2.3.2.1 (Figure A.3) (in addition to the data generated from the experiments described in Section 2.2.3). Figure A.3 collectively shows that the indirect and direct estimates of $q_{\mathrm{e}_i}^{\mathrm{s}}$ and $q_{\mathrm{e}_i}^{\mathrm{d}}$ are similar (as described in Section 2.3.2.1), and therefore the indirect estimates are considered reliable when used in determining the ISIAS model parameters. For the $q_{\mathrm{e}_i}^{\mathrm{d}}$ estimates for benzene and toluene corresponding to the higher $M_{\mathrm{err}_i}^{\mathrm{d}}$, as described above, these data are positioned sightly further from the 1:1 line in Figure A.3, as indicated by the data with red outlines.

2.3.2.3 Single-solute sorption and desorption equilibrium time

Temporal sorption and desorption data for single-solute benzene and toluene are shown on Figure 2.3(a, b) at high (i.e., 31.1 ± 5.5 mg/L [average between solutes]) and low (i.e., 3.5 ± 1.3 mg/L [average between solutes]) C_{o_i} over 0.5 to 48 hours (2 days). Figure 2.3(a, b) shows that sorption equilibrium was reached quickly for benzene and toluene at both C_{o_i} given that the solid phase concentrations ($q_{\mathrm{t}_i}^{\mathrm{s}}$) were relatively constant after 0.5 hours (characteristic behaviour of benzene and toluene in contact with PAC [130, 33, 133]). Figure 2.3(a, b) shows the desorption data from 0.5 to 24 hours (1 day), which was extended from 72 hours (3 days) to 720 hours (30 days) in Figure 2.3(c) for benzene and Figure 2.3(d) for toluene. After 0.5 hours of desorption (in Figure 2.3(a, b)) no substantial change in the solid phase concentrations ($q_{\mathrm{t}_i}^{\mathrm{d}}$) were observed for either solute, suggesting that sufficient time was provided for desorption equilibrium. Equilibrium conditions after 0.5 hours of benzene or toluene sorption or desorption is also supported by the consistency between the temporal data (corresponding to both C_{o_i}) and the single-solute sorption isotherms and desorption equilibrium data from Figure 2.2(a, b) (shown in Figure A.4(a, b)). Given that sufficient time was provided for desorption equilibrium, diffusion limitations during desorption [32] do not appear to be the cause of the suspected single-solute hysteretic behaviour identified in Figure 2.2(a, b). Instead, the suspected hysteretic behaviour is likely be attributed to a time irrelevant process (e.g., permanent chemical bonding [38] or pore deformation [41, 42]), as described in Section 1.1.1.

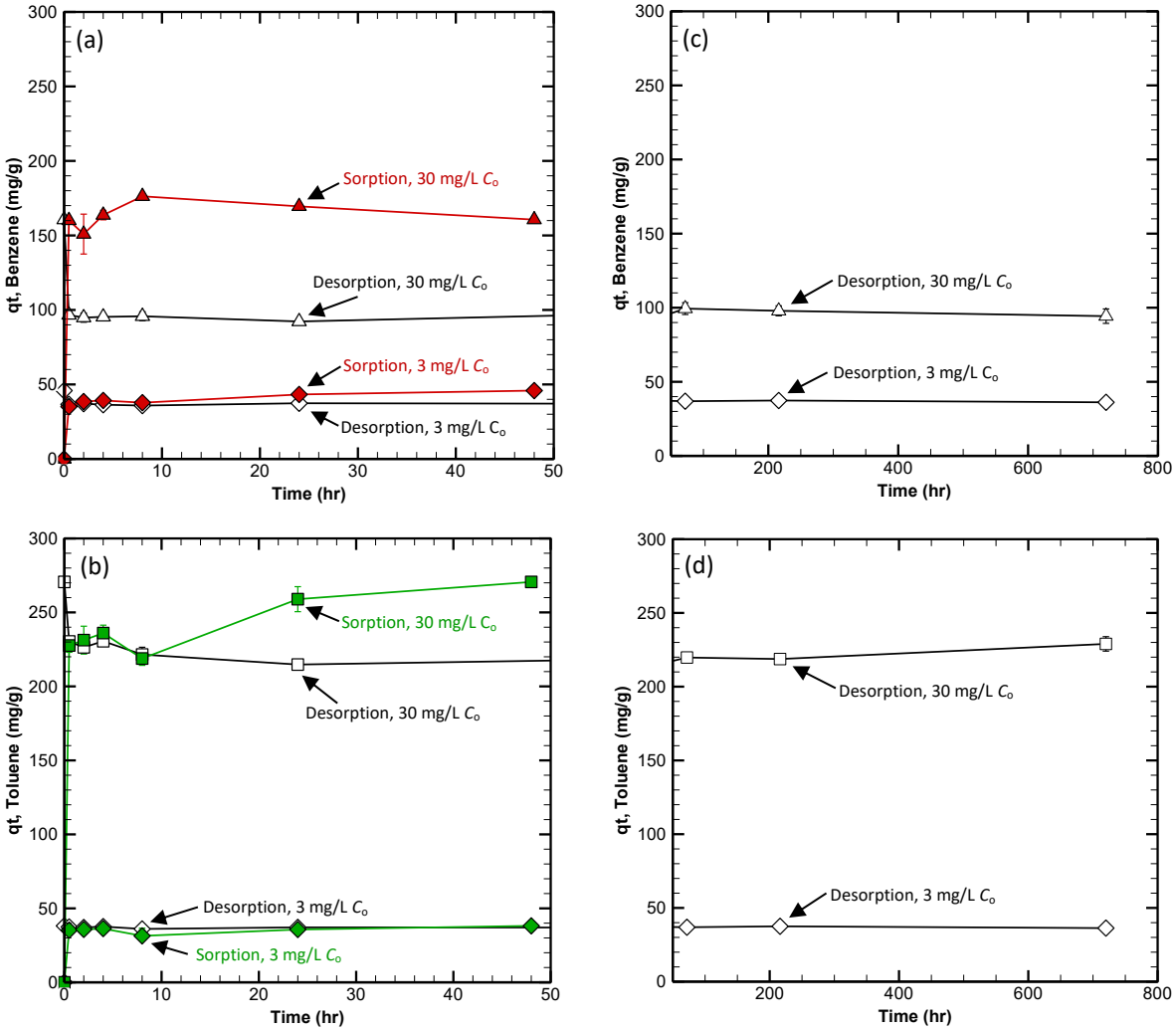

Figure 2.3: Temporal sorption and desorption data for single-solute (a) benzene and (b) toluene over 48 hours (2 days) and at 3 and 30 mg/L initial aqueous phase concentrations (C_{o_i}). The solid phase concentration for sorption and desorption and for both solutes is denoted as q_t (mg/g) versus time (hours). At the C_{o_i} of 30 mg/L the sorption data is represented as filled (a) red triangles for benzene and (b) green squares for toluene, and the desorption data is represented as the same unfilled shapes as the sorption data. At the C_{o_i} of 5 mg/L the sorption data is represented as filled (a) red diamonds for benzene and (b) green diamonds for toluene, and the desorption data is represented as unfilled diamonds. Desorption data from 72 hours (3 days) to 720 hours (30 days) is shown for (c) benzene and (d) toluene. The standard deviation of triplicate measurements is represented as ± error bars.

As expected, the percentage of total mass sorbed or desorbed within the system once equilibrium conditions were reached was dependent on the solute and C_{o_i}. For instance, between solutes at the lower average C_{o_i} (3.5 ± 1.3 mg/L), 51% of benzene mass and 86% of toluene mass was

sorbed (i.e., T > B), while at the higher average C_{o_i} (31.1 ± 5.5 mg/L) 22% of benzene mass and 49% of toluene mass were sorbed (i.e., T > B). In contrast, 26% of benzene mass and 7% of toluene mass were desorbed at the lower average C_{o_i} (i.e., B > T), and 45% of benzene mass and 25% of toluene mass was desorbed at the higher average C_{o_i} (i.e., B > T). These results are consistent with the isotherms for each single solute which showed toluene sorbed more than benzene, and that benzene desorbed more than toluene. Additionally, for both solutes more partitioning occurred at lower average C_{o_i} (with less desorption), and less partitioning occurred at the higher average C_{o_i} (with higher desorption) due to a reduction in available sorption sites [40, 131].

The $M_{err_i}^{d}$ for benzene and toluene were 7.2 ± 5.8% and 7.5 ± 2.7%, respectively, at the low average C_{o_i} between solutes (Figure A.5(a)) and the $M_{err_i}^{d}$ for benzene and toluene were 12.6 ± 5.5% and 15.2 ± 0.6%, respectively, at the high average C_{o_i} between solutes (Figure A.5(b)), showing mass lost or gained slightly increased with increased C_{o_i} for both solutes (see Table A.4 for the $M_{err_i}^{d}$ estimates corresponding to each C_{o_i}). As described for the multi-solute equilibrium data in Section 2.3.2.2, the slight increase in $M_{err_i}^{d}$ with increasing C_{o_i} may be related to aqueous phase volatilization of benzene and toluene given that more desorption to the aqueous phase occurs at higher C_{o_i}. The $q_{t_i}^{d}$ for benzene and toluene indirectly estimated from Equation (2.2) using aqueous phase temporal data versus the direct measurements from solid phase temporal data are shown on the same scatterplot as the single- and multi-solute data described in Section 2.3.2.1 and 2.3.2.2 (Figure A.3). Figure A.3 indicates that collectively the indirect and direct estimates of $q_{t_i}^{d}$ are similar (as described in Sections 2.3.2.1 and 2.3.2.2) and are considered reliable. As expected from the slightly higher $M_{err_i}^{d}$ estimates corresponding to the high C_{o_i}, the $q_{t_i}^{d}$ for benzene and toluene are positioned slightly further from the 1:1 line relative to the rest of the single- and multi-solute sorption and desorption q_{e_i} or q_{t_i} data as indicated by the data in Figure A.3 with yellow outlines.

2.4 Conclusion

The WPC PAC used in this research has been characterized previously in the literature for pH_{pzc}, particle diameter, surface area and pore volume [124, 122, 123]. The SEM images generated as part of the research shows a heterogeneous size distribution between PAC particles with an average measured diameter of 11.5 ± 4.4 µm, which is similar to the value of 13.1 µm reported by S.

Hakimabadi (2023) using a more accurate measurement methodology (i.e., laser diffraction) [123]. SEM images also reveal that the PAC surface is rough and irregular with potential macropore openings identified (0.83 ± 0.27 μm).

Also consistent with the literature [21, 29, 28, 33], the single-solute (benzene, toluene or *o*-xylene) and multi-solute (BTX) sorption equilibrium data for each solute in contact with the PAC showed partitioning followed X > T > B. Whereas the single- and multi-solute single-step desorption equilibrium data showed the magnitude of desorption followed B > T > X. Between the single- or multi-solute sorption and single-step desorption processes the desorption equilibrium data do not align with the sorption equilibrium data, with the single-solute desorption data lying outside of the 95% confidence envelopes surrounding the single-solute sorption isotherms. The difference in sorption and desorption data is indicative of hysteresis, which suggests the sorption and desorption processes are dissimilar; however, given the limited nature of these data, with only one desorption step, hysteresis was not fully explored. Between the single- and multi-solute sorption systems the sorption equilibrium capacity of all solutes were reduced relative to the single-solute systems due to competitive sorption and a reduction in the number of available sorption sites for all solutes. Collectively, the sorption and desorption equilibrium behaviour described here are due to the differences in the chemical properties between solutes, which is well documented in the literature for AC systems exposed to BTX [28, 21, 16, 29].

Single-solute Freundlich and multi-solute ISIAS sorption equilibria best-fit model parameters were generated by non-linear regression of the sorption equilibrium data. The isotherm model parameters were generated for the purpose of applying them to more complex AC amended systems with bioactivity (discussed in Chapter 3), and to determine if the ideal isotherms are representative of the sorption equilibrium behaviour in bioactive systems (addressing Q1 [Section 1.2]). The best-fit single-solute Freundlich isotherm model parameter for benzene, toluene and *o*-xylene in contact with WPC PAC were 36.1 ± 3.8, 88.2 ± 7.7 and 132 ± 20 for K_{f_i} ([mg/g][L/mg]^n) and 0.484 ± 0.045, 0.421 ± 0.044 and 0.371 ± 0.099 for n_{f_i} (-), respectively. The multi-solute ISIAS model competition factors (a_i) for benzene, toluene and *o*-xylene in contact with WPC PAC were 1.42 ± 0.38, 1.43 ± 0.16 and 1.08 ± 0.08, respectively.

Temporal sorption and desorption data up to 48 or 24 hours, respectively, showed the time to reach sorption and desorption equilibrium for single-solute benzene and toluene at initial

concentrations of 3 and 30 mg/L was rapid (≤ 0.5 hours). The desorption process was also extended up to 720 hours to observe if diffusion limitations during desorption may be the cause of the suspected single-solute hysteretic behaviour in the isotherm systems; however, no additional desorption occurred after 0.5 hours and therefore sufficient time was deemed to be provided for desorption equilibrium. The suspected hysteretic behaviour is more likely attributed to a time irrelevant process (e.g., permanent chemical bonding or pore deformation). The equilibrated sorption and desorption temporal data from ≥ 0.5 hours to 48 hours for sorption and up to 720 hours for desorption were additionally compared to the single-solute isotherms and equilibrium desorption data for benzene and toluene. The consistency in equilibrium partitioning between the equilibrium capacity and time experiments indicates that the temporal data represents equilibrium conditions after 0.5 hours of contact between benzene or toluene and the PAC at both initial concentrations.

Mass balance between single- and multi-solute sorption ($M^{\mathrm{s}}_{\mathrm{err}_i}$) and desorption ($M^{\mathrm{d}}_{\mathrm{err}_i}$) estimates of q_{e_i} or q_{t_i} indirectly estimated from aqueous phase data or observed directly from solid phase data was carried out to determine the degree of error or mass lost or gained from the systems (e.g., from PAC particle removal during decanting steps, BTX volatilization, or inter-bottle variation in C_{o_i} or the m_{PAC}). Mass balance between the indirect aqueous phase derived estimates and the directly measurement solid phase estimates of single- and multi-solute $q^{\mathrm{s}}_{\mathrm{e}_i}$ also provided an indication of the reliability associated with the indirectly derived $q^{\mathrm{s}}_{\mathrm{e}_i}$ estimates used to generate the Freundlich and ISIAS model parameters. For most single- and multi-solute systems the average $M^{\mathrm{s}}_{\mathrm{err}_i}$ and $M^{\mathrm{d}}_{\mathrm{err}_i}$ for all C_{o_i} was low (< 10%), showing minimal mass was lost or gained. However, the $M^{\mathrm{d}}_{\mathrm{err}_i}$ estimates (from $q^{\mathrm{d}}_{\mathrm{e}_i}$) for benzene (77.5 ± 7.9%) and toluene (26.1 ± 21.8%) in the multi-solute system and the $M^{\mathrm{d}}_{\mathrm{err}_i}$ estimates (from $q^{\mathrm{d}}_{\mathrm{t}_i}$) for benzene (12.6 ± 5.5%) and toluene (15.2 ± 0.6%) in the single-solute systems, all corresponding to high C_{o_i}, were elevated. The elevated $M^{\mathrm{d}}_{\mathrm{err}_i}$ for benzene and toluene may be attributed to volatilization during sampling or decanting steps given more mass resides in the aqueous phase at higher C_{o_i} and volatility follows B > T > X. Collectively, between all equilibrium and temporal systems the single- and multi-solute indirect and direct estimates of q_{e_i} or q_{t_i} were similar to a 1:1 line, which confirms that the indirect estimates of q_{e_i} used in determining the Freundlich and ISIAS model parameters are reliable.

Chapter 3

Anaerobic biodegradation of benzene, toluene and *o*-xylene in the presence of powdered activated carbon particulate amendments – Microcosm study

3.1 Introduction

Prior microcosm investigations in the literature have shown that the anaerobic biodegradation of petroleum hydrocarbons (PHCs) such as naphthalene are stimulated in the presence of powdered activated carbon (PAC) [115, 111]. Additionally, the presence of PAC has been found to reduce the lag time prior to the initiation of methanogenesis and is associated with increased methane (CH_4) yields [117]. Genera enriched in PAC amended microcosms were also linked to direct interspecies electron transfer (DIET), including *Geobacter* [115, 117, 111] and *Methanosarcina* [115, 117].

This research specifically investigates the biodegradation behaviour of other PHCs, including benzene, toluene and *o*-xylene (BTX), in simplified single-solute (toluene-only) and more complex multi-solute (BTX) PAC amended microcosms. Microcosms were assembled and monitored under sulfate reducing and methanogenic conditions in addition to sulfate enhanced or electron acceptor (EA) amended conditions and tracked for 1 year. First, the single-solute (toluene only) and multi-solute (BTX) activated carbon (AC) sorption isotherms generated under ideal conditions (in Chapter 2) were compared to the microcosm data to determine if the isotherms are representative of the sorption behaviour in bioactive systems. Differences in geochemical parameters (e.g., sulfate, sulfide, CH_4 and total inorganic carbon [TIC]), and quantitative polymerase chain reaction (qPCR) and next generation sequencing (NGS) data were then compared between microcosms with and without AC to determine if the presence of AC influences the microbial community dynamics during PHC biodegradation. Finally, high-resolution aqueous and solid phase PHC data were used to investigate if the AC sorption capacity is regenerated during biodegradation, and if the PHC biodegradation rate is enhanced in the presence of AC. Collectively, the assembled microcosm dataset was used to assess the long-term behaviour of AC sorption and anaerobic biodegradation, and if the AC enhances or influence the biodegradation of toluene or BTX relative to systems without AC.

3.2 Materials and methods

The same benzene, toluene and *o*-xylene used in the sorption and desorption experiments (Section 2.2) were used as pure phase additions to an artificial groundwater (AGW) for the microcosms.

The AGW solution for the microcosms consisted of the same salts dissolved in Milli-Q water as described in Section 2.2 for the sorption and desorption experiments (and at same concentrations as listed in Table A.1), apart from potassium hydrogen phosphate (Sigma-Aldrich, St. Louis, MO, USA) used in place of monosodium phosphate. Higher concentrations of both potassium hydrogen phosphate and potassium dihydrogen phosphate, as buffering agents, were also used relative to the AGW for the sorption and desorption experiments. Additionally, a trace mineral stock solution was added to the microcosm AGW, and was comprised of boric acid, sodium molybdate dihydrate, cobalt (II) chloride hexahydrate, aluminum sulfate octadecahydrate, manganese (II) chloride tetrahydrate (Sigma-Aldrich, St. Louis, MO, USA), zinc chloride, nickel (II) chloride hexahydrate, copper (II) chloride dihydrate and sodium selenite (Alfa Aesar, Fisher Scientific, Ottawa, ON, CA). Other additions to the microcosm AGW solution consisted of a sodium bicarbonate (EMD Millipore Corporation, Darmstadt, HE, DE) stock solution, and an amorphous ferrous sulfide (FeS) stock solution as a reducing agent. The FeS stock solution was comprised of ammonium iron (II) sulfate hexahydrate (Sigma-Aldrich, St. Louis, MO, USA) and sodium sulfide nonahydrate (Alfa Aesar, Fisher Scientific, Ottawa, ON, CA). The concentration of each chemical in the AGW used for the microcosms is listed in Appendix B.1.

Specific microcosms were amended with sodium azide (Section 2.2) and mercuric chloride (Sigma-Aldrich, St. Louis, MO, USA) as biocides, and/or resazurin (Abcam, UK) as a colour indicator for the detection of oxygen (the resazurin recipe is provided in Appendix B.1).

For liquid-liquid and solid-liquid benzene, toluene and *o*-xylene extractions the same dichloromethane (DCM) containing internal standards of *m*-fluorotoluene and 2-fluorobiphenyl, as described in Section 2.2, was used.

The PAC (WPC, [Calgon Carbon Corporation, Pittsburgh, PA, USA]) used in this investigation is thoroughly described in Chapter 2.

Aquifer material was sourced from Canadian Forces Base (CFB) Borden, Ontario, Canada in the sand pit research area, which has been used for hydrogeologic research since the 1970's [134]. The Borden aquifer is unconfined and comprised of primarily horizontal discontinuous lenses of well sorted medium-

to fine-grained and silty fine-grained sand with infrequent layers of silt, silty-clay and coarse sand, representing microscale local heterogeneities in hydraulic conductivity [135, 136]. The aquifer deposits are glaciolacustrine in origin and grade into a clayey and sandy silt aquitard located approximately 9 m below ground surface (bgs) [137, 135, 134]. The groundwater table is encountered approximately 1 m bgs with seasonal oscillations, and flow occurs in the north to northeast direction at approximately 9 cm/day [137, 135, 138, 136]. Geochemistry is dominated by calcium (Ca^{2+}) (50 to 100 mg/L) and alkalinity (as HCO_3^-) (100 to 300 mg/L), in addition to sulfate (SO_4^{2-}) (10 to 30 mg/L) [135, 138, 139]. A detailed summary of the hydrogeologic and geochemical characteristics of the Borden aquifer are listed in Table B.1.

Prior microbiological studies confirm the microbial populations within the Borden aquifer are predominantly aerobic and heterotrophic in the upper region of the aquifer near the water table, and have the potential for anaerobic reduction by microaerophilic or facultative microorganisms with depth and in the presence of electron acceptors [140, 141, 142]. Field and laboratory experiments reported in the literature have demonstrated indigenous Borden microorganisms are capable of BTEX biodegradation under both aerobic [143, 144, 145, 146] and anaerobic (e.g., nitrate reducing [143, 147, 148], and iron reducing [148]) conditions. Microbiological characterization studies also indicate that the microbial populations are variable, sparse and spatially heterogeneous within small areas of the Borden aquifer, and communities are locally and metabolically distinct from one another and often limited by dissolved organic carbon, nutrients (e.g., nitrogen) or oxygen [140, 141].

For this research, aquifer material was collected from the middle of three longitudinally adjoined and hydraulically isolated sheet-piled experimental gates (each gate is 21 m long, 7.5 m wide and 7 m bgs) within the sand pit research area. The experimental gates are positioned parallel to the average annual ambient groundwater flow direction, which allows for groundwater to enter from the open, upgradient end and exit from the downgradient end, equipped with an open funnel-and-gate system for groundwater treatment. Within the middle experimental gate two separate PHC injections occurred within the upgradient end to create a dissolved phase PHC plume. PHC injections occurred from 1.25 to 2.25 m bgs, and both PHC injection solutions were comprised of 100 L of pure phase: isopentane (25 L [15.4 kg]), 2,2,4-trimethylpentane (20 L [13.8 kg]), hexane (20 L [13.2 kg]), cyclopentane 10 L [7.5 kg]), octane (10 L [7 kg]), pentane (10 L [6.3 kg]), benzene (2.5 L [2.2 kg]), toluene (1.25 L [1.1 kg]), naphthalene (0.8 kg), *o*-xylene (0.5 L [0.5 kg]) and 1,2,4-trimethylbenzene (0.4 L [0.4 kg]). Within the middle experimental gate, Borden aquifer material was collected within an anaerobic zone downgradient of the PHC injection location

and known to contain sulfate reducing bacteria (SRB) [149, 150]. Within the anaerobic zone, aquifer material was collected at 9 locations from 1.5 to 4.5 m bgs within 17 polyvinyl chloride (PVC) core liners (Geoprobe, Salina, KS, USA) 126 days after the second PHC source was established. The collected cores were stored in the dark at 4ºC for 274 and 232 days prior to use in the single-solute (toluene only) and multi-solute (BTX) microcosm experiments, respectively. Prior to use each core was cut into 0.3-meter sections to allow for transport and handling within an anaerobic chamber (Coy, Grass Lake, MI, USA) (N_2/H_2 atmosphere). The open ends of each core were immediately capped and transported into the anaerobic chamber, and approximately 2.5 cm of aquifer material on all severed core ends were discarded to remove aquifer material exposed to oxygen during cutting. The remainder of the aquifer material from each 0.3-meter section of the core liners were then loaded into 0.6 × 0.91-meter sterile polypropylene autoclave bags (VWR, Padnor, PA, USA), and all aquifer material (51.6 kg) was thoroughly manually homogenized in preparation for laboratory experimental use. See Figure B.1 for a schematic of the location of core extractions from the middle experimental research gate in the sandpit research area, and images of the 17 cores collected.

3.2.1 Microcosm design

To address research Questions 1 to 4 (Section 1.2) a series of microcosms were assembled. Microcosm types included: (1) abiotic killed controls (KC) and (2) KC with PAC (KC+PAC) and PHCs to account for potential abiotic mass losses and sorption to BS and PAC; (3) bioactive starved controls (SC) to account for potential biodegradation of other substrates in the absence of PHCs; (4) bioactive positive controls with low sulfate concentrations (i.e., 10 to 20 mg/L SO_4^{2-}, representative of background concentrations in the Borden aquifer [Table B.1]) (BA-PC) and (5) BA-PC with additional electron acceptor (EA) amendments (i.e., 138 to 275 mg/L SO_4^{2-}) (BA-PC+EA) and PHCs to account for the biodegradation of PHCs in the absence of PAC; and (6) bioactive microcosms with PAC and low sulfate concentrations (i.e., 10 to 20 mg/L SO_4^{2-}) (BA+PAC) and (7) BA+PAC with additional EA amendments (i.e., 138 to 275 mg/L SO_4^{2-}) (BA+PAC+EA) and PHCs to account for the biodegradation of PHCs in the presence of PAC. Each microcosm type was prepared in a simplified single-solute (toluene-only) system and a more complex multi-solute (BTX) system. See Table B.2 for the experimental details, and amendments to each microcosm type.

Microcosms were set up in triplicate in 250 mL clear glass screw top serum bottles (Pierce Chemical Company, Rockford, IL, USA) in an anaerobic chamber. All single- and multi-solute microcosms were loaded with 81.5 g of anaerobic Borden sand (BS) (68.5 g dry mass) containing indigenous microorganisms from the cores described in Section 3.2 (Figure B.1). For the KC and KC+PAC microcosms, following BS addition the bottles were additionally autoclaved three times, for 15 minutes on three consecutive days at 121ºC. All microcosms intended to be amended with or without PAC were then loaded with 155 or 175 mL, respectively, of anaerobic AGW. All microcosm bottles were then sealed with Mininert valve screw caps lined with Teflon septa (Precision Sampling Corporation, Baton Rouge, LA., USA), leaving 30 mL of headspace for gas collection (for bottles with 175 mL of AGW). Once sealed, the KC and KC+PAC microcosms were injected with 2.5 mL of mercuric chloride (2.71 g/ 100 mL) and 0.45 mL of sodium azide (5 g/ 100 mL) through the opened Mininert valves using a disposable plastic syringe (Air-Tite, Virginia Beach, VA, USA) equipped with a luer-lock fitting and assembled to a 22-gauge needle (Exel Int., USA). In one replicate non-PAC microcosm bottle within each triplicate set, 0.1 mL of resazurin was also injected through open Mininert valves. Microcosms without PAC were selected for resazurin amendments given resazurin sorbs to PAC, and only 1 replicate was amended to control against a potential reaction with any of the bottle contents. All microcosm bottles were left to incubate for 2 weeks to allow any residual oxygen to deplete, and to ensure the contents were anaerobic.

Following the incubation period (Day 0), a series of amendments were made using sterile glass microliter syringes (Hamilton, Reno, NV, USA) for toluene or BTX, or disposable plastic syringes equipped with luer-lock fittings and attached to 22-gauge needles for sulfate. Electron donor (BTX) and EA (sulfate) amendments included: 4 µL of pure phase toluene into all single-solute microcosms (except the SC microcosms) to achieve a target aqueous concentration of 20 mg/L, 12 µL of a 1:1:1 stock solution of pure phase BTX into all multi-solute microcosms (except the SC microcosms) to achieve an aqueous concentration of 20 mg/L per solute (or 60 mg/L total BTX), or 0.77 mL of the sodium sulfate (Sigma Aldrich, St. Louis, MO, USA) stock solution (listed in Appendix B.1) into all single- and multi-solute BA-PC+EA or BA+PAC+EA microcosms to achieve a target aqueous concentration of 275 mg/L. Once the amendments were added, all microcosms were vigorously shaken by hand and left undisturbed for 2 days. On Day 2 an anaerobic slurry of 15 mg of PAC and 20 mL of AGW was injected into the microcosm bottles intended to be amended with PAC. The PAC slurry allowed for a precise loading of the PAC particulates into microcosm bottles, relative to a dry addition of the PAC. The 20 mL PAC slurry increased aqueous

volume from 155 to 175 mL in the PAC amended microcosms, which was the same aqueous volume as all other microcosms without PAC. The ratio of PAC mass in the PAC amended microcosm bottles to the volume of toluene or BTX was determined based on predicted partitioning behaviour between the aqueous and the gas [151], BS [152] or PAC phases (using the partitioning coefficients listed in Tables B.3 and Table 2.2), while allowing the for detection of each solute in all phases (see Table B.3 for the estimated single-solute [toluene-only] or multi-solute [BTX] partitioning between phases, based on the solute injection volume(s) and PAC mass). Sealed microcosm bottles were then vigorously shaken by-hand to homogenize the bottle contents and left undisturbed for an additional 2 days to allow for toluene or BTX equilibrium partitioning.

All microcosms were stored undisturbed in the anaerobic chamber. Microcosms were positioned horizontally with the aqueous phase covering the septa to minimize gas diffusion through the Mininert valve caps and were stored under non-transparent plastic sheets to limit direct light exposure. Over the 1-year monitoring period, reamendments of the electron donors (i.e., toluene and BTX, using the same volume additions and target aqueous concentrations listed above) and/or EA (i.e., 0.39 or 0.77 mL of the sulfate stock solution to achieve target aqueous concentrations of 138 or 275 mg/L, respectively) were made to microcosms when toluene or BTX and sulfate were depleted (i.e., $\leq$ 1 mg/L).

3.2.2 Sampling

For the single- or multi-solute microcosm experiments 114 bottles were set up and subdivided into 38 sets of triplicates that were further subdivided for each microcosm type (listed in Table B.2). The multiple sets of triplicate microcosm bottles facilitated a repetitive and sacrificial sampling procedure over 1-year. For the KC, KC+PAC and SC microcosms, two triplicate sets of microcosms were set-up, with the first triplicate set repetitively sampled for the aqueous phase during five separate sampling events prior to being sacrificed on the sixth sampling event for aqueous and solid phase sampling. During the seventh to thirteenth sampling events for the KC, KC+PAC and SC microcosms the second triplicate set of microcosm bottles were repetitively sampled prior to being sacrificed on the fourteenth sampling event. Each sampling event took place over 1-month intervals, except for the first and second sampling events which took place on Day 2 (following the initial toluene or BTX dose, and prior to PAC amendments) and Day 7-8 (following PAC amendments). For the BA-PC, BA+PAC, BA-PC+EA and BA+PAC+EA microcosms, 8 triplicate sets of microcosms were set-up. All microcosm sets were repetitively sampled for the aqueous phase once

prior to being sacrificed during the next sampling event for aqueous and solid phase sampling, followed by a new microcosm set being sampled during the next repetitive sampling event. The sampling intervals for the BA-PC and BA+PAC microcosms were the same as those described for the KC, KC+PAC and SC microcosms. However, for the BA-PC+EA and BA+PAC+EA microcosms the last 2 sets of triplicate bottles were sampled for the aqueous and solid phases as separate replicates during each sampling event and the sampling events occurred at higher sampling frequencies (i.e., sampling intervals were 4 to 17 days) to estimate zero-order biodegradation rates during these sampling times. Additionally, the first and second sampling events for the BA-PC, BA+PAC, BA-PC+EA and BA+PAC+EA microcosms were sacrificial to measure the change in concentration attributed to the expected partitioning of toluene or BTX between all phase before (i.e., sampling Day 2) relative to after the PAC addition (i.e., sampling Day 7-8 between the single- and multi-solute experiments) (Tables B.3). The repetitive and sacrificial sampling design allowed for: (1) the minimization of substantial toluene or BTX partitioning between phases, potentially resulting from large aqueous or gaseous volume removal from the same microcosm bottles during multiple sampling events over the 1-year monitoring period; and (2) solid phase sample collection during each sacrificial sampling event. For all single- and multi-solute microcosm types 14 to 16 timepoints were collected over the 1-year monitoring period, and Figure 3.1 provides a detailed schematic of the sampling timeline associated with each microcosm type described above.

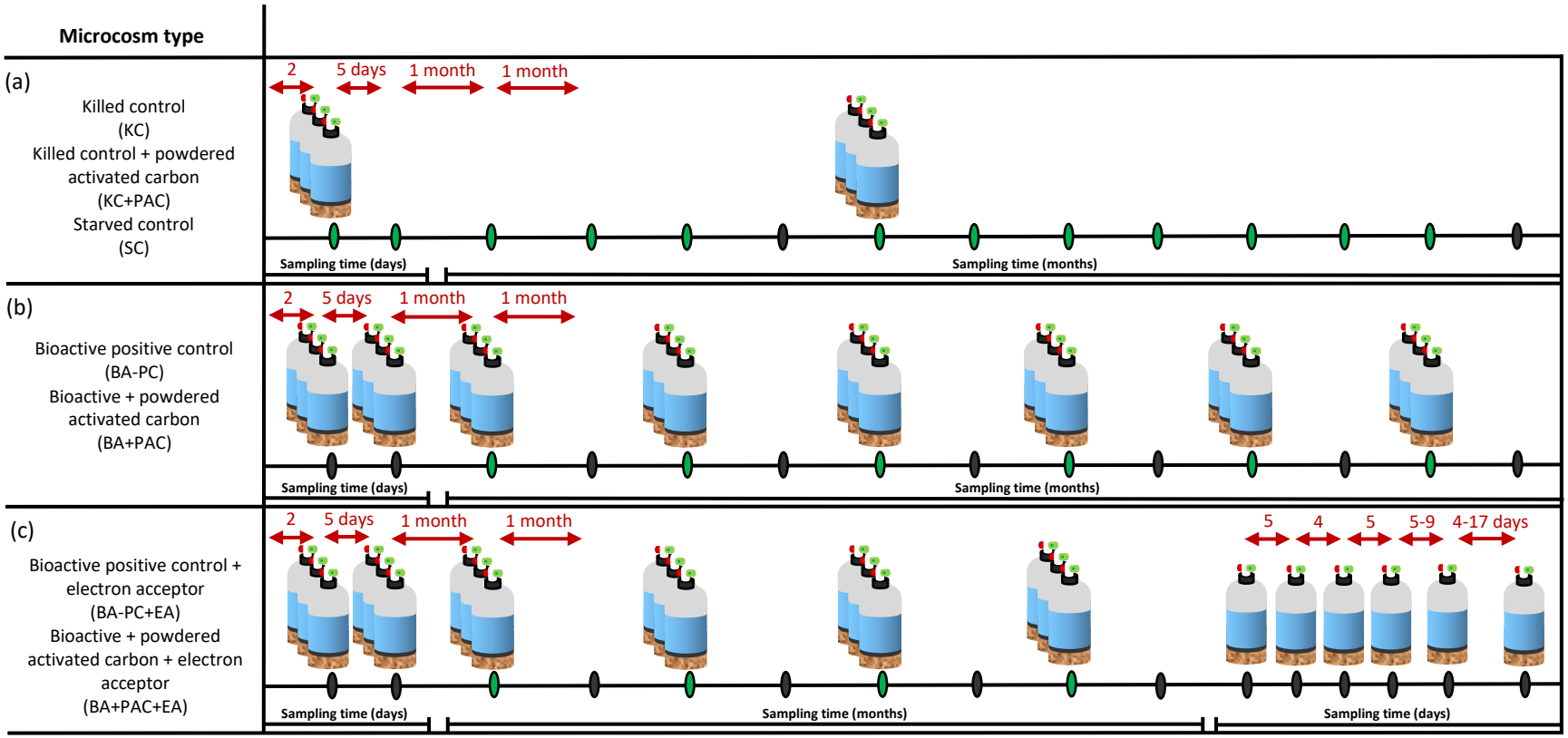

Figure 3.1: Repetitive and sacrificial sampling design for the single-solute (toluene-only) or multi-solute (benzene, toluene and *o*-xylene [BTX]) (a) KC, KC+PAC and SC; (b) BA-PC and BA+PAC; and (c) BA-PC+EA and BA+PAC+EA microcosms. Repetitive and sacrificial sampling intervals are represented as green and black hash marks, respectively, on the horizontal axes. The microcosm bottle locations on the horizontal axes represent when a new bottle or triplicate set was sampled following a prior sacrificial sampling event.

All microcosms were sampled anaerobically within the anaerobic chamber, and 1 day prior to sampling the triplicate sets of microcosm bottles designated to be sampled were manually shaken by hand for several minutes to homogenize the bottle contents. During each repetitive sampling event aqueous phase sample collection included: 2 mL for BTX; 1 mL for sulfate, dissolved oxygen (DO), pH and the oxidation reduction potential (ORP); and 1 mL for sulfide. During each sacrificial sampling event, aqueous phase sample collection included: 2 mL for BTX; 5 mL for sulfate, DO, pH and ORP; 10 mL for sulfide; and 3.5 mL for dissolved inorganic carbon (DIC). Additionally, DIC was sampled during the first repetitive sampling event for the KC, KC+PAC and SC microcosms to establish baseline conditions for this parameter. During both repetitive and sacrificial sampling 5 mL of the gas phase were sampled for methane (CH_4) and carbon dioxide (CO_2). During sacrificial sampling events the solid phase (BS and PAC) were analyzed for BTX, and on the last sacrificial sampling events the solid phase was split in half for BTX and deoxyribonucleic acid (DNA) analysis. Several sub-samples for DNA were also collected from the homogenized BS (described in Section 3.2) prior to addition to the microcosm bottles to characterize the microbial community before exposure to the experimental conditions (i.e., background).

Aqueous samples for BTX were collected in 4 mL glass screw top vials preloaded with 1 mL of dichloromethane (DCM) containing internal standards of *m*-fluorotoluene and 2-fluorobiphenyl (25 mg/L) for liquid-liquid extractions. Following the collection of all sacrificial aqueous samples, solid samples for BTX were collected by decanting the remaining AGW in the microcosms (~150 mL) with a 100 mL glass syringe with a luer-lock fitting (Cadence Science, Cranston, RI, USA) attached to an 18-gauge stainless steel needle (Ace Glass, Vineland, NJ, USA) while ensuring minimal disturbance to the solids. Once decanted, the BS and PAC were saturated with 20 mL of DCM (containing *m*-fluorotoluene and 2-fluorobiphenyl [25 mg/L]) for liquid-solid extractions (10 mL of DCM was used during the last sacrificial sampling event given the soil sample was reduced by half, as described above), and the bottles were then vigorously shaken by-hand for several minutes and vented. Aqueous sample vials and microcosm bottles containing the solid phase samples were sealed with Teflon lined silicon septa screw caps, and the extraction and analytical methodologies used are described in Section 2.2.2.

Samples for sulfate, DO, pH and ORP were syringe filtered (0.45 µm, Basix nylon filter [Pall Corporation, Ann Arbor, MI, USA]) into 5 mL disposable ion chromatography (IC) autosampler vials (Thermo Scientific, Waltham, MA, USA), and diluted with Milli-Q water for a final sample volume of 5 mL (if necessary).

Samples for sulfide were collected in 10 mL disposable syringes with luer-lock fittings attached to 22-gauge disposable needles. Prior to analysis the needle tips were plugged with rubber stoppers to preserve the sample. In preparation of analysis, the rubber stoppers were removed, and the sulfide samples were syringe filtered (0.45 µm, nylon filter) into 10 mL glass cuvettes, and diluted with Milli-Q water for a final sample volume of 10 mL (if necessary).

Samples for DIC were collected in 4 mL glass screw top vials preloaded with 1.4% of a mercuric chloride stock solution (2.71 g/ 100 mL) and sealed with butyl rubber lined caps. Turbid samples were syringe filtered (0.45 µm, nylon filter) prior to analysis (if necessary).

Gas samples for CH_4 and CO_2 were collected in 10 mL gas tight sampling syringes with luer-lock fittings (Sigma Aldrich, St. Louis, MO, USA), equipped with a 1-way polycarbonate stopcock and 22-gauge disposable needle. Prior to analysis the stopcock was closed to retain the gas sample and the syringe was stored in a water bath to limit sample loss. For analysis, gas samples were diluted with purified helium (if necessary).

Solid phase samples for DNA were collected in 50 mL plastic screw top tubes (Eppendorf, Hamburg, DE), and immediately stored at -80ºC and shipped to the BioZone Centre for Applied Bioscience and Bioengineering (University of Toronto) for molecular analyses. A portion of the soil sample (0.25 g) was extracted for genomic DNA using the MagAttract PowerSoil Pro DNA Kit (Qiagen, Germantown, MD, USA) according to the manufacturer's procedure.

3.2.3 Analyses

DO, pH and ORP samples were measured anaerobically in the anaerobic chamber using an Oakton double junction epoxy ORP probe, an Oakton pHTestr® 50S Spear-Tip Waterproof Pocket Tester (Cole-Palmer, Vernon Hills, IL, USA) and a Thermo Scientific Orion 083005MD polarographic DO probe (Themo Fischer Scientific, Waltham, MA, USA). Following DO, pH and ORP analysis the remainder of the samples were transported out of the anaerobic chamber and analyzed aerobically.

Sulfate samples were analyzed on a Dionex ICS-1100 IC equipped with a Dionex AS-DV Autosampler (Dionex Corporation, Sunnyvale, CA, USA). Twenty-five (25) µL of sample was injected onto a AG4A-SC (4 × 50mm) guard column and AS4A-SC (4 × 250mm) column, and operating conditions, included: 1.8 mM Na_2CO_3/1.7 mM $NaHCO_3$ eluent concentration, 2.0 mL/min flow rate, ambient temperature, suppressed conductivity detection using a Dionex Anion Self-Regenerating Suppressor

(Dionex ADRS 600 4mm) in AutoSuppression Recycle Mode, and 32 mA applied current (method detection limit [MDL] of 0.1 mg/L).

Sulfide samples were analyzed on a Hach DR 1900 portable spectrophotometer (Hach, Loveland, CO, USA) using the methylene blue method (Hach method 8131) [153] (detection limit: 5 to 800 µg/L).

DIC samples were analyzed on a Dohrmann DC-190 (Rosemount Analytical Inc., Shakopee, MN, USA). Two hundred (200) µL of sample was manually injected into the instrument at a flow rate of 200 ± 5 cm^3/min and acidified with 20% H_3PO_4 (Sigma-Aldrich, St. Louis, MO, USA) at ambient temperature. The sample was then loaded on a catalyst bed and held at an elevated temperature until the carbon in the sample was converted to CO_2 through combustion. The evolved CO_2 was measured by a non-dispersive infrared detector (NDIR).

Gas samples were analyzed on a Shimadzu GC-2014 gas chromatograph for greenhouse gas analysis (Shimadzu, Kyoto, JPN) by injecting 5 mL of sample into the sample loop. The sample was passed on a 1.5 m × 3.2 mm HayeSep N 80/100 mesh stainless steel precolumn that traps and backflushes water vapour. The retained gas was then passed on a 5.0 m × 3.2 mm HayeSep D 80/100 mesh stainless steel column to separate CO_2 and CH_4, and the gas was measured by a thermal conductivity detector (TCD) or flame ionization detector (FID) with a methanizer. Operating conditions included: 80ºC oven temperature, 100ºC split temperature, 250ºC FID temperature (flame: air 50 kPa, Hydrogen 66 kPa), 100ºC TCD temperature (TCD 125mA, TCD Reference 57.5 kPa), 380ºC methanizer temperature, 80ºC valve temperature, and 14-minute run time (detection limit: 0.005 mg/L CH_4 and 0.1 mg/L CO_2).

DNA samples were assayed by quantitative polymerase chain reaction (qPCR) using the primer pairs listed in Table B.4 and reaction conditions summarized by Toth et al. 2021 [154]. Reaction mixtures (20 µL) contained 500 nM of each forward and reverse primer, 2 µL of template DNA, 10 µL 2 × SsoFast EvaGreen Supermix (Bio-Rad Laboratories, Hercules, CA, USA) and UltraPure DNase/Rnase-Free Distilled Water (Invitrogen, Carlsbad, CA, USA). Serial dilutions of plasmids containing corresponding targeted gene fragments were used to generate standard curves. Each qPCR reaction was performed in duplicate on a Bio-Rad CFX96 real time PCR machine. Thermal cycling conditions included: 98°C initial denaturation step temperature (2 min), 40 cycles of denaturation (5 sec, 98°C) and annealing/extension (10 sec, see Table B.4 for annealing temperature), and 65 to 95°C melt curve analysis temperature with an increase of 0.5°C every 10 sec. qPCR results were analyzed using Bio-Rad CFX Manager software [154]. The amplification efficiency for each qPCR run batch ranged from 93.6% to 101.5% Bac, 87.2% to

104.1% Arch, 93.7% to 99.8% ORM2, 92.8% to 98.2% Dsp, and 86.3% to 94.3% Pep with R^2 values of > 0.996.

16S ribosomal ribonucleic acid (rRNA) gene amplicon sequencing (MiSeq 300PE, paired-end) was carried out at Genome Quebec Innovation Centre at McGill University. Amplicon sequence reads were generated using modified staggered end primers to improve sequencing quality. Primers included 926F (AAACTYAAAKGAATWGRCGG) and 1392R (ACGGGCGGTGWGTRC) (V6-V8), where 0 to 3 random bases were inserted between the primer and Illumina adaptor sequences. Read processing and sequencing analysis was completed in QIIME 2 version 2022.2. Raw reads were trimmed of primer sequences and staggered ends, truncated and denoised using the DADA2 pipeline within QIIME 2 [155]. Quality filtered forward (260 bp) and reverse (240 bp) reads were merged with a maximum of 2 expected errors in the overlap region. Chimeric sequences and sequences < 400 nucleotides in length were removed. The final amplicon sequence variants (ASVs) were classified against the SSU SILVA 132 database trained on the targeted 16S rRNA gene region. Taxonomy of the 100 most abundant ASV were screened against the NCBI and RDP databases to ensure correct classification [154].

3.2.4 Mass balance estimates

The mass of total inorganic carbon (TIC) (M_{TIC}), was estimated from the sum of the mass of aqueous DIC ($M_{\mathrm{DIC_{(aq)}}}$) and gaseous CO_2 ($M_{\mathrm{CO_{2(g)}}}$) (mg) as defined by

$$M_{\mathrm{TIC}} = M_{\mathrm{DIC_{(aq)}}} + M_{\mathrm{CO_{2(g)}}} = (C_{\mathrm{DIC_{(aq)}}} \times V_{(\mathrm{aq})}) + (C_{\mathrm{CO_{2(g)}}} \times V_{(\mathrm{g})} \times \frac{\mathrm{M.W._C}}{\mathrm{M.W._{CO_2}}}) \quad (3.1)$$

where $C_{\mathrm{DIC_{(aq)}}}$ is the aqueous phase concentration of DIC (mg/L), $V_{(\mathrm{aq})}$ is the aqueous phase volume (L), $C_{\mathrm{CO_{2(g)}}}$ is the gas phase concentration of CO_2 (mg/L), $V_{(\mathrm{g})}$ is the gas phase volume (L), and $\mathrm{MW._C}$ and $\mathrm{MW._{CO_2}}$ are the molecular weights of carbon (12.01) and CO_2 (44.01), respectively, (g/mol).

The total mass of benzene, toluene or *o*-xylene was estimated from the sum of the mass of each solute *i* in all phases ($M_{i_{\mathrm{T}}}$), including gas ($M_{i_{(\mathrm{g})}}$), aqueous ($M_{i_{(\mathrm{aq})}}$) and solid ($M_{i_{(\mathrm{s})}}$) which is comprised of both BS ($M_{i_{(\mathrm{BS})}}$) and PAC ($M_{i_{(\mathrm{PAC})}}$) (mg), as defined by,

$$M_{i_T} = M_{i_{(g)}} + M_{i_{(aq)}} + M_{i_{(BS)}} + M_{i_{(PAC)}} = (K_{h_i} \times C_{i_{(aq)}} \times V_{(g)}) + (C_{i_{(aq)}} \times V_{(aq)}) + (K_{d_i} \times C_{i_{(aq)}} \times m_{BS}) + (M_{i_{(s)}} - M_{i_{(BS)}}) \quad (3.2)$$

where, K_{h_i} is the Henry's constant of solute *i* (dimensionless), $C_{i_{(aq)}}$ is the aqueous phase concentration of solute *i* (mg/L), K_{d_i} is the soil-water partitioning coefficient of solute *i* (L/kg), and m_{BS} is the mass of BS (g). K_{d_i} was estimated as defined below,

$$\log K_{oc_i} = \log K_{ow_i} - 0.21 \quad (3.3)$$

$$K_{d_i} = K_{oc_i} \times f_{oc} \quad (3.4)$$

where, K_{oc_i} is the organic carbon partitioning coefficient defining equilibrium conditions between solute *i* and the BS (cm^3/g), K_{ow_i} is the octanol water portioning coefficient of solute *i* in water (dimensionless) (Table A.3) and f_{oc} is the fraction of organic carbon in the BS (dimensionless) (2.4×10^{-4} [156]) (refer to Table B.1 for the f_{oc} of the BS [135], and Table B.3 for the K_{h_i} [151] and estimated K_{d_i} [152] values for each solute in contact with the gas phase or BS, respectively). From Equation (3.1) and (3.2) $C_{i_{(aq)}}$ and $M_{i_{(s)}}$ were directly measured, $M_{i_{(g)}}$ and $M_{i_{(BS)}}$ were estimated from the K_{h_i} and K_{d_i}, respectively, and $M_{i_{(PAC)}}$ was estimated from mass balance between the solid phases (i.e., $M_{i_{(PAC)}} = M_{i_{(s)}} - M_{i_{(BS)}}$).

3.3 Results and discussion

Fifteen (15) days prior to the initiation of the single- and multi-solute microcosm experiments the homogenized BS loaded into the microcosm bottles was analyzed for the same 11 compounds present in the PHC injection solution described in Section 3.2 (in addition to qPCR and NGS analysis) to determine background conditions and the initial mass of PHCs within the microcosm bottles prior to toluene or BTX additions. Using the same sampling and analytical methods described in Sections 3.2.2 and 3.2.3, respectively, all PHCs were ≤ MDL (i.e., ≤ 52 µg/L for naphthalene and ≤ 5.5 µg/L for all other compounds). The absence of PHCs detected in the BS indicates that any residual mass within the cores (emanating from the PHC plume, located directly upgradient of the locations of core collection [described in Section 3.2, and details shown in Figure B.1]) were either absent from the cores at the time of

collection or, if present, were biodegraded by the indigenous microbial population present within the aquifer material.

Microcosm sampling and amendments occurred over a monitoring period of 366 and 372 days for the single- and multi-solute systems, respectively (see Table B.5 for the sampling and amendments days for each microcosm type and experiment). Toluene-only or BTX and sulfate as electron donors or an electron acceptor, respectively, were amended into designated microcosm types one to several times throughout the monitoring period, resulting in variations in the cumulative target masses as shown in Table 3.1. From Table 3.1 the single-solute microcosms received toluene only, and the multi-solute microcosms received BTX, as described in Section 3.2.1; however, following the first dosing event the multi-solute microcosms only received additional amendments of toluene and *o*-xylene (not benzene). Additionally, the total cumulative mass of sulfate was lower in the KC, KC+PAC, SC, BA-PC and BA+PAC microcosms relative to the EA amended BA-PC+EA and BA+PAC+EA microcosms, with the lower concentration range (10-20 mg/L SO_4^{2-}) being representative of the background sulfate concentration in the groundwater within the Borden aquifer (Table B.1) (i.e., location of BS collection as described in Section 3.2). The low target sulfate concentration was initially present in all microcosms, including the EA amended, given the source of sulfate was from the sodium sulfate in the AGW described in Section 3.2 (Appendix B.1). Additional sulfate was amended into the BA-PC+EA and BA+PAC+EA microcosms (using the stock solution listed in Appendix B.1) to achieve a target aqueous concentration of 275 mg/L during sulfate dosing events. Although, during the last sulfate dosing event on Day 269 and 310 (prior to high frequency sampling as described in Section 3.2.2) for the single- and multi-solute microcosms, respectively, a lower target sulfate concentration of 138 mg/L was used. In the single-solute BA-PC+EA and BA+PAC+EA microcosms, a higher cumulative mass of sulfate was present relative to the multi-solute microcosms due to one additional unintended sulfate amendment to the target concentration of 275 mg/L on Day 149. See Table B.2 for the target concentrations of toluene, BTX and sulfate for each microcosm type.

Table 3.1: Cumulative target mass and number of amendments of toluene-only, BTX or sulfate added to each single- and multi-solute microcosm type over a 1-year monitoring period.

		Cumulative Mass (mg) (number of amendments) [1]					
		Benzene	Toluene	*o*-Xylene	Sulfate		
	Microcosm				Background (10-20 mg/L)	EA amended (275 mg/L)	EA amended (138 mg/L)
Single-solute (toluene-only)	KC, KC+PAC, SC, BA-PC or BA+PAC		3.5 (1)		3.5 (1)		
	BA-PC+EA		20.8 (6)		3.5 (1)	144.4 (3)	24.2 (1)
	BA+PAC+EA		24.3 (7)		3.5 (1)	144.4 (3)	24.2 (1)
Multi-solute (BTX)	KC, KC+PAC, SC, BA-PC or BA+PAC	3.5 (1)	3.5 (1)	3.5 (1)	1.8 (1)		
	BA-PC+EA	3.5 (1)	10.4 (3)	10.6 (3)	1.8 (1)	96.3 (2)	24.2 (1)
	BA+PAC+EA	3.5 (1)	10.4 (3)	10.6 (3)	1.8 (1)	96.3 (2)	24.2 (1)

Notes:
1. The volume of toluene, BTX and sulfate added to each microcosm is described in section 3.2.1 and the target concentrations are shown in Table B.2.

Periodically the microcosms were monitored to ensure any bottles under pressure (i.e., from CO_2 or CH_4 formation during anaerobic biodegradation) were degassed. Degassing of microcosm bottles was accomplished by inserting a 20 mL glass syringe with a luer-lock fitting attached to a 22-gauge stainless steel needle into the open Mininert valves to allow any gas under pressure to passively release into the syringe barrel (the volume and concentration of any collected gas were to be measured and recorded for mass balance considerations). Degassing events took place on: Day 63 (BTX system), Day 170 (toluene-only system) and Day 205 (toluene-only system); however, no gas under high pressure was removed from the microcosm bottles.

Throughout the duration of the microcosm experiments some Mininert valve caps were replaced due to damage, including cracks and/or leakages. Cracked Mininert valve caps were replaced for select microcosms, including BA-PC-set 7 (two replicates) and BA+PAC-set 8 (one replicate) on Day 170 (toluene-only system). Leakages were primarily noticed from the KC or KC+PAC microcosms due to an abiotic degradation reaction between the biocides (discussed in Section 3.2.1) and the septa of the Mininert valves. Due to observed aqueous phase bottle leakages (i.e., KC-set 4 [one replicate] on Day 99 [toluene-only system]) or noted reductions in the aqueous phase volumes within bottles, the KC and KC+PAC microcosms were positioned vertically upright, as opposed to horizontal as described in Section 3.2.1, from Day 63 and Day 105 onwards for the single- and multi-solute microcosm experiments, respectively.

3.3.1 Isotherm comparison

The directly measured aqueous and corresponding solid phase concentrations of toluene (corrected to include only the $M_{i_{(\mathrm{PAC})}}$ per gram of PAC) within the single-solute KC+PAC, BA+PAC and BA+PAC+EA microcosms at each sacrificial event (shown in Figure 3.1) were plotted in Figure 3.2(a) relative to the single-solute sorption isotherm for toluene determined in Chapter 2 (using the single-solute Freundlich model parameters for toluene [K_{f_i} and n_{f_i}] [Table 2.2]). Figure 3.2(a) shows all microcosm data lie outside and below of the 95% confidence envelope surrounding the sorption isotherm for toluene, indicating that the Freundlich isotherm model overestimates the solid phase concentration of toluene within the PAC amended single-solute microcosms. The directly measured solid phase concentrations of benzene, toluene and *o*-xylene (corrected to include only the $M_{i_{(\mathrm{PAC})}}$ per gram of PAC) within the multi-solute KC+PAC, BA+PAC and BA+PAC+EA microcosms at each sacrificial event (shown in Figure 3.1) were plotted in Figure 3.2(b) against the predicted equilibrium solid phases concentrations of each solute generated from the improved simplified ideal adsorption solution (ISIAS) model (using the single-solute Freundlich model parameters for each solute [K_{f_i} and n_{f_i}] and the multi-solute ISIAS competition factors for each solute [a_i] [Table 2.2]), and displayed against a 1:1 line (representing a perfect correlation between measured and predicted values). Figure 3.2(b) shows that the magnitude of difference between the data points for each solute and the 1:1 line varies following X > T > B indicating that the multi-solute model better predicts the solid phase concentration of benzene, followed by toluene and then *o*-xylene. Additionally, between solutes most of the multi-solute data resides above the 1:1 line indicating that, like the single-solute Freundlich isotherm for toluene, the multi-solute ISIAS model overestimates the magnitude of BTX sorption in the PAC amended multi-solute microcosms.

Difference between the single-solute Freundlich isotherm or multi-solute ISIAS model predictions of the equilibrium solid phase concentrations of toluene or BTX, respectively, relative to the directly measured solid phase concentrations from the single- and multi-solute KC+PAC, BA+PAC and BA+PAC+EA microcosms may be related to several factors. First, the microcosm systems may require longer times for toluene or BTX to equilibrate between phases relative to the isotherm systems (0.5 hours, as described in Section 2.3.2.3). Differences in toluene or BTX equilibrium times between the isotherm and microcosm systems may be related to the variation in mixing conditions, where the isotherm vials were continually shaken for 1 day prior to equilibrium sampling (as described in Section 2.2.2). Whereas the microcosm bottles were left undisturbed between sampling episodes and manually shaken for only several minutes following electron donor and electron acceptor amendments or prior to a sampling event

(as described in Sections 3.2.1 and 3.2.2). In Figure 3.2(a) the microcosm data with red outlines correspond to sampling events 5 days following a toluene dosing event, and given these data reside furthest from the sorption isotherm for toluene (relative to all other data corresponding to sampling events > 5 days following a toluene dosing event) they may represent the additional time required for partitioning within the single-solute microcosms. Similarly, in Figure 3.2(b) the microcosm data for BTX with red outlines correspond to sampling events within 6 to 64 days following a TX dosing event, and given these data reside furthest from 1:1 line (relative to all other data corresponding to sampling events > 9 to 64 days), these data may represent the range in additional time required for partitioning within the multi-solute microcosms. For the remainder of the single- and multi-solute microcosm data residing closer but remaining below the sorption isotherm for toluene in Figure 3.2(a) or above the 1:1 line for BTX in Figure 3.2(b), sorption may have been influenced by differences in the solution matrix chemistry (e.g., increasing the ionic strength may reduce the availability of surface area on the PAC or block pores due to the formation of agglomerations [157]) between the AGW used for the microcosms (0.020 M [KC+PAC and BA+PAC microcosms] to 0.028 M [BA+PAC+EA microcosms] ionic strength [Appendix B.1]) relative to the simplified AGW solution used for the isotherm experiments (0.0068 M ionic strength [Table A.1]). The reduced solid phase toluene or BTX concentrations measured in microcosm systems relative to Freundlich or ISIAS predicted solid phase concentrations may also be associated with interferences (e.g., competition) with other sorbing components within the microcosm systems that were absent from the isotherm systems (e.g., metabolites generated during anaerobic BTX biodegradation [60], methane generated as a by-product of methanogenesis [158, 159], or other sources of organic carbon in the BS). Finally, if a microbial biofilm layer surrounds the PAC particles this is also expected to reduce the sorption capacity of PAC within the KC+PAC, BA+PAC or BA+PAC+EA microcosms relative to the isotherm systems, with the magnitude of reduction dependent on the biofilm layer thickness (where increased thickness increases the diffusional resistance of solutes [37]) and the microbial activity within the biofilm layer (where microbes can potentially biodegrading solute(s) prior to sorption, or inhibit sorption due to the secretion and pore filling of extracellular polymeric substances [EPS] [110, 107, 13, 108]). For the multi-solute system specifically (Figure 3.2(b)), *o*-xylene was likely most influenced by the factors limiting sorption within the microcosms, followed by toluene and then benzene, given that the magnitude of multi-solute sorption is highest for *o*-xylene (followed by toluene and then benzene) as discussed in the Section 2.3.2.2.

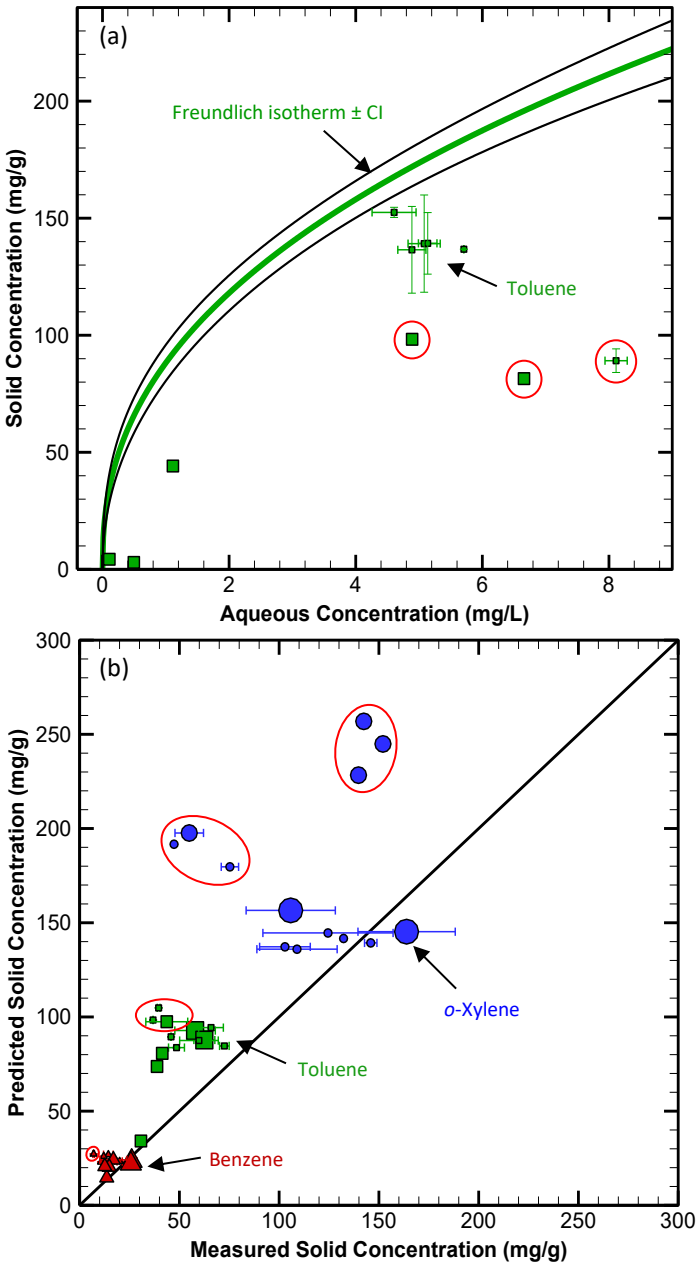

Figure 3.2: Measured solid phase concentrations within the KC+PAC (large sized symbols), BA+PAC+EA (medium sized symbols) and BA+PAC (small sized symbols) microcosms for (a) single-solute toluene (filled green squares) against the measured aqueous phase concentrations at each sacrificial sampling time, and (b) multi-solute benzene (filled red triangles), toluene (filled green squares) and *o*-xylene (filled blue circles) (BTX) against the predicted solid phase concentration generated from the improved simplified ideal adsorption solution (ISIAS) model (using the single-solute Freundlich model parameters for each solute [K_{f_i} and n_{f_i}] and the multi-solute ISIAS competition factors for each solute [a_i] [listed in Table 2.2]). The single-solute Freundlich isotherm for toluene with a 95% confidence envelope (black solid band) is represented as a solid green line in (a), and a black solid 1:1 line is shown in (b). The standard deviation of triplicate measurements is represented as ± error bars on each data point. The red circles indicate data corresponding to sampling times (a) < 5 days following a toluene dosing event, or (b) between 6 and 64 days following a TX dosing event.

3.3.2 Killed and starved controls

Between the single-solute (toluene-only) and multi-solute (BTX) KC (Figure B.2(a) and Figure B.3(a)) and KC+PAC (Figure B.2(e) and Figure B.3(e)) microcosms, the aqueous and solid phase concentrations of toluene and BTX differed following the PAC amendment to the KC+PAC microcosms on Day 2 and over the remainder of the 1-year monitoring period. For the KC microcosms the average aqueous toluene or BTX concentration decreased slightly after Day 2 to the end of the monitoring period (17.4 ± 1.8 mg/L on Day 2 to 14.4 ± 0.7 mg/L on Day 366 or 372 for the single- or multi-solute KC microcosms, respectively) and the average solid phase concentration remained low (0.001 ± 0.0006 mg/g between single- and multi-solute systems). The limited change in aqueous or solid phase concentrations indicates mass was conserved within the KC microcosms and limited partitioning of toluene or BTX between phases occurred. Contrarily, for the KC+PAC microcosms a reduction in the average aqueous concentration of toluene (18 mg/L on Day 2 to 5.8 mg/L on Day 366) in the single-solute system, or benzene (20.9 mg/L on Day 2 to 13.6 mg/L on Day 372), toluene (20.4 mg/L on Day 2 to 10 mg/L on Day 372) and *o*-xylene (17.8 mg/L on Day 2 to 3.8 mg/L on Day 372) in the multi-solute system were observed. With the reduction in aqueous phase concentrations in the KC+PAC microcosms, a corresponding increase in the average solid phase concentrations of benzene (25.9 ± 0.3 mg/g), toluene (60.2 ± 3.3 mg/g) and *o*-xylene (134.8 ± 41.1 mg/g) were also observed in the multi-solute system after Day 2 which is attributed to BTX partitioning from the aqueous to solid PAC phase (no solid phase data is available for toluene in the single-solute KC+PAC microcosm). Like the multi-solute partitioning behaviour discussed in Section 2.3.2.2, the magnitude of partitioning between solutes followed X > T > B which is due to difference in the magnitude of chemical properties between solutes (e.g., high molecular weight and hydrophobicity generally yields higher partitioning relative to lower values, as described in Section 2.3.2). The difference in chemical properties between solutes in the multi-solute system resulted in the chemically favourable solute (i.e., *o*-xylene) preferentially sorbing more than the other solutes (i.e., toluene then benzene) (see Table A.3 for the chemical properties of BTX). Additionally, the magnitude of toluene partitioning was greater in the single-solute KC+PAC microcosm relative to the multi-solute microcosm (when comparing the average aqueous phase data only) due to a reduction in the total number of sorption sites accessible to toluene in the competitive multi-solute system [28, 21, 16, 29].

In the single-solute (Figure B.2(b-c, f-g)) and multi-solute (Figure B.3(b-c, f-g)) KC and KC+PAC microcosms negligible sulfide (≤ 5 µg/L) or CH_4 (≤ 0.03 mg/L) were generated and minimal

change in the average sulfate concentrations were observed over the 1-year monitoring period (18 ± 2.9 mg/L [toluene-only] to 10.8 ± 1.9 [BTX]). Contrarily, the average mass of TIC slightly increased from 2.4 ± 0.2 mg to 5.3 ± 1 mg between the single- and multi-solute systems which may be attributed to an abiotic reaction between the biocide (sodium azide) and some other bottle material forming inorganic carbon given that sodium azide is known to act as an oxidant or reductant [160] (Figures B.2(c, g) and Figure B.3(c, g)). Figures B.2(d, h) and Figure B.3(d, h) show that the average DO concentration was consistently low (0.3 ± 0.3 mg/L), pH was neutral (7.2 ± 0.3) and the ORP was oxidizing (+250 ± 22 mV) between the single- and multi-solute microcosms KC and KC+PAC microcosms over the 1-year monitoring period. Additionally, from the qPCR data at the conclusion of the 1-year monitoring period a reduction in abundance of total bacteria, total archaea and *Desulfosporosinus* was shown for the KC and KC+PAC microcosms relative to the BS on Day -15 (i.e., background) (Figure 3.3(a, b) and see Table B.6 for the qPCR data for the single- and multi-solute microcosms). In general, the stability in the geochemical parameters monitored combined with the reduced abundance of bacteria and archaea indicates that anaerobic biodegradation (specifically sulfate reduction or methanogenesis) was absent from the KC or KC+PAC microcosms over the 1-year monitoring period, as expected (see Table B.7 for the chemical reactions associated with BTX oxidation coupled to sulfate reduction, and the changes in geochemical parameters expected under sulfate reducing conditions).

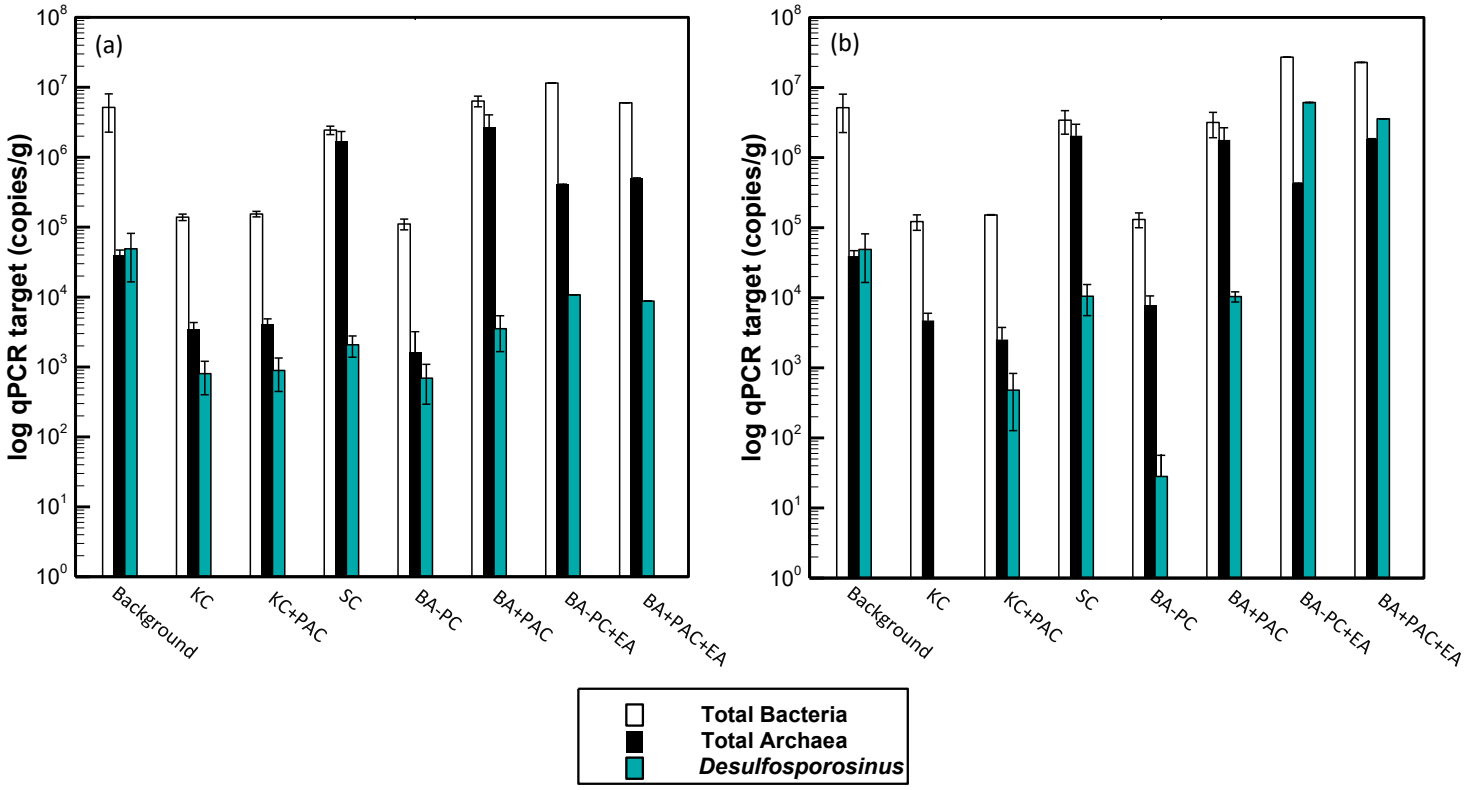

Figure 3.3: Abundance of total bacteria, total archaea and *Desulfosporosinus* detected using quantitative polymerase chain reaction (qPCR) analysis for all (a) single-solute (toluene-only) and (b) multi-solute (benzene, toluene and *o*-xylene [BTX]) microcosm types after 1-year relative to background conditions. Error bars represent ± 1 standard error.

Mass balance estimates generated from Equation (3.2) show that for the single- and multi-solute KC microcosms the average M_{i_T} decreased from 3.3 ± 0.3 mg (Day 2) to 2.4 ± 0.09 mg (on Day 366 [toluene-only] or 372 [BTX]), and for the KC+PAC microcosms the average M_{i_T} decreased from 3.4 ± 0.2 mg (Day 2) to 2.6 ± 0.3 mg (Day 366 [toluene-only] or 372 [BTX]) (see Table B.8 for the M_{i_T} estimates of each solute and for each microcosm type over the 1-year monitoring period). Given that the geochemical data (i.e., sulfate, sulfide, TIC and CH_4) described above indicate biodegradation was absent from the KC and KC+PAC microcosms, mass loss reflected in the M_{i_T} estimates are more likely associated with inter-bottle variation in $C_{i_{(aq)}}$ between triplicate sets of microcosm bottles, M_{i_T} removal during repetitive sampling (described in Section 3.2.2) or bottle leakages (described in Section 3.3),

and/or unintended $M_{i_{(PAC)}}$ removal during sacrificial sampling and aqueous phase decanting (as described in Section 3.2.2).

In the single- and multi-solute SC microcosms, toluene or BTX were ≤ MDL (Section 2.2.2) in the aqueous or solid phases from Day 2 to the end of the 1-year monitoring period (Figure B.4(a, e)). Geochemically, the average sulfate concentration slowly depleted (from 7.7 ± 1.7 mg/L to 0.2 ± 0.01 mg/L) while negligible sulfide was formed (≤ 3 µg/L), TIC remained stable (2.3 ± 0.5 mg) and some CH_4 was generated (concentration increased from 0.02 ± 0.02 mg/L to 1.7 mg/L [single-solute] or 7 mg/L [multi-solute]) between the single- and multi-solute SC microcosms (Figure B.4(b-c, f-g)). Additionally, the average DO concentration remained low (0.2 ± 0.2 mg/L), pH was neutral (7.4 ± 0.2) and the ORP was consistently reduced in the multi-solute SC microcosm (-209.5 ± 48 mV) and more variable in the single-solute SC microcosm (217 ± 155 mV) (Figure B.4(d, h)). The gradual depletion of sulfate with the corresponding slight increase in CH_4 and limited sulfide or TIC production in both the single- and multi-solute SC microcosms suggests that some sulfate reduction and methanogenesis occurred. Given that the concentration of CH_4 increased as the concentration of sulfate was reduced in both the single- and multi-solute SC microcosm, this likely represents a shift to methanogenesis after the higher energy yielding redox condition, with sulfate as an EA, was essentially depleted.

Methanogenesis in the single- and multi-solute SC microcosms is supported by the qPCR data at the end of the 1-year monitoring period relative to background, which shows an enrichment in the average abundance of total archaea ($1.9 \times 10^{+6} \pm 2.4 \times 10^{+5}$ copies/g versus $3.9 \times 10^{+4} \pm 7.7 \times 10^{+3}$ copies/g [average background abundance]) (Figure 3.3(a, b) and see Table B.6 for the qPCR data for the single- and multi-solute microcosms). The NGS data between the single-solute (Figure 3.4(a-c)) and multi-solute (Figure 3.5(a-c)) SC microcosms, reveal that the average relative abundance of archaea from the Euryarchaeota and Halobacterota phyla were enriched relative to background conditions (0.0%). Within these phyla, the average relative abundance of genera enriched between the single- and multi-solute SC microcosms included: *Methanomethylovorans* (5 ± 5.3% [single- and multi-solute]), which are canonically methylotrophic methanogens that convert methylated compounds to CH_4 [161]; *Methanosaeta* (2.4 ± 0.1% [single-solute]), which contains acetoclastic methanogens [162, 161]; and *Methanobacterium* (2.5 ± 1.5% [single-solute] and 5.9 ± 2.3% [multi-solute]), whose members are versatile methanogens able to grow on H_2, CO_2 or formate [67] (see Table B.9 for the NGS data for the single- and multi-solute microcosms). Enrichment of these archaea in the absence of PHCs, combined

with the gradual formation of CH_4 under reduced redox conditions, indicates methanogenesis involving alternate carbon or hydrogen sources (other than metabolic products generated from the oxidation of toluene or BTX) occurred in the single- and multi-solute SC microcosms. For example, H_2 gas can be used as an electron donor by sulfate reducers and methanogens during CO_2 reduction [66, 67], and H_2 is present in the headspace of all microcosms due to exposure to the anaerobic chamber atmosphere [163, 164, 111]).

Unlike the archaeal enrichment for the single- and multi-solute SC microcosms, the qPCR data did not show an enrichment in the abundance of total bacteria or *Desulfosporosinus* relative to background (Figure 3.3(a, b) and see Table B.6 for the qPCR data for the single- and multi-solute microcosms). However, the NGS data did show an enrichment of anaerobic bacteria between the single-solute (Figure 3.4(a-c)) and multi-solute (Figure 3.5(a-c)) SC microcosms relative to background conditions (0.0-0.3%). Bacteria enriched between the single- and multi-solute SC microcosms include: the genus *Deferrisoma* from the phylum Deferrisomatota (0.8 ± 0.1% [single-solute] and 7.9 ± 1.1% [multi-solute]); the family Desulfocapsaceae from the phylum Desulfobacterota (1.4 ± 0.04% [single-solute]), which are SRB capable of using sulfur compounds as electron donors and acceptors [165, 166, 167]; the genus *Edwardsbacteria* from the phylum Edwardsbacteria (1.9 ± 1.4% [single- and multi-solute]); the family Geobacteraceae from the phylum Desulfobacterota (5.1 ± 4.8% [multi-solute]), which are associated with iron reduction [168, 169]; the family Peptococcaceae from the phylum Firmicutes (6.6 ± 6.6% [single-solute]), which are associated with sulfate and iron reduction [170, 171]; and the genus *Sulfuricurvum* from the phylum Campilobacterota (13.4 ± 18.5% [single-solute]), which are sulphur-oxidizing facultative anaerobes [172, 173] (see Table B.9 for the NGS data for the single- and multi-solute microcosms). Like the enriched archaea, enrichment of these bacteria are likely associated with the anaerobic biodegradation of background carbon or hydrogen substrates (other than toluene or BTX). Additionally, given that sulfate was depleted from the SC microcosm at the time of molecular monitoring (i.e., at the conclusion of the 1-year monitoring period) theses bacteria likely coexisted with the enriched archaea under methanogenic conditions or competed for common substrates (e.g., H_2 or acetate) [65, 68, 66, 67].

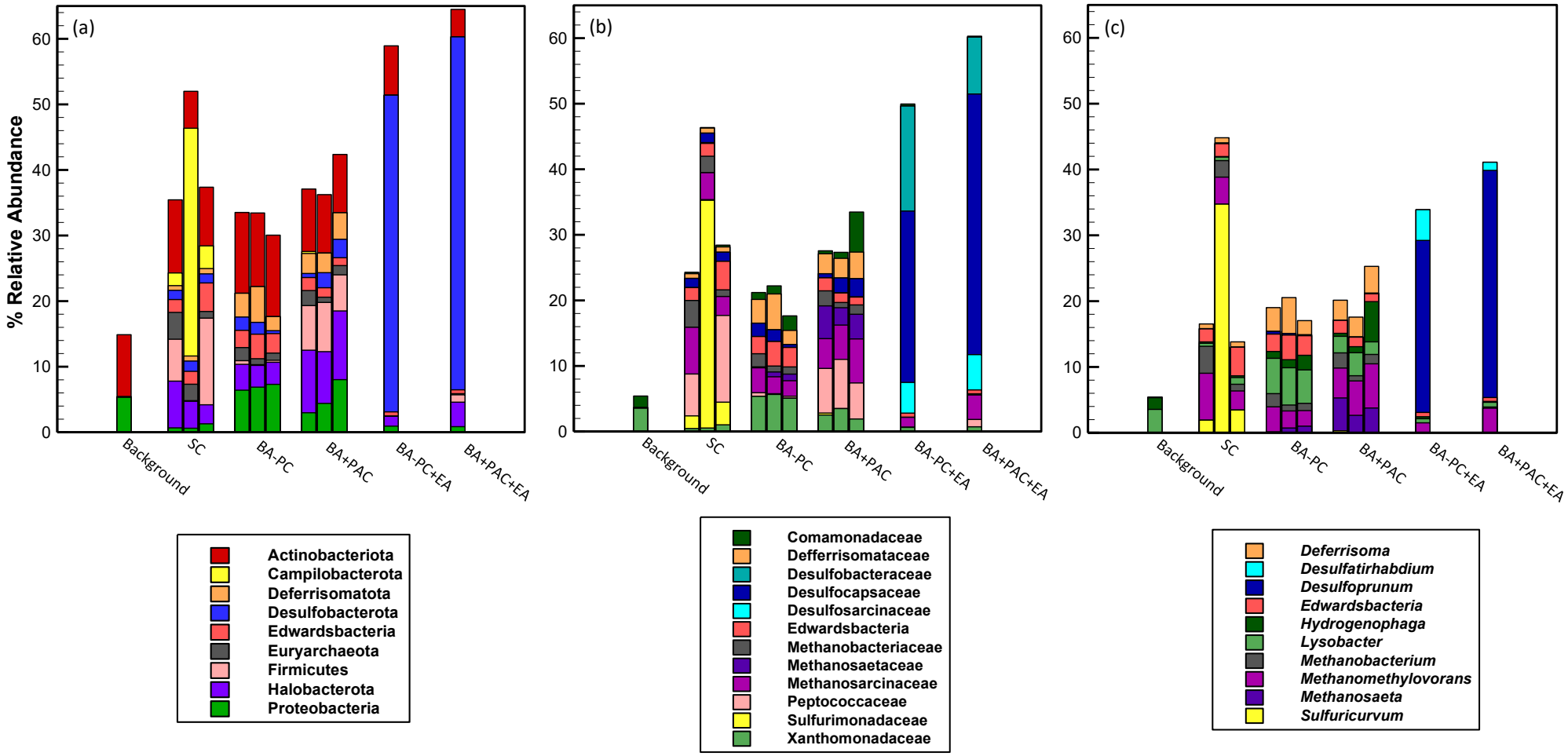

Figure 3.4: Relative abundance (≥ 4%) of bacteria and archaea at the (a) phylum, (b) family and (c) genus taxonomic levels detected using 16S ribosomal ribonucleic acid (rRNA) next generation sequencing (NGS) for the SC, BA-PC, BA+PAC, BA-PC+EA and BA+PAC+EA single-solute (toluene-only) microcosms after 1-year relative to background conditions. The relative abundance of all replicate bottles (A, B and C) is shown for the SC, BA-PC and BA+PAC microcosms, whereas the relative abundance of a single replicate bottle (C) is shown for the BA-PC+EA and BA+PAC+EA microcosms.

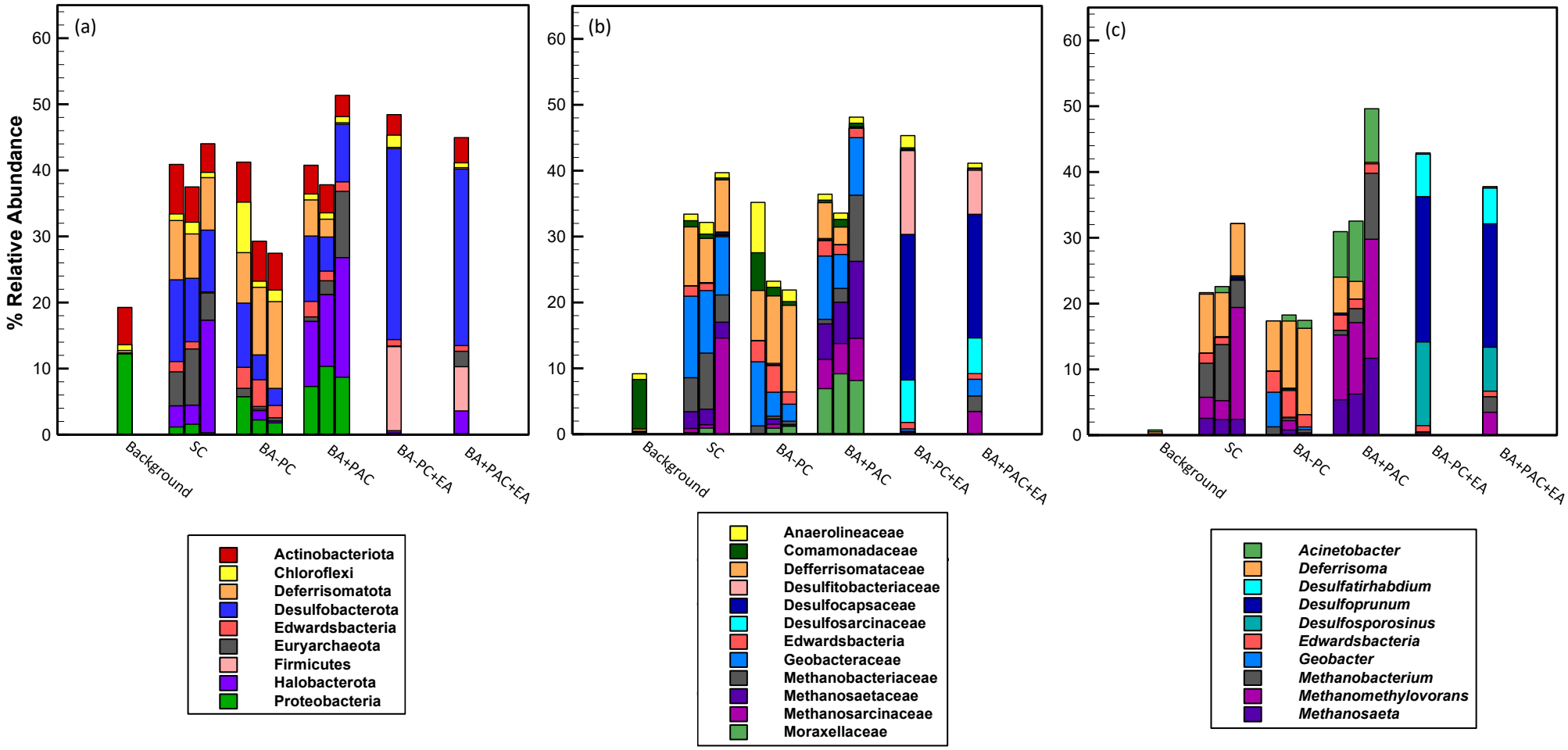

Figure 3.5: Relative abundance (≥ 4%) of bacteria and archaea at the (a) phylum, (b) family and (c) genus taxonomic levels detected using 16S ribosomal ribonucleic acid (rRNA) next generation sequencing (NGS) for the SC, BA-PC, BA+PAC, BA-PC+EA and BA+PAC+EA multi-solute (benzene, toluene and *o*-xylene [BTX]) microcosms after 1-year relative to background conditions. The relative abundance of all replicate bottles (A, B and C) is shown for the SC, BA-PC and BA+PAC microcosms, whereas the relative abundance of a single replicate bottle (C) is shown for the BA-PC+EA and BA+PAC+EA microcosms.

3.3.3 Bioactive systems (no electron acceptor amendment)

The aqueous and solid phases concentrations of toluene and BTX in the BA-PC and BA+PAC single-solute (Figure 3.6(a, d)) and multi-solute (Figure 3.7(a, d)) microcosms are similar to the behaviour of these solutes in the single- and multi-solute KC (Figure B.2(a) and Figure B.3(a)) and KC+PAC (Figure B.2(e) and Figure B.3(e)) microcosms, indicating minimal toluene or BTX mass were removed from the bioactive system (without EA amendments). Limited mass removal is supported by a slight reduction in the average M_{i_T} between the single- and multi-solute BA-PC and BA+PAC microcosms from Day 2 (3.6 ± 0.3 mg) to the end of the 1-year monitoring period on Day 366 (toluene-only) or 372 (BTX) (2.8 ± 0.2 mg [BA-PC] and 2.9 ± 0.2 mg [BA+PAC]), which may be due to the same sources of mass loss as described for the KC and KC+PAC microcosms in Sections 3.3.2 (see Table B.8 for the M_{i_T} estimates of each solute and for each microcosm type over the 1-year monitoring period). For the single- and multi-solute BA-PC microcosms, the average aqueous phase concentration between solutes decreased slightly after Day 2 to the end of the 1-year monitoring period (19.1 ± 1.4 mg/L on Day 2 to 15 ± 1.2 mg/L on Day 366 [toluene-only] or 372 [BTX]), and the average solid phase concentration of each solute remained low over the same monitoring period ($9.1 \times 10^{-4} \pm 1.1 \times 10^{-3}$ mg/g [toluene-only]; and $5.6 \times 10^{-4} \pm 4.3 \times 10^{-4}$ mg/g benzene, $8.3 \times 10^{-4} \pm 6.6 \times 10^{-4}$ mg/g toluene and $1.4 \times 10^{-3} \pm 7.1 \times 10^{-4}$ mg/g *o*-xylene [BTX]). Contrarily, larger shifts in the aqueous phase concentrations of toluene or BTX were observed in the single- and multi-solute BA+PAC microcosms, including a reduction in the aqueous phase concentrations of toluene (20.4 mg/L on Day 2 to 5.1 mg/L on Day 366) in the single-solute system and benzene (21.6 mg/L on Day 2 to 15.9 mg/L on Day 372), toluene (21.2 mg/L on Day 2 to 10.3 mg/L on Day 372) and *o*-xylene (18.4 mg/L on Day 2 to 3.8 mg/L on Day 372) in the multi-solute system. The reduction in aqueous phase concentrations in the BA+PAC microcosms corresponded with increases in the solid phase concentrations of toluene (89.1 mg/g on Day 7 to 139.3 mg/g on Day 366) in the single-solute system and benzene (16 mg/g on Day 2 to 12.1 mg/g on Day 372), toluene (36.8 mg/g on Day 2 to 45.8 mg/g on Day 372) and *o*-xylene (47.3 mg/g on Day 2 to 132.3 mg/g on Day 372) in the multi-solute system. The larger shift in the aqueous and solid phase toluene or BTX concentrations in the single- and multi-solute BA+PAC microcosms relative to the BA-PC microcosms is due to partitioning primarily from the aqueous to the PAC phase and is consistent with the behaviour described for the KC+PAC microcosms in Section 3.3.2.

The geochemistry within the single-solute (Figure 3.6(b-c, e-f) and multi-solute (Figure 3.7(b-c, e-f)) BA-PC and BA+PAC microcosms indicates that anaerobic biodegradation occurred, including a

slow depletion in the average sulfate concentration from 9.2 ± 1.5 mg/L [single solute] and 7.3 ± 0.3 mg/L [multi-solute] on Day 2 to < 1 mg/L on Day 64 to 128 between microcosms. Despite the reduction in sulfate, minimal sulfide (as the reduced form of sulfate) was generated in the single- and multi-solute BA-PC and BA+PAC microcosms over the 1-year monitoring period (≤ 7 µg/L). As opposed to a lack of sulfate reduction, the low average sulfide concentration may be due to an abiotic reaction between ferric iron in the BS and any generated sulfide (H_2S and HS^-) which is known to form FeS precipitates [53, 54] that are undetected during aqueous phase monitoring. In addition to the minimal sulfide detected, limited TIC formation was observed between the single- and multi-solute BA-PC and BA+PAC microcosms (2.2 ± 0.2 mg) from Day 2 to Day 64-128, as sulfate was reduced to < 1 mg/L. Following sulfate reduction (i.e., after Day 64 to 128) to the end of the 1-year monitoring period the average mass of TIC slightly increased between the single- and multi-solute BA-PC and BA+PAC microcosms (2.5 ± 0.5 mg), except for the single-solute BA+PAC microcosm which remained stable over the monitoring period (2.2 ± 0.2 mg). The concentration of CH_4 also increased between the single- and multi-solute BA-PC and BA+PAC microcosms (from 0.2 ± 0.07 mg/L on Day 2 to 6.6 ± 1.1 mg/L or 22.9 ± 13.5 mg/L for the BA-PC or BA+PAC microcosms, respectively, by Day 372 [toluene-only] or 366 [BTX]) indicating methanogenesis occurred following sulfate reduction. Notably between the single- and multi-solute microcosms, the concentration of CH_4 was also consistently higher in the BA+PAC microcosms relative to the BA-PC microcosms which may indicate that the presence of PAC provided support for methanogenesis and archaeal growth [76]. Other indicators of anaerobic biodegradation between the single-solute (Figure B.5(a-b, e-f)) and multi-solute (Figure B.5(a-b, e-f)) BA-PC and BA+PAC microcosms include consistently low DO (0.2 ± 0.2 mg/L), neutral pH (7.4 ± 0.2) and reduced ORP (-223.2 ± 42.9 mV). Although the geochemical data indicate sulfate reduction and methanogenesis occurred in the single- and multi-solute BA-PC and BA+PAC microcosms, only a small change in M_{i_T} was observed for toluene and BTX, as described above. Therefore, a fraction of the toluene or BTX mass may have been oxidized within the single- and multi-solute PC-BA and BA+PAC microcosms; however, biodegradation may also be associated with other sources of carbon or hydrogen other than toluene and BTX, like the behaviour described for the SC microcosms in Section 3.3.2 where no toluene or BTX was present. Although, relative to the SC microcosms without PAC, notably more CH_4 generation occurred in the BA+PAC microcosms with PAC.

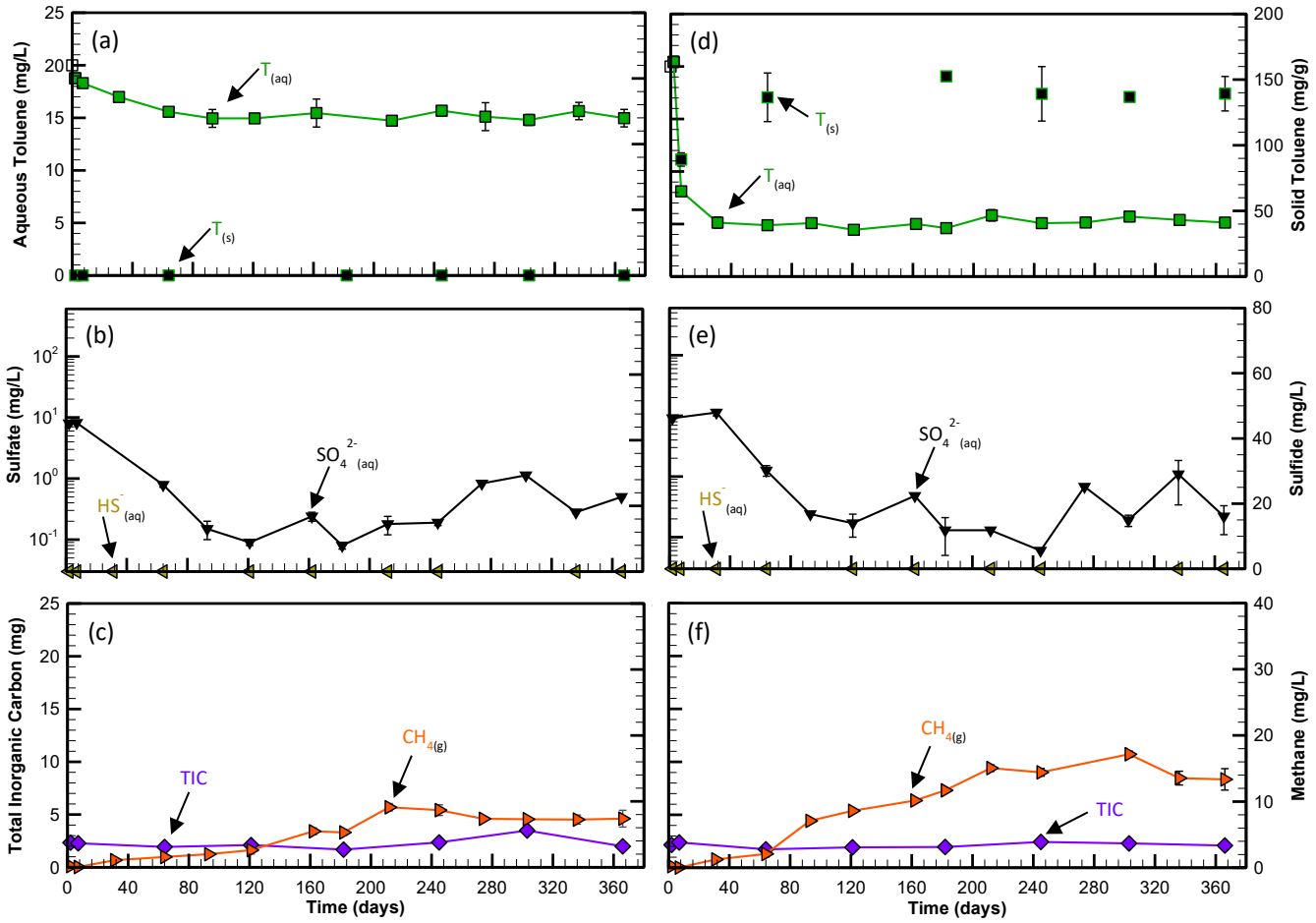

Figure 3.6: Temporal changes in the (a, d) aqueous and solid phase toluene concentrations ($T_{(aq)}$ and $T_{(s)}$) (green and black filled squares, respectively), (b, e) aqueous sulfate ($SO_4^{2-}{}_{(aq)}$) (black filled gradient symbols) and sulfide ($HS^-_{(aq)}$) (yellow filled left triangles) concentrations, and (c, f) total inorganic carbon (TIC) (purple filled diamonds) and gaseous methane concentration ($CH_{4(g)}$) (orange filled right triangles) for the single-solute (toluene-only) (a-c) BA-PC and (d-f) BA+PAC microcosms. Each timepoint represents the average of three values and the error bars are ± 1 standard deviation.

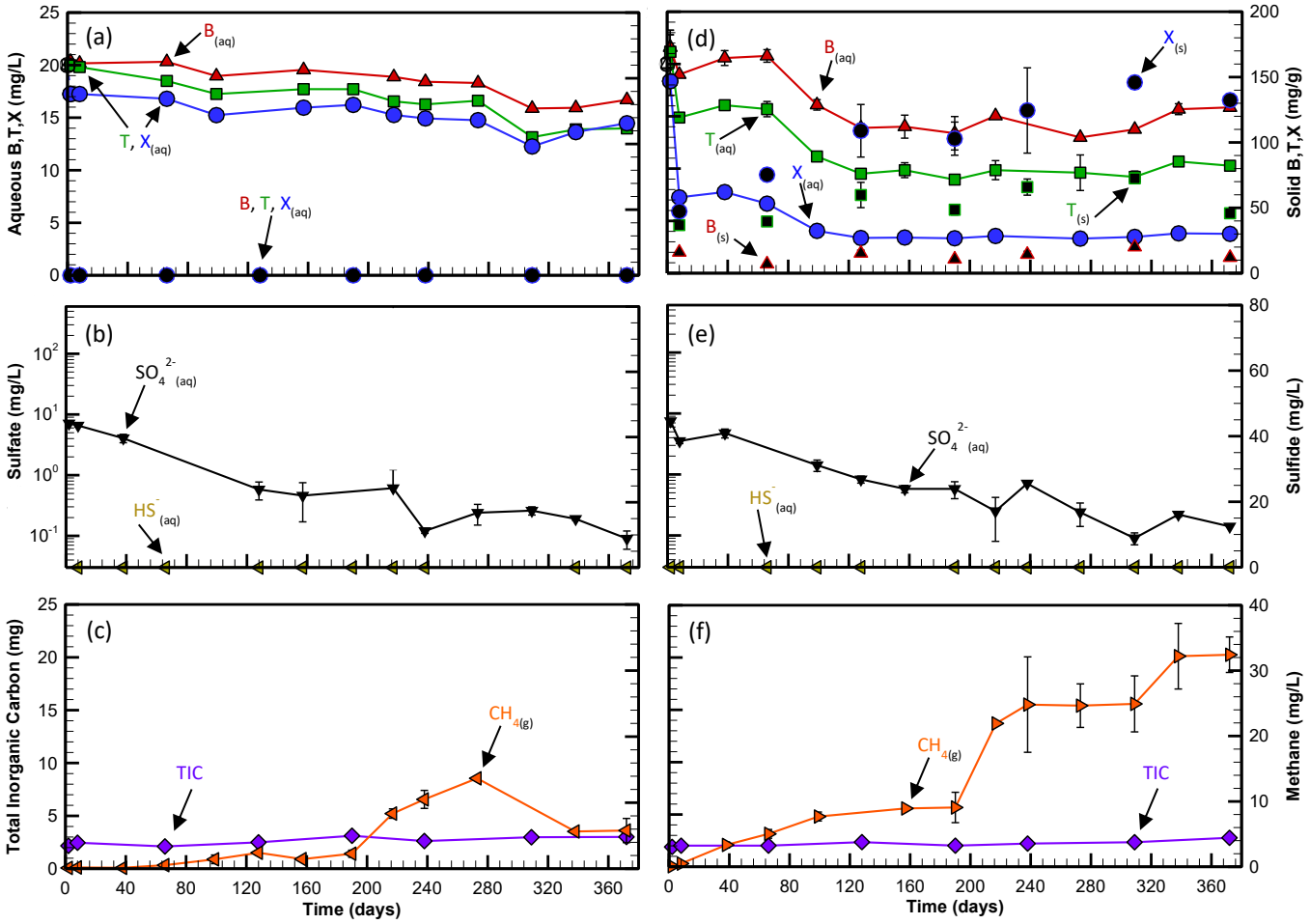

Figure 3.7: Temporal changes in the (a, d) aqueous phase benzene, toluene and *o*-xylene (BTX) ($B,T,X_{(aq)}$) (red filled triangle [B], green filled squares [T] and blue filled circles [X]) and solid phase BTX ($B,T,X_{(s)}$) (black filled triangles [B], squares [T] and circles [X]) concentrations, (b, e) aqueous sulfate ($SO_4^{2-}{}_{(aq)}$) (black filled gradient symbols) and sulfide ($HS^-_{(aq)}$) (yellow filled left triangles) concentrations, and (c, f) total inorganic carbon (TIC) (purple filled diamonds) and gaseous methane concentration ($CH_{4(g)}$) (orange filled right triangles) for the multi-solute (BTX) (a-c) BA-PC and (d-f) BA+PAC microcosms. Each timepoint represents the average of three values and the error bars are ± 1 standard deviation.

Like the SC microcosms (described in Section 3.3.2), the qPCR data shows an enrichment in the average abundance of total archaea relative to background conditions between the single- and multi-solute BA+PAC microcosms ($2.2 \times 10^{+6} \pm 6.3 \times 10^{+5}$ copies/g versus $3.9 \times 10^{+4} \pm 7.7 \times 10^{+3}$ copies/g [average background abundance]). However, enrichment in the average abundance of total archaea was not observed between the single- and multi-solute BA-PC microcosms ($4.7 \times 10^{+3} \pm 4.4 \times 10^{+3}$ copies/g versus $3.9 \times 10^{+4} \pm 7.7 \times 10^{+3}$ copies/g [average background abundance]) (Figure 3.3(a, b) and see Table B.6 for the qPCR

data for the single- and multi-solute microcosms). The NGS data for the single-solute (Figure 3.4(a-c) and multi-solute (Figure 3.5(a-c) BA-PC and BA+PAC microcosms shows methanogenic enrichment relative to background conditions (0.0%), with higher average relative abundances consistently observed between the single- and multi-solute BA+PAC microcosms relative to the BA-PC microcosms. Higher methanogenic enrichment in BA+PAC relative to the BA-PC microcosm may be associated with the presence of the PAC, known to enhance archaeal growth and accelerate substrate conversion to CH_4 [115, 117, 108]. Archaea enriched in the single- and multi-solute BA-PC and BA+PAC microcosms were consistent with those detected in the SC microcosms, including: *Methanomethylovorans* (single-and multi-solute: 5.3 ± 1% [BA+PAC] > 1.6 ± 1.5% [BA-PC]), *Methanosaeta* (single-and multi-solute: 5.8 ± 3.2% [BA+PAC] > 0.5 ± 0.4% [BA-PC]) and *Methanobacterium* (single-solute: 1.5 ± 0.8 % [BA+PAC] > 1.3 ± 0.6% [BA-PC], and multi-solute: 4.3 ± 5% [BA+PAC] > 0.7 ± 0.5% [BA-PC]). Although consistent with the SC microcosms, the relative abundance of enriched archaea were higher in the BA+PAC microcosms relative to the SC microcosms without PAC (see Table B.9 for the NGS data for the single- and multi-solute microcosms). Of the enriched archaea, *Methanosaeta* and *Methanobacterium* are commonly associated with DIET in AC amended systems [112, 118, 117] which may explain the higher relative abundance of these archaea in the BA+PAC relative to the BA-PC microcosms. Specifically, members of the genus *Methanosaeta* are acetoclastic (as described in Section 3.3.2) and able to convert acetate to CO_2 and CH_4 with limited capacity to consume H_2; however, through PAC-mediated DIET *Methanosaeta* can also reduce CO_2 to CH_4 by directly accepting electrons transferred from bacteria through the PAC similar to hydrogenotrophic methanogens that often rely on interspecies hydrogen transfer (IHT) [78, 73, 118, 174].

In the single- and multi-solute BA-PC or BA+PAC microcosms the qPCR data showed total bacteria and *Desulfosporosinus* were not enriched relative to background (Figure 3.3(a, b) and see Table B.6 for the qPCR data for the single- and multi-solute microcosms). Although, like the SC microcosms described in Section 3.3.2 the NGS data showed enrichment in the average relative abundance of anaerobic bacteria between the single-solute (Figure 3.4(a-c)) and multi-solute (Figure 3.5(a-c)) BA-PC or BA+PAC microcosms relative to background conditions (0.0-0.3%). Most of the anaerobic bacteria enriched in the single- and multi-solute BA-PC and BA+PAC microcosms are the same as those enriched within the SC microcosms, including: *Deferrisoma* (single-solute: 3.7 ± 1.7% [BA-PC] and 3.4 ± 0.6% [BA+PAC], and multi-solute: 10.3 ± 2.8% [BA-PC] and 2.8 ± 2.6% [BA+PAC]) [175], Desulfocapsaceae (single-solute: 1.2 ± 0.8% [BA-PC] and 1.9 ± 1.1% [BA+PAC]) [176], *Edwardsbacteria* (single- and

multi-solute: 3.1 ± 0.8% [BA-PC] and 1.6 ± 0.4% [BA+PAC]), Geobacteraceae (multi-solute: 1.7 ± 0.6% [BA-PC] and 3.9 ± 2.4% [BA+PAC]) and Peptococcaceae (single-solute: 5.9 ± 1.2% [PAC+BA]) (see Table B.9 for the NGS data for the single- and multi-solute microcosms). Although many of these families and genera are associated with PHC biodegradation [177, 178, 179, 162, 46, 176, 175], the similarity in enriched bacteria between the SC, and the BA-PC and BA+PAC microcosms may indicate some or all the bacteria were primarily sustained by other carbon or hydrogen substrates in the microcosms, as described in Section 3.3.2. Enrichment of other bacteria also associated with PHC biodegradation in the multi-solute BA+PAC microcosms included *Acinetobacter* (8.1 ± 1.1% [BA+PAC] versus 0.3% [average background relative abundance]) from the phylum Proteobacteria [180], whose members are known to participate in manganese, iron or sulfate reduction [181, 182]. Additionally, members of the family Anaerolineaceae from the phylum Chloroflexi were enriched in one multi-solute BA-PC replicate microcosm bottle (7.6% [BA-PC] versus 0.9% [average background relative abundance]), which are acetogenic microbes that play key syntrophic roles in methanogenic PHC degrading consortiums (e.g., providing acetate to acetoclastic methanogens, such as *Methanosaeta*) [183].

3.3.4 Bioactive electron acceptor amended systems

In contrast, to the single- and multi-solute BA-PC and BA+PAC microcosms without additional EA amendments (described in Section 3.3.3), a reduction in PHCs was observed in the EA amended BA-PC+EA and BA+PAC+EA microcosms. Toluene was replenished 5 and 6 times in the single-solute BA-PC+EA and BA+PAC+EA microcosms, respectively (Figure 3.8(a, d)), and toluene and *o*-xylene were replenished twice in the multi-solute BA-PC+EA and BA+PAC+EA microcosms (Figure 3.9(a, d)). The initial sulfate concentration was the only difference between the BA-PC and BA+PAC (10-20 mg/L) and the BA-PC+EA and BA+PAC+EA (138-275 mg/L) microcosms (see Table B.2 for the microcosm experimental design), and therefore the lack of toluene or BTX biodegradation in the single- or multi-solute BA-PC and BA+PAC microcosms was most likely attributed to the stoichiometric limitation of sulfate for sulfate reduction coupled to toluene or BTX oxidation (see Table B.7 for the chemical reactions associated with toluene or BTX biodegradation under sulfate reducing conditions).

In the BA-PC+EA and BA+PAC+EA microcosms a brief lag period of stabilized aqueous concentration(s) occurred until between Day 31 and 64 for the single-solute microcosms and between Day 38 and 66 for the multi-solute microcosms (there was no detectable difference in the length of the lag time

between the single- or multi-solute PC+EA and BA+PAC+EA microcosms), which is assumed to be representative of an initial growth period of the indigenous microbes [184] within the BS. Following the initial lag period to Day 269 or 310 in the single- or multi-solute microcosms, respectively, the M_{i_T} for toluene in the BA-PC+EA and BA+PAC+EA microcosms was repeatedly reduced to ≥ 98.1% of the initial mass (i.e., 3.5 mg [Table B.3]) within 12 to 64 days in the single-solute microcosms or 45 to 66 days in the multi-solute microcosms. During high-resolution monitoring (where the initial mass of toluene amended into the microcosms was measured, in place of assuming the target initial concentration as was done prior to high-resolution monitoring), the M_{i_T} for toluene in the BA-PC+EA and BA+PAC+EA microcosms was reduced to ≥ 98.3% of the initial mass within 23 or 23 to 40 days for the single-solute (over Day 269 to 292) or multi-solute (over Day 310 to 350) microcosms, respectively (neglecting for the single-solute BA-PC+EA microcosm, where the M_{i_T} for toluene was reduced to 92.4% over 23 days) (see Figure B.6(a-b, e-f) for the change in single- and multi-solute toluene mass in all phases during high-resolution monitoring, and Table B.8 for the M_{i_T} estimates). The repetitive reduction in the M_{i_T} of toluene from the single- and multi-solute BA-PC+EA and BA+PAC+EA microcosms suggests that the mass of toluene was bioavailable in all phases. Specifically, for the BA+PAC+EA microcosms the reduction in the M_{i_T} of toluene supports desorption of toluene from the PAC during biodegradation and shows that the AC sorption of toluene is reversible with bioactivity. Although some residual toluene remained sorbed to the PAC prior to each toluene reamendment to the single- and multi-solute BA+PAC+EA microcosms, the $M_{i_{(S)}}$ of toluene was reduced to ≥ 95.5% over each biodegradation cycle which shows that the PAC can be repetitively regenerated multiple times, allowing for continued sorption.

The change in M_{i_T} of toluene from the BA-PC+EA and BA+PAC+EA microcosms during high-resolution monitoring over Day 269 to 292 or 310 to 350 in the single- or multi-solute microcosms, respectively (see Figure B.6(a-b, e-f) for the mass of toluene in all phases during high-resolution monitoring), are shown in Figure B.7(a, b) and the zero-order biodegradation rate constants associated with the M_{i_T} reduction during this monitoring period are listed in Table B.10. The zero-order rate constants for toluene were determined during the high-resolution monitoring period given that biodegradation of toluene was generally faster than the 1-month sampling intervals used prior to high-resolution monitoring (i.e., over Day 0 to 269 or 310 in the single- or multi-solute microcosms, respectively). Between the single-solute BA-PC+EA (0.10 ± 0.14 mg/day) and BA+PAC+EA (0.51 ±

0.79 mg/day) microcosms or the multi-solute BA-PC+EA (0.14 ± 0.11 mg/day) and BA+PAC+EA (0.14 ± 0.11 mg/day) microcosms, there was no difference in the biodegradation rate constants for toluene during high-resolution monitoring. Therefore, the presence of the PAC did not enhance the rate of anaerobic toluene biodegradation within the single- or multi-solute BA+PAC+EA microcosms relative to the BA-PC+EA microcosms without PAC.

In the multi-solute BA-PC+EA and BA+PAC+EA microcosms toluene was consistently biodegraded to depletion (≤ MDL) prior to *o*-xylene (Figure 3.9(a, d)), which is due to the competitive inhibition of *o*-xylene in the presence of toluene (or metabolic intermediates of toluene) [159, 185, 148]. The competitive inhibition of *o*-xylene in the presence of toluene commonly occurs when a single enzymatic pathway (e.g., fumarate addition by benzylsuccinate synthase [bss] [186]) is involved in the biodegradation of multiple solutes, with one being more easily oxidized (i.e., toluene) relative to the other(s) (i.e., *o*-xylene) [54, 56, 187]. Prior to high-resolution monitoring (over Day 0 to 310), the M_{i_T} for *o*-xylene in the multi-solute microcosms was reduced to ≥ 98.9% of the initial target mass (i.e., 3.5 mg [Table B.3]) within ≤ 120 days from the dosing of *o*-xylene or ≤ 62 days following the depletion in the M_{i_T} of toluene. Relative to toluene, the residual $M_{i_{(s)}}$ of *o*-xylene was consistently higher during each sacrificial sampling event likely due to the difference in multi-solute sorption capacities between solutes (i.e., X > T) described in Section 3.3.2, and the preferential biodegradation of toluene prior to *o*-xylene (see Table B.8 for the M_{i_T} estimates of each solute). During high-resolution monitoring, the M_{i_T} of *o*-xylene in the multi-solute BA-PC+EA and BA+PAC+EA microcosms was not reduced (see Figure B.6(g-h) for the mass of *o*-xylene in all phases during high-resolution monitoring) given toluene was preferentially biodegraded over the entire 40 day monitoring period (see Figure B.6(e-f) for the mass of toluene in all phases during high-resolution monitoring). Although the M_{i_T} of *o*-xylene remained relatively stable over the high-resolution monitoring period within the multi-solute BA+PAC+EA microcosm, the $M_{i_{(PAC)}}$ and $M_{i_{(aq)}}$ of *o*-xylene slightly increased on the PAC (from 2.36 mg on Day 310 to 2.73 mg on Day 333) and correspondingly decreased within the aqueous phase (from 2.03 mg on Day 310 to 0.70 mg on Day 333), respectively (see Figure B.6(h)). The shift in *o*-xylene mass between phases within the BA+PAC+EA microcosm occurred as the M_{i_T} of toluene decreased from 3.28 mg to 0.02 mg over the same monitoring period (see Figure B.6(f)), supporting partitioning of *o*-xylene to a greater

number of vacant sorption sites on the PAC as the mass of toluene was biodegraded and desorbed from the PAC.

Minimal change in the M_{i_T} of benzene occurred over the monitoring period from Day 0 to 350 in the multi-solute BA-PC+EA (3.56 mg on Day 2 to 3.08 mg on Day 350) or BA+PAC+EA (3.74 mg on Day 2 to 2.69 mg on Day 350) microcosms (Figure 3.9(a, d) and see Table B.8 for the M_{i_T} estimates of benzene over the 1-year monitoring period). The limited change in the M_{i_T} of benzene over the monitoring period suggests a lack of biodegradation potentially due to several reasons well documented within the literature, including: the absence of benzene degraders or other syntrophic microbes [188, 189]; the slow growth of benzene degraders and a lack of sufficient incubation time [188]; and/or the presence of other preferentially degrading solutes (e.g., T and X over B given the high energetic requirements for benzene ring cleavage [190, 191]) and the build up of metabolic by-products [54, 185, 154]. Given the recalcitrant nature of benzene, following the depletion in the M_{i_T} of toluene and *o*-xylene an extended 4-month monitoring period was provided for the multi-solute BA-PC+EA and BA+PAC+EA microcosms from Day 66 to 193 to observe if the biodegradation of benzene would initiate in the absence of the other solutes. During the extended monitoring period the aqueous and solid phase concentrations of benzene remained relatively stable in the multi-solute BA-PC+EA microcosm, indicating benzene was not biodegraded. Whereas in the BA+PAC+EA microcosm partitioning of benzene from the aqueous to the PAC phase occurred, given that a greater number of sorption sites were available to benzene in the absence of the other competing and preferentially sorbing solutes (i.e., *o*-xylene and toluene) [21, 29]. The partitioning behaviour of benzene in the multi-solute BA+PAC+EA microcosm is demonstrated in Figure B.8, which shows the aqueous and corresponding solid phase concentrations of benzene over Day 66 to 193 are positioned closer to the single-solute Freundlich isotherm for benzene (determined in Chapter 2) relative to all other timepoints before Day 66 or after Day 193. Therefore, during Day 66 to 193 the partitioning of benzene in the multi-solute system approached single-solute equilibrium conditions, but remained lower than the sorption isotherm potentially due to the reasons described in Section 3.3.1 in addition to some residual $M_{i_{(\mathrm{PAC})}}$ of toluene and *o*-xylene remaining on the PAC (see Table B.8 for the $M_{i_{(\mathrm{PAC})}}$ estimates of each solute). Following the second reamendment of toluene and *o*-xylene on Day 193 benzene partitioned again between phases, with the aqueous and corresponding solid phase concentrations more representative of multi-solute microcosm partitioning in the presence of toluene and *o*-xylene (Figure 3.2(b)). Given the limited evidence of benzene

biodegradation, the slight reduction in the M_{i_T} of benzene over the 1-year monitoring period may be associated with the same sources of mass loss as described for the KC and KC+PAC microcosms in Section 3.3.2.

The anaerobic biodegradation of toluene and *o*-xylene in the single-solute (Figure 3.8(b, e)) and multi-solute (Figure 3.9(b, e)) BA-PC+EA and BA+PAC+EA microcosms were coupled to sulfate reduction due to the reduction in the aqueous sulfate concentration three times. Specifically, in the single-solute BA-PC+EA and BA+PAC+EA microcosms the sulfate concentration was reduced to 5.2% and 22.1% of the total mass added (144.4 mg [Table 3.1]), respectively, by Day 292, and in the multi-solute BA-PC+EA and BA+PAC+EA microcosms the sulfate concentration was reduced to 0.4% and 7% of the total mass added (96.3 mg [Table 3.1]), respectively, by Day 350. The aqueous sulfide concentration also increased from < 4 µg/L prior to high-resolution monitoring (i.e., over Day 0 to 269 or 310 in the single- or multi-solute microcosms, respectively) to average concentrations of 53.3 ± 0.9 mg/L and 54.2 ± 30.3 mg/L in the single- and multi-solute microcosms, respectively, during high-resolution monitoring (i.e., from Day 269 to Day 292 in the single-solute microcosms or from Day 310 to Day 350 in the multi-solute microcosms). Prior to the high-resolution monitoring period, the low aqueous sulfide concentration was likely the result of an abiotic reaction between the generated sulfide (H_2S and HS^-) and ferric iron in the BS, forming black FeS precipitates [53, 54]. The formation of presumed FeS precipitates were observed in all single- and multi-solute BA-PC+EA and BA+PAC+EA microcosms over the 1-year monitoring period, as shown for a subset of sacrificial microcosm bottles in Figure B.9(a) on Day 278 (single-solute) or 319 (multi-solute) for the BA-PC+EA microcosms. In support of FeS formation a sulphuric odour emanated from the single- and multi-solute BA-PC+EA and BA+PAC+EA bottles when opened during each sacrificial sampling event. During high-resolution monitoring, the elevated sulfide concentrations were likely attributed to either the aqueous detection of sulfide prior to the precipitation reaction, or a depletion in free ferric iron within the BS preventing further FeS formation. During the high-resolution monitoring period, when only toluene was biodegraded as described above, the oxidation of toluene coupled to sulfate reduction was also verified from the mole ratios between toluene and sulfate (4.5 ± 0.3 moles) and sulfate and sulfide (1.1 ± 0.3 moles) in the single- and multi-solute BA-PC+EA and BA+PAC+EA microcosms (Table B.11), which were consistent with the theoretical ratios (Table B.7).

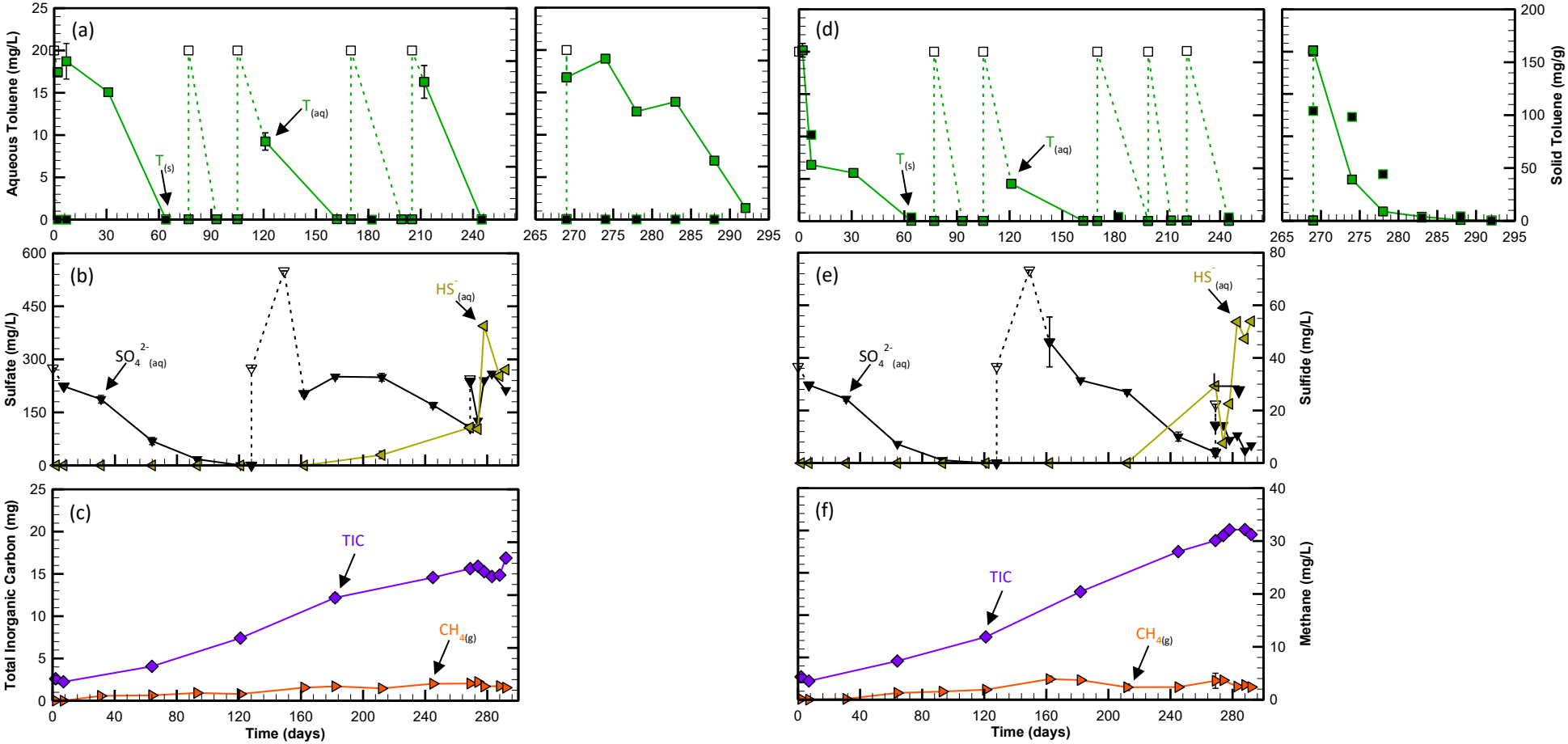

Figure 3.8: Temporal changes in the (a, d) aqueous and solid phase toluene concentrations ($T_{(aq)}$ and $T_{(s)}$) (green and black filled squares, respectively), (b, e) aqueous sulfate ($SO_4^{2-}{}_{(aq)}$) (black filled gradient symbols) and sulfide ($HS^-_{(aq)}$) (yellow filled left triangles) concentrations, and (c, f) total inorganic carbon (TIC) (purple filled diamonds) and gaseous methane concentration ($CH_{4(g)}$) (orange filled right triangles) for the single-solute (toluene-only) (a-c) BA-PC+EA and (d-f) BA+PAC+EA microcosms. Empty symbols and dashed lines represent target (non-measured) concentrations or trends, respectively. Each timepoint represents the average of three values and the error bars are ± 1 standard deviation.

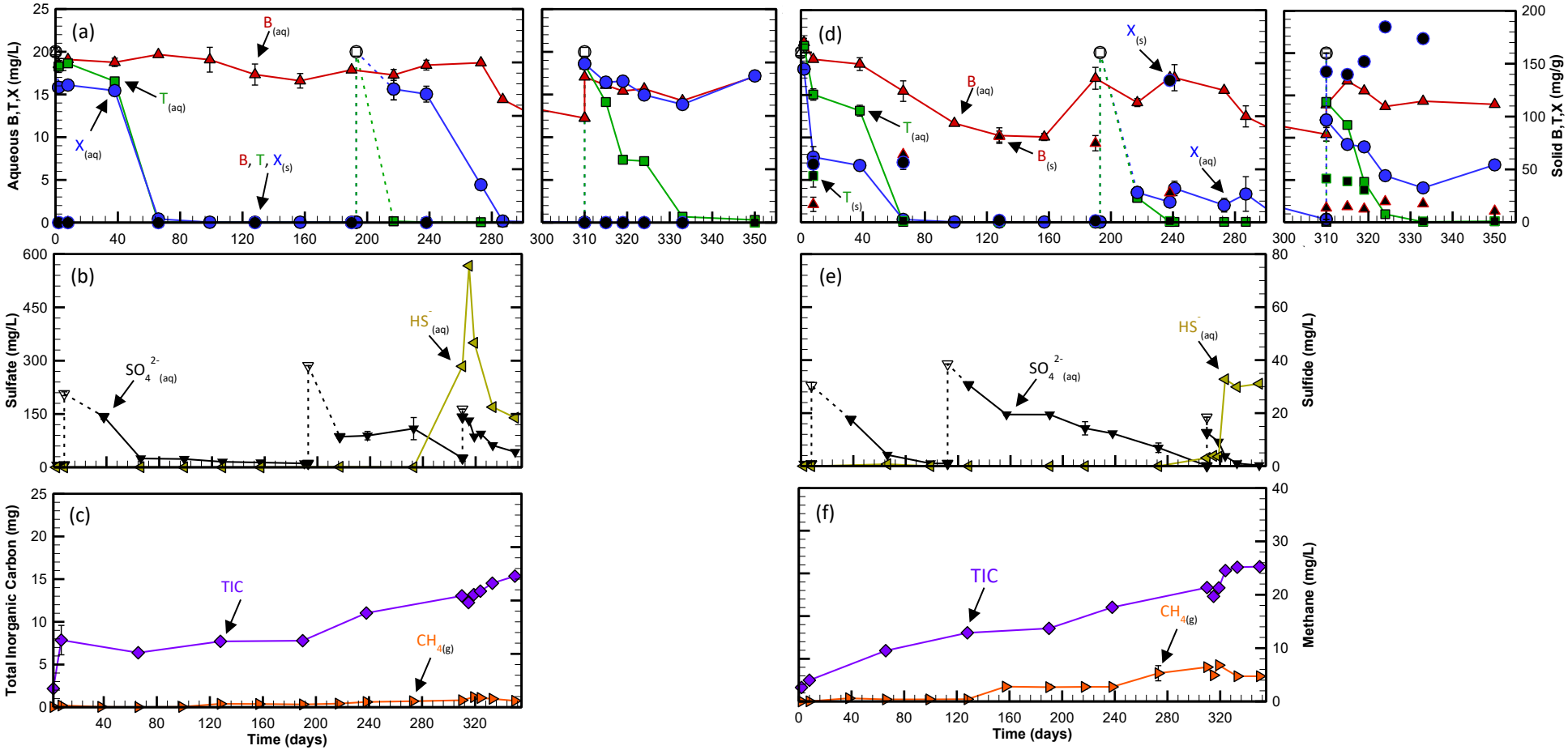

Figure 3.9: Temporal changes in the (a, d) aqueous phase benzene, toluene and *o*-xylene (BTX) ($B,T,X_{(aq)}$) (red filled triangle [B], green filled squares [T] and blue filled circles [X]) and solid phase BTX ($B,T,X_{(s)}$) (black filled triangles [B], squares [T] and circles [X]) concentrations, (b, e) aqueous sulfate ($SO_4^{2-}{}_{(aq)}$) (black filled gradient symbols) and sulfide ($HS^-_{(aq)}$) (yellow filled left triangles) concentrations, and (c, f) total inorganic carbon (TIC) (purple filled diamonds) and gaseous methane concentration ($CH_{4(g)}$) (orange filled right triangles) for the multi-solute (BTX) (a-c) BA-PC+EA and (d-f) BA+PAC+EA microcosms. Empty symbols and dashed lines represent target (non-measured) concentrations or trends, respectively. Each timepoint represents the average of three values and the error bars are ± 1 standard deviation.

Between the single-solute (Figure 3.8(c, f)) and multi-solute (Figure 3.9(c, f)) BA-PC+EA and BA+PAC+EA microcosms, the average mass of TIC increased from 2.3 ± 0.5 mg to 16.6 ± 2.7 mg over the 1-year monitoring period as by-products of toluene and *o*-xylene oxidation (Table B.7). Contrary to the BA-PC and BA+PAC microcosms (described in Section 3.3.3), minimal CH_4 was generated (i.e., increasing from 0.06 ± 0.06 to 4 ± 2 mg/L) between the single- and multi-solute BA-PC+EA and BA+PAC+EA microcosm over the 1-year monitoring period indicating that methanogenesis was limited under sulfate-reducing conditions, as expected [65, 192, 66, 69]. The average DO concentrations remained consistently low (< 1 mg/L) and the average ORP gradually decreased from -179.6 ± 24.8 mV to highly reduced conditions of -380.2 ± 13.1 mV between all single- and multi-solute BA-PC+EA and BA+PAC+EA microcosm over the 1-year monitoring period. The average pH within all single- and multi-solute BA-PC+EA and BA+PAC+EA microcosm slightly increased from neutral (7.3 ± 0.03) to alkaline conditions (8.1 ± 0.2) (Figure B.5(c-d, g-h), potentially due to a hydrolysis reaction between the sulfide formed (predominating as HS^- at pH 8) and water generating hydroxyl ions (OH^-) (i.e., $HS^- + H_2O \rightleftharpoons H_2S + OH^-$ [193]). Collectively, there appears to be minimal difference in the long-term geochemical behaviour between the single-solute (Figure 3.8(b-c, e-f) and Figure B.5(c-d)) and multi-solute (Figure 3.9(b-c, e-f) and Figure B.5(g-h)) BA-PC+EA and BA+PAC+EA microcosms, indicating that that the presence of PAC in the BA+PAC+EA microcosms had limited influence on the microbial activity within the EA amended microcosms relative to the BA-PC+EA microcosms.

The qPCR data show an enrichment in the average abundance of total archaea between the single- and multi-solute BA-PC+EA ($4.2 \times 10^{+5} \pm 1.5 \times 10^{+4}$ copies/g) and BA+PAC+EA ($1.2 \times 10^{+6} \pm 9.6 \times 10^{+5}$ copies/g) microcosms relative to background conditions ($3.9 \times 10^{+4} \pm 7.7 \times 10^{+3}$ copies/g) (Figure 3.3(a, b) and see Table B.6 for the qPCR data for the single- and multi-solute microcosms). The NGS data shows, between single- and multi-solute BA-PC+EA (0.9 ± 0.8%) and BA+PAC+EA (3.6 ± 0.2%) microcosms *Methanomethylovorans* were enriched, and in the multi-solute BA+PAC+EA (2.4%) microcosm the genus *Methanobacterium* were enriched relative to background conditions (0.0%) (Figure 3.4(a-c) and Figure 3.5(a-c) and see Table B.9 for the NGS data for the single- and multi-solute microcosms). Relative to the single and multi-solute BA+PAC microcosm (described in Section 3.3.3), less archaeal enrichment occurred in the single- and multi-solute BA-PC+EA and BA+PAC+EA microcosms which is likely attributed to the inhibition of substantial methanogenesis under sulfate reducing conditions [65, 192, 66, 69].

The qPCR data show minimal enrichment in the abundance of total bacteria in the single-solute ($8.8 \times 10^{+6} \pm 3.9 \times 10^{+6}$ copies/g) and multi-solute ($2.5 \times 10^{+7} \pm 3 \times 10^{+6}$ copies/g) BA-PC+EA and BA+PAC+EA microcosms relative to background ($5.2 \times 10^{+6} \pm 2.9 \times 10^{+6}$ copies/g). However, *Desulfosporosinus,* whose members are SRB associated with PHC biodegradation [194, 195, 162, 196], was highly enriched in the multi-solute BA-PC+EA and BA+PAC+EA microcosms ($4.8 \times 10^{+6} \pm 1.8 \times 10^{+6}$ copies/g) relative to background ($4.9 \times 10^{+4} \pm 3.3 \times 10^{+4}$ copies/g) (Figure 3.3(a, b) and see Table B.6 for the qPCR data for the single- and multi-solute microcosms). Enrichment of *Desulfosporosinus* in the multi-solute BA-PC+EA and BA+PAC+EA microcosms is supported by the NGS data (9.7 ± 4.3% versus 0.06% [average background relative abundance]) (Figure 3.5(a-c)). The higher enrichment of this SRB within the multi-solute microcosms relative to the single-solute microcosms may indicate this bacterial lineage was more involved in *o*-xylene biodegradation as opposed to toluene. Other SRB detected in both the single-solute (Figure 3.4(a-c)) and multi-solute (Figure 3.5(a-c)) BA-PC+EA and BA+PAC+EA microcosms relative to background (≤ 0.05%), include the genera *Desulfoprunum* (25.4 ± 6.8%) and *Desulfatirhabdium* (4.4 ± 2.3%) [197] from the phylum Desulfobacterota. SRB enriched in only the single-solute BA-PC+EA and BA+PAC+EA microcosms relative to background conditions (0.0%), include several families from the phylum Desulfobacterota comprised of Desulfobacteraceae (12.4 ± 5.2%), which contain metabolically versatile bacteria [198, 199], Desulfocapsaceae (3.3 ± 2.7%) and Desulfosarcinaceae (4.1% [BA+PAC+EA only]) [166] (see Table B.9 for the NGS data for the single- and multi-solute microcosms). The high enrichment of SRB between the single- and multi-solute BA-PC+EA and BA+PAC+EA microcosms supports sulfate reduction dominating within the EA amended microcosms. However, given the limited difference in the enrichment of SRB between the single and multi-solute BA-PC+EA microcosms relative to the BA+PAC+EA microcosms the presence of the PAC appears to have had limited influence on the microbial activity (supported by the limited difference in geochemical parameters between microcosms, as described above).

3.4 Conclusion

Following PAC amendment to the single-solute (toluene-only) and multi-solute (BTX) KC+PAC, BA+PAC and BA+PAC+EA microcosms, rapid reductions in the aqueous phase toluene or BTX concentrations and corresponding increases in the solid phase concentrations were evident due to partitioning. The magnitude of toluene sorption to the PAC was greater in the single-solute microcosms relative to the multi-solute microcosms, and the magnitude of the multi-solute sorption followed X > T >

B due to the difference in chemical properties between solutes and competitive sorption (consistent with the results described in Chapter 2).

The directly measured aqueous and solid phase toluene concentrations from the single-solute KC+PAC, BA+PAC and BA+PAC+EA microcosms were compared to the single-solute Freundlich isotherm (determined in Chapter 2). Similarly, the directly measured aqueous and solid phase benzene, toluene and *o*-xylene concentrations from the multi-solute KC+PAC, BA+PAC and BA+PAC+EA microcosms were compared to the ISIAS model predicted solid phase concentrations. Both the single- and multi-solute Freundlich and ISIAS models, respectively, overestimated the equilibrium sorption of toluene or BTX to the PAC in the microcosm systems. Difference between the single-and muti-solute sorption isotherms and the microcosm data may be due to several factors such as differences in equilibrium times caused by variation in mixing conditions between systems, differences in solution matrix chemistries between systems (e.g., ionic strength), interferences (e.g., competition) caused by other sorbing components within the microcosm system that are absent from the isotherm systems (e.g., metabolites generated from anaerobic biodegradation), and/or the influence of a potential biofilm layer surrounding the PAC particles (causing diffusional resistance or pore filling of EPSs that may limit solute sorption). Specifically, for the multi-solute PAC amended microcosms *o*-xylene deviated the most from the ISIAS model predicted solid phase concentrations followed by toluene and then benzene, which is attributed to difference in the magnitude of sorption between solutes (i.e., following X > T > B).

Over the 1-year monitoring period evidence of methanogenesis coupled to a background substrate (other than substantial toluene or BTX mass) was evident from the geochemical (i.e., CH_4 production) and molecular (i.e., archaeal enrichment) data within the sulfate-limited (i.e., 10-20 mg/L SO_4^{2-}) single- and multi-solute SC, BA-PC and BA+PAC microcosms. Between the single- and multi-solute BA-PC (and SC) and BA+PAC microcosms the CH_4 concentrations and archaeal enrichment (including *Methanomethylovorans*, *Methanosaeta* and *Methanobacterium*) were consistently higher in the BA+PAC relative to the BA-PC (and SC) microcosms without PAC, which supports the presence of PAC providing support for methanogenesis and archaeal growth (e.g., through AC mediated DIET).

Contrary to the SC, BA-PC and BA+PAC microcosms, within the EA amended (i.e., 138-275 mg/L SO_4^{2-}) single- and multi-solute BA-PC+EA and BA+PAC+EA microcosms sulfate reduction was coupled to the oxidation of toluene, evidenced by the repetitive reduction in toluene and the geochemical (i.e., SO_4^{2-} reduction, and HS^- and TIC formation) and molecular (i.e., enrichment of SRB, including *Desulfosporosinus*, *Desulfoprunum* and Desulfobacteraceae) data. In the multi-solute EA amended BA-

PC+EA and BA+PAC+EA microcosms, *o*-xylene (not benzene) was additionally biodegraded following toluene (due to the preferential biodegradation of toluene over *o*-xylene). Between the single- and multi-solute PC+EA and BA+PAC+EA microcosms the total mass of toluene was repetitively reduced by ≥ 92.4% within 12 to 66 days, and in the single- and multi-solute BA+PAC+EA microcosms the PAC was regenerated multiple times as shown by the repetitive reduction in the solid phase mass of toluene by ≥ 95.5%. The reduction in the solid phase concentration of toluene is attributed to the continual desorption of toluene during anaerobic biodegradation and confirms that the AC sorption of toluene is almost entirely reversible with bioactivity. Although toluene and *o*-xylene were anaerobically biodegraded within the single- and multi-solute BA-PC+EA and BA+PAC+EA microcosms over the 1-year monitoring period, there was no substantial difference in the PHC, geochemical or molecular data between the microcosms indicating that from the parameters monitored the presence of the PAC (in the BA+PAC+EA microcosms) did not influence the anaerobic microbial activity relative to the microcosms without PAC (the BA-PC+EA microcosms). In support of the limited difference in microbial activity over the 1-year monitoring period, the zero-order rate constants for toluene during high-resolution monitoring showed no difference between the single- and multi-solute BA-PC+EA and BA+PAC+EA microcosms which indicates that the presence of PAC did not enhance the anaerobic biodegradation of toluene within the BA+PAC+EA microcosms relative to the BA-PC+EA microcosms. Collectively the assembled data over the 1-year monitoring period shows that the presence of PAC did not generate any discernible differences in the anaerobic biodegradation of toluene between the EA amended bioactive microcosm with and without PAC.

Chapter 4

Anaerobic biodegradation of benzene, toluene and *o*-xylene in powdered activated carbon particulate amended aquifer material – Column study

4.1 Introduction

The combination of activated carbon (AC) sorption and biodegradation has been applied to various water treatment technologies, including biological AC (BAC) fluidized or flow-through reactors for application in wastewater treatment [36, 100, 101, 38, 39], and permeable reactive barriers (PRBs) or biobarriers (BBs) for application in groundwater treatment [104, 105, 106]. These technologies operate similarly as compared to an injected AC PRB for groundwater treatment [102, 103], involving the rapid reduction in contaminant concentrations due to sorption followed by biodegradation to regenerate sorption sites (discussed in Section 1.1.3). One of the primary benefits of the combined use of AC sorption and biodegradation pertains to the consistently reduced or stabilized depletion in contaminant concentrations under variable contaminant loading conditions due to enhanced sorption relative to systems with only biodegradation (showing higher effluent concentrations) [36, 100, 101, 37]. Although this is well known, the degree to which the microbial activity is influenced due to the presence of the AC and relative to unamended anaerobic groundwater system without AC is uncertain.

To investigate if a powdered AC (PAC) zone installed in aquifer material influences the anaerobic biodegradation of benzene, toluene and *o*-xylene (BTX) in groundwater relative to systems without PAC, a series of simplified single-solute (toluene-only) and more complex multi-solute (benzene, toluene and *o*-xylene [BTX]) column experiments were conducted. Column types included columns with only a PAC zone to track sorption behaviour in the absence of anaerobic biodegradation, bioactive columns without a PAC zone to track anaerobic biodegradation behaviour in the absence of sorption, and bioactive columns with a PAC zone to track the combination of sorption and anaerobic biodegradation relative to sorption or bioactivity alone. Columns were assembled and monitored under sulfate reducing and methanogenic conditions, which are representative of the reducing conditions where a PAC zone may be installed below the vadose zone at the mature petroleum hydrocarbon (PHC) contaminated site. The columns were monitored for 2 years to show long-term trends in multiple parameters, including aqueous and solid phase PHCs (toluene as a single-solute, or BTX combined), aqueous phase geochemical

parameters (primarily sulfate, sulfide, dissolved inorganic carbon [DIC] and methane [CH_4]), molecular biomarkers through solid phase analysis (i.e., deoxyribonucleic acid [DNA] analysis using quantitative polymerase chain reaction [qPCR] and next generation sequencing [NGS]) and isotopes through aqueous phase analysis (i.e., carbon and/or hydrogen isotopes for DIC and BTX using compound specific isotope analysis [CSIA]). To assess if the PAC zone influenced microbial activity during PHC biodegradation within the bioactive column with a PAC zone, relative to the columns with only bioactivity or a PAC zone, changes in the PHC, geochemical and molecular data were compared between columns. Additionally, to investigate how the bioactive column with a PAC zone, relative to the columns with only bioactivity or a PAC zone, responded to changes in PHC loading a series of step increases in influent PHC concentrations were carried out and any changes in the effluent for the aqueous parameters monitored were compared between columns. Finally, given evidence of fractionation due to abiotic processes such as sorption have been reported [86, 87, 88, 89] (as discussed in Section 1.1.2.1), shifts in the isotopes of the PHCs were compared between the bioactive column with a PAC zone relative to the columns with only a PAC zone or bioactivity to understand if CSIA can distinguish biodegradation from AC sorption in bioactive systems. Collectively, the AC sorption and anaerobic biodegradation behaviour between the single-solute (toluene-only) and multi-solute (BTX) columns was used to provide evidence to support how the presence of AC impacts the long-term behaviour and monitoring of anaerobic PHC biodegradation in AC PRB systems relative to systems without AC.

4.2 Materials and methods

The chemicals (i.e., BTX, AGW, sodium sulfate stock solution and biocide) and aquifer material (i.e., Borden sand [BS]) used during the column experiments are described in Section 2.2 and 3.2, with some amendments, including the omission of the amorphous ferrous sulfide (FeS) stock solution from the AGW (i.e., step 5 and 11 in Appendix B.1), and only sodium azide used for a biocide (no mercuric chloride). The BS was collected 307, 333 and 336 days prior to use in the single-solute (toluene only) and multi-solute (BTX) columns with only a PAC zone, only bioactivity, or a PAC zone and bioactivity, respectively, and stored in the dark at 4ºC until use (a detailed description of the Borden aquifer, and the methodologies associated with collecting and handling the aquifer material is described in Section 3.2 and listed in Table B.1).

4.2.1 Column description

To address research Questions 2, 5 and 6 (Section 1.2) three types of single-solute (toluene-only) and multi-solute (BTX) columns were constructed, including: killed controls with a PAC zone (KC+PACz) to account for sorption to aquifer material or PAC in the absence of biodegradation, bioactive positive controls (BA-PC) without a PAC zone to account for anaerobic biodegradation of PHCs in the absence of PAC, and bioactive columns with a PAC zone (BA+PACz) to account for anaerobic biodegradation of PHCs in the presence of PAC (see Table C.1 for the experimental design).

Acrylic columns (37 cm length × 3.75 cm inner diameter [ID]) were packed in an anaerobic glove bag (Sigma-Aldrich, St. Louis, MO, USA) with a N_2 atmosphere using sterile equipment. The influent (bottom) end of each column was first sealed with an acrylic end cap that was laser cut with orb web shaped indentations on the interior face to distribute fluid flow. End caps were fit with rubber O-rings (Sigma-Aldrich, St. Louis, MO, US), and fastened to the columns using six thumbscrews and nuts. Prior to loading BS within the columns, enclosure materials were placed directly adjacent to the interior face of the installed influent end cap by spreading the material with an acrylic rod that extended the entire length of the column. The enclosure material included a circular large mesh (U.S. mesh 20) stainless steel (SS) screen (~3.7 cm diameter), followed by a layer of evenly spread glass wool, and another circular fine mesh (U.S. mesh 80) SS screen (~3.7 cm diameter) (Sigma-Aldrich, St. Louis, MO, USA) all used to assist with even flow distribution and to prevent fines in the BS from migrating out of the columns. The BA-PC and BA+PACz columns were then packed with 875.3 ± 35.8 g of BS in 1 cm increments by thoroughly compacting each layer with the acrylic rod. In the central region of the BA+PACz columns a PAC zone extending 14 to 20 cm (6 cm length) from the influent end was emplaced to mimic a reactive PAC barrier. The PAC zone was comprised of 0.5% wt/wt of WPC PAC thoroughly homogenized with the BS under anaerobic conditions. The PAC loading was selected based on estimated ideal PHC breakthrough times (see Appendix C.1 for the equation used) to ensure that the columns with PAC zones would not be sorption dominated during monitoring (i.e., non-detect of PHCs in the column effluent). During BA-PC and BA+PACz column packing several subsamples of the BS were collected for PHC and DNA analysis using qPCR, following the sampling and analytical methodologies described in Section 3.2.2 and 3.2.3, respectively. The DNA and PHC samples collected during column packing were used to determine if any PHCs were initially present in the BS (see Section 3.2 for details pertaining to the PHC contamination at the site of BS collection) and to characterize the background microbial population within the BS. Prior to packing the

KC+PACz columns 1.5 kg of moist BS was autoclaved three times on three consecutive days for 15 min at 121˚C. Following autoclaving the mass of water removed during autoclaving (i.e., 16% volumetric water content) was added back to the dry BS as deoxygenated Milli-Q water in an anaerobically glove bag. The moist sterile BS was then packed into the KC+PACz columns (862.7 ± 12.8 g) following the same methodology as described for the BA+PACz columns. Once packed, the same enclosure materials that were placed at the influent (bottom) ends of each column were placed at the effluent (top) ends of each column directly adjacent to the packed BS. Each column was then sealed with effluent end caps, as described for the influent ends. The exterior sides of the influent and effluent end caps were fit with 316 SS fittings (SS-200-1-OR) (Swagelok, Solon, OH, USA) that were attached to 10 cm (influent end) and 80 cm (effluent end) lengths of 1.6 mm ID non-transparent SS tubing (used to prevent direct light exposure and limit microbial colonization inside the tubing). Prior to moving the columns to the bench-top for operation, the open ends of the influent and effluent SS tubing were temporarily sealed to prevent O_2 exposure to the BS, and the exterior of the columns were wrapped in aluminum foil to limit direct light exposure.

Once positioned on the benchtop, the influent SS tubing was connected to the Luer-slip outlet base of a 25 mm SS microsyringe filter holder (MilliporeSigma, Burlington, MA, USA) with 3 cm of 1.42 mm ID non-transparent flexible Viton tubing (Cole-Parmer, Vernon Hills, IL, USA). The SS filter holder was equipped with a polytetrafluoroethylene (PTFE) flat gasket, followed by a SS support screen, a 25 mm 0.22 µm nylon filter (Ezflow, Fox Life Sciences, Londonderry, NH, USA) and a PTFE O-ring which were held in place by fastening the Luer-Lok inlet cover of the SS filter holder to the Luer-slip outlet base. The inlet cover of the SS filter holder was attached to 30 cm of SS tubing which connected to the outlet of a 3-way SS ball valve (SS-41GXS2) (Swagelok, Solon, OH, USA). The ball valve was equipped with a sampling port lined with rubber septum, which served as the influent sampling port. The inlet of the SS ball valve was attached to a 170 cm length of SS tubing which fed into Masterflex L/S Viton pump tubing (RK-96428-14) at the outlet end of a Masterflex L/S® peristaltic pump (Cole-Parmer, Vernon Hills, IL, USA). The inlet end of the pump tubing was attached to a second SS filter holder, which was connected to an 80 cm length of SS tubing. The 80 cm length of SS tubing was fastened to the SS fitting on the inlet of a dedicated sterile 10 L Tedlar sampling bag (SKC Inc., Eighty Four, PA, USA) which was used to contain the influent source of anaerobic AGW.

At the effluent ends of each column, the 80 cm length of SS tubing was attached to the inlet of a second 3-way SS ball valve which served as the effluent sampling port. The outlet of the SS ball valve was attached to a 70 cm length of SS tubing which was connected to the inlet cover of a third 25 mm SS filter

holder. The outlet of the SS filter holder was attached to a 10 cm length of SS tubing which fed into a rubber stopper enclosing the opening of 1 L Erlenmeyer glass flask (Corning Life Sciences, Corning, NY, USA) which served as containment for effluent waste collection. In-line connections for all columns were made with SS fittings on the exterior faces of the end caps or to the 3-way ball valves or 3 cm non-transparent flexible Viton tubing for all other connections. Figure 4.1 shows a schematic of the column set-up in up-flow mode, and Figure C.1 shows an image of the column set-up for the single- and multi-solute KC+PACz columns.

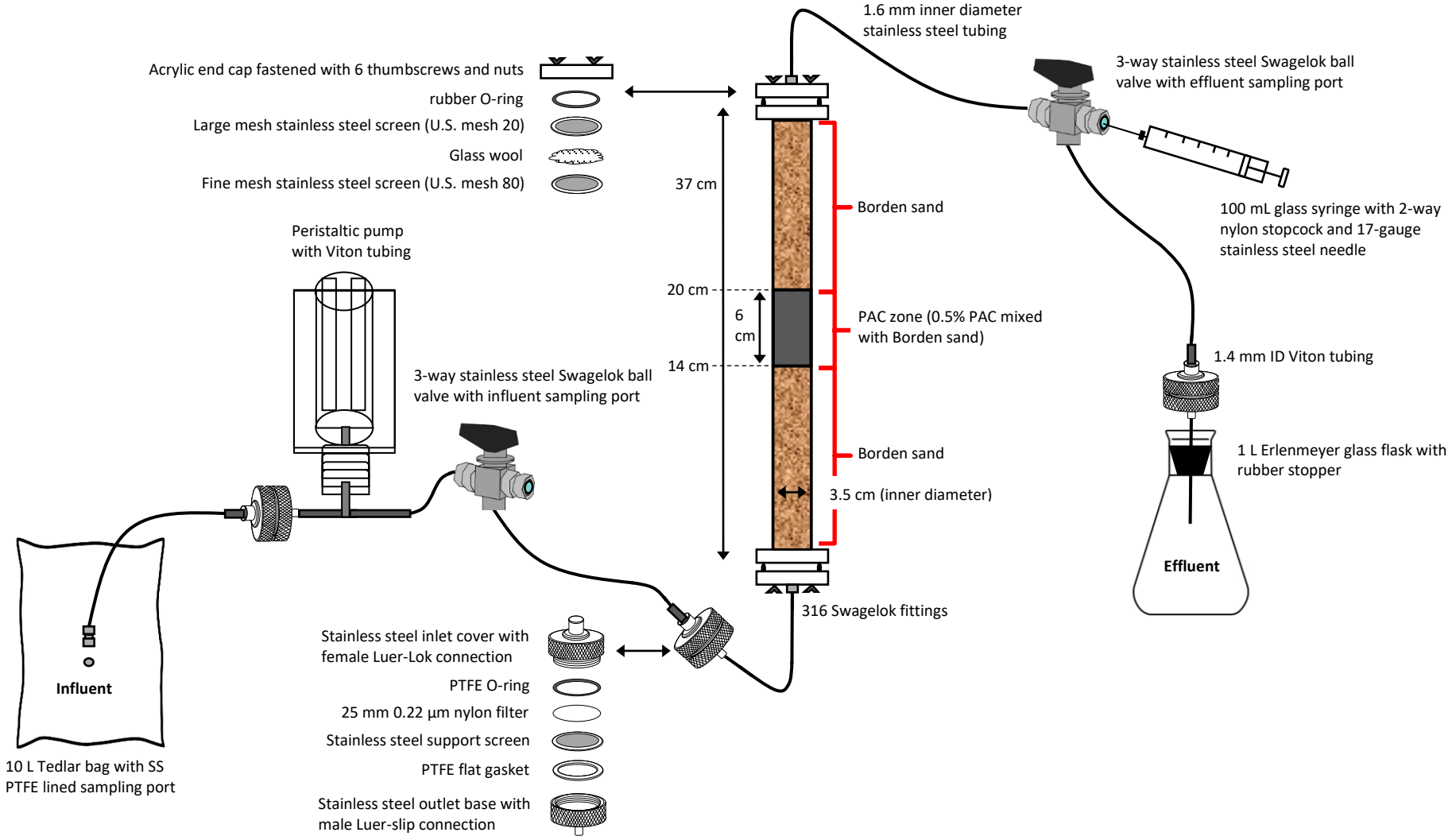

Figure 4.1: Schematic of the column set-up in up-flow mode for a column with an installed powdered activated carbon (PAC) zone.

Prior to column operation a bromide tracer test was performed to determine the effective porosity. An anaerobic sodium bromide solution (1000 mg/L) was pumped into a dedicated sterile 10 L Tedlar bag as the influent solution. The test was performed at a flow rate of 1 mL/min with 25 mL of solution fed into each column as a pulse followed by anaerobic AGW, and 19 samples per column were collected over 3 hours. The column porosities of each column were similar (0.29 ± 0.027 [Table C.2]), suggesting that the hydraulic behaviour would also be similar.

4.2.2 Operation

Influent anaerobic AGW was prepared in 8-9 L batches following the recipe listed in Appendix B.1 with the omission of the FeS stock solution from the AGW (i.e., step 5 and 11 in Appendix B.1, as described in Section 4.2) to prevent FeS precipitates from obstructing the in-line filtration system. Following preparation of the AGW, the solution was stored in a mixing vessel housed within an N_2 filled glove bag. The glove bag was connected to a 2 m length of 1.57 mm ID Teflon tubing that was installed through a port located on the side of the bag. Within the glove bag the Teflon tubing was fed inside the AGW mixing vessel, extending to the bottom of the solution, and outside of the glove bag the Teflon tubing was connected in-line to the influent side of a peristaltic pump. The effluent side of the peristaltic pump was then connected to the SS inlet valve of a sterile dedicated Tedlar bag, and once connected the anaerobic AGW was pumped from the mixing vessel into the Tedlar bag. Once the Tedlar bag was filled with AGW, amendments were made (depending on the column requirements) by injection through the SS PTFE lined sampling port. For the single- or multi-solute columns pure phase analytical grade toluene or BTX (1:1:1 concentration ratio), respectively, were added to the AGW using a sterile glass microliter syringe (Hamilton, Reno, NV, USA), and sodium sulfate (using the stock solution listed in Appendix B.1) was added to the AGW using a disposable plastic syringe equipped with a luer-lock fitting (Air-Tite, Virginia Beach, VA, USA) and attached to a 22-gauge needle (Exel Int., USA) (injection volume was variable and dependent on the AGW volume and the desired solution concentration). The KC+PACz columns were also amended with 2.5 mL of a 5% sodium azide solution per L of AGW using a disposable plastic syringe equipped with a luer-lock fitting and attached to a 22-gauge needle. Following amendments to the transparent Tedlar bags, each bag was covered with a non-transparent black plastic sheet to limit direct light exposure and agitated on a platform shaker (Barnstead Thermolyne, Dubuque, IA, USA) for one day at ~10 rotations per minute (RPM) to ensure a well-mixed solution.

Columns were operated for a 1-year (Year-1) acclimation period at nominal flow rates ranging between 0.02 mL/min (equivalent to 0.2-0.3 pore volumes per day) and 0.8 mL/min (equivalent to 8.3-11.1

pore volumes per day). Following the Year-1 acclimation period, the nominal flow rate of 0.02 mL/min was maintained for an additional year (Year- 2). The flow rates during Year-1 and Year-2 were measured for each column from the volume of effluent solution collected in dedicated 1 L Erlenmeyer glass flasks. During Year-2 the influent toluene and BTX (1:1:1) concentrations (as the electron donors) were sequentially adjusted in a stepwise manner from a target concentration of 5 mg/L per solute to 10 mg/L per solute and then to 20 mg/L per solute to investigate how the columns respond to variable PHC loading. Similarly, the sulfate concentration (as an electron acceptor [EA]) was increased from a target concentration of 5 mg/L to 20 mg/L and then to 30 mg/L (see Table C.1 for the experimental design).

4.2.3 Sample collection and analyses

All columns were sampled from the influent and effluent 3-way SS ball valves by temporarily shifting the flow direction of the sampling ports shown in Figure 4.1 and Figure C.1. Samples were collected in dedicated 100 mL glass sampling syringes (Cadence Science, Cranston, RI, USA), equipped with 2-way nylon stopcocks (Masterflex, Gelsenkirchen, NRW, DE) attached to 5.1 cm 17-gauge SS needles (Ace Glass, Vineland, NJ, US) which were inserted into the rubber septa of the sampling ports. During sample collection, the syringe barrels were positioned vertically on plexiglass stands with the 2-way stopcocks temporarily positioned open which allowed the plungers to slowly lift as the total sample volume was anaerobically collected (Figure C.1). Influent and effluent samples were collected with the intention of sampling the same pore volume (PV) of AGW, and therefore effluent samples were collected 3-4 days (representing 1 PV when accounting for the residence time) following the influent samples (Table C.2). Given that the influent sampling ports are positioned before the columns, influent samples were collected at a temporarily increased flow rate of 0.4 mL/min (versus 0.02 mL/min for effluent samples).

Year-1 aqueous phase influent and effluent sample collection included toluene or BTX (2 mL) only. Whereas during Year-2 aqueous phase influent sample collection (25 mL of AGW) was comprised of several parameters, including, toluene-only or BTX (2 mL); sulfate, dissolved oxygen (DO), pH and the oxidation reduction potential (ORP) (5 mL); sulfide (10 mL); DIC (3.5 mL); and CH_4 (4.5 mL). Aqueous phase effluent sample collection (45 mL of AGW) included all influent sampling parameters (25 mL) in addition to the carbon and/or hydrogen isotopes for benzene, toluene, *o*-xylene and DIC (i.e., δ^{13}C-B,T,X; δ^{2}H-B,T,X; and δ^{13}C-DIC) (20 mL). Subsamples of the pure phase BTX injected into the

Tedlar bags as described in Section 4.2.2 (~5 mL) and the $NaHCO_3$ used in the AGW recipe (Appendix B.1, step 4.) (~5 g) were submitted for the same isotope analysis as the effluent isotope samples to determine the carbon and hydrogen isotope signatures of BTX and similarly the signature of the DIC in the influent AGW solution. Following sample collection, the total sample volume was dispensed into designated vials for each parameter being analyzed; however, the sample for sulfate, DO, pH and ORP were left in the sealed sampling syringes and transported into an anaerobic glove bag for analysis. The remainder of the methodologies associated with sample collection or sample preparation prior to analysis, in addition to the analytical methods for toluene-only or BTX, sulfate, ORP, pH, DO, sulfide and DIC are described in Section 3.2.2 and 3.2.3.

Samples for aqueous CH_4 were collected in 4 mL (Thermoscientific, Rockwood, TN, USA) glass screw top vials preloaded with 1% of a 5% sodium azide stock solution and sealed with Teflon lined silicon septa screw caps. Aqueous CH_4 samples were drawn into 10 mL gas tight sampling syringes with luer-lock fittings (Sigma Aldrich, St. Louis, MO, USA), equipped with a 1-way polycarbonate stopcock and a 22-gauge disposable needle. The samples were then diluted with purified helium, shaken vigorously by hand and left to equilibrate for 1 hour prior to analysis by gas chromatography (GC). Analytical methods for CH_4 analysis are described in Section 3.2.3.

Isotope samples were collected in 20 mL (Sci Spec, Hanover, MD, USA) glass screw top vials preloaded with 1% of a 5% sodium azide stock solution and sealed with Teflon lined silicon septa screw caps. Compound specific carbon and hydrogen isotope ratios of BTX were determined using a purge and trap thermal desorption system coupled to a GC-C-IRMS. Samples were manually injected into a CDS 7000 (CDS Analytical LLC, Oxford, PA, US) sparger vessel and purged with helium for 10 minutes. The trap was then heated to 300ºC, and analytes were separated by a DB 624 GC column on a Trace GC (Thermo Finnigan, Millan Italy). The GC temperature program was set to 35ºC for 2 min, then 80ºC at 15ºC/min and 120ºC at 20ºC/min. Analytes were combusted in a GC–Combustion III interface operating at 1450°C for ^{2}H or 940°C for ^{13}C, and isotope ratios were measured on a Thermo Finnigan Delta XP Plus XP isotope ratio mass spectrometer (Thermo Finnigan, Bremen, Germany) (5‰ VSMOW precision for $\delta^{2}H$ and 0.3‰ VPDB precision for $\delta^{13}C$). For $\delta^{13}C$-DIC samples, an aliquot of sample equivalent to 0.2 mg of carbonate was removed through the septum of the sample vial and injected into a helium filled 12 mL Labco Exetainer vial preloaded with 0.5 mL of 85% phosphoric acid (H_3PO_4). The vial was then shaken to catalyze a reaction between the DIC and H_3PO_4 and left to equilibrate for 3 hours to convert the

DIC to CO_2 in the headspace. Samples were transferred to a CTC PAL autosampler and analyzed by a Delta V Plus isotope ratio mass-spectrometer (IRMS) with Gasbench as a peripheral (Thermo-Finnigan, Bremen, Germany) (0.2‰ VPDB precision).

To determine the spatial distribution of solid phase toluene or BTX and DNA at the end of Year-2 the BA-PC and BA+PACz columns were subsampled from top to bottom in an anaerobic glove bag. For the BA-PC columns, five 2-cm thick increments of BS spaced 4 to 5 cm apart were subsampled, extending 3-5, 9-11, 16-18, 23-25 and 29-31 cm from the bottom (or influent end) of the column. For the BA+PACz columns, the PAC zone was subsampled at a higher frequency compared to outside of the PAC zone, where six 1-cm thick increments were subsampled along the length of the PAC zone, extending 14-20 cm from the bottom of the column. Adjacent to the PAC zone, two 2-cm think increments were subsampled, extending 11-13, 13-14, 20-21 and 21-23 cm from the bottom of the column. Away from the PAC zone, three 2 to 3 cm thick increments spaced 1 cm apart were subsampled, extending 1-4, 5-7, 8-10, 24-26, 27-29 and 33-36 cm from the bottom of the column. Each increment contained 20 to 60 g of BS (and PAC for the BA+PACz column) (i.e., 20 g/ cm increment), which was first manually homogenized with a sterile SS sampling spoon and then subsampled for toluene or BTX and DNA analyses. For a toluene or BTX sample, 5 g of solids was placed in a 20 mL glass screw top vial (Sci Spec, Hanover, MD, USA), and 4 mL of DCM (containing the internal standards *m*-fluorotoluene and 2-fluorobiphenyl (25 mg/L)) was added. The vials were then sealed with a Teflon lined silicon septa screw cap, shaken vigorously by hand for several minutes and vented. The remainder of the methodology associated with sample preparation prior to toluene or BTX analysis (i.e., sample shaking and extract transfer to autosampler vials) is detailed in Section 2.2.2. For a DNA sample, 2 to 5 g of solids were placed in a 50 mL plastic screw top Eppendorf tube and sealed with a plastic cap, then immediately frozen at -80ºC. Details pertaining to the analytical methodologies associated with solid phase toluene or BTX and DNA analyses are described in Section 2.2.2 and 3.2.3.

Solid phase DNA samples for NGS were unintentionally contaminated during sample extraction from the DNA extraction kits used. To address the sample contamination all amplicon sequence variants (ASVs) present in the extraction black (Eblank) samples were removed, assuming any ASVs in the Eblanks were likely contaminants from the DNA extraction kits. Thirty (30) ASVs representing common contaminants were removed; however, sample contamination may have remained. See Table C.3 for the 30 ASVs removed and the relative abundance per sample prior to ASV removal.

4.3 Results and discussion

During the Year-1 acclimation period the average measured flow rate between single- and multi-solute columns varied from 0.017 ± 0.006 to 0.76 ± 0.12 mL/min. Higher flow rates during Year-1 were used to induce breakthrough in the KC+PACz and BA+PACz columns, while lower flow rates were used during column maintenance or to address design tweaks (e.g., mixing of influent AGW solutions; testing different Tedlar bag options due to bag liner leakages, corrosion from contact with biocides, or BTX sorption to the linear material; and changing column tubing from transparent 1.57 mm ID Teflon to non-transparent 1.57 mm ID SS in addition to adding SS filters holders to prevent microbial growth in the tubing). As a result, the flow rate and mass injected between columns were variable during Year-1. The mass injected varied from 56 to 165 mg of toluene (average influent concentration of 1.6 ± 1.2 mg/L between single-solute columns) for the toluene-only columns, and from 56 to 177 mg of benzene (average influent concentration of 2.5 ± 0.6 mg/L between multi-solute columns), 48 and 159 mg of toluene (average influent concentration of 2.1 ± 0.7 mg/L between multi-solute columns), and 47 and 113 mg of *o*-xylene (average influent concentration of 1.7 ± 0.7 mg/L between multi-solute columns) for the BTX columns. During Year-1, sorption is presumed to have resulted in a change in cumulative mass between the influent and effluent (ΔM) of -61.2 mg of toluene (37.1% reduction) in the toluene-only KC+PACz column, and -16.6 mg of benzene (9.4% reduction), -41.5 mg of toluene (26.1% reduction) and -90.5 mg of *o*-xylene (81.2% reduction) in the BTX KC+PACz column. Biodegradation is presumed to have resulted in a ΔM of -39.4 mg of toluene (71% reduction) in the toluene-only BA-PC column, and -25.8 mg of benzene (46.3% reduction), -27.6 mg of toluene (57.2% reduction) and -11.7 mg of *o*-xylene (25.1% reduction) in the BTX BA-PC column. Sorption and biodegradation are presumed to have resulted in a ΔM of -87.4 mg of toluene (96.5% reduction) in the toluene-only BA+PACz column, and -78.3 mg of benzene (59.5% reduction), -87.6 mg of toluene (81.4% reduction) and -84.3 mg of *o*-xylene (91.7% reduction) in the BTX BA+PACz column (see Table C.4 for the cumulative influent and effluent mass, and ΔM of toluene and BTX per column during Year-1). The Year-1 change in aqueous phase influent and effluent concentrations are shown in Figure C.2(a-f) for the single- and multi-solute KC+PACz (Figure C.2(a, d)), BA-PC (Figure C.2(b, e)) and BA+PACz (Figure C.2(c, f)) columns.

During Year-2 of column operation the average measured flow rate was 0.023 ± 0.019 mL/min which yielded an average groundwater velocity and residence time of 0.0062 ± 0.0006 cm/min and 4.16 ±

0.43 days, respectively, between columns (Table C.2), which is representative of the Borden aquifer (0.0063 cm/min [135] [Table B.1]) and therefore deemed sufficient for anaerobic biodegradation [149, 150]. As described in Section 4.2.3, effluent samples were collected at a lower measured flow rate of 0.017 ± 0.004 mL/min, whereas influent samples were collected at a temporarily higher measured flow rate of 0.04 ± 0.014 mL/min. The variation in flow rates during sample collection resulted in effluent and influent sample collection over 1.8 and 0.4 days, respectively.

During Year-2 of column operation, the average influent toluene and BTX concentrations were sequentially adjusted in a stepwise manner between the single- and multi-solute columns from 4.7 ± 1.1 mg/L for the first 20.2 ± 4.1 PVs to 8.6 ± 1.3 mg/L from PV 22.2 ± 4.4 to 26.6 ± 4.6 to 17.4 ± 2.5 mg/L from PV 27.9 ± 4.8 to 58.8 ± 10 (note that an injection concentration of 10 mg/L was unintentionally not used for the single-solute BA-PC column, instead the concentration increased from 5 mg/L directly to 20 mg/L). Relative to Year-1, less variability in the cumulative injected mass between all solutes and columns occurred during Year-2, with an average injected mass of 78.1 ± 10.7 mg. In the multi-solute KC+PACz column the ΔM followed X (-32.2 mg or 42.2% reduction) > T (-21.4 mg or 25.4% reduction) > B (-4.6 mg or 5.2% reduction) which is attributed to competitive sorption, with *o*-xylene having the highest sorption capacity followed by toluene and then benzene [21, 29], as described in Chapter 2 and 3. Between the single- and multi-solute KC+PACz columns the ΔM of toluene was greater for the single-solute column (74.6% reduction) relative to the multi-solute column (25.4% reduction) given that the sorption capacity of toluene was reduced in the multi-solute competitive system. In the multi-solute BA-PC and BA+PACz columns with bioactivity the ΔM followed T > X > B. For the multi-solute BA-PC column this behaviour is attributed to the preferential biodegradation of toluene (-38.3 mg or 59.2% reduction) [54, 56, 187] prior to *o*-xylene (-11.3 mg or 16.9% reduction) and the limited biodegradation of benzene (-6 mg or 8.3% reduction) due to the recalcitrance of benzene, as described in Section 3.3.4 [54, 185, 154]. Whereas, for the multi-solute BA+PACz column the ΔM between solutes is likely attributed to the preferential biodegradation of toluene (-88.9 mg or 98.5% reduction) and the greater sorption of benzene (-14.3 mg or 14.4% reduction) and *o*-xylene (-74.7 mg or 85.2% reduction) as toluene was biodegraded and the availability of sorption sites increased (see Table C.4 for the cumulative influent and effluent mass, and ΔM of toluene and BTX per column during Year-2). Between the toluene-only columns the ΔM of toluene followed BA+PACz (-68.1 mg or 99.5% reduction) > KC+PACz (-54.9 mg or 74.6% reduction) > BA-PC (-38.8 mg or 44.4% reduction), showing that toluene mass was reduced more due to the combination of

sorption and biodegradation, as opposed to sorption or biodegradation alone. Similarly, between the multi-solute columns the ΔM of toluene was greatest for the BA+PACz column (-88.9 mg or 98.5% reduction), followed by the BA-PC (-38.3 mg or 59.2% reduction) and KC+PACz (-21.4 mg or 25.4% reduction) columns.

The average sulfate concentration, as a source of electron acceptor, was increased in a similar manner between the single- and multi-solute columns as compared to the influent toluene and BTX concentrations during Year-2, staring at 6.3 ± 3.6 mg/L over PV 0 to 4.7 ± 0.9 to 22.2 ± 3.5 mg/L over PV 9.2 ± 1.6 to 11.7 ± 5.3 to 26.5 ± 4.6 mg/L over PV 27.9 ± 4.8 to 58.8 ± 10 (note that an injection concentration of 30 mg/L was unintentionally not used for the single-solute KC+PACz column). The average cumulative mass of sulfate injected into all single- and multi-solute columns during Year-2 was 159 ± 22.7 mg. The ΔM of sulfate between the single- and multi-solute KC+PACz columns was -6.8 mg (4.8% reduction) and -2.2 mg (1.5% reduction), respectively, and -162.5 ± 26.1 mg (97.4 ± 3.6% reduction) between all single- and multi-solute BA-PC and BA+PACz columns. The ΔM of sulfate between the single- and multi-solute BA-PC and BA+PACz columns in combination with the production of other biodegradation by-products expected under sulfate-reducing (i.e., $C_7H_8 + 4.5SO_4^{2-} + 3H_2O \longrightarrow 7HCO_3^- + 2.25HS^- + 2.25H_2S + 0.25H^+$) and methanogenic (i.e., $4H_2 + HCO_3^- + H^+ \longrightarrow CH_4 + 3H_2O$ [hydrogenotrophic] or $CH_3COO^- + H_2O \longrightarrow CH_4 + HCO_3^-$ [acetoclastic]) conditions supports anaerobic biodegradation. Specifically, between the single- and multi-solute BA-PC and BA+PACz columns the average ΔM of CH_4 and DIC was 97.8 ± 22.1 mg (99.9% increase) and 109.1 ± 23.6 mg (60.2% increase), respectively, relative to the ΔM of CH_4 and DIC between the single- and multi-solute abiotic KC+PACz columns which was 0.0 mg (0.0% increase) and 32.4 ± 6.5 mg (53.5% increase), respectively (see Table C.4 for the cumulative influent and effluent mass, and ΔM of sulfate, CH_4 and DIC per column during Year-2).

To estimate the fraction of toluene consumption attributed to anaerobic biodegradation between the single- and multi-solute columns during Year-2, the stoichiometrically estimated mass of DIC generated from sulfate reduction coupled to toluene oxidation (i.e., determined using the ΔM of sulfate and the stoichiometric mass ratios between DIC and sulfate during sulfate reduction [0.19]) or methanogenesis (i.e., determined using the ΔM of CH_4 and the stoichiometric mass ratios between DIC and CH_4 during methanogenesis [0.75]) were compared to the measured ΔM of DIC (listed in Table C.4). Between the single- and multi-solute KC+PACz columns minimal DIC production was stoichiometrically estimated (0.9

± 0.6 mg) given the limited ΔM of sulfate consumed (-4.5 ± 3.2 mg or 3.1 ± 2.3% reduction) and no ΔM of methane produced (0.0 mg or 0.0% increase). However, the average measured ΔM of DIC between the single- and multi-solute KC+PACz columns indicates DIC was produced (32.4 ± 6.5 mg or 53.5 ± 3.6% increase). As opposed to DIC production associated with biodegradation, the difference between the average stoichiometric estimate and measured ΔM of DIC between the single- and multi-solute KC+PACz columns is likely attributed to an abiotic reaction between the biocide (sodium azide) and some other material within the columns forming inorganic carbon given that sodium azide is known to act as an oxidant or reductant [160] (similarly observed in the single- and multi-solute KC and KC+PAC microcosms described in Section 3.3.2). Contrarily the stoichiometrically estimated mass of DIC relative to the measured ΔM of DIC for both the single- and multi-solute BA-PC and BA+PACz columns were similar, indicating that the DIC produced was coupled to both sulfate reduction and methanogenesis (i.e., 98.4 ± 16.9% of the average stoichiometrically estimated mass of DIC generated was accounted for relative to the average measured ΔM of DIC between columns) (see Table C.5 for the measured ΔM of DIC and toluene relative to stoichiometric estimates during sulfate reduction and methanogenesis per single- and multi-solute column during Year-2).

Between the single- and multi-solute BA-PC and BA+PACz columns, given that the average ΔM of sulfate (-162.5 ± 26.1 mg or 97.4 ± 3.6% reduction), DIC (109.1 ± 23.6 mg or 60.2 ± 7.1% increase), CH_4 (97.8 ± 22.1 mg or 99.9 ± 0.2% increase) and toluene (-38.6 ± 0.4 mg or 51.8 ± 10.5% reduction [BA-PC] and -78.5 ± 14.7 mg or 99 ± 0.7% reduction [BA+PACz]) were similar this suggests that the toluene was primarily biodegraded in the multi-solute BA-PC and BA+PACz columns as opposed to other solutes (e.g., *o*-xylene) also being consumed. For substantial *o*-xylene mass to have been consumed from the multi-solute BA-PC and BA+PACz columns higher ΔM of all parameters monitored, relative to those observed in Table C.4, would have been stoichiometrically expected. The slight reduction in the average measured ΔM of *o*-xylene in the multi-solute BA-PC column during Year-2 (-11.3 mg or 16.9% reduction) may be associated with co-metabolism during toluene biodegradation [64] and/or error (substantial retardation of *o*-xylene to the BS is unlikely based on the K_{d_i} in Table B.3). Whereas the larger change in ΔM of *o*-xylene observed in the multi-solute BA+PACz column (-74.7 mg or 85.2% reduction) is likely primarily related to PAC sorption given *o*-xylene is preferentially sorbed to the PAC (as described in Chapter 2).

Like the comparison between the stoichiometrically estimated mass of DIC generated relative to the measured ΔM of DIC, the stoichiometrically estimated mass of toluene consumed from sulfate reduction

(i.e., determined using the ΔM of sulfate and the stoichiometric mass ratios between toluene and sulfate during sulfate reduction [0.21]) was compared to the measured ΔM of toluene (listed in Table C.4) for each single- and multi-solute column during Year-2. For the single- and multi-solute KC+PACz columns the average mass of toluene stoichiometrically estimated for consumption during sulfate reduction was minimal (1 ± 0.7 mg) given that limited sulfate was consumed (-4.5 ± 3.2 mg or 3.1 ± 2.3% reduction), which supports the absence of toluene biodegradation in KC+PACz columns, as expected. However, the average measured ΔM of toluene between the single- and multi-solute KC+PACz columns indicates mass was consumed (-54.9 mg or 74.6% reduction [single-solute] and -21.4 mg or 25.4% reduction [multi-solute]) which is attributed to PAC sorption. For the single- and multi-solute BA-PC and BA+PACz columns the average measured ΔM of toluene were -38.6 ± 0.4 mg (51.8 ± 10.5% reduction) and -78.5 ± 14.7 mg (99 ± 0.7% reduction), respectively. Contrary to the KC+PACz columns, relative to the average stoichiometric estimates of toluene consumed during sulfate reduction 78.6 ± 3.9% and 50 ± 4.2% of the average measured ΔM of toluene were accounted for in the single- and multi-solute BA-PC and BA+PACz columns, respectively, which supports anaerobically biodegradation of toluene. Between the single- and multi-solute BA-PC and BA+PACz columns, the stoichiometrically estimated and measured mass of toluene consumed were closer for the BA-PC columns without PAC zones relative to the BA+PACz columns with PAC zones given that the fraction of toluene sorbed to the PAC in the BA+PACz columns was not accounted for in the stoichiometric estimates of biodegradation (see Table C.5 for the measured ΔM of DIC and toluene relative to stoichiometric estimates per column during Year-2).

The formation of a black precipitate at the influent ends of the single- and multi-solute BA-PC and BA+PACz columns after 1.6 years of operation (see Figure C.3(i-l) for images) relative to Day 0 (see Figure C.3(c-f) for images) is presumed to be attributed to an abiotic oxidation-reduction reaction between sulfide (H_2S and HS^-) generated from sulfate reduction coupled to toluene oxidation and ferric iron in the BS [200, 53, 54, 201] (as was similarly described in Section 3.3.4 for the electron acceptor (EA) amended microcosms). FeS formation in the single- and multi-solute BA-PC and BA+PACz columns is further supported by a strong sulfur odour noted during column dismantling and excavation. The absence of FeS precipitates at the downgradient ends of the single- and multi-solute BA-PC and BA+PACz columns may indicate an absence of sulfate reduction (or H_2S and HS- production) in these locations due to the exhaustion of the sulfate source at the influent ends. FeS formation was not observed in the sterile single- and multi-solute KC+PACz columns within the BS after 1.6 years of operation (see Figure C.3(g-h) for images)

relative to Day 0 (see Figure C.3(a-b) for images), as expected, given anaerobic sulfate reduction was not stoichiometrically coupled to toluene oxidation, as described above.

The following Sections (4.3.1 to 4.3.3) pertain to data collected over Year-2 only, where PV = 0 is the start of Year-2.

4.3.1 Killed control columns

In the single-solute KC+PACz column during the first two stepwise increases in the influent concentration of toluene from 5 to 10 mg/L the PAC was unsaturated (i.e., influent ≠ effluent concentration) after 19.6 and 6.1 PVs, respectively (Figure 4.2(a)). Although during the highest increase in influent concentrations to 20 mg/L breakthrough of toluene was observed after 15.7 PVs in the single-solute KC+PACz column. In the multi-solute KC+PACz column, the PAC was saturated (i.e., influent = effluent concentration) with benzene after 9, 5.3 and 3.7 PVs, when the influent concentrations were 5, 10 and 20 mg/L, respectively, showing more PVs were required to saturate the PAC with benzene at lower influent concentrations, as expected (for all solutes). For toluene or *o*-xylene in the multi-solute KC+PACz column saturation was only achieved at the highest influent concentration of 20 mg/L after 21.6 and 24.4 PVs for toluene and *o*-xylene, respectively (Figure 4.3(a)). Between solutes in the multi-solute KC+PACz column, the number of PVs to saturate the PAC at the highest influent concentration of 20 mg/L followed X > T > B which is related to the difference in sorption capacities between solutes with more PVs required to achieve saturation of *o*-xylene relative to toluene then benzene [29, 202], as described in Section 4.3. Between the KC+PACz columns more toluene sorption occurred in the single-solute column relative to the multi-solute column due to the higher sorption capacity of toluene in the single-solute system without the presence of other competing solutes [29, 202], as described in Section 4.3.

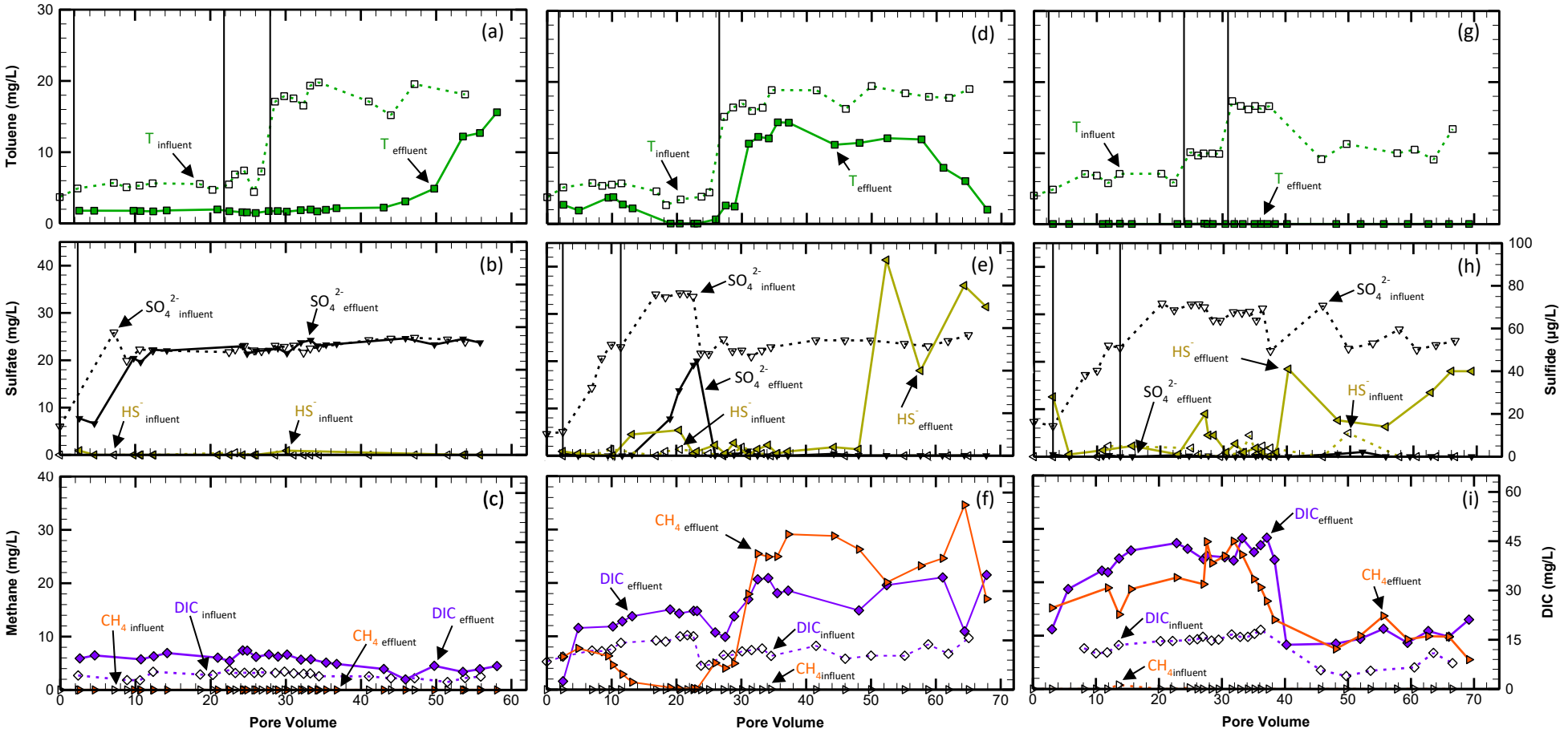

Figure 4.2: Influent (dashed lines with open symbols) and effluent (solid lines with closed symbols) aqueous concentrations of (a, d, g) toluene, (b, e, h) sulfate (SO_4^{2-}) and sulfide (HS^-), and (c, f, i) methane (CH_4) and dissolved inorganic carbon (DIC) from the single-solute (toluene-only) KC+PACz (left panel), BA-PC (middle panel) and BA+PACz (right panel) columns. The vertical solid lines represent an increase in influent concentration.

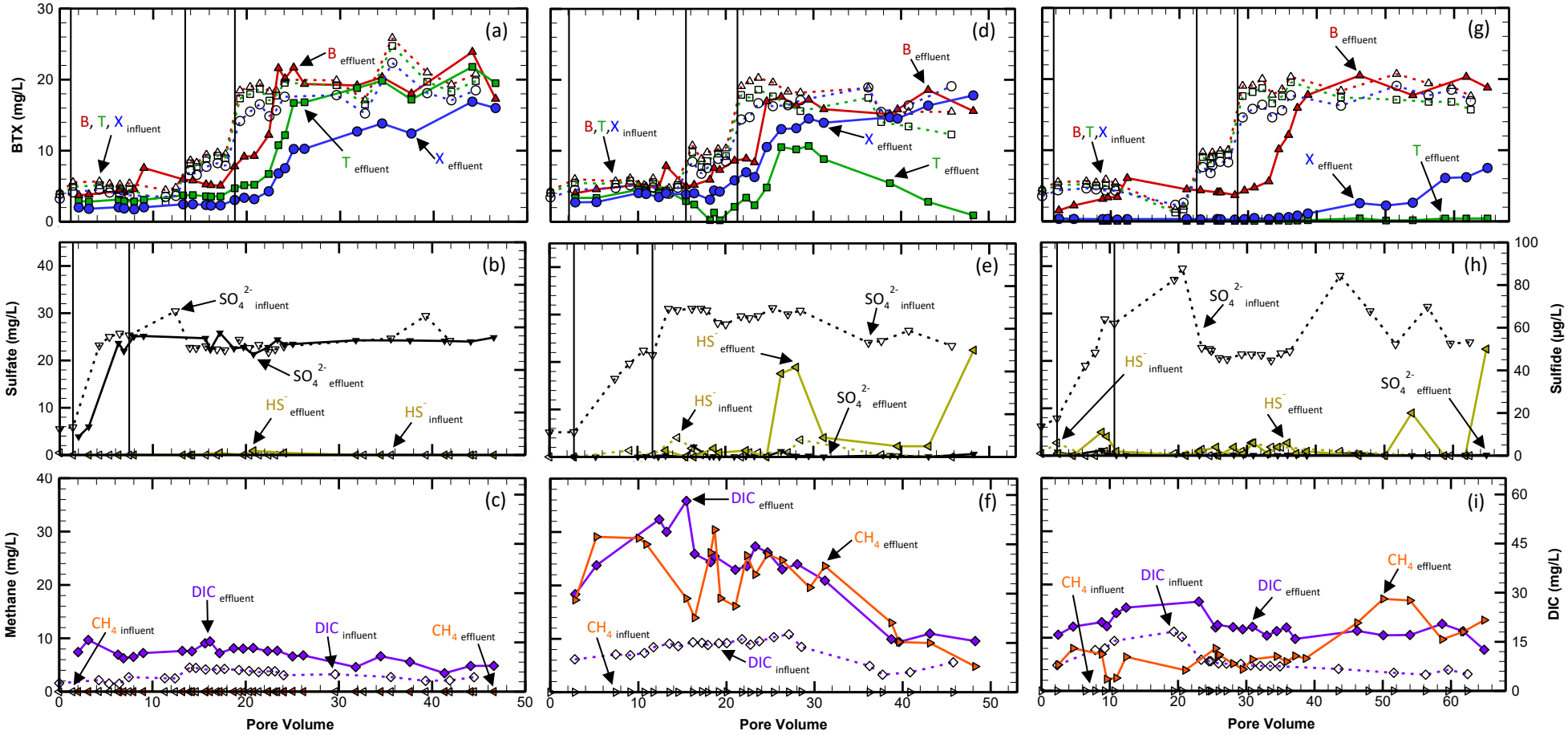

Figure 4.3: Influent (dashed lines with open symbols) and effluent (solid lines with closed symbols) aqueous concentration of (a, d, g) benzene, toluene and *o*-xylene (BTX), (b, e, h) sulfate (SO_4^{2-}) and sulfide (HS^-), and (c, f, i) methane (CH_4) and dissolved inorganic carbon (DIC) from the multi-solute (BTX) KC+PACz (left panel), BA-PC (middle panel) and BA+PACz (right panel) columns. The vertical solid lines represent an increase in influent concentration.

As expected, no change in markers of microbial activity, typically observed during sulfate reduction or methanogenesis, were detected in the effluent of the single- or multi-solute KC+PACz columns during Year-2, including stabilized sulfate concentrations between the influent and effluent and negligible CH_4 or sulfide (H_2S and HS^-) production (i.e., ≤ method detection limit [MDL] [Section 3.2.3]) (Figure 4.2(b, c) and Figure 4.3(b, c)). Additionally, no change in the average DO (2.6 ± 1.3 mg/L), pH (7.2 ± 0.2) or the ORP (185.7 ± 33.8 mV) were observed between the influent and effluent of the single- and multi-solute KC+PACz columns (Figure C.4(a-d)). Between the single- and multi-solute KC+PACz columns 10.3 ± 0.2 mg/L of DIC was produced, although DIC production was not stoichiometrically coupled to toluene oxidation, as described in Section 4.3 (Figure 4.2(c) and Figure 4.3(c)).

For the single-solute KC+PACz column, no change in the values of δ^{13}C-toluene (T) were shown over PV 4.6-55.8 relative to the AGW signature (-27.8 ± 0.2‰ [sample average over PVs] versus -27.8‰ [AGW signature]) (Figure 4.4(a) and see Table C.6 for the isotope data). For the multi-solute KC+PACz column no change in the values of δ^{13}C-T (-27.8 ± 0.4‰ versus -27.8‰) or δ^{13}C-*o*-xylene (X) (-30.1‰ versus -29.9‰) were also shown over PV 3.1-15.6 and 44.1 for toluene or PV 3.1 for *o*-xylene relative to the AGW signatures. However, over PV 26.2-37.6 and 15.6-37.6 for toluene and *o*-xylene, respectively, slight reductions in the values of δ^{13}C-T (-28.6 ± 0.1‰ versus -27.8‰) and δ^{13}C-X (-30.9 ± 0.2‰ versus -29.9‰) were observed. Contrarily, for benzene (B) in the multi-solute KC+PACz column a slight increase in the values of δ^{13}C-B were observed (-24.5 ± 0.5‰ versus -25.6‰) over all PVs (3.1-37.6) relative to the AGW signature (Figure 4.5(a) and see Table C.6 for the isotope data). The values of δ^{2}H-T (-66.9 ± 5.9‰ versus -82.1‰) from the effluent of the single-solute KC+PACz column, in addition to δ^{2}H-B (-74.5 ± 8.4‰ versus -98.4‰), δ^{2}H-T (-63.2 ± 4.8‰ versus -82.1‰) and δ^{2}H-X (-79.7 ± 8.2‰ versus -132.1‰) in the effluent of the multi-solute KC+PACz column increased over all PVs (4.6-55.8 [toluene-only] and 3.1-44.1 [BTX]) relative to the AGW signatures which indicates enrichment in ^{2}H-B,T,X (Figure 4.4(b) and Figure 4.5(b) and see Table C.6 for the isotope data). Larger changes in the values δ^{2}H-B,T,X relative to δ^{13}C-B,T,X were expected, given that hydrogen isotope fractionation is often substantially larger than carbon isotope fractionation due to differences in the relative mass between the stable isotopes of both elements with the difference being greater for hydrogen [83, 84]. Enrichment in ^{2}H-B,T,X, presumably due to ^{1}H sorption to the PAC (given the absence of biodegradation in the single- and multi-solute KC+PACz columns) is notable [87] as sorption is not expected to substantially influence the isotope ratios [79, 80, 81, 82]. Increases in the values of δ^{13}C-DIC were also observed in the effluent of the single-solute KC+PACz column (2.6 ± 1.9‰ versus -2.9‰) and the multi-solute KC+PACz

column (3.7 ± 1.0‰ versus -2.9‰) over all PVs (4.6-55.8 [toluene-only] and 3.1-44.1 [BTX]), indicating ^{13}C-DIC enrichment (Figure 4.4(c) and Figure 4.5(c) and see Table C.6 for the isotope data), and may be related to the formation of DIC as described in Section 4.3 (Figure 4.2(c) and Figure 4.3(c)).

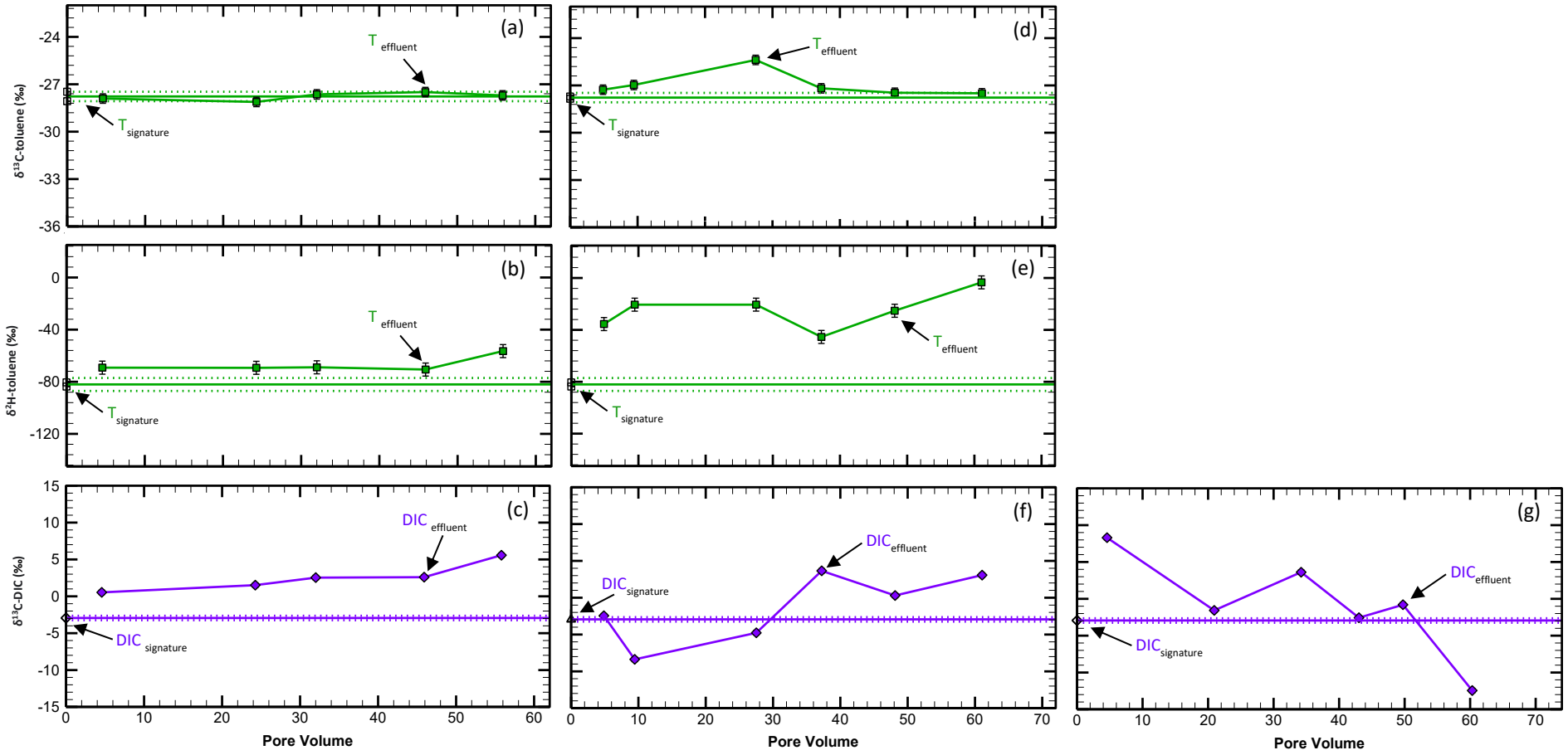

Figure 4.4: Influent isotope source signature (open symbols) and effluent (a, d) δ^{13}C-toluene, (b, e) δ^{2}H-toluene and (c, f, g) δ^{13}C-DIC (dissolved inorganic carbon) isotopes (solid lines with closed symbols) for the single-solute (toluene-only) KC+PACz (left panel), BA-PC (middle panel) and BA+PACz (right panel) columns. Solid horizontal lines represent the average of the influent isotope source signatures and dashed horizontal lines and error bars on data represent the error, including ±0.3‰ (2σ) for δ^{13}C-T, ±5‰ (2σ) for δ^{2}H-T and ±0.2‰ (2σ) for δ^{13}C-DIC.

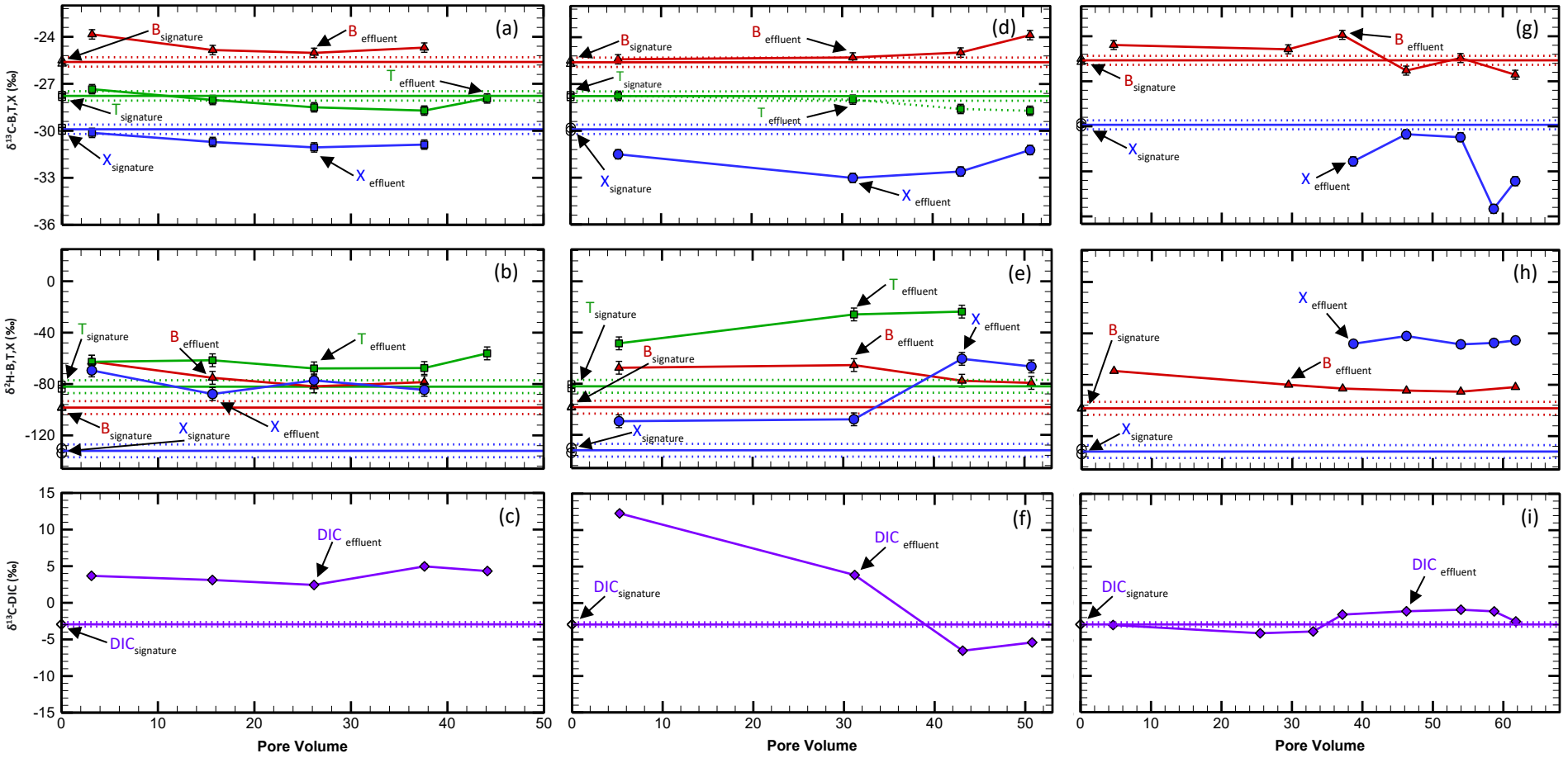

Figure 4.5: Influent isotope source signature (open symbols) and effluent (a, d, g) δ^{13}C-benzene (B), toluene (T), and *o*-xylene (X), (b, e, h) δ^{2}H-B,T,X and (c, f, i) δ^{13}C-DIC (dissolved inorganic carbon) isotopes (solid lines with closed symbols) for the multi-solute (BTX) KC+PACz (left panel), BA-PC (middle panel) and BA+PACz (right panel) columns. Solid horizontal lines represent the average of the influent isotope signatures and dashed horizontal lines and error bars on data represent the error, including ±0.3‰ (2σ) for δ^{13}C-B,T,X, ±5‰ (2σ) for δ^{2}H-B,T,X and ±0.2‰ (2σ) for δ^{13}C-DIC.

4.3.2 Toluene-only bioactive system

In the single-solute (toluene-only) BA-PC column the effluent toluene concentration was reduced from an average of 4.4 ± 1 mg/L over PV 2.5-27.5 to < MDL (Section 2.2.2) by PV 19, and from 17.5 ± 1.4 mg/L over PV 28.9-67.8 to 2 mg/L by PV 67.8 (Figure 4.2(d)). However, for the single-solute BA+PACz column the effluent toluene concentration was reduced from 6.1 ± 1.2 mg/L, 9.9 ± 0.2 mg/L, 16.6 ± 0.4 mg/L and 10.6 ± 1.5 mg/L over PV 3-24.5, 27.1-31.9, 33.2-40.2 and 48.1-69.2, respectively, to 0.06 ± 0.02 mg/L over PV 3-27.1 and < MDL by PV 27.6 (Figure 4.2(g)). The near depletion in effluent toluene from the BA+PACz column during Year-2 is attributed to a combination of PAC sorption and anaerobic biodegradation [36, 100, 101, 39], as opposed to the higher effluent toluene concentrations from the BA-PC column with only anaerobic biodegradation (Figure 4.2(d)) or from the single-solute KC+PACz column with only PAC sorption (Figure 4.2(a)).

The average solid phase toluene concentration along the length of the BA-PC column (4 to 30 cm from the influent [i.e., median sample distances within the incrementally collected and homogenized solid phase samples, described in Section 4.2.3]) in addition to the upgradient (2.5 to 13.5 cm from the influent) and downgradient (20.5 to 34.5 cm from the influent) sections of the BA+PACz column (outside of the PAC zone) was $2.9 \times 10^{-4} \pm 4.6 \times 10^{-4}$ mg/g (Figure 4.6(a, f)). Comparatively, in the 6 cm PAC zone within the BA+PACz column (14.5 to 19.5 cm from the influent), the solid phase toluene concentration was 1 to 3 orders of magnitude higher than outside of the PAC zone. At the leading edge of the PAC zone (14.5 cm from the influent) a peak concentration of 0.18 mg/g of toluene was detected followed by a gradual reduction in toluene concentration to 8.5×10^{-3} mg/g towards the end of the PAC zone (19.5 cm from the influent). The gradient in toluene concentration within the PAC zone of the BA+PACz column shows that toluene was regenerated from the PAC due to biodegradation, with greater mass removal sustained towards the end of the PAC zone furthest from the influent source of toluene being continually replenished.

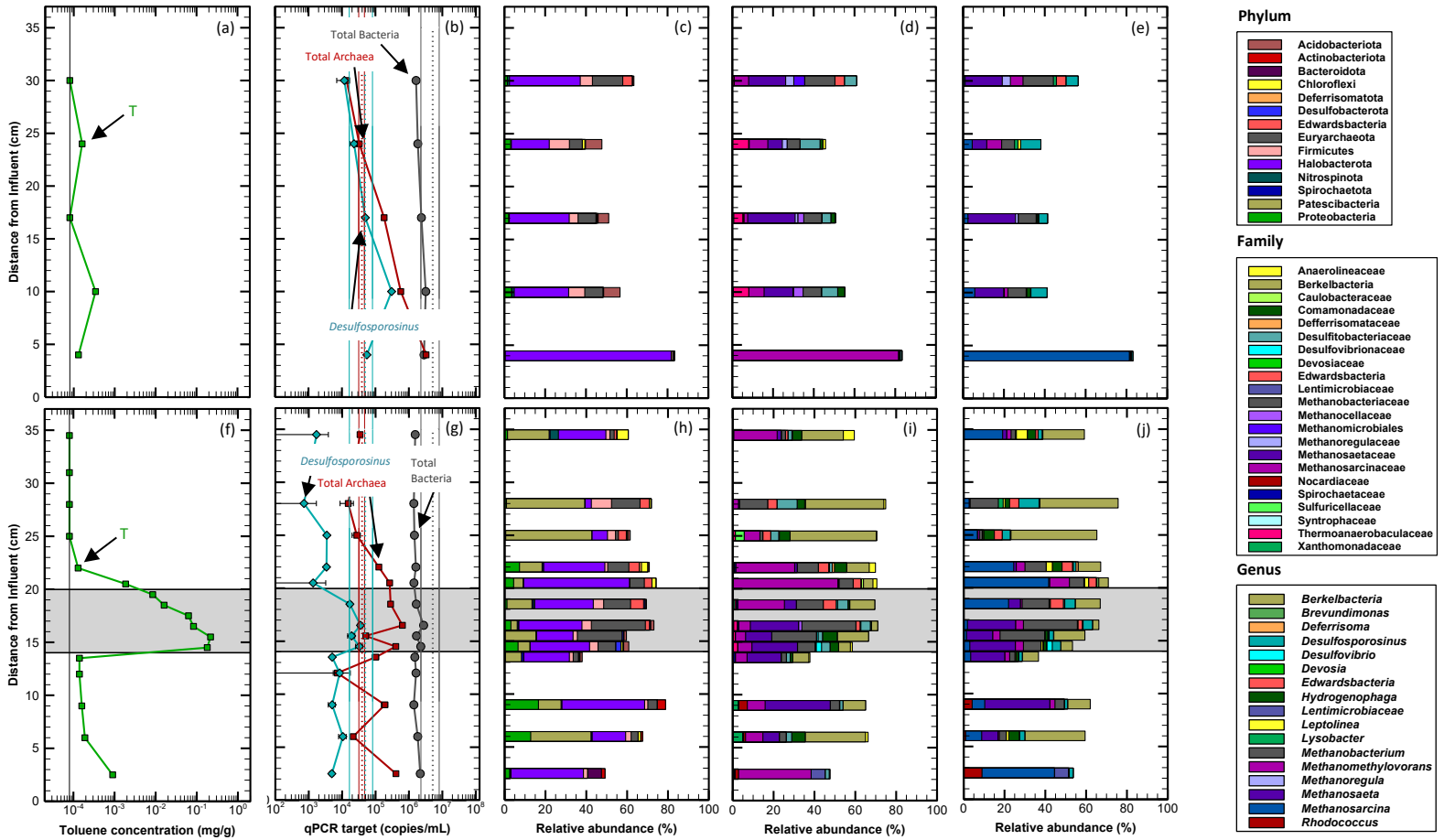

Figure 4.6: Solid phase (a, f) concentration of toluene (green filled squares); (b, g) abundance of *Desulfosporosinus* (light blue filled diamonds), total bacteria (grey filled circles) and total archaea (dark red filled squares) from quantitative polymerase chain reaction (qPCR) analysis; and relative abundance (≥ 4%) of bacteria and archaea detected at the (c, h) phylum, (d, i) family and (e, j) genus taxonomic levels using 16S ribosomal ribonucleic acid (rRNA) next generation sequencing (NGS) for the single-solute (toluene-only) BA-PC (top panel) and BA+PACz (bottom panel) columns after Year-2 of column operation. The grey region in the bottom panel represents the powdered activated carbon (PAC) zone. The vertical line in (a, f) represents the method detection limit of solid phase toluene (8.0×10^{-5} mg/g). The data in (b, g) represent the average of three measurements and the dashed vertical lines represent the background abundances. Error bars and solid vertical lines in (b, g) are ± 1 standard deviation. The phylum, family and genus legends correspond to (c, h), (d, i) and (e, j), respectively. Sample depths from the influent represent the median distance of incrementally collected samples that were homogenized.

Anaerobic biodegradation in the single-solute BA-PC and BA+PACz columns is supported by geochemical activity including a reduction in the average effluent sulfate concentration, as a source of electron acceptor for PHC oxidation [53, 203, 54, 55], to 0.1 ± 0.2 mg/L between columns following all three stepwise increases in the influent sulfate concentration (listed in Section 4.3). Between the single-solute BA-PC and BA+PACz columns the effluent sulfate concentration was reduced over all PVs (2.5-13.2 and 26-67.8 [BA-PC], and 3-69.2 [BA+PACz]), neglecting during the highest influent concentration for the BA-PC column where the effluent sulfate concentration gradually increased from 0.17 to 20.1 mg/L over PV13.2-23.2 but decreased again to near depletion (0.09 mg/L) by PV 25 (Figure 4.2(e, h)). The slight increase in the effluent sulfate concentration within the BA-PC column, relative to the BA+PACz column (showing no increase), may be related to the absence of a PAC zone (which provided sustained desorption of toluene in the BA+PACz column) potentially resulting in less toluene oxidation coupled to sulfate reduction over PV 13.2-23.2. Sulfate reduction in the BA-PC and BA+PACz columns is also supported by the production of biodegradation by-products including sulfide (Figure 4.2(e, h)) and DIC (Figure 4.2(f, i)) that were produced at concentrations greater than from the single-solute KC+PACz column (Figure 4.2(b, c)). Specifically, between the BA-PC and BA+PACz columns the average effluent sulfide concentration increased from 1.7 ± 2.7 µg/L in the influent over all PVs (2.8 ± 0.4 to 68.5 ± 1) to 46.4 ± 26 µg/L over PV 46.3 ± 8.6 to 68.5 ± 1 (Figure 4.2(e, h)). The accumulation of FeS precipitates at the influent ends of the single-solute BA-PC and BA+PACz columns, as described in Section 4.3 (Figure C.3(i, j)), may explain the low average effluent sulfide concentration at PV < 46.3 ± 8.6 as opposed to a lack of sulfide production during sulfate reduction. The average effluent DIC concentration was variable between the BA-PC and BA+PACz columns, but generally increased from 12.2 ± 3.4 to 28.4 ± 10.8 mg/L over all PVs (Figure 4.2(f, i)). Additionally, within the effluent of the single-solute BA-PC and BA+PACz columns the average DO concentration was consistently low (0.5 ± 0.3 mg/L), as expected under anaerobic reducing conditions; the pH was neutral (6.9 ± 0.2), within the range of optimal conditions for microbial degradation [54]; and the ORP decreased from 174.5 ± 32.2 mV in the influent to a range in values from -141.9 to 140.9 mV over all PVs [49, 204] (Figure C.5(a, b)).

Sulfate reduction at the influent ends of the single-solute BA-PC and BA+PACz columns is supported by the qPCR data which shows a higher average abundance of *Desulfosporosinus*, whose members are sulfate reducing bacteria (SRB) associated with PHC biodegradation [195, 162, 196] (as described in Section 3.3.4), within the influent regions (i.e., 2.5 to 13.5 cm from the influent) ($1.8 \times 10^{+5}$ ±

$1.8 \times 10^{+5}$ copies/mL [BA-PC] and $6.8 \times 10^{+3} \pm 2.6 \times 10^{+3}$ copies/mL [BA+PACz]) relative to the effluent ends (i.e., 20 to 35 cm from the influent) ($1.7 \times 10^{+4} \pm 8 \times 10^{+3}$ copies/mL [BA-PC] and $2.1 \times 10^{+3} \pm 1.2 \times 10^{+3}$ copies/mL [BA+PACz]). *Desulfosporosinus* was only enriched (i.e., > the background abundance) at 10 cm from the influent in the BA-PC column ($3.1 \times 10^{+5}$ copies/mL versus $4.9 \times 10^{+4} \pm 3.3 \times 10^{+4}$ copies/mL [average background abundance]), and in the BA+PACz column the average abundance of *Desulfosporosinus* was highest within the PAC zone ($2.6 \times 10^{+4} \pm 9.4 \times 10^{+3}$ copies/mL) (Figure 4.6(b, g) and see Table C.7 for the qPCR data). The reduction in the abundance of *Desulfosporosinus* with distance from the influent of the BA-PC and BA+PACz columns (where the sources of sulfate and toluene were continually replenished) may be attributed to a depletion in sulfate with distance from the influent ends [205, 206] (supported by the localized formation of FeS within the influent regions, as discussed in Section 4.3 [Figure C.3(i, j)]). For the BA+PACz column, the elevated abundance of *Desulfosporosinus* within the PAC zone may have been sustained by the continual desorption of toluene from the PAC (Figure 4.6(f)) and the use of other substrates as electron acceptors (e.g., fumarate) [66] if sulfate was depleted within the PAC zone or potentially AC-mediated direct interspecies electron transfer (DIET) [112, 78, 108]. The NGS data confirms the relative abundance of *Desulfosporosinus* was elevated within the influent end of the BA-PC column (7.9% at 10 cm from the influent), although the average relative abundance remained elevated further downgradient (5.2 ± 1.1% at 17 and 30 cm from the influent) and reached a peak value of 9.9% at 24 cm from the influent (Figure 4.6(c-e) and see Table C.8 for the NGS data). Additionally, the NGS data confirms the average relative abundance of *Desulfosporosinus* was elevated within the PAC zone of the BA+PACz column (4 ± 1.3% over 14.5 to 18.5 cm from the influent) relative to the influent (2.1 ± 0.5% over 2.5 to 13.5 cm from the influent) and effluent (1.9 ± 1.5% over 20.5 to 25 and 34.5 cm from the influent) ends, neglecting at 28 cm from the influent (downgradient of the PAC zone) where the relative abundance was highest (9.9%) (Figure 4.6(h-j) and see Table C.8 for the NGS data).

From the qPCR data, the abundance of total bacteria within the single-solute BA-PC and BA+PACz columns was numerous along the column lengths, as expected, but not enriched relative to the background abundance ($1.9 \times 10^{+6} \pm 5.4 \times 10^{+5}$ copies/mL [average abundance between columns] versus $5.2 \times 10^{+6} \pm 2.2 \times 10^{+6}$ copies/mL [average background abundance]) (Figure 4.6(b, g) and see Table C.7 for the qPCR data). The NGS data show that along the BA-PC column length (from 10 to 24 cm from the influent) the families Thermoanaerobaculaceae, who are anaerobic bacteria associated with PHC

degradation [207, 208] (6.7 ± 2%) and Comamonadaceae, whose members are primarily denitrifying bacteria associated with PHC degradation [209, 210] (1.4 ± 0.07%), were the most abundant bacteria (Figure 4.6(c-e) and see Table C.8 for the NGS data). Whereas, at the influent (6 cm from the influent) and effluent (25 to 34.5 cm from the influent) ends of the BA+PACz column the relative abundance of the genera *Berkelbacteria* from the phylum Patescibacteria, whose members participate in syntrophic interactions with other bacteria and archaea [211, 212] (29.5% [influent] and 33.6 ± 11.6% [effluent]), and *Hydrogenophaga* from the family Comamonadaceae, who are associated with PHC contamination [213] (5.2% [influent] and 3.9 ± 1.5% [effluent]), were elevated. Within the PAC zone of the BA+PACz column (at 14.5 cm from the influent) the relative abundance of *Desulfovibrio*, which are metabolically versatile SRB associated with BTEX degradation [47, 162, 214] and can grow syntrophically with methanogens in the absence of sulfate [215] (2.6%) and Thermoanaerobaculaceae (2.4%) were elevated (coinciding with the location of highest solid phase toluene concentration, as described above [Figure 4.6(f)]). In the downgradient region of the BA+PACz column the average relative abundance of the genera *Edwardsbacteria* (4.7 ± 1.17% from 18.5 to 28 cm from the influent) and *Leptolinea*, which are anaerobic bacteria [216] (5.4% at 34.5 cm from the influent), and the family Sulfuricellaceae, which are sulfur oxidizers [217] (4.4% from 25 cm from the influent), were elevated (Figure 4.6(h-j) and see Table C.8 for the NGS data).

Variable CH_4 was detected in the effluent of the single-solute BA-PC and BA+PACz columns (15.2 ± 9.2 mg/L [average between columns]) relative to the average influent concentration (0.02 ± 0.1 mg/L) over all PVs (2.8 ± 0.4 to 68.5 ± 1) (Figure 4.2(f, i)). The CH_4 produced is associated with methanogenic reactions driven partly by the utilization of metabolites from sulfate reduction [205, 218, 219, 60]. The change in the effluent CH_4 concentrations also coincides with the change in effluent DIC concentrations over the same PVs (Figure 4.2(f, i)), potentially suggesting acetoclastic methanogenesis (i.e., $CH_3COO^- + H_20 \longrightarrow CH_4 + HC0_3^-$). Methanogenesis in the BA-PC column is supported by the qPCR data which show the average abundance of total archaea was enriched at the influent end ($3.3 \times 10^{+6}$ copies/mL at 4 cm from the influent versus $3.9 \times 10^{+4} \pm 7.7 \times 10^{+3}$ copies/mL [average background abundance]), followed by a gradual reduction to less than background at the effluent end ($1.4 \times 10^{+4}$ copies/mL at 30 cm from the influent) (Figure 4.6(b) and see Table C.7 for the qPCR data). The NGS data also show a high relative abundance of archaea at the influent end of the BA-PC column. Specifically, members of the genus *Methanosarcina*, which is a versatile methanogen capable of growing on

methylated compounds, acetate or hydrogen [220, 117], was most abundant at 4 cm from the influent (81.4%) of the BA-PC column. Further downgradient from 10 to 30 cm from the influent the average relative abundance of the genera *Methanosaeta*, which contains acetoclastic methanogens as described in Section 3.3.2 [162, 161, 46] (15.7 ± 6.8%), and *Methanobacterium*, whose members are versatile and able to grow on H_2, CO_2 or formate [67] as described in Section 3.3.2 (9.7 ± 3.6%), were elevated (Figure 4.6(c-e) and see Table C.8 for the NGS data). The most abundant archaea (*Methanosarcina* and *Methanosaeta*) are capable of acetoclastic methanogenesis [220, 70, 162] which supports the production of DIC in tandem with CH_4 (Figure 4.2(f, i)). Other archaea of elevated relative abundance at select locations along the BA-PC column length included the genus *Methanoregula,* who are hydrogenotrophic methanogens that require acetate for growth and are associated with benzene degradation activity [221, 222, 223] (4% at 30 cm from the influent), and the families Methanocellaceae (4.7% at 10 cm from the influent) and Methanomicrobiales (5.3% at 30 cm from the influent), who are hydrogenotrophic methanogens associated with syntrophic toluene metabolism [224, 225]. In the BA+PACz column the qPCR data show that the average abundance of total archaea at the influent ($1.5 \times 10^{+5} \pm 1.6 \times 10^{+5}$ copies/mL at 2.5 to 13.5 cm from the influent) and effluent ($9.3 \times 10^{+4} \pm 1.1 \times 10^{+5}$ copies/mL at 20.5 to 34.5 cm from the influent) ends were less than within the PAC zone ($3.4 \times 10^{+5} \pm 2.4 \times 10^{+5}$ copies/mL at 14.5 to 18.5 cm from the influent) (Figure 4.6(g)), potentially suggesting the PAC provided support for archaeal growth [117]. The NGS data for the BA+PACz column show that *Methanosarcina* is most abundant at the influent end (2.5 cm from the influent) (35.5% relative abundance). Within the downgradient end of the PAC zone within the BA+PACz column (18.5 to 22 cm from the influent) the average relative abundance of *Methanosarcina* was also elevated (29.4 ± 10.7%) in addition to *Methanomethylovorans*, which are canonically methylotrophic methanogens [161] as described in Section 3.3.2 (7 ± 3.8% from 20.5 to 22 cm from the influent), which coincides with the location of lower solid phase toluene concentration as shown in Figure 4.6(f). Within the upgradient regions of the PAC zone in the BA+PACz column (from 9 to 16.5 cm from the influent), where the solid phase toluene concentration was highest as shown in Figure 4.6(f), the genus *Methanosaeta*, which are acetoclastic as described above but also capable of CO_2 reduction to CH_4 by directly accepting electrons transferred from bacteria through the PAC as described in Section 3.3.3 [78, 73, 118, 174] (21.4 ± 7.3%), is most abundant. From 15.5 to 18.5 cm from the influent within the PAC zone of the BA+PACz column, the average relative abundance of the genus *Methanobacterium* was also elevated (20.5 ± 6.7%) (Figure 4.6(h-j) and see Table C.8 for

the NGS data). The proliferation of *Methanosaeta* [112, 118, 117] and *Methanosarcina* [76, 119, 117] within the PAC zone is notable given these genera are associated with AC-mediated DIET, and the elevated relative abundances within the PAC zone shows that the presence of PAC influenced the microbial activity within the single-solute BA+PACz column.

Isotope data for the single-solute BA-PC column shows no change in the values of effluent δ^{13}C-T relative to the AGW signature except from at PV 9.4 and 27.5 where an increase in δ^{13}C-T was observed (-26.2 ± 1.1‰ [sample average over PVs] versus -27.8‰ [AGW signature]). The increase in δ^{13}C-T in the single-solute BA-PC column indicates ^{13}C-T enrichment which suggests anaerobic biodegradation of toluene occurred at PV 9.4 and 27.5 (Figure 4.4(d) and see Table C.6 for the isotope data). Increases in the values of δ^{2}H-T were also observed in the effluent of the BA-PC column (-25.1 ± 14.4‰ versus -82.1‰) over all PVs (4.9-61.1) relative to the AGW signature, which additionally supports the anaerobic biodegradation of toluene (Figure 4.4(e) and see Table C.6 for the isotope data). Relative to the single-solute KC+PACz column (Figure 4.4(a, b)), in the BA-PC column the average value of δ^{2}H-T was 41.8‰ higher which shows a larger shift in the hydrogen isotope ratio during anaerobic biodegradation (in the BA-PC column) as opposed to sorption to the PAC (in the KC+PACz column), as expected [84, 45]. Isotope data for toluene (δ^{13}C-T and δ^{2}H-T) in the single-solute BA+PACz column is unavailable since the effluent toluene concentration was depleted (Figure 4.2(g)), which prevented a direct comparison of the carbon and hydrogen isotope fractionation of toluene between the single-solute KC+PACz, BA-PC and BA+PACz columns.

The values of effluent δ^{13}C-DIC were variable, showing increases or decreases for the BA-PC column (ranging from -8.4‰ at PV 9.4 to 3.6‰ at PV 37.2 versus -2.9‰ [AGW signature]) and BA+PACz column (ranging from -12.5‰ at PV 60.3 to 8.3‰ at PV 4.6 versus -2.9‰) relative to the AGW signature (Figure 4.4(f, g) and see Table C.6 for the isotope data). Similar to the effluent CH_4 concentrations, the change in value of δ^{13}C-DIC coincided with the changes in the effluent DIC concentrations over the same PVs (Figure 4.2(f, i)), which is contrary to the typical shift in δ^{13}C-DIC associated with PHC biodegradation under sulfate reducing conditions (i.e., ^{13}C-DIC depletion is expected as ^{1}H-T and ^{12}C-T are oxidized and the generated ^{12}C-DIC becomes enriched [95]). Enrichment or depletion in ^{13}C-DIC is also expected when coupled to methanogenic reactions that consume ^{12}C-DIC to form ^{12}C-CH_4 which enriches the remaining ^{13}C-DIC (e.g., hydrogenotrophic methanogenesis) [226, 227, 228, 205, 229], or methanogenic reactions that generate ^{12}C-DIC from ^{12}C products (e.g., acetoclastic

methanogenesis), respectively. As a result of either methanogenic reaction (i.e., hydrogenotrophic or acetoclastic methanogenesis) the change in the DIC concentration is expected to be inverse of the shift in δ^{13}C-DIC which was not observed in the single-solute BA-PC or BA+PACz columns, and therefore the cause of the change in the carbon isotopes of DIC are inconclusive.

4.3.3 BTX bioactive system

In the multi-solute (BTX) BA-PC column the effluent toluene concentration was reduced from an average of 5.2 ± 0.6 to 3.7 ± 0.8 mg/L over PV 2.8-16.4, 9 ± 0.9 to 1.4 ± 1.4 mg/L over PV 18.2-22.3, and 16 ± 2.2 to 10.5 ± 0.3 mg/L over PV 26.3-29.5 followed by a reduction to 0.9 mg/L by PV 48.2 (Figure 4.3(d)). The reduction in the effluent toluene concentration was similar between the multi-solute BA-PC column and the single-solute BA-PC column discussed in Section 4.3.2 (Figure 4.2(d)). Contrarily, over all PVs (2.8-48.2) only a minor reduction in the effluent *o*-xylene concentration and minimal change in the effluent benzene concentration occurred for the BA-PC column. Limited biodegradation of benzene and *o*-xylene were expected due to the recalcitrance of benzene [54, 185, 154], and the preferential biodegradation of toluene prior to *o*-xylene [54, 56, 187] (as described in Section 4.3) combined with the continual replenishment of toluene in the influent. Despite the limited biodegradation of benzene and *o*-xylene, over each stepwise increase in influent concentration the effluent *o*-xylene concentration was reduced slightly more than benzene. Differences in the effluent concentrations between benzene and *o*-xylene included reductions from 4.6 ± 0.4 to 3.6 ± 0.6 mg/L (*o*-xylene, 21.9% reduction) versus 5.6 ± 0.5 to 5.2 ± 1.1 mg/L (benzene, 7.9% reduction) over PV 2.8-16.4, 8 ± 0.8 to 4.9 ± 1.5 mg/L (*o*-xylene, 38.8% reduction) versus 10 ± 0.7 to 7.7 ± 1.2 mg/L (benzene, 23.3% reduction) over PV 18.2-22.3, and 16.6 ± 1.6 to 13.5 ± 3.2 mg/L (*o*-xylene, 18.5% reduction) versus 18 ± 1.9 to 15.8 ± 2.8 mg/L (benzene, 12.7% reduction) over PV 23.3-48.2 (Figure 4.3(d)). The slightly higher reduction in the effluent *o*-xylene concentration relative to benzene may be related to co-metabolism of *o*-xylene during toluene biodegradation [64], as described in Section 4.3, or potentially slightly higher retardation of *o*-xylene to the BS relative to benzene (with *o*-xylene sorbing more than benzene due to difference in the K_{d_i} [Table B.3]).

Like the single-solute BA+PACz column (Figure 4.2(g)), the combination of PAC sorption and anaerobic biodegradation in the multi-solute BA+PACz column resulted in a larger reduction in the effluent toluene concentration relative to biodegradation alone (in the BA-PC column [Figure 4.3(d)]) or

sorption alone (in the KC+PACz column [Figure 4.3(a)]). The effluent toluene concentration from the multi-solute BA+PACz column was nearly depleted (0.2 ± 0.1 mg/L) over all PVs (2.4-64.9) with influent concentrations of 4 ± 1.6 mg/L over PV 2.4-23.1, 9 ± 0.5 mg/L over PV 25.5-29.5 and 17.4 ± 1 mg/L over PV 30.9-64.9 (Figure 4.3(g)). Therefore, similar to the single-solute BA+PACz column the multi-solute BA+PACz column also maintained nearly depleted effluent toluene concentrations over each stepwise increase in the influent BTX concentrations; however, dissimilar to the single-solute BA+PACz column, this was accomplished in the presence of other solutes (benzene and *o*-xylene) likely competing for sorption sites on the PAC as toluene was desorbed and biodegraded. For *o*-xylene in the BA+PACz column, the effluent concentration was depleted to 0.3 ± 0.03 mg/L when the influent concentrations were 3.9 ± 0.9 mg/L over PV 2.4-23.1 and 7.8 ± 0.6 mg/L over PV 25.5-29.5. However, when the influent *o*-xylene concentration was increased to the highest concentration of 16.7 ± 1.4 mg/L over PV 30.9-64.9 the effluent *o*-xylene concentration gradually increased from 0.5 mg/L to 7.5 mg/L. The increase in the effluent *o*-xylene concentration from the BA+PACz column may be due to breakthrough or saturation of the PAC capacity for *o*-xylene in the absence of substantial biodegradation given that *o*-xylene is competitively inhibited during toluene biodegradation (Figure 4.3(g)). In the BA+PACz column the influent benzene concentration was increased from 4.5 ± 1.7 mg/L over PV 2.4-23.1 to 9.7 ± 0.4 mg/L over PV 25.5-29.5 to 19.1 ± 1 mg/L over PV 30.9-64.9, while the effluent benzene concentration increased from 1.6 to 4.4 mg/L over PV 2.4-23.1, stabilized at 4.1 ± 0.2 mg/L from PV 25.5-29.5, and increased from 4.8 to 18.8 mg/L over PV 30.9-64.9 (Figure 4.3(g)). The increase in the effluent benzene concentration over most stepwise increases in influent concentration shows breakthrough in the BA+PACz column which was expected given that the PAC sorption capacity for benzene was lowest (relative to toluene and *o*-xylene) [28, 21, 29, 202], as described in Section 4.3.

Similar to the single-solute BA+PACz column (described in Section 4.3.2), at the leading edge of the PAC zone in the multi-solute BA+PACz column (14.5 cm from the influent [i.e., median sample distance within the incrementally collected and homogenized solid phase sample, described in Section 4.2.3]) the solid phase concentration of toluene was highest (0.003 mg/g), and only at this location was the solid phase concentration of toluene greater than benzene (0.001 mg/g). Additionally, between solutes the solid phase concentration of *o*-xylene (0.02 mg/g) was highest at the leading edge of the PAC zone due to the preferential sorption and higher sorption capacity of *o*-xylene relative to both toluene and benzene. Directly downgradient of the leading edge to the end of the PAC zone the solid phase

concentration of toluene gradually decreased to 0.004 mg/g (at 19.5 cm from the influent), whereas the solid phase concentrations of *o*-xylene (0.8 mg/g) and benzene (0.03 mg/g) increased (Figure 4.7(f)). The variation in sorption between solutes within the PAC zone is due to the biodegradation of toluene and regeneration of sorption sites on the PAC (with greater mass removal towards the end of the PAC zone furthest from the influent source of BTX being continually replenished), resulting in higher sorption capacities of *o*-xylene and benzene. The average solid phase BTX concentrations within the BA+PACz column in the upgradient (0.0022 ± 0.0032 mg/g [X] > $6.9 \times 10^{-4} \pm 9.6 \times 10^{-4}$ mg/g [T] > $4.9 \times 10^{-4} \pm 0.8 \times 10^{-4}$ mg/g [B]) and downgradient (0.0034 ± 0.0054 mg/g [X] > 0.0011 ± 0.0024 mg/g [B] > $2.4 \times 10^{-4} \pm 3.9 \times 10^{-4}$ mg/g [T]) regions outside of the PAC zone, in addition to along the entire column length of the BA-PC column ($0.0012 \pm 2.2 \times 10^{-4}$ mg/g [X] > $8.5 \times 10^{-5} \pm 1.2 \times 10^{-5}$ mg/g [T] > 8×10^{-5} mg/g [B]) were 1 to 3 orders of magnitude lower than within the PAC zone (Figure 4.7(a, f)), which is similar to the results described for toluene in the single-solute BA-PC and BA+PACz columns (Figure 4.6(a, f)) (Section 4.3.2).

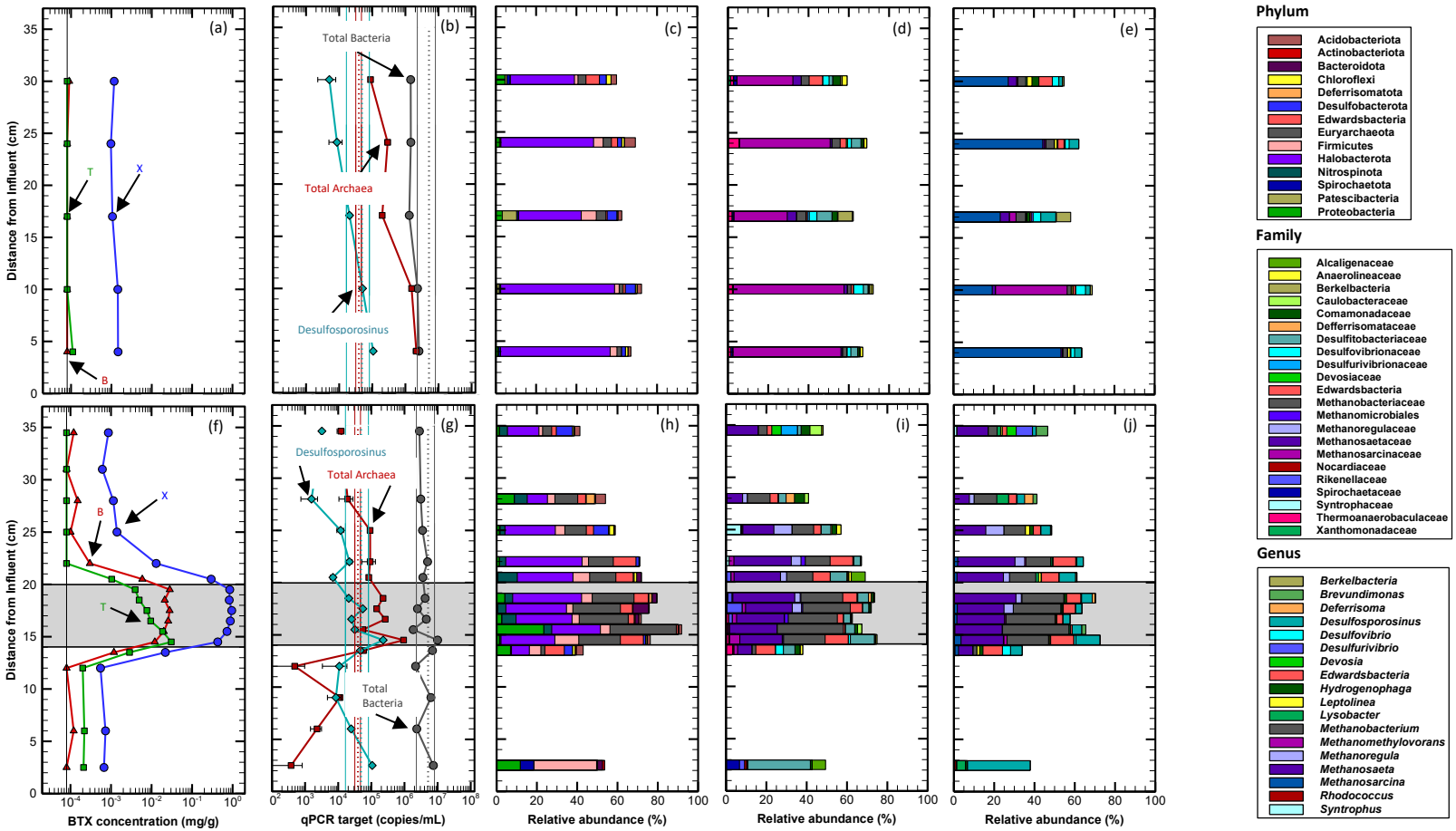

Figure 4.7: Solid phase (a, f) concentration of benzene (red filled triangles), toluene (green filled squares) and *o*-xylene (blue filled circles) (BTX); (b, g) abundance of *Desulfosporosinus* (light blue filled diamonds), total bacteria (grey filled circles) and total archaea (dark red filled squares) from quantitative polymerase chain reaction (qPCR) analysis; and relative abundance (≥ 4%) of bacteria and archaea detected at the (c, h) phylum, (d, i) family and (e, j) genus taxonomic levels using 16S ribosomal ribonucleic acid (rRNA) next generation sequencing (NGS) for the multi-solute (BTX) BA-PC (top panel) and BA+PACz (bottom panel) columns after Year-2 of column operation. The grey region in the bottom panel represents the powdered activated carbon (PAC) zone. The vertical line in (a, f) represents the method detection limit of solid phase BTX (8.0×10^{-5} mg/g). The data in (b, g) represent the average of three measurements and the dashed vertical lines represent the background abundances. Error bars and solid vertical lines in (b, g) are ± 1 standard deviation. The phylum, family and genus legends correspond to (c, h), (d, i) and (e, j), respectively. Sample depths from the influent represent the median distance of incrementally collected samples that were homogenized.

Anaerobic biodegradation in the multi-solute BA-PC and BA+PACz columns is supported by similar geochemical activity as described for the single-solute columns in Section 4.3.2, including a reduction in the influent sulfate concentrations listed in Section 3.4 to an average effluent sulfate concentration of 0.2 ± 0.4 mg/L between columns over PV 2.6 ± 0.3 to 56.6 ± 11.8 (Figure 4.3(e, h)). Sulfate reduction is also supported by increases in the average effluent DIC and sulfide concentrations between the BA-PC and BA+PACz columns, including influent concentrations of 10.9 ± 3.9 mg/L for DIC and 2.1 ± 2.5 µg/L for sulfide relative to effluent concentrations of 28 ± 12.13 mg/L for DIC over all PVs (2.6 ± 0.3 to 56.6 ± 11.8) and a peak value of 50 µg/L for sulfide by PV 56.6 ± 11.8 (Figure 4.3(e-f, h-i)). In support of methanogenesis, between the BA-PC and BA+PACz columns the average effluent CH_4 concentration increased from 0.01 ± 0.03 to 13.7 ± 8.5 mg/L over PV 2.6 ± 0.3 to 56.6 ± 11.8 (Figure 4.3(f, i)). Additionally, the average effluent DO concentration remained low (0.5 ± 0.3 mg/L), the effluent pH was neutral (7 ± 0.2) and the effluent ORP ranged from 160.4 to -140.2 mV relative to a higher average influent value (175 ± 32.4 mV) for the BA-PC and BA+PACz columns (Figure C.5(c, d)). From the geochemical parameters monitored, given the limited difference in the magnitude of change between the multi-solute columns this indicates that the PAC zone within the BA+PACz column did not substantially influence the microbial activity during PHC biodegradation relative to the BA-PC column without a PAC zone.

The qPCR data shows an enrichment in *Desulfosporosinus* at the influent ends of the multi-solute BA-PC ($1.1 \times 10^{+5}$ copies/mL at 4 cm from the influent) and BA+PACz ($1.1 \times 10^{+6}$ copies/mL at 2.5 cm from the influent) columns relative to background ($4.9 \times 10^{+4} \pm 3.3 \times 10^{+4}$ copies/mL). Enrichment of *Desulfosporosinus* at the influent ends of the multi-solute columns, closet to the influent source of toluene and sulfate and at the location of FeS formation (Figure C.3(k, l)) as discussed in Section 4.3, supports sulfate reduction at these locations. With distance from the influent end of the BA-PC column the abundance of *Desulfosporosinus* gradually decreased to an average abundance of $6.8 \times 10^{+3} \pm 2.5 \times 10^{+3}$ copies/mL at 24 to 30 cm from the influent (Figure 4.7(b) and see Table C.7 for the qPCR data). The NGS data also show that *Desulfosporosinus* was detected in the influent end (4 cm from the influent) of the BA-PC column (3.4%), although similar to the single-solute BA-PC column (described in Section 4.3.2) a peak value of 7.5% was detected further downgradient at 17 cm from the influent (Figure 4.7(c-e) and see Table C.8 for the NGS data). Like the PC-BA column, the qPCR data for the BA+PACz column show that the average abundance of *Desulfosporosinus* decreased downgradient of the PAC zone at 28 to 34.5 cm from the influent ($2.4 \times 10^{+3} \pm 1.2 \times 10^{+3}$ copies/mL) in addition to upgradient of the PAC zone at 6 to 12 cm from the influent ($1.5 \times 10^{+4} \pm 8.7 \times 10^{+3}$ copies/mL) relative to the influent and background abundances. Although, within the PAC zone of the BA+PACz column (15.5 to 20.5 cm from the influent)

the average abundance of *Desulfosporosinus* was similar to background ($3.3 \times 10^{+4} \pm 1.5 \times 10^{+4}$ copies/mL), neglecting at 14.5 cm from the influent where *Desulfosporosinus* was enriched ($2.3 \times 10^{+5}$ copies/mL) (Figure 4.7(g) and see Table C.7 for the qPCR data) which coincides with the location of highest solid phase toluene concentration, as described above (Figure 4.7(f)). The NGS data, also show that the relative abundance of *Desulfosporosinus* was highest at the influent end of the BA+PACz column (31.17% at 2.5 cm from the influent), in addition to the leading edge of the PAC zone (11.9% at 14.5 cm from the influent) relative to all other locations along the column length (4.4 ± 1.8% at 13.5 and 15.5 to 34.5 cm from the influent) (Figure 4.7(h-j) and see Table C.8 for the NGS data). Like the BA-PC column, the relative abundance of *Desulfosporosinus* was highest where the sulfate and/or toluene concentrations were presumed to be highest which suggests this SRB was involved in toluene biodegradation.

The qPCR data show the abundance of total bacteria within the multi-solute BA-PC and BA+PACz columns was similar to the single-solute columns described in Section 4.3.2, being numerous along the column lengths but not enriched relative to background (i.e., $3.8 \times 10^{+6} \pm 2.3 \times 10^{+6}$ copies/mL [average abundance between columns] versus $5.2 \times 10^{+6} \pm 2.2 \times 10^{+6}$ copies/mL [average background abundance]) (Figure 4.7(b, g) and see Table C.7 for the qPCR data). The NGS data show that along the BA-PC column length (4 to 30 cm from the influent) the genus *Desulfovibrio* is the most abundant bacterium (3.2 ± 1.3%). Other bacteria with elevated relative abundances at select locations along the BA-PC column length included the genera *Berkelbacteria* (7.1% at 17 cm from the influent) and *Edwardsbacteria* (6.7% at 30 cm from the influent), and the family Thermoanaerobaculaceae (5.3% at 24 cm from the influent) (Figure 4.7(c-e) and see Table C.8 for the NGS data). In the upgradient region of the BA+PACz column at 2.5 cm from the influent the family Spirochaetaceae, whose members can produce acetate by fermentation and are associated with anaerobic PHC degradation [230] (6.7%), and the genus Lysobacter (4.2%) were elevated. Within the PAC zone of the BA+PACz column the NGS data showed that the relative abundance of the phylum Nitrospinota, whose members are involved in nitrification [231] (5.8 ± 2.6% from 15.5 to 20.5 cm from the influent), and the family Rikenellaceae (7.7% at 17.5 cm from the influent) were elevated. As was similarly observed in the single-solute BA+PACz column (as described in Section 4.3.2), in the downgradient region of the PAC zone in the BA+PACz column (from 18.5 to 22 cm from the influent) the average relative abundance of *Edwardsbacteria* was elevated (9 ± 2.1%). At 14.5 cm from the influent within the PAC zone (the location of highest solid phase toluene concentration, as described above [Figure 4.7(f)]), *Edwardsbacteria* (9.7%) and *Desulfovibrio* (4%) were the most abundant genera detected which was also observed in the single-solute BA+PACz column for *Desulfovibrio* (as described in Section 4.3.2).

In the downgradient region of the BA+PACz column the relative abundance of several bacteria were elevated including the phyla Nitrospinota (5.3 ± 1.7% from 28 to 34.5 cm from the influent) and Vicinamibacterales, which are associated with PHC degradation using nitrite [232] (4.9% at 28 cm from the influent); the family Comamonadaceae (4.7 ± 0.4% from 28 to 34.5 cm from the influent); and the genera *Lysobacter* (5.9% at 28 cm from the influent), *Syntrophus*, whose members produce acetate, hydrogen and CO_2 through the fermentation of benzoate [233, 234, 209] (7.3% at 25 cm from the influent), *Brevundimonas*, which are associated with aerobic PHC degradation [235] that could have potentially been sustained by the residual O_2 at the effluent end of the column (Figure C.5(d)) (5.8% at 34.5 cm from the influent), *Desulfurivibrio*, who are SRB [236] (8.1% at 34.5 cm from the influent) and *Devosia* (4.7% at 34.5 cm from the influent) (Figure 4.7(h-j) and see Table C.8 for the NGS data).

Similar to the single-solute BA-PC column described in Section 4.3.2, the qPCR data for the multi-solute BA-PC column show an enrichment in total archaea ($2.1 \times 10^{+6}$ copies/mL versus $3.9 \times 10^{+4} \pm 7.7 \times 10^{+3}$ copies/mL [average background abundance]) within the influent end (4 cm from the influent), followed by a gradual reduction ($8.9 \times 10^{+4}$ copies/mL) within the effluent end (30 cm from the influent) (Figure 4.7(b) and see Table C.7 for the qPCR data). The NGS data show that the influent end of the multi-solute BA-PC column was dominated by the genus *Methanosarcina* at 4 cm from the influent (53.4% relative abundance) and, although detected at a reduced average relative abundance, *Methanosarcina* was also detected along the remainder of the column length (28.5 ± 11% from 10 to 30 cm from the influent). The relative abundance of *Methanomethylovorans* was elevated primarily at 10 cm from the influent within the BA-PC column (35.6%), which are methylotrophic methanogens that convert methylated compounds to CH_4 [161], as described in Section 3.3.2. Within the downgradient region of the BA-PC column the average relative abundance of the genera *Methanosaeta* (4.3 ± 0.3% at 17 and 30 cm from the influent) and *Methanobacterium* (4.3 ± 0.4% at 17 to 30 cm from the influent) were slightly elevated (Figure 4.7(c-e) and see Table C.8 for the NGS data), which is similar to the spatial distribution of these methanogens within the single-solute BA-PC column (described in Section 4.3.2 [Figure 4.6(c-e)]). The detection of these archaea indicates methylotrophic or acetoclastic methanogenesis may have predominated within the multi-solute BA-PC column which supports the production of DIC and CH_4 [70] shown in Figure 4.3(f, i). Contrary to the single-solute BA+PACz column, the qPCR data show that the average abundance of total archaea was lowest within the influent end of the multi-solute BA+PACz column ($1.1 \times 10^{+3} \pm 1.1 \times 10^{+3}$ copies/mL versus $3.9 \times 10^{+4} \pm 7.7 \times 10^{+3}$ copies/mL [average background abundance]) from 2.5 to 6 and 12 cm from the influent. However, like the single-solute BA+PACz column the average abundance of total archaea was highest and enriched within the PAC zone of the

multi-solute BA+PACz column ($3.9 \times 10^{+5} \pm 3.7 \times 10^{+5}$ copies/mL) from 14.5 and 16.5 to 18.5 cm from the influent (Figure 4.7(g) and see Table C.7 for the qPCR data). Consistent with the single-solute BA+PACz column described in Section 4.3.2, the NGS data show that the archaea of highest average relative abundance primarily within the PAC zone of the multi-solute BA+PACz column includes the genera *Methanosaeta* (24.8 ± 3.4% from 14.5 to 22 cm from the influent) and *Methanobacterium* (24.4 ± 5% 14.5 to 18.5 cm from the influent). However, dissimilar to the single-solute BA+PACz column *Methanosarcina* was detected at a lower relative abundance as compared to the other archaea and primarily at 14.5 cm from the influent (3.4%), coinciding with the location of highest solid phase toluene concentration as shown in Figure 4.7(f). Additionally, the average relative abundance of *Methanoregula* was elevated within the PAC zone to the downgradient region of the BA+PACz column from 17.5 to 28 cm from the influent (4.6 ± 2.5%) (i.e., further downgradient of the location of the elevated solid phase toluene concentration [Figure 4.7(f)]) (Figure 4.7(h-j) and see Table C.8 for the NGS data). Consistent with the single-solute BA+PACz column, the enriched archaeal community at higher relative abundances within the PAC zone, as compared to regions outside of the PAC zone, demonstrates that the PAC spatially influenced the microbial growth of methanogens relative to the BA-PC column. The presence of the PAC zone in the BA+PACz columns may be providing support for biofilm formation [36, 38, 111], or potentially AC-mediated DIET as described in Section 1.1.3 [112, 76, 78, 108].

Isotope data for the multi-solute BA-PC column showed no change in the effluent values of δ^{13}C-B,T from PV 5.2-43.1 for benzene (-25.2 ± 0.2‰ [sample average over PVs] versus -25.6‰ [AGW signature]) and PV 5.2-31.2 for toluene (-27.9 ± 0.2‰ versus -27.8‰) relative to the AGW signatures. However, at PV 50.8 for benzene and from PV 43.1-50.8 for toluene increases in the values of δ^{13}C-B (-23.9‰ versus -25.6‰) and decreases in the values of δ^{13}C-T (-28.7 ± 0.08‰ versus -27.8‰) were observed relative to the AGW signatures. Contrarily, the values of δ^{13}C-X were consistently reduced relative to the AGW signature (-32.1 ± 0.9‰ versus -29.9‰) over all PV (5.2-50.8) within the BA-PC column (Figure 4.5(d) and see Table C.6 for the isotope data) which was similarly observed in the multi-solute BA+PACz column (-32.6 ± 2.1‰ versus -29.9‰) over all PVs (38.7-61.8). The values of effluent δ^{13}C-B in the multi-solute BA+PACz column were variable, showing an increase in δ^{13}C-B from PV 4.6-37.2 (-24.5 ± 0.5‰ versus -25.6‰), a decreases at PV 46.3 and 61.8 (-26.4 ± 0.2‰ versus -25.6‰), and no change relative to the AGW signature at PV 54.0 (-25.5‰ versus -25.6‰) (Figure 4.5(g) and see Table C.6 for the isotope data). The change in the values of δ^{13}C-B,T between the multi-solute BA-PC or BA+PACz columns were similar to those observed for the multi-solute KC+PACz column, described in Section 4.3.1 (Figure 4.5(a)), potentially indicating that the change in the carbon isotopes of benzene and

toluene are not associated with anaerobic biodegradation. The reduction in the values of δ^{13}C-X in all multi-solute columns indicates a depletion in ^{13}C-X occurred (Figure 4.5(a, d, g)); however, more fractionation of the carbon isotopes of *o*-xylene occurred in the BA-PC and BA+PACz columns relative to the KC+PACz column. Although notable, the cause of ^{13}C-X depletion in the multi-solute columns is inconclusive given that isotope shifts associated with anaerobic biodegradation or sorption are expected to enrich ^{13}C-X due to the consumption [164, 84, 80, 85] or sorption [86, 87, 88, 89], respectively, of the lighter isotope (^{12}C-X). Depletion in ^{13}C-X is also expected due to the desorption of the lighter isotope (^{12}C-X), although this is likely not the cause of the ^{13}C-X depletion between the multi-solute columns given the high solid phase concentration of *o*-xylene shown in the Figure 4.7(a, f). Isotope data for toluene (δ^{13}C-T) in the multi-solute BA+PACz column is unavailable since the effluent toluene concentration was depleted (Figure 4.3(g)), which prevented a direct comparison of the carbon isotope fractionation of toluene between the multi-solute KC+PACz, BA-PC and BA+PACz columns.

The values of δ^{2}H-B,T,X increased relative to the AGW signatures for the multi-solute BA-PC column over all PVs (5.2-50.8) (-72.5 ± 7‰ [sample average for B over all PVs] versus -98.4‰ [AWG signature of B], -32.7 ± 13.7 [sample average of T over all PVs] versus -82.1‰ [AWG signature of T], and -86.1 ± 26.1‰ [sample average of X over all PVs] versus -132.1‰ [AWG signature of X]) (Figure 4.5(e) and see Table C.6 for the isotope data). Given that the PHC data in Figure 4.3(d) and the ΔM of benzene or *o*-xylene in Table C.4 (described in Section 4.3) do not support substantial anaerobic biodegradation of benzene or *o*-xylene, increases in the values of δ^{2}H-B,X (indicating enrichment in ^{2}H-B,X) are likely attributed to causes other than biodegradation (e.g., partial substrate oxidation through co-metabolism during toluene oxidation [64], as described in Section 4.3). Relative to benzene and *o*-xylene, the values of δ^{2}H-T were higher indicating that more enrichment in ^{2}H-T occurred in the multi-solute BA-PC column, which is attributed to the anaerobic biodegradation of toluene as supported by the PHC data in Figure 4.3(d) and the ΔM of toluene in Table C.4 (described in Section 4.3). The magnitude of ^{2}H-T enrichment in the BA-PC column was also similar to the single-solute column described in Section 4.3.2 (Figure 4.4(e)), and relative to the multi-solute KC+PACz column with sorption only (Figure 4.5(b)) the average value of δ^{2}H-T was 30.5‰ higher due to anaerobic biodegradation (in the BA-PC column), as expected [84, 45]. For the multi-solute BA+PACz column over all PVs (4.6-61.8) the values of δ^{2}H-B were elevated relative to the AGW signature (-80.7 ± 5.9‰ versus -82.1‰), indicating enrichment in ^{2}H-B which was similar to the magnitude of enrichment in the multi-solute KC+PACz (Figure 4.5(b)) and BA-PC (Figure 4.5(e)) columns. In the BA+PACz column the values of δ^{2}H-X were also elevated relative to the AGW signature (-46.3 ± 2.6‰ versus -132.1‰) over all PVs (38.7-61.8) (Figure 4.5(h) and see

Table C.6 for the isotope data), with the average value of δ^2H-X 54‰ and 58‰ greater than the average values in the multi-solute KC+PACz and BA-PC columns, respectively. The higher values of δ^2H-X in the BA+PACz column relative to both the KC+PACz and BA-PC columns supports higher ^{2}H-X enrichment associated with enhanced *o*-xylene sorption to the PAC zone within the BA+PACz column as toluene was desorbed and biodegraded (enhanced sorption of *o*-xylene did not occur in the KC+PACz column due to the presence of toluene). Sorption as opposed to anaerobic biodegradation of *o*-xylene in the multi-solute BA+PACz column is supported by the high solid phase concentration of *o*-xylene (relative to the other solute) as shown in Figure 4.7(f), in addition to the PHC data in Figure 4.3(g) and the ΔM of *o*-xylene in Table C.4 (described in Section 4.3) that do not support substantial *o*-xylene biodegradation. Isotope data for toluene (δ^2H-T) in the multi-solute BA+PACz column is unavailable since the effluent toluene concentration was depleted (Figure 4.3(g)), which prevented a direct comparison of the hydrogen isotope fractionation of toluene between the multi-solute KC+PACz, BA-PC and BA+PACz columns.

The values of effluent δ^{13}C-DIC were variable for the multi-solute BA-PC column, showing increases at PV 5.2 (12.3‰) and 31.2 (3.8‰) and reductions (-6‰ ± 0.8 [sample average over PVs]) over PV 43.1-50.8 relative to the AGW signature (-2.9‰) (Figure 4.5(f) and see Table C.6 for the isotope data). However, for the multi-solute BA+PACz column minimal change in the values of δ^{13}C-DIC were observed from the effluent (2.3 ± 1.3‰ versus -2.9‰) over all PVs (4.6-61.8) (Figure 4.5(i) and see Table C.6 for the isotope data). Like the single-solute BA-PC and BA+PACz columns described in Section 4.3.2 (Figure 4.4(f, i)), the shift in the carbon isotope ratios of DIC coincides with the change in the effluent DIC concentrations (Figure 4.2(f, i) and Figure 4.3(f, i)) which is contrary to the expected shift in δ^{13}C-DIC under sulfate reducing or methanogenic conditions. Therefore, like the single-solute system the cause of the change in the carbon isotopes of DIC are inconclusive for the multi-solute BA-PC or BA+PACz columns.

4.4 Conclusion

During the Year-1 and Year-2 of column operation the total ΔM of toluene between the influent and effluent of the single-solute (toluene-only) and multi-solute (BTX) columns was highest for the BA+PACz columns due to a combination of biodegradation and sorption, relative to the BA-PC or KC+PACz columns due to biodegradation alone or sorption alone, respectively. For instance, during Year-2 within the single-solute system the ΔM of toluene between the influent and effluent followed BA+PACz

(99.5% reduction) > KC+PACz (74.6% reduction) > BA-PC (44.4% reduction). Similarly, between the multi-solute columns the ΔM of toluene between the influent and effluent followed BA+PACz (98.5% reduction) > BA-PC (59.2% reduction) > KC+PACz (25.4% reduction). Between the single- and multi-solute KC+PACz columns with sorption alone, the ΔM of toluene between the influent and effluent during Year-2 was greater for the single-solute column (74.6% reduction) relative to the multi-solute column (25.4% reduction) given that the sorption capacity of toluene was greater in the single-solute system in the absence of multi-solute competitive sorption. Between the single- and multi-solute bioactive BA+PACz columns with PAC zones, a depletion in effluent toluene mass over sequential increases in the influent concentration from 5 to 10 to 20 mg/L was consistently demonstrated during Year-2. However, for the other solutes in multi-solute BA+PACz column (benzene and *o*-xylene) breakthrough was observed due to the recalcitrance of benzene and the competitive inhibition of *o*-xylene during toluene biodegradation.

In the multi-solute KC+PACz column, the ΔM of BTX between the influent and effluent during Year-2 followed X (42.2% reduction) > T (25.4% reduction) > B (5.2% reduction), given that *o*-xylene has the highest sorption capacity followed by toluene and then benzene (consistent with the results described in Chapter 2). In the multi-solute BA-PC column the ΔM of BTX between the influent and effluent followed T (59.2% reduction) > X (16.9% reduction) > B (8.3% reduction) due to the preferential biodegradation of toluene prior to *o*-xylene and the recalcitrance of benzene (as observed in Chapter 3 during the microcosm investigation). Comparatively, the ΔM of BTX between the influent and effluent of the multi-solute BA+PACz column followed T (98.5% reduction) > X (85.2% reduction) > B (14.4% reduction) due to the preferential biodegradation of toluene and preferential sorption of *o*-xylene as toluene was biodegraded. Enhanced sorption of *o*-xylene (and benzene) directly downgradient of the leading edge within the PAC zone of the multi-solute BA+PACz column was shown from the higher solid phase concentration of *o*-xylene (then benzene) relative to the leading edge, which was due to the increased availability of sorption sites as toluene was continually desorbed and biodegraded. However, at the leading edge of the PAC zone the solid phase concentration of toluene was higher due to the direct contact with the continually replenished influent source of BTX, which resulted in the magnitude of solid phase sorption following X > T > B.

During Year-2 anaerobic biodegradation (sulfate reduction and methanogenesis) within the bioactive single- and muti-solute BA-PC and BA+PACz columns was supported by the reduction of sulfate, and formation of sulfide, DIC and CH_4 in the column effluents. Contrarily, no change in the effluent sulfate, sulfide or CH_4 concentrations were observed in the single- or multi-solute KC+PACz columns due to the lack of anaerobic biodegradation (some DIC was abiotically generated). Like the microcosm systems (in Chapter 3), there was no distinguishable difference in the magnitude of change of the geochemical

parameters monitored between the single- and multi-solute BA-PC or BA+PACz columns, showing that the presence of a PAC zone did not influence the microbial activity during PHC biodegradation. However, the PAC did influence the spatial distribution of anaerobic microbes along the bioactive single and multi-solute BA-PC or BA+PACz columns lengths. Between the single- and multi-solute BA-PC columns the abundance of *Methanosarcina* and *Methanomethylovorans* were highest at the influent ends of the columns relative to the effluent ends. However, for the single- and multi-solute BA+PACz columns the abundances of *Methanosaeta*, *Methanobacterium* and *Methanosarcina* were highest within the PAC zone relative outside of the PAC zone, in addition to being higher in abundance relative to all bacteria detected within the PAC zone (primarily *Desulfosporosinus*, *Edwardsbacteria* and *Berkelbacteria*). In the multi-solute BA+PACz column, the abundance of *Desulfosporosinus* was also notably elevated at the leading edge of the PAC zones (coinciding with the location of the highest solid phase toluene concentration).

Given that hydrogen isotope fractionation is often substantially larger than carbon isotope fractionation, changes in the values of δ^2H-B,T,X provided more insight into the mass reduction or removal processes occurring during Year-2 relative to δ^{13}C-B,T,X. Enrichment of ^{2}H-T was shown in the single- and multi-solute BA-PC and KC+PACz columns, although the average value of δ^2H-T between the BA-PC columns with bioactivity was 36.1 ± 8‰ greater than in the KC+PACz columns with only sorption, as expected. The magnitude of hydrogen isotope fractionation of toluene associated with a combination of PAC sorption and biodegradation in the BA+PACz columns is unknown given toluene was depleted. Unlike toluene, a direct comparison of the hydrogen isotope fractionation of *o*-xylene between the multi-solute columns showed that the average value of δ^2H-X was 54‰ and 58‰ greater in the BA+PACz column relative to the BA-PC and KC+PACz columns, respectively. ^{2}H-X enrichment in the multi-solute BA+PACz column was presumably due to a significant amount of *o*-xylene sorption to the PAC as toluene was biodegraded as opposed to substantial *o*-xylene biodegradation (supported by the solid phase data).

Chapter 5

5.1 Conclusion

Injected activated carbon (AC) particulate amendments for the *in situ* treatment of groundwater impacted by petroleum hydrocarbons (PHCs) is relatively new, and relies on a combination of AC sorption and biodegradation. Currently the performance of this technology remains unclear, primarily related to the long-term interplay between sorption and biodegradation and whether the presence of AC enhances the anaerobic biodegradation of PHCs relative to systems without AC. To address these uncertainties, this research investigated the sorption and anaerobic biodegradation (sulfate reducing and methanogenic) behaviour of toluene (as a single-solute) or benzene, toluene and *o*-xylene (BTX) (combined in a multi-solute system) in microcosm experiments amended with AC and column experiments designed to mimic an AC permeable reactive barrier (PRB) over a period of 1 to 2 years. Specific research question asked as part of this research included:

Q1. Are AC sorption isotherms generated under ideal conditions representative of sorption behaviour in bioactive AC systems?
Q2. Does AC influence microbial activity during PHC biodegradation?
Q3. Does biodegradation regenerate AC sorption capacity?
Q4. Does AC enhance the biodegradation rate of PHCs?
Q5. How do bioactive systems with AC respond to variable PHC loading?
Q6. Can CSIA distinguish biodegradation from AC sorption in bioactive systems?

The powdered AC (PAC) used in this research (WPC from Calgon Carbon Corporation) was characterized in Chapter 2, using scanning electron microscopy (SEM). The SEM results showed the PAC had a rough, irregular surface with potential macropore openings of 0.8 ± 0.3 μm, and variable particle sizes with an average diameter of 11.5 ± 4.4 μm. Additionally, the PAC sorption and desorption of BTX in single-solute (benzene [B], toluene [T], or *o*-xylene [X]) and multi-solute (BTX) systems were investigated. The sorption and desorption behaviour were driven by differences in chemical properties between solutes, which resulted in the magnitude of single- or multi-solute BTX sorption to the PAC following X > T > B and the magnitude of desorption reversed. Between the single- and multi-solute

systems the magnitude of sorption in the multi-solute system was reduced relative to the single-solute systems due to competitive sorption and a reduction in the availability of sorption sites for all solutes. The sorption and desorption processes differed, which is indicative of hysteresis; however, hysteresis was not explored as part of this research given the limited nature of only a single desorption step. Temporal sorption (up to 48 hours) and desorption (up to 720 hours) data showed the time to reach sorption and desorption equilibrium for single-solute benzene and toluene was rapid (≤ 0.5 hours). The rapid sorption and desorption time indicates that diffusion limitations (or other time-dependent factors) effecting desorption do not appear to be the cause of the suspected single-solute hysteretic behaviour between the sorption and desorption processes.

In Chapter 2 single- and multi-solute sorption isotherms were also developed for B, T or X and BTX in contact with PAC under ideal conditions and were compared to the aqueous and solid phase microcosm data in Chapter 3 to address Q1. The best-fit single-solute Freundlich isotherm model parameters for benzene, toluene and *o*-xylene in contact with the PAC were 36.1 ± 3.8, 0.484 ± 0.045, and 88.2 ± 7.7 for K_{f_i} ([mg/g][L/mg]^n) and 0.421 ± 0.044, 132 ± 20 and 0.371 ± 0.099 for n_{f_i} (-), respectively. The multi-solute improved simplified ideal adsorption solution (ISIAS) model competition factors (a_i) for benzene, toluene and *o*-xylene in contact with the PAC were 1.42 ± 0.38, 1.43 ± 0.16 and 1.08 ± 0.08, respectively. Mass balance between the directly measured aqueous and solid phases relative to the initial mass within the isotherm systems releveled that in general minimal mass was lost or gained from both the single- and multi-solute sorption and desorption isotherm systems (i.e., < 10% average mass lost or gained, neglecting 29.6 ± 37.7% for benzene and 12.2 ± 14.6% for toluene during desorption in the multi-solute system presumably due to volatilization during sampling). The limited mass lost or gained from the sorption equilibrium systems supports the reliability of the indirect estimate of the solid phase B, T or X and BTX concentrations (i.e., difference between the initial and equilibrium aqueous phase concentrations) used to generate the Freundlich and ISIAS sorption isotherms through non-linear regression.

In Chapter 3 single-solute (toluene-only) and multi-solute (BTX) abiotic and bioactive (including sulfate-limited [10-20 mg/L SO_4^{2-}]) or sulfate amended [138-275 mg/L SO_4^{2-}]) microcosms with and without PAC were constructed (in addition to starved controls without toluene, BTX or PAC). PAC sorption of single-solute toluene or multi-solute BTX within the PAC amended abiotic and bioactive microcosms showed similar magnitudes of sorption between solutes (i.e., X > T > B) and systems (i.e., single-solute > multi-solute sorption) as described in Chapter 2. The aqueous and solid phase toluene or BTX

concentrations from the single- and multi-solute PAC amended microcosms were compared to single- and multi-solute Freundlich or ISIAS model predictions of the equilibrium solid phases. In general, the Freundlich or ISIAS models were found to overestimate the measured solid phase concentrations in the microcosm systems (**addressing Q1**). Differences in solid phase concentrations between the isotherm and microcosm systems may be related to several factors, including: differences in equilibrium times; differences in solution matrix chemistries (e.g., ionic strengths); interferences or competition from other sorbing components within the microcosm systems, not found in the isotherm systems (e.g., within the BS, or metabolites from biodegradation); and/or the presence of a biofilm layer surrounding the PAC particles (generating diffusional resistance or pore filling from of extracellular polymeric substances [EPS]). For the multi-solute PAC amended abiotic and bioactive microcosms *o*-xylene deviated the most from the ISIAS model predicted solid phase concentrations followed by toluene and then benzene, which is attributed to differences in the magnitude of sorption between solutes (i.e., following X > T > B).

In the subset of single-solute (toluene-only) and multi-solute (BTX) sulfate-limited (i.e., 10-20 mg/L SO_4^{2-}) bioactive microcosms evidence of methanogenesis coupled to a background substrate (other than substantial toluene or BTX mass) was evident from the geochemical (i.e., CH_4 production) and molecular (i.e., *Methanomethylovorans*, *Methanosaeta* and *Methanobacterium* enrichment) data. Notably, methane production and methanogenic enrichment were consistently more elevated in the sulfate limited microcosms with PAC relative to the sulfate limited microcosms without PAC, potentially supporting enhanced methanogenesis and archaeal growth in the presence of the PAC (e.g., through AC mediated direct interspecies electron transfer [DIET]) (**in support of Q2**). Contrarily in the single-solute (toluene-only) and multi-solute (BTX) sulfate amended bioactive microcosms (i.e., 138-275 mg/L SO_4^{2-}) sulfate reduction was coupled to the oxidation of toluene or *o*-xylene (not benzene, which was recalcitrant). Biodegradation in the sulfate amended bioactive microcosms was evidenced by the repetitive or preferential reduction in toluene within the single- and multi-solute microcosms (≥ 92.4% reduction of total mass within 12 to 66 days) followed by *o*-xylene in the multi-solute microcosms (≥ 98.9% reduction of total mass within ≤ 120 days following BTX dosing or ≤ 62 days following the depletion of toluene) and supported by the geochemical (i.e., SO_4^{2-} reduction, and HS^- and TIC formation) and molecular (i.e., enrichment of sulfate reducing bacteria, including *Desulfosporosinus*, *Desulfoprunum* and Desulfobacteraceae) data. Within the sulfate and PAC amended bioactive microcosms the solid phase mass of toluene was also found to be repetitively reduced by ≥ 95.5% during anaerobic biodegradation showing PAC regeneration (**addressing Q3**) and the reversibility of toluene sorption with bioactivity. Although anaerobic biodegradation of toluene

and *o*-xylene were repetitively demonstrated, there was no substantial difference in the PHC, geochemical or molecular data between the sulfate amended bioactive microcosms with and without PAC indicating that the presence of PAC did not influence the anaerobic microbial activity during PHC biodegradation (**addressing Q2**). Additionally, there was no difference in the zero-order biodegradation rate constants for toluene between the microcosms with and without PAC during high-resolution monitoring, which confirms that in the microcosm system the presence of PAC did not enhance the anaerobic biodegradation of toluene (**addressing Q4**). Collectively, the microcosm data assembled over the 1-year monitoring period from the sulfate amended single- and multi-solute bioactive microcosms revealed that the presence of PAC did not generate any discernible differences in the anaerobic biodegradation of toluene between the microcosms with and without PAC.

In Chapter 4 three types of single-solute (toluene-only) and multi-solute (BTX) columns (37 cm long, 3.75 cm inner diameter) were constructed to represent PAC sorption alone, bioactivity alone, and PAC sorption with bioactivity. The columns were operated for approximately 2 years, with Year-1 serving as an acclimation period, and Year-2 used for high-resolution temporal monitoring. For the columns containing PAC, a 6-cm long PAC zone (0.5% wt/wt) was located near the middle of the column to mimic an AC PRB. During Year-2 the overall column mass balance (i.e., estimated by subtracting the cumulative effluent mass from the cumulative mass injected) for the multi-solute column with an installed PAC zone and no bioactivity showed a change in BTX mass between the influent and effluent following X (42.2% reduction) > T (25.4% reduction) > B (5.2% reduction) given that *o*-xylene has the highest sorption capacity followed by toluene and then benzene. Between the single- and multi-solute columns with PAC zones and no bioactivity the change in toluene mass between the influent and effluent was greater for the single-solute column (74.6% reduction) relative to the multi-solute column (25.4% reduction) given that the sorption capacity of toluene was greater in the single-solute system in the absence of multi-solute competitive sorption. For the multi-solute bioactive column without a PAC zone the change in BTX mass between the influent and effluent ends of the column followed T (59.2% reduction) > X (16.9% reduction) > B (8.3% reduction) due to the preferential biodegradation of toluene prior to *o*-xylene and the recalcitrance of benzene (as similarly shown in Chapter 3). For the multi-solute bioactive column with a PAC zone the change in BTX mass between the influent and effluent ends of the column followed T (98.5% reduction) > X (85.2% reduction) > B (14.4% reduction) due to the preferential biodegradation of toluene and preferential sorption of *o*-xylene as toluene was biodegraded. Sorption, as opposed to anaerobic biodegradation of *o*-xylene in the multi-solute bioactive column with a PAC zone is supported by the high

solid phase concentration of *o*-xylene, relative to the other solutes (benzene > toluene) sorbed to the PAC directly downgradient of the leading edge of the PAC zone. The increased sorption of *o*-xylene and benzene to the PAC in the multi-solute BA+PACz column was due to the desorption and biodegradation of toluene in the downgradient regions of the PAC zone, which increased the availability of sorption sites primarily for *o*-xylene in addition to benzene. At the leading edge of the PAC zone, closest to the influent source of BTX being continually replenished, the solid phase concentration of toluene was higher than the downgradient regions with the magnitude of solid phase sorption following X > T > B.

Consistently observed, the largest change in toluene mass between the influent and effluent was attributed to a combination of sorption and biodegradation, as opposed to sorption alone or biodegradation alone. For example, among the single-solute columns the mass removal of toluene was greatest for the bioactive column with a PAC zone (99.5% reduction), followed by the column with only a PAC zone (74.6% reduction) and the column with only bioactivity (44.4% reduction). Similarly, between the multi-solute columns the mass removal of toluene was greatest for the bioactive column with a PAC zone (98.5% reduction), followed by the column with only bioactivity (59.2% reduction) and the column with only a PAC zone (25.4% reduction). The depletion in the effluent toluene concentration ($< 0.5 \pm 0.1$ mg/L) during Year-2 was consistent between the single- and multi-solute bioactive columns with PAC zones during sequential increases in the influent concentrations (**addressing Q5**). For the other solutes (benzene and *o*-xylene) in the multi-solute bioactive column with a PAC zone breakthrough was observed given the recalcitrance of benzene and the competitive inhibition of *o*-xylene during toluene biodegradation.

Anaerobic biodegradation within the single- and multi-solute bioactive columns was supported by changes in geochemical parameters that would be expected under sulfate reducing and methanogenic conditions (i.e., SO_4^{2-} reduction, and HS^-, TIC and CH_4 formation). Like the microcosm systems, there was no difference in the magnitude of change of the geochemical parameters monitored between columns with or without PAC, suggesting that the PAC zone in the bioactive columns did not influence microbial activity during PHC biodegradation. However, the PAC did influence the spatial distribution of anaerobic microbes along the bioactive column lengths (**addressing Q2)**. For the single- and multi-solute bioactive columns without a PAC zone, the relative abundance of *Methanosarcina* and *Methanomethylovorans* were highest at the influent ends relative to the effluents. However, for the single- and multi-solute bioactive columns with a PAC zone the relative abundance of *Methanosaeta*, *Methanobacterium* and *Methanosarcina* were highest within the PAC zone relative to outside of the PAC zone, in addition to being higher in abundance relative to all bacteria detected within the PAC zone (primarily *Desulfosporosinus*, *Edwardsbacteria* and

Berkelbacteria). In the multi-solute bioactive columns with a PAC zone, the abundance of *Desulfosporosinus* was also notably elevated at the leading edge of the PAC zones (coinciding with the location of the highest solid phase toluene concentration).

Between the single- and multi-solute columns, compound specific isotope analysis (CSIA) showed enrichment of ^{2}H-T in the columns with only bioactivity or a PAC zone, although the average value of δ^{2}H-T between the single- and multi-solute columns with only bioactivity was 36.1 ± 8‰ greater than for the columns with only a PAC zone, as expected. The magnitude of hydrogen isotope fractionation of toluene associated with a combination of PAC sorption and biodegradation, is unknown given toluene was depleted in the bioactive column with a PAC zone (**in support of Q6**). Unlike toluene, a direct comparison of the hydrogen isotope fractionation of *o*-xylene between the multi-solute columns showed that the average value of δ^{2}H-X was 54‰ and 58‰ greater in the bioactive column with a PAC zone relative to the columns with only a PAC zone or only bioactivity, respectively. ^{2}H-X enrichment in the multi-solute bioactive column with a PAC zone was presumably due to a significant amount of *o*-xylene sorption to the PAC as toluene was biodegraded as opposed to substantial *o*-xylene biodegradation (supported by the solid phase data).

Collectively the compiled data sets provide comprehensive insight into how AC particulate amendments behave in anaerobic systems in contact with PHCs, and the interplay between BTX sorption and anaerobic biodegradation under sulfate reducing and methanogenic conditions. These data provide direct evidence that the presence of PAC particulate amendments does not enhance the biodegradation of BTX relative to systems with no PAC under sulfate reducing conditions. Instead, the presence of the PAC provides rapid reductions in contaminant concentrations relative to systems without PAC and sustains reductions in the aqueous phase concentration of the most preferentially degraded solute under variable loading conditions as the PAC is regenerated. The PAC also influences microbial activity during PHC biodegradation by promoting microbial growth on the PAC, with notably high methanogenic enrichment. This research also provides evidence that ideal isotherms are not representative of the sorption behaviour in bioactive systems with AC and tend to overestimate sorption. Finally, PAC sorption, most notably for the most preferentially sorbed solute in the multi-solute system, generates substantial hydrogen isotope enrichment which may lead to overestimations in the fractionation presumed to be associated with biodegradation when integrating CSIA into monitoring approaches for bioactive systems with AC.

5.2 Recommendations for future work

To address the limitations of this research, several recommendations are provided which may provide further insight into the sorption and anaerobic biodegradation behaviour in bioactive systems with AC in future research. For the sorption experiments described in Chater 2, given that the single-solute Freundlich and multi-solute ISIAS isotherm model parameters developed under ideal conditions were found to overestimate the solid phase toluene or BTX concentrations in bioactive microcosms with AC, the development of sorption isotherms in the systems they will be applied to (as opposed to controlled ideal laboratory conditions) may provide more accurate estimates of the solid phase concentrations. Additionally, other single-solute sorption equilibria isotherm models (e.g., those listed in Table 1.1 [Section 1.1.1]) or multi-solute sorption equilibria models (versus the Freundlich and ISIAS models used in this research) may be explored to determine if the sorption behaviour is better represented by other models. It is also recommended to carry out multiple desorption steps (as opposed to the single desorption step used as part of this research) to further investigate the presumed hysteretic behaviour observed between the single- and multi-solute sorption and desorption processes. Finally, given that the sorption and desorption equilibrium times were rapid (i.e., ≤ 0.5 hours), equilibrium time experiments can be conducted utilizing higher resolution monitoring, with a focus on the first 0.5 hours of sorption or desorption. For the microcosm systems described in Chapter 3, the sampling frequency during long-term monitoring can be increased from monthly to potentially weekly sampling intervals which may allow for the estimation of PHC biodegradation rates during the long-term monitoring period. Biodegradation rates were not estimated during long-term monitoring as part of this research given that the rate of toluene biodegradation in the sulfate amended bioactive microcosms was generally faster than the 1-month sampling interval used. Instead, the estimation of the biodegradation rate of toluene was limited to the high-resolution monitoring period at the end of the experimental duration (i.e., during the last 23 to 40 days). In multi-solute microcosm systems competitive inhibition of solutes (e.g., *o*-xylene) during the biodegradation of preferentially degraded solutes (e.g., toluene) should also be accounted for to ensure that the biodegradation of all solutes can be monitored, which was not accomplished for *o*-xylene during the 40-day high-resolution monitoring period as only toluene was biodegraded. For the column experiments described in Chapter 4, increases in the influent single- and multi-solute PHC concentrations may potentially generate detectable effluent concentrations for the most preferentially biodegraded solute(s) which may allow for more enhanced monitoring between columns. In this research, given that

toluene was depleted from the effluent of the bioactive columns with PAC zones this prevented CSIA for toluene which would have assisted in answering Q6 by directly comparing the isotope fractionation of toluene between columns with bioactivity or PAC sorption alone versus bioactivity and PAC sorption. Estimation of the biodegradation rate constants between bioactive columns with and without PAC zones may also be determined to provide more insight into Q4. For bioactive columns with PAC zones, the biodegradation rates of PHCs can be determined by applying the ideal stoichiometric ratios between the PHC(s) and other electron acceptor(s) or the reduced or oxidized by-products of the biodegradation reaction(s), to the change in concentrations between the influent and effluent for parameters that are not depleted in the effluent or sorbed to the PAC.

Future investigations should fundamentally consider multi-solute systems given that preferential sorption and biodegradation heavily influence contaminant treatment within multi-solute groundwater systems which are most frequently encountered at contaminated field sites where AC particulate amendments may be installed. In this research only substantial toluene mass was removed in the bioactive columns with a PAC zone and limited *o*-xylene biodegradation occurred due to competitive inhibition; however, the potential for the mass reduction of *o*-xylene may also be explored in columns with longer PAC zones relative to the 6 cm length used as part of this research. With an extended length of the PAC zone preferential biodegradation of toluene may occur upgradient, potentially allowing for the desorption and biodegradation of *o*-xylene further downgradient at locations where toluene is depleted. Additionally, the installation of sampling ports along the length of columns will allow for depth discrete aqueous phase sampling and monitoring, which may provide insight into the potential zonation of AC sorption and biodegradation processes that are expected to vary between solutes. Sampling ports will allow for enhanced monitoring of the column system, as opposed to only assessing changes in the influent and effluent concentrations for each solute as was done as part of this research. Columns can also be monitored in replicate, allowing for replicate aqueous phase measurements, or sacrificial sampling of the solid phase material over the monitoring period as opposed to a single timepoint at the end of the experiment as was done as part of this research.

References

[1] Nadim, F., G.E. Hoag, S. Liu, R.J. Carley, and P. Zack, "Detection and remediation of soil and aquifer systems contaminated with petroleum products: an overview," *Journal of Petroleum Science and Engineering,* vol. 26, no. 1-4, pp. 169-178, 2000.

[2] Khan, F.I., T. Husain, and R. Hejazi, "An overview and analysis of site remediation technologies," *Journal of Environmental Management,* vol. 71, no. 2, pp. 95-122, 2004.

[3] Farhadian, M., C. Vachelard, D. Duchez, and C. Larroche, "In situ bioremediation of monoaromatic pollutants in groundwater: A review," *Bioresource Technology,* vol. 99, no. 13, pp. 5296-5308, 2008.

[4] Ossai, I.C., A. Ahmed, A. Hassan, and F.S. Hamid, "Remediation of soil and water contaminated with petroleum hydrocarbon: A review," *Environmental Technology & Innovation,* vol. 17, p. 100526, 2020.

[5] McDougall, G.J., "The physical nature and manufacture of activated carbon," *Journal of the South African Institute of Mining and Metallurg,* vol. 91, no. 4, pp. 109-120, 1991.

[6] Menéndez-DíazaI, J.A., and I. Martín-Gullónb, "Chapter 1 Types of carbon adsorbents and their production," *Interface Science and Technology,* vol. 7, pp. 1-48, 2006.

[7] Menya, E., P.W. Olupot, H. Storz, M. Lubwama, and Y. Kiros, "Production and performance of activated carbon from rice husks for removal of natural organic matter from water: A review," *Chemical Engineering Research and Design,* vol. 129, pp. 271-296, 2018.

[8] Lewoyehu, M., "Comprehensive review on synthesis and application of activated carbon from agricultural residues for the remediation of venomous pollutants in wastewater," *Journal of Analytical and Applied Pyrolysis,* vol. 159, p. 105279, 2021.

[9] Harris, P.J.F., Z. Liu, and K. Suenaga, "Imaging the atomic structure of activated carbon," *Journal of Physics: Condensed Matter,* vol. 20, no. 36, p. 362201, 2008.

[10] Pre, P., G. Huchet, D. Jeulin, J-N. Rouzaud, M. Sennour, and A. Thorel, "A new approach to characterize the nanostructure of activated carbons from mathematical morphology applied to high resolution transmission electron microscopy images," *Carbon,* vol. 52, no. 45, pp. 239-258, 2013.

[11] Pawlyta, M., "Transmission electron microscope studies on carbon nanostructured materials," *Archives of Material Science and Engineering,* vol. 63, no. 2, pp. 58-67, 2013.

[12] Raad, M.T., H. Behnejad, and M.E.l. Jamal, "Equilibrium and kinetic studies for the adsorption of benzene and toluene by graphene nanosheets: a comparison with carbon nanotubes," *Surface and Interface Analysis,* vol. 48, no. 3, pp. 117-125, 2016.

[13] Cecen, F., and O. Aktas, Activated Carbon for Water and Wastewater Treatment, Weinheim, Germany: Wiley-VCH, 2012.

[14] Ando, N., Y. Matsui, R. Kurotobi, Y. Nakano, T. Matsushita, and K. Ohno, "Comparison of natural organic matter adsorption capacities of super-powdered activated carbon and powdered activated Carbon," *Water Research,* vol. 44, no. 14, pp. 4127-4136, 2010.

[15] Partlan, E., K. Davis, Y. Ren, O.G. Apul, O.T. Mefford, T. Karanfil, and D.A. Ladner, "Effect of bead milling on chemical and physical characteristics of activated carbons pulverized to superfine sizes," *Water Research,* vol. 89, pp. 161-170, 2016.

[16] Valderrama, C., X. Gamisans, X. de las Heras, A. Farran, and J.L. Cortina, "Sorption kinetics of polycyclic aromatic hydrocarbons removal using granular activated carbon: Intraparticle diffusion coefficients," *Journal of Hazardous Materials,* vol. 157, no. 2-3, pp. 386-396, 2008.

[17] Yuan, M., S. Tong, S. Zhao, and C.Q. Jia, "Adsorption of polycyclic aromatic hydrocarbons from water using petroleum coke-derived porous carbon," *Journal of Hazardous Materials,* vol. 181, no. 1-3, pp. 1115-1120, 2010.

[18] Boehm, H.P., "Some aspects of the surface chemistry of carbon blacks and other carbons," *Carbon,* vol. 32, no. 5, pp. 759-769, 1994.

[19] Srivastava, A., B. Gupta, A. Majumder, A.K. Gupta, and S.K. Nimbhorkar, "A comprehensive review on the synthesis, performance, modifications, and regeneration of activated carbon for the adsorptive removal of various water pollutants," *Journal of Environmental Chemical Engineering,* vol. 9, no. 5, p. 106177, 2021.

[20] Yonge, D.R., T.M. Keinath, K. Poznanska, and Z.P. Jiang, "Single-solute irreversible adsorption on granular activated carbon," *Environmental Science & Technology,* vol. 19, no. 8, pp. 690-694, 1985.

[21] Daifullah, A.A.M., and B.S. Girgis, "Impact of surface characteristics of activated carbon on adsorption of BTEX adsorption of BTEX," *Colloids and Surfaces A: Physicochemical and Engineering Aspects,* vol. 214, no. 1-3, pp. 181-193, 2002.

[22] Bu, J., G. Loh, C.G. Gwie, S. Dewiyanti, M. Tasrif, and A. Borgna, "Desulfurization of diesel fuels by selective adsorption on activated carbons: Competitive adsorption of polycyclic aromatic sulfur heterocycles and polycyclic aromatic hydrocarbons," *Chemical Engineering Journal,* vol. 166, no. 1, pp. 207-217, 2011.

[23] Mojoudi, N., N. Mirghaffari, M. Soleimani, H. Shariatmadari, C. Belver, and J. Bedia, "Phenol adsorption on high microporous activated carbons prepared from oily sludge: equilibrium, kinetic and thermodynamic studies," *Scientific Reports,* vol. 9, no. 1, p. 19352, 2019.

[24] Williams, P.T., and A.R. Reed, "Development of activated carbon pore structure via physical and chemical activation of biomass fibre waste," *Biomass Bioenergy,* vol. 30, no. 2, pp. 144-152, 2006.

[25] Wang, X., D. Li, W. Li, J. Peng, H. Xia, L. Zhang, S. Guo, and G. Chen, "Optimization of mesoporous activated carbon from coconut shells by chemical activation with phosphoric acid," *Bioresources,* vol. 8, no. 4, pp. 6184-6195, 2013.

[26] Sweetman, M.J., S. May, N. Mebberson, P. Pendleton, and K. Vasilev, "Activated carbon, carbon nanotubes and graphene: Materials and composites for advanced water purification," *Journal of Carbon Research,* vol. 3, no. 2, p. 18, 2017.

[27] Pelekani, C., and V.L. Snoeyink, "Competitve adsorption in natural water: Role of activated carbon pore size," *Water Research,* vol. 33, no. 5, pp. 1209-1219, 1999.

[28] El-Dib, M.A., A.S. Moursy, and M.I. Badawy, "Role of adsorbents in the removal of soluble aromatic hydrocarbons from drinking waters," *Water Research,* vol. 12, no. 12, pp. 1131-1137, 1978.

[29] de Souza, S.M.A.G.U., A.D. da Luz, A. da Silva, and A.A.U. de Souza, "Removal of mono- and multicomponent BTX compounds from effluents using activated carbon from coconut shell as the adsorbent," *Industrial & Engineering Chemistry Research,* vol. 51, no. 18, pp. 6461-6469, 2012.

[30] Majd, M.M., V. Kordzadeh-Kermani, V. Ghalandari, A. Askari, and M. Sillanpää, "Adsorption isotherm models: A comprehensive and systematic review (2010−2020)," *Science of the Total Environment,* vol. 812, p. 151334, 2022.

[31] El-Dib, M., and M.I. Badawy, "Adsorption of soluble aromatic hydrocarbons on granular activated carbon," *Water research,* vol. 13, no. 3, pp. 255-258, 1979.

[32] Chatzopoulos, D., A. Varma, and R.L. Irvine, "Activated carbon adsorption and desorption of toluene in the aqueous phase," *AIChE Journal,* vol. 39, no. 12, pp. 2027-2041, 1993.

[33] Stähelin, P.M., A. Valério, S.M.A.G.U. de Souza, A. da Silva, J.A.B. Valle, and A.A.U. de Souza, "Benzene and toluene removal from synthetic automotive gasoline by mono and bicomponent adsorption process," *Fuel,* vol. 231, pp. 45-52, 2018.

[34] Hackbarth, V.F., V.J.P. Vilar, G.B. De Souza, S.M.A.G.U. de Souza, and A.A. U. de Souza, "Benzene, toluene and o-xylene (BTX) removal from aqueous solutions through adsorptive processes," *Adsorption,* vol. 20, no. 4, pp. 577-590, 2014.

[35] Mohammed, J., N.S. Nasri, M.A.A. Zaini, U.D. Hamza, and F.N. Ani, "Adsorption of benzene and toluene onto KOH activated coconut shell based carbon treated with NH3," *International Biodeterioration & Biodegradation,* vol. 102, pp. 245-255, 2015.

[36] Voice, T.C., D. Pak, X. Zhao, J. Shi, and R.F. Hickey, "Biological activated carbon in fludized bed reactors for the treatment of groundwater contaminated with volatile aromatic hydrocarbons," *Water Research,* vol. 26, no. 10, pp. 1389-1401, 1992.

[37] Mason, C.A., G. Ward, K. Abu-Salah, O. Keren, and C.G. Dosoretz, "Biodegradation of BTEX by bacteria on powdered activated carbon," *Bioprocess Engineering ,* vol. 23, pp. 331-336, 2000.

[38] Aktas, O., and F. Cecen, "Bioregeneration of activated carbon: A review," *International Biodeterioration & Biodegradation,* vol. 59, no. 4, pp. 257-272, 2007.

[39] Zhang, W., W. Ding, and W. Ying, "Biological activated carbon treatment for removing BTEX from groundwater," *Journal of Environmental Engineering,* vol. 139, no. 10, pp. 1246-1254, 2013.

[40] Walters, R.W., and R.G. Luthy, "Equilibrium adsorption of polycyclic aromatic hydrocarbons from water onto activated carbon," *Environmental Science & Technology,* vol. 18, no. 6, pp. 395-403, 1984.

[41] Braida, W.J., .J.J. Pignatello, Y. Lu, P.I. Ravikovitch, A.V. Neimark, and B. Xing, "Sorption hysteresis of benzene in charcoal particles," *Environmental Science & Technology,* vol. 37, no. 2, pp. 409-417, 2003.

[42] Yang, K., and B. Xing, "Desorption of polycyclic aromatic hydrocarbons from carbon nanomaterials in water," *Environmental Pollution,* vol. 145, no. 2, pp. 529-537, 2007.

[43] Jia, Y.F., and K.M. Thomas, "Adsorption of cadmium ions on oxygen surface sites in activated carbon," *Langmuir,* vol. 16, no. 3, pp. 1114-1122, 2000.

[44] Tessmer, C.H., R.D. Vidic, and L.J. Uranowski, "Impact of oxygen-containing surface functional groups on activated carbon adsorption of phenols," *Environmental Science & Technology,* vol. 31, no. 7, pp. 1872-1878, 1997.

[45] Mancini, S.A., A.C. Ulrich, G. Lacrampe-Couloume, B. Sleep, E.A. Edwards, and B. Sherwood Lollar, "Carbon and hydrogen isotopic fractionation during anaerobic biodegradation of benzene," *Applied and Environmental Microbiology,* vol. 69, no. 1, pp. 191-198, 2003.

[46] Lueders, T., "The ecology of anaerobic degraders of BTEX hydrocarbons in aquifers," *FEMS Microbiology Ecology,* vol. 93, no. 1, p. fiw220, 2017.

[47] Bombach, P., H.H. Richnow, M. Kastner, and A. Fischer, "Current approaches for the assessment of in situ biodegradation," *Applied Microbiology and Biotechnology,* vol. 86, no. 3, pp. 839-852, 2010.

[48] Vroblesky, D.A., and F.H. Chapelle, "Temporal and spatial changes of terminal electron-accepting processes in a petroleum hydrocarbon-contaminated aquifer and the significance for contaminant biodegradation," *Water Resources Research,* vol. 30, no. 5, pp. 561-157, 1994.

[49] Borden, R.C., C.A. Gomez, and M.T. Becker, "Geochemical indicators of intrinsic bioremediation," *Ground Water,* vol. 33, no. 2, pp. 180-189, 1995.

[50] Christensen, T.H., P.L. Bjerg, S.A. Banwart, R. Jakobsen, G. Heron, and H-J. Albrechtsen, "Characterization of redox conditions in groundwater contaminant plumes," *Journal of Contaminant Hydrology,* vol. 45, no. 3-4, pp. 165-241, 2000.

[51] Kao, C.M., and C.C. Wang, "Control of BTEX migration by intrinsic bioremediation at a gasoline spill site," *Water Research,* vol. 34, no. 13, pp. 3413-3423, 2000.

[52] Chapelle, F.H., P.M. Bradley, D.R. Lovley, K. O'Neill, and J.E. Landmeyer, "Rapid evolution of redox processes in a petroleum hydrocarbon-contaminated aquifer," *Gorundwater ,* vol. 40, no. 4, pp. 353-360, 2002.

[53] Beller, H.R., D. Grbic-Galic, and M. Reinhard, "Microbial degradation of toluene under sulfate-reducing conditions and the influence of iron on the process," *Applied and Environmental Microbiology,* vol. 58, no. 3, pp. 786-793, 1992.

[54] Edwards, E.A., L.E. Wills, M. Reinhard, and D. Grbic-Galic, "Anaerobic degradation of toluene and xylene by aquifer microorganisms under sulfate-reducing conditions," *Applied and Enviromental Microbiology,* vol. 58, no. 3, pp. 794-800, 1992.

[55] Rabus, R., R. Nordhaus, W. Ludwig, and F. Widdel, "Complete oxidation of toluene under strictly anoxic conditions by a new sulfate-reducing bacterium," *Applied and Environmental Microbiology,* vol. 59, no. 5, pp. 1444-1451, 1993.

[56] Phelps, C.D., and L.Y. Young, "Anaerobic biodegradation of BTEX and gasoline in various aquatic sediments," *Biodegradation,* vol. 10, no. 1, pp. 15-25, 1999.

[57] Anderson, R.T., and D.R. Lovley, "Anaerobic bioremediation of benzene under sulfate-reducing conditions in a petroleum-contaminated aquifer," *Environmental Science and Technology,* vol. 34, no. 11, pp. 2261-2266, 2000.

[58] Flanagan, P.V., B.P. Kelleher, and C.C.R. Allen, "Assessment of anaerobic biodegradation of aromatic hydrocarbons: The impact of molecular biology approaches," *Geomicrobiology Journal,* vol. 31, no. 4, pp. 276-284, 2014.

[59] Dorer, C., C. Vogt, T.R. Neu, H. Stryhanyuk, and H-H. Richnow., "Characterization of toluene and ethylbenzene biodegradation under nitrate-, iron(III)- and manganese(IV)-reducing conditions by compound-specific isotope analysis," *Environmental Pollution,* vol. 211, pp. 271-281, 2016.

[60] Gieg, L.M., and C.R.A. Toth, Signature metabolite analysis to determine in situ anaerobic hydrocarbon biodegradation, in Handbook of Hydrocarbon and Lipid Microbiology: Anaerobic Utilization of Hydrocarbons, Oils, and Lipids, New York, NY: Springer International Publishing, 2017.

[61] Griebler, C., M. Safinowski, A. Vieth, H.H. Richnow, and R.U. Meckenstock, "Combined application of stable carbon isotope analysis and specific metabolites determination for assessing in situ degradation of aromatic hydrocarbons in a tar oil-contaminated aquifer," *Environmental Science and Technology,* vol. 38, no. 2, pp. 617-631, 2004.

[62] Washer, C. E., and E.A. Edwards, "Identification and expression of benzylsuccinate synthase genes in a toluene-degrading methanogenic consortium," *Applied and Environmental Microbiology,* vol. 73, no. 4, pp. 1367-1369, 2007.

[63] Winderl, C., S. Schaefer, and T. Lueders, "Detection of anaerobic toluene and hydrocarbon degraders in contaminated aquifers using benzylsuccinate synthase (bssA) genes as a functional marker," *Environmental Microbiology,* vol. 9, no. 4, pp. 1035-1046, 2007.

[64] Foght, J., "Anaerobic biodegradation of aromatic hydrocarbons: Pathways and prospects," *Journal of Molecular Microbiology and Biotechnology,* vol. 15, no. 2-3, pp. 93-120, 2008.

[65] Winfrey, M.R., and J.G. Zeikus, "Effect of sulfate on carbon and electron flow during microbial methanogenesis in freshwater sediments," *Applied and Environmental Microbiology,* vol. 33, no. 2, pp. 275-281, 1977.

[66] Raskin, L., B.E. Rittmann, and D.A. Stahl, "Competition and coexistence of sulfate-reducing and methanogenic populations in anaerobic biofilms," *Applied and Environmental Microbiology,* vol. 62, no. 10, pp. 3847-3857, 1996.

[67] Stams, A.J.M., C.M. Plugge, F.A.M. de Bok, B.H.G.W. van Houten, P. Lens, and H. Dijkman, "Metabolic interactions in methanogenic and sulfate-reducing bioreactors," *Water Science & Technology,* vol. 52, no. 1, pp. 13-20, 2005.

[68] Holmer, M., and E. Kristensen, "Coexistence of sulfate reduction and methane production in an organic-rich sediment," *Marine Ecology Progress Series,* vol. 107, pp. 177-184, 1994.

[69] Sela-Adler, M., Z. Ronen, B. Herut, G. Antler, H. Vigderovich, W. Eckert, and O. Sivan, "Co-existence or methanogenesis and sulfate reduction with common substrates in sulfate-rich estuarine sediments," *Frontiers in Microbiology,* vol. 8, p. 766, 2017.

[70] Mesle, M., G. Dromart, and P. Oger, "Microbial methanogenesis in subsurface oil and coal," *Research in Microbiology,* vol. 164, no. 9, pp. 959-972, 2013.

[71] Stams, A.J.M., and C.M. Plugge, "Electron transfer in syntrophic communities of anaerobic bacteria and archaea," *Nature Reviews Microbiology,* vol. 7, no. 8, pp. 568-577, 2009.

[72] Gieg, L.M., S.J. Fowler, and C. Berdugo-Clavijo, "Syntrophic biodegradation of hydrocarbon contaminants," *Current Opinion in Biotechnology,* vol. 27, pp. 21-29, 2014.

[73] Baek, G., J. Kim, J. Kim, and C. Lee, "Role and potential of direct interspecies electron transfer in anaerobic digestion," *Energies,* vol. 11, no. 1, p. 107, 2018.

[74] Park, J-H., H-J. Kang, K-H. Park, and H-D. Park, "Direct interspecies electron transfer via conductive materials: A perspective for anaerobic digestion applications," *Bioresource Technology,* vol. 254, pp. 300-311, 2018.

[75] Shrestha, P.M., A-E. Rotaru, M. Aklujkar, F. Liu, M. Shrestha, Z.M. Summers, N. Malvankar, D.C. Flores, and D.R. Lovley, "Syntrophic growth with direct interspecies electron transfer as the primary mechanism for energy exchange," *Environmental Microbiology Reports,* vol. 5, no. 6, pp. 904-910, 2013.

[76] Rotaru, A-E., P.M. Shrestha, F. Liu, B. Markovaite, S. Chen, K.P. Nevin, and D.R. Lovley, "Direct interspecies electron transfer between Geobacter metallireducens and Methanosarcina barkeri," *Applied and Environmental Microbiology,* vol. 80, no. 15, pp. 4599-4605, 2014.

[77] Holmes, D.E., P.M. Shrestha, D.J.F. Walker, Y. Dang, K.P. Nevin, T.L. Woodard, and D.R. Lovley, "Metatranscriptomic evidence for direct interspecies electron transfer between Geobacter and Methanothrix species in methanogenic rice paddy soils," *Applied and Environmental Microbiology,* vol. 83, no. 9, pp. e00223-17, 2017.

[78] Lovley, D.R., "Syntrophy goes electric: Direct interspecies electron transfer," *Annual Review of Microbiology,* vol. 71, no. 1, pp. 643-664, 2017.

[79] Harrington, R.R., S.R. Poulson, J.I. Drever, P.J.S. Colberg, and E.F. Kelly, "Carbon isotope systematics of monoaromatic hydrocarbons: vaporization and adsorption experiments," *Organic Geochemistry,* vol. 30, no. 8, pp. 765-775, 1999.

[80] Richnow, H.H E. Annweiler, W. Michaelis, and R.U. Meckenstock, "Microbial in situ degradation of aromatic hydrocarbons in a contaminated aquifer monitored by carbon isotope fractionation," *Journal of Contaminant Hydrology,* vol. 65, no. 1-2, pp. 101-120, 2003.

[81] Schuth, C., H. Taubald, N. Bolano, and K. Maciejczyk, "Carbon and hydrogen isotope effects during sorption of organic contaminants on carbonaceous materials," *Journal of Contaminant Hydrology,* vol. 64, no. 3-4, pp. 269-281, 2003.

[82] Vieth, A., M. Kastner, M. Schirmer, H. Wei, S. Godeke, R.U. Meckenstock, and H.H. Richnow, "Monitoring in situ biodegradation of benzene and toluene by stable carbon isotope fractionation," *Environmental Toxicology and Chemistry,* vol. 24, no. 1, pp. 51-60, 2005.

[83] Ward, J.A.M., J.M.E. Ahad, G. Lacrampe-Couloume, G.F. Slater, E.A. Edwards, and B. Sherwood Lollar, "Hydrogen isotope fractionation during methanogenic degradation of toluene: Potential for direct verification of bioremediation," *Environmental Science & Technology,* vol. 34, no. 21, pp. 4577-4581, 2000.

[84] Mancini, S.A., G. Lacrampe-Couloume, H. Jonker, B.M. Van Breukelen, J. Groen, F. Volkering, and B. Sherwood Lollar, "Hydrogen isotopic enrichment: An indicator of biodegradation at a petroleum hydrocarbon contaminated field site," *Environmental Science & Technology,* vol. 36, no. 11, pp. 2464-2470, 2002.

[85] Steinbach, A., R. Seifert, E. Annweiler, and W. Michaelis, "Hydrogen and carbon isotope fractionation during anaerobic biodegradation of aromatic hydrocarbons - A field study," *Environmental Science and Technology,* vol. 38, no. 2, pp. 609-616, 2004.

[86] Kopinke, F-D., A. Georgi, M. Voskamp, and H.H. Richnow, "Carbon isotope fractionation of organic contaminants due to retardation on humic substances: Implications for natural attenuation studies in aquifers," *Environmental Science & Technology,* vol. 39, no. 16, pp. 6052-6062, 2005.

[87] Van Breukelen, B.M., and H. Prommer, "Beyond the rayleigh equation: Reactive transport modeling of isotope fractionation effects to improve quantification of biodegradation," *Environmental Science & Technology,* vol. 42, no. 7, pp. 2457-2463, 2008.

[88] Hohener, P., and O. Atteia, "Multidimensional analytical models for isotope ratios in groundwater pollutant plumes of organic contaminants undergoing different biodegradation kinetics," *Advances in Water Resources,* vol. 33, no. 7, pp. 740-751, 2010.

[89] Qiu, S., D. Eckert, O.A. Cirpka, M. Huenniger, P. Knappett, P. Maloszewski, R.U. Meckenstock, C. Griebler, and M. Elsner, "Direct experimental evidence of non-first order degradation kinetics and sorption-induced isotopic fractionation in a mesoscale aquifer: 13C/12C analysis of a transient toluene pulse," *Environmental Science & Technology,* vol. 47, no. 13, pp. 6892-6899, 2013.

[90] Fischer, A., I. Herklotz, S. Herrmann, M. Thullner, S.A.B. Weelink, A.J.M. Stams, M. Schlomann, H-H. Richnow, and C. Vogt, "Combined carbon and hydrogen isotope fractionation investigations for elucidating benzene biodegradation pathways," *Environmental Science & Technology,* vol. 42, no. 12, pp. 4356-4363, 2008.

[91] Mancini, S.A., C.E. Devine, M. Elsner, M.E. Nandi, A.C. Ulrich, E.A. Edwards, and B.S. Lollar, "Isotopic evidence suggests different initial reaction mechanisms for anaerobic benzene biodegradation," *Environmental Science & Technology,* vol. 42, no. 22, pp. 8290-8296, 2008.

[92] Vogt, C., E. Cyrus, I. Herklotz, D. Schlosser, A. Bahr, S. Herrmann, H-H. Richnow, and A. Fischer, "Evaluation of toluene degradation pathways by two-dimensional stable isotope fractionation," *Environmental Science & Technology,* vol. 42, no. 21, pp. 7793-7800, 2008.

[93] Herrmann, S., C. Vogt, A. Fischer, A. Kuppardt, and H-H. Richnow, "Characterization of anaerobic xylene biodegradation by two-dimensional isotope fractionation analysis," *Environmental Microbiology Reports,* vol. 1, no. 6, pp. 535-544, 2009.

[94] Solano, F.M., M. Marchesi, N.R. Thomson, D. Bouchard, and R. Aravena, "Carbon and hydrogen isotope fractionation of benzene, toluene, and o-xylene during chemical oxidation by persulfate," *Groundwater Monitoring & Remediation,* vol. 38, no. 4, pp. 62-72, 2018.

[95] Bouchard, D., D. Hunkeler, E.L. Madsen, T. Buscheck, E. Daniels, R. Kolhatkar, C.M. DeRito, R. Aravena, and N.R. Thomson, "Application of diagnostic tools to evaluate remediation performance at petroleum hydrocarbon-impacted sites," *Groundwater Monitoring & Remediation,* vol. 38, no. 4, pp. 88-98, 2018.

[96] Yargicoglu, E.N., and. K.R. Reddy, "Review of biological diagnostic tools and their applications in geoenvironmental engineering," *Reviews in Environmental Science and Biotechnology,* vol. 14, pp. 161-194, 2015.

[97] Buermans, H.P.J., and J.T. den Dunnen, "Next generation sequencing technology: Advances and applications," *Biochimica et Biophysica Acta,* vol. 1842, no. 10, pp. 1932-1941, 2014.

[98] Ambardar, S., R. Gupta, D. Trakroo, R. Lal, and J. Vakhlu, "High throughput sequencing: An overview of sequencing chemistry," *Indian Journal of Microbiology,* vol. 56, no. 4, pp. 394-404, 2016.

[99] Malik, S., M. Beer, M. Megharaj, and R. Naidu, "The use of molecular techniques to characterize the microbial communities in contaminated soil and water," *Environment International,* vol. 34, no. 2, pp. 265-276, 2008.

[100] Shi, J., X. Zhao, R.F. Hickey, and T.C. Voice, "Role of adsorption in granular activated carbon-fluidized bed reactors," *Water Environment Research,* vol. 67, no. 3, pp. 302-309, 1995.

[101] Zhao, X., K. Doh, C.S. Criddle, and T.C. Voice, "Accumulation of metabolic intermediates during shock loads in biological fluidized bed reactors," *Journal of Environmental Engineering,* vol. 123, no. 12, pp. 1185-1193, 1997.

[102] Fan, D., E.J. Gilbert, and T. Fox, "Current state of in situ subsurface remediation by activated carbon-based amendments," *Journal of Environmental Management,* vol. 204, pp. 793-803, 2017.

[103] Ottosen, C.B., P.L. Bjerg, D. Hunkeler, J. Zimmermann, N. Tuxen, D. Harrekilde, L. Bennedsen, G. Leonard, L. Brabæk, I.L. Kristensen, and M.M. Broholm, "Assessment of chlorinated ethenes degradation after field scale injection of activated carbon and bioamendments: Application of isotopic and microbial analyses," *Journal of Contaminant Hydrology,* vol. 240, p. 103794, 2021.

[104] Gibert, O., A.S. Ferguson, R.M. Kalin, R. Doherty, K.W. Dickson, K.L. McGeough, J. Robinson, and R. Thomas, "Performance of a sequential reactive barrier for bioremediation of coal tar contaminated groundwater," *Environmental Science and Technology,* vol. 41, no. 19, pp. 6795-6801, 2007.

[105] Careghini, A., S. Saponaro, and E. Sezenna, "Biobarriers for groundwater treatment: A review," *Water Science & Technology,* vol. 67, no. 3, pp. 453-468, 2013.

[106] Obiri-Nyarko, F., S.J. Grajales-Mesa, and G. Malina, "An overview of permeable reactive barriers for in situ sustainable groundwater remediation," *Chemosphere,* vol. 111, pp. 243-259, 2014.

[107] Simpson, D.R., "Biofilm processes in biologically active carbon water purification," *Water Research,* vol. 42, no. 12, pp. 2839-2848, 2008.

[108] Redwan, A.M., and K. Millerick, "Anaerobic bacterial responses to carbonaceous materials and implications for contaminant transformation: Cellular, metabolic, and community level findings," *Bioresource Technology,* vol. 341, p. 125738, 2021.

[109] Abu-Salah, K., G. Shelef, D. Levanoxf, R. Armonb, and C.G. Dosoretza, "Microbial degradation of aromatic and polyaromatic toxic compounds adsorbed on powdered activated carbon," *Journal of Biotechnology,* vol. 51, no. 3, pp. 265-272, 1996.

[110] Zhao, X., R.F. Hickey, and T.C. Voice, "Long-term evaluation of adsorption capacity in a biological activated carbon fluidized bed reactor system," *Water Research,* vol. 33, no. 13, pp. 2983-2991, 1999.

[111] Pagnozzi, G., S. Carroll, D.D. Reible, and K. Millerick, "Powdered activated carbon (PAC) amendment enhances naphthalene biodegradation under strictly sulfate-reducing conditions," *Environmental Pollution,* vol. 268, p. 115641, 2021.

[112] Liu, F., A.E. Rotaru, P.M. Shrestha, N.S. Malvankar, K.P. Nevin, and D.R. Lovley, "Promoting direct interspecies electron transfer with activated carbon," *Energy & Environmental Science,* vol. 5, pp. 8982-8989, 2012.

[113] Summers, Z.M., H.E. Fogarty, C. Leang, A.E. Franks, N.S. Malvankar, and D.R. Lovley, "Direct exchange of electrons within aggregates of an evolved syntrophic coculture of anaerobic bacteria," *Science,* vol. 330, no. 6009, pp. 1413-1415, 2010.

[114] Lee, J-Y. S-H. Lee, and H-D. Park, "Enrichment of specific electro-active microorganisms and enhancement of methane production by adding granular activated carbon in anaerobic reactor," *Bioresource Technology,* vol. 205, pp. 205-212, 2016.

[115] Bonaglia, S., E. Broman, B. Brindefalk, E. Hedlund, T. Hjorth, C. Rolff, F.J.A. Nascimento, K. Udekwu, and J.S. Gunnarsson, "Activated carbon stimulates microbial diversity and PAH biodegradation under anaerobic conditions in oil-polluted sediments," *Chemosphere,* vol. 248, p. 126023, 2020.

[116] Pagnozzi, G., S. Carroll, D.D. Reible, and K. Millerick, "Biological natural attenuation and contaminant oxidation in sediment caps: Recent advances and future opportunities," *Current Pollution Reports,* vol. 6, pp. 281-294, 2020.

[117] Ma, J., H. Wei, Y. Su, W. Gu, B. Wang, and B. Xie, "Powdered activated carbon facilitates methane productivity of anaerobic codigestion via acidification alleviating: Microbial and metabolic insights," *Bioresource Technology,* vol. 313, p. 123706, 2020.

[118] Yang, L., B. Si, Y. Zhang, J. Watson, M. Stablein, J. Chen, Y. Zhang, X. Zhou, and H. Chu, "Continuous treatment of hydrothermal liquefaction wastewater in an anaerobic biofilm reactor: Potential role of granular activated carbon," *Journal of Cleaner Production,* vol. 276, p. 122836, 2020.

[119] Xu, S., C. He, L. Luo, F. Lü, P. He, and L. Cui, "Comparing activated carbon of different particle sizes on enhancing methane generation in upflow anaerobic digester," *Bioresource Technology,* vol. 196, pp. 606-612, 2015.

[120] Hornig, G., K. Northcott, I. Snape, and G. Stevens, "Assessment of sorbent materials for treatment of hydrocarbon contaminated ground water in cold regions," *Cold Regions Science and Technology,* vol. 53, no. 1, pp. 83-91, 2008.

[121] Calgon Carbon Corporation, "Data sheet: WPC powdered activated carbon," 2015.

[122] Liu, Y., "Treatment of cyanotoxins cylindrospermopsin, microcystin-LR, and anatoxin-a by activated carbon in drinking water," MASc. Thesis, Department of Civil and Environmental Engineering, University of Waterloo. Waterloo, Ontario, Canada, 2017.

[123] Hakimabadi, S.G., *Factors affecting the adsorption of per- and polyfluoroalkyl substances by activated carbon [unpublished],* PhD Thesis, Department of Civil and Environmental Engineering, University of Waterloo. Waterloo, Ontario, Canada, 2023.

[124] Boyd, S.A., J.B. Sallach, Y. Zhang, R. Crawford, H.Li, C.T. Johnston, B.J. Teppen, and N.E. Kaminski, "Sequestration of 2,3,7,8-tetrachlorodibenzo-p-dioxin by activated carbon eliminates bioavailability and the supression of immune function in mice," *Environmental Toxicology and Chemistry,* vol. 36, no. 10, pp. 2671-2678, 2017.

[125] Anjum, H., K. Johari, N. Gnanasundaram, and A. Appusamy, "Investigation of green functionalization of multiwall carbon nanotubes and its application in adsorption of benzene, toluene & p-xylene," *Journal of Cleaner Production,* vol. 221, pp. 323-338, 2019.

[126] Henderson, J.E., G.R. Peyton, and W.H. Glaze., A convenient liquid-liquid extraction method for the determination of halomethanes in water at the parts-per-billion level. Chapt. 7: Identification and analysis of organic pollutants in water, Ann Arbor, Michigan: Ann Arbor Science, 1976.

[127] Freitas, J.G., and J.F. Barker, "Sampling VOCs with porous suction samplers in the presence of ethanol: How much are we losing?," *Ground Water Monitoring & Remediation,* vol. 28, no. 3, pp. 83-92, 2008.

[128] Aktas, O., and F. Cecen, "Competitive adsorption and desorption of a bi-solute mixture: effect of activated carbon type," *Adsorption,* vol. 13, no. 2, pp. 159-169, 2007.

[129] Yonge, D.R., and T.M. Keinath, "The effects of non-ideal competition on multi-component adsorption equilibria," *Water Pollution Control Federation,* vol. 58, no. 1, pp. 77-81, 1986.

[130] Saha, D., N. Mirando, and A. Levchenko, "Liquid and vapor phase adsorption of BTX in lignin derived activated carbon: Equilibrium and kinetics study," *Journal of Cleaner Production,* vol. 182, pp. 372-378, 2018.

[131] Elhadded, E., "The sorption fate of aromatic pollutants in different sorbents," *Environmental Processes,* vol. 4, no. 3, pp. 573-585, 2017.

[132] Aktas, O., and F. Cecen, "Effect of type of carbon activation on adsorption and its reversibility," *Journal of Chemical Technology and Biotechnology,* vol. 81, no. 1, pp. 94-101, 2006.

[133] Anjum, H., K. Johari, N. Gnanasundaram, A. Appusamy, and M. Thanabalan, "Impact of surface modification on adsorptive removal of BTX onto activated carbon," *Journal of Molecular Liquids,* vol. 280, pp. 238-251, 2019.

[134] Sudicky, E.A., and W.A. Illman, "Lessons learned from a suite of CFB Borden experiments," *Ground Water,* vol. 49, no. 5, pp. 630-648, 2011.

[135] Mackay, D.M., D.L. Freyberg, P.V. Roberts, and J.A. Cherry, "A natural gradient experiment on solute transport in a sand aquifer 1. Approach and overview of plume movement," *Water Resources Research,* vol. 22, no. 13, pp. 2017-2029, 1986.

[136] Sudicky, E.A., "A natural gradient experiment on solute transport in a sand aquifer: Spatial variability of hydraulic conductivity and its role in the dispersion process," *Water Resources Research,* vol. 22, no. 13, pp. 2069-2082, 1986.

[137] MacFarlane, D.S., J.A. Cherry, R.W. Gillham, and E.A. Sudicky, "Migration of contaminants in groundwater at a landfill: A case study 1. Groundwater flow and plume delineation," *Journal of Hydrology,* vol. 63, no. 1-2, pp. 1-29, 1983.

[138] King, M.W.G., and J.F. Barker, "Migration and natural fate of a coal tar creosote plume 1. Overview and plume development," *Journal of Contaminant Hydrology,* vol. 39, no. 3-4, pp. 249-279, 1999.

[139] Schillig, P.C., J.F. Devlin, J.A. Roberts, G.P. Tsoflias, and M.A. McGlashan, "Transient heterogeneity in an aquifer undergoing bioremediation of hydrocarbons," *Ground Water,* vol. 49, no. 2, pp. 184-196, 2011.

[140] Barbaro, S.E., H-J. Albrechtsen, B.K. Jensen, C.I. Mayfield, and J.F. Barker, "Relationships between aquifer properties and microbial populations in the Borden aquifer," *Gromicrobiology Journal,* vol. 12, no. 3, pp. 203-219, 1994.

[141] Butler, B.J., S.E. Barbaro, F.H. Crocker, and C.I. Mayfield, "Characterization of microbial populations of the Borden aquifer," *Geomicrobiology Journal,* vol. 14, no. 4, pp. 253-268, 1997.

[142] King, M.W.G., J.F. Barker, J.F. Devlin, and B.J. Butler, "Migration and natural fate of a coal tar creosote plume 2. Mass balance and biodegradation indicators," *Journal of Contaminant Hydrology,* vol. 39, no. 3-4, pp. 281-307, 1999.

[143] Major, D.W., C.I. Mayfield, and J.F. Barker, "Biotransformation of benzene by denitrification in aquifer sand," *Ground Water,* vol. 26, no. 1, pp. 8-14, 1988.

[144] Barker, J.F., G.C. Patrick, and D. Major, "Natural attenuation of aromatic hydrocarbons in a shallow sand aquifer," *Groundwater Monitoring & Remediation,* vol. 7, no. 1, pp. 64-71, 1987.

[145] Bianchi-Mosquera, G.C., R.M. Allen-King, and D.M. Mackay, "Enhanced degradation of dissolved benzene and toluene using a solid oxygen-releasing compound," *Groundwater Monitoring & Remediation,* vol. 14, no. 1, pp. 120-128, 1994.

[146] Devlin, J.F., D. Katic, and J.F. Barker, "In situ sequenced bioremediation of mixed contaminants in groundwater," *Journal of Contaminant Hydrology,* vol. 69, no. 3-4, pp. 233-261, 2004.

[147] Barbaro, J.R., J.F. Barker, L.A. Lemon, and C.I. Mayfield, "Biotransformation of BTEX under anaerobic, denitrifying conditions: Field and laboratory observations," *Journal of Contaminant Hydrology,* vol. 11, no. 3-4, pp. 245-272, 1992.

[148] Chen, Y.D., J.F. Barker, and L. Gui, "A strategy for aromatic hydrocarbon bioremediation under anaerobic conditions and the impacts of ethanol: A microcosm study," *Journal of Contaminant Hydrology,* vol. 96, no. 1-4, pp. 17-31, 2008.

[149] Wei, Y., N.R. Thomson, R. Aravena, M. Marchesi, J.F. Barker, E.L. Madsen, R. Kolhatkar, T. Buscheck, D. Hunkeler, and C.M. DeRito, "Infiltration of sulfate to enhance sulfate reduction of petroleum hydrocarbons," *Groundwater Monitoring & Remediation,* vol. 38, no. 4, pp. 73-87, 2018.

[150] Bartlett, C.K., R.M. Slawson, and N.R. Thomson, "Response of sulfate-reducing bacteria and supporting microbial community to persulfate exposure in a continuous flow system," *Environmental Science Processes & Impacts,* vol. 21, no. 7, pp. 1193-1203, 2019.

[151] Sander, R., "Compilation of Henry's law constants (version 4.0) for water as solvent," *Atmospheric Chemsitry and Physics,* vol. 15, no. 8, pp. 4399-4981, 2015.

[152] Doucette, W.J., "Quantitative structure - activity relationships for predicting soil-sediment sorption coefficients for organic chemicals," *Environmental Toxicology and Chemistry,* vol. 22, no. 8, pp. 1771-1788, 2003.

[153] Hach Company , "Sulfide, Methylene Blue Method 8131," 2018.

[154] Toth, C.R.A., F. Luo, N. Bawa, J. Webb, S. Guo, S. Dworatzek, and E.A. Edwards, "Anaerobic benzene biodegradation linked to the growth of highly specific bacterial clades," *Environmental Science & Technology,* vol. 55, no. 12, pp. 7970-7980, 2021.

[155] Callahan, B.J., P.J. McMurdie, M.J. Rosen, A.W. Han, A.J.A. Johnson, and S.P. Holmes, "DADA2: High resolution sample inference from Illumina amplicon data," *Nature Methods,* vol. 13, no. 7, pp. 581-583, 2016.

[156] Xu, X., and N.R. Thomson, "Estimation of the maximum consumption of permanganate by aquifer solids using a modified chemical oxygen demand test," *Journal of Environmental Engineering,* vol. 134, no. 5, pp. 353-361, 2008.

[157] Yu, F., J. Ma, J. Wang, M. Zhang, and J. Zheng, "Magnetic iron oxide nanoparticles functionalized multi-walled carbon nanotubes for toluene, ethylbenzene and xylene removal from aqueous solution," *Chemosphere,* vol. 146, pp. 162-172, 2016.

[158] Grbic-Galic, D., and T.M. Vogel, "Transformation of toluene and benzene by mixed methanogenic cultures," *Applied and Environmental Microbiology,* vol. 53, no. 2, pp. 254-260, 1987.

[159] Edwards, E.A., and D. Grbic-Galic, "Anaerobic degradation of toluene and o-xylene by a methanogenic consortium," *Applied and Environmental Microbiology,* vol. 60, no. 1, pp. 313-322, 1994.

[160] Hendrix, K., N. Bleyen, T. Mennecart, C. Bruggeman, and E. Valcke, "Sodium azide used as microbial inhibitor caused unwanted by-products in anaerobic geochemical studies," *Applied Geochemistry,* vol. 107, pp. 120-130, 2019.

[161] Fowler, S.J., C.R.A. Toth, and L.M. Gieg, "Community structure in methanogenic enrichments provides insight into syntrophic interactions in hydrocarbon-impacted environments," *Frontiers in Microbiology,* vol. 7, p. 562, 2016.

[162] Ramos, D.T., M.L.B. da Silva, C.W. Nossa, P.J.J. Alvarez, and H.X. Corseuil, "Assessment of microbial communities associated with fermentative–methanogenic biodegradation of aromatic hydrocarbons in groundwater contaminated with a biodiesel blend (B20)," *Biodegradation,* vol. 25, no. 5, pp. 681-691, 2014.

[163] Edwards, E.A., and D. Grbic-Galic, "Complete mineralization of benzene by aquifer microorganisms under strictly anaerobic conditions," *Applied and Environmental Microbiology,* vol. 58, no. 8, pp. 2663-2666, 1992.

[164] Ahad, J.M.E., B.S. Lollar, E.A. Edwards, G.F. Slater, and B.E. Sleep, "Carbon isotope fractionation during anaerobic biodegradation of toluene: Implications for intrinsic bioremediation," *Environmental Science & Technology,* vol. 34, no. 5, pp. 892-896, 2000.

[165] Bell, E., T. Lamminmäki, J. Alneberg, C. Qian, W. Xiong, R.L. Hettich, M. Frutschi, and R. Bernier-Latmani, "Active anaerobic methane oxidation and sulfur disproportionation in the deep terrestrial subsurface," *The ISME Journal,* vol. 6, no. 16, pp. 1583-1593, 2022.

[166] Maltsev, A., D. Zelenina, and A. Safonov, "Microbial diversity and authigenic mineral formation of modern bottom sediments in the littoral zone of Lake Issyk-Kul, Kyrgyz Republic (Central Asia)," *Biology,* vol. 12, no. 642, pp. 18-19, 2023.

[167] Song, J., J. Hwang, I. Kang, and J-C. Cho, "A sulfate-reducing bacterial genus, Desulfosediminicola gen. nov., comprising two novel species cultivated from tidal-flat sediments," *Scientific Reports,* vol. 11, no. 1, p. 19978, 2021.

[168] Chen, M., X. Ma, S. Wei, X. An, Y. Li, L. Liang, and T. Jiang, "Seasonal and spatial variations in functional genes and microbial community of Feammox and its associated processes in urban green heart soil," *Water,* vol. 15, no. 6, p. 1024, 2023.

[169] Rakitin, A.L., S. Begmatov, A.V. Beletsky, D.A. Philippov, V.V. Kadnikov, A.V. Mardanov, S.N. Dedysh, and N.V. Ravin, "Highly distinct microbial communities in elevated strings and submerged flarks in the boreal aapa-type mire," *Microorganisms,* vol. 10, no. 1, p. 170, 2022.

[170] Burkhardt, E-M., S. Bischoff, D.M. Akob, G. Buchel, and K. Kusel, "Heavy metal tolerance of Fe(III)-reducing microbial communities in contaminated creek bank soils," *Applied and Environmental Microbiology,* vol. 77, no. 9, pp. 3132-3136, 2011.

[171] Santos, A.L., and D.B. Johnson, "Design and application of a low pH upflow biofilm sulfidogenic bioreactor for recovering transition metals from synthetic waste water at a Brazilian copper mine," *Frontiers in Microbiology,* vol. 9, p. 2051, 2018.

[172] Huang, Y., W. Hu, M. Dong, Y. Yang, X. Yang, H. Huang, S. Yang, W. Jia, B. Wang, and M. Xu, "Cable bacteria accelerate the anaerobic removal of pyrene in black odorous river sediments," *Journal of Hazardous Materials,* vol. 443, p. 130305, 2023.

[173] Reiss, R.A., P. Guerra, and O. Makhnin, "Metagenome phylogenetic profiling of microbial community evolution in a tetrachloroethene-contaminated aquifer responding to enhanced reductive dechlorination protocols," *Standards in Genomic Sciences,* vol. 11, no. 88, 2016.

[174] Xiao, L., E. Lichtfouse, and P.S. Kumar, "Advantage of conductive materials on interspecies electron transfer-independent acetoclastic methanogenesis: A critical review," *Fuel,* vol. 305, p. 121577, 2021.

[175] Ruan, M-Y., B. Liang, S.M. Mbadinga, L. Zhou, L-Y. Wang, J-F. Liu, J-D. Gu, and B-Z. Mu, "Molecular diversity of bacterial bamA gene involved in anaerobic degradation of aromatic hydrocarbons in mesophilic petroleum reservoirs," *International Biodeterioration & Biodegradation,* vol. 114, pp. 122-128, 2016.

[176] Murphy, C.W.M., G.B. Davis, J.L. Rayner, T. Walsh, T.P. Bastow, A.P. Butler, G.J. Puzon, and M.J. Morgan, "The role of predicted chemotactic and hydrocarbon degrading taxa in natural source zone depletion at a legacy petroleum hydrocarbon site," *Journal of Hazardous Materials,* vol. 2022, no. 430, p. 128482, 2022.

[177] Rooney-Varga, J.N., C.V. Gaw, and D.R. Lovley, "Anaerobic benzene oxidation in the Fe(III) reduction zone of petroleum-contaminated aquifers," *Environmental Science & Technology,* vol. 32, no. 9, pp. 1222-1229, 1998.

[178] Botton, S., M. van Harmelen, M. Braster, J.R. Parsons, and W.F.M. Roling, "Dominance of Geobacteraceae in BTX-degrading enrichments from an iron-reducing aquifer," *FEMS Microbiology Ecology,* vol. 62, no. 1, pp. 118-130, 2007.

[179] van der Zaan, B.M., F.T. Saia, A.J.M. Stams, C.M. Plugge, W.M. de Vos, H. Smidt, A.A.M. Langenhoff, and J. Gerritse, "Anaerobic benzene degradation under denitrifying conditions: Peptococcaceae as dominant benzene degraders and evidence for a syntrophic process," *Environmental Microbiology,* vol. 14, no. 5, pp. 1171-1181, 2012.

[180] Vanbroekhoven, K., A. Ryngaert, P. Wattiau, R. De Mot, and D. Springael, "Acinetobacter diversity in environmental samples assessed by 16S rRNA gene PCR–DGGE fingerprinting," *FEMS Microbiology Ecology,* vol. 50, no. 1, pp. 37-50, 2004.

[181] Das, S., C-C. Liu, J-S. Jean, and T. Liu, "Dissimilatory arsenate reduction and in situ microbial activities and diversity in arsenic-rich groundwater of Chianan plain, southwestern Taiwan," *Environmental Microbiology,* vol. 71, no. 2, pp. 365-374, 2016.

[182] Lu, S., Y. Yang, H. Yin, X. Su, K. Yu, and C. Sun, "Microbial community structure of arsenic-bearing groundwater environment in the riverbank filtration zone," *Water,* vol. 14, no. 10, p. 1548, 2022.

[183] Liang, B., L-Y. Wang, Z. Zhou, S.M. Mbadinga, L. Zhou, J-F. Liu, S-Z. Yang, J-D. Gu, and B-Z. Mu, "High frequency of Thermodesulfovibrio spp. and Anaerolineaceae in association with Methanoculleus spp. in a long-term incubation of n-alkanes-degrading methanogenic enrichment culture," *Frontiers in Microbiology,* vol. 7, p. 1431, 2016.

[184] Winderl, C., H. Penning, F. von Netzer, R.U. Meckenstock, and T. Lueders, "DNA-SIP identifies sulfate-reducing Clostridia as important toluene degraders in tar-oil-contaminated aquifer sediment," *The ISME Journal,* vol. 4, pp. 1314-1325, 2010.

[185] Nales, M., B.J. Butler, and E.A. Edwards, "Anaerobic benzene biodegradation: A microcosm survey," *Bioremediation Journal,* vol. 2, no. 2, pp. 125-144, 1998.

[186] Callaghan, A.V., "Metabolomic investigations of anaerobic hydrocarbon-impacted environments," *Current Opinion in Biotechnology,* vol. 24, no. 3, pp. 506-515, 2013.

[187] Meckenstock, R.U., R.J. Warthmann, and W. Schafer, "Inhibition of anaerobic microbial o-xylene degradation by toluene in sulfidogenic sediment columns and pure cultures," *FEMS Microbiology Ecology,* vol. 47, no. 3, pp. 381-386, 2004.

[188] Kazumi, J., M.E. Caldwell, J.M. Suflita, D.R. Lovley, and L.Y. Young, "Anaerobic degradation of benzene in diverse anoxic environments," *Environmental Science & Technology,* vol. 31, no. 3, pp. 813-818, 1997.

[189] Weiner, J.M., and D.R. Lovley, "Anaerobic benzene degradation in petroleum-contaminated aquifer sediments after inoculation with a benzene-oxidizing enrichment," *Applied and Environmental Microbiology,* vol. 64, no. 2, pp. 775-778, 1998.

[190] Weelink, S.A.B., M.H.A. van Eekert, and A.J.M. Stams, "Degradation of BTEX by anaerobic bacteria: Physiology and application," *Reviews in Environmental Science and Biotechnology,* vol. 9, no. 4, pp. 359-385, 2010.

[191] Vogt, C., S. Kleinsteuber, and H-H. Richnow, "Anaerobic benzene degradation by bacteria," *Microbial Biotechnology,* vol. 4, no. 6, pp. 710-724, 2011.

[192] Senior, E., E.B. Lindstrom, I.M. Banat, and D.B. Nedwell, "Sulfate reduction and methanogenesis in the sediment of a saltmarsh on the east coast of the United Kingdom," *Applied and Environmental Microbiology,* vol. 43, no. 5, pp. 987-996, 1982.

[193] Cattony, E.B.M., F.A. Chinalia, R. Ribeiro, M. Zaiat, E. Foresti, and M.B.A. Varesche, "Ethanol and toluene removal in a horizontal-flow anaerobic immobilized biomass reactor in the presence of sulfate," *Biotechnology and Bioengineering,* vol. 91, no. 2, pp. 244-253, 2005.

[194] Franzmann, P.D., W.J. Robertson, L.R. Zappia, and G.B. Davis, "The role of microbial populations in the containment of aromatic hydrocarbons in the subsurface," *Biodegradation,* vol. 13, no. 1, pp. 65-78, 2002.

[195] Fowler, S.F., M-L. Gutierrez-Zamora, M. Manefield, and L.M. Gieg, "Identification of toluene degraders in a methanogenic enrichment culture," *FEMS Microbiology Ecology,* vol. 89, no. 3, pp. 625-636, 2014.

[196] Sun, W., X. Sun, and A.M. Cupples, "Identification of Desulfosporosinus as toluene-assimilating microorganisms from a methanogenic consortium," *International Biodeterioration & Biodegradation,* vol. 88, pp. 13-19, 2014.

[197] Frolov, E.N., A.V. Gololobova, A.A. Klyukina, E.A. Bonch-Osmolovskaya, N.V. Pimenov, N.A. Chernyh, and A.Y. Merkel, "Diversity and activity of sulfate-reducing prokaryotes in Kamchatka hot springs," *Microorganisms,* vol. 9, no. 10, p. 2072, 2021.

[198] Kummel, S., F-A. Herbst, A. Bahr, M. Duarte, D.H. Pieper, N. Jehmlich, J. Seifert, M. von Bergen, P. Bombach, H.H. Richnow, and C. Vogt, "Anaerobic naphthalene degradation by sulfate

reducing Desulfobacteraceae from various anoxic aquifers," *FEMS Microbiology Ecology,* vol. 91, no. 3, p. fiv006, 2015.

[199] Roth, S., B.A. Poulin, Z. Baumann, X. Liu, L. Zhang, D.P. Krabbenhoft, M.E. Hines, J.K. Schaefer, and T. Barkay, "Nutrient inputs stimulate mercury methylation by syntrophs in a subarctic peatland," *Frontiers in Microbiology,* vol. 12, p. 741523, 2021.

[200] Acton, D.W., and J.F. Barker, "In situ biodegradation potential of aromatic hydrocarbons in anaerobic groundwaters," *Journal of Contaminant Hydrology,* vol. 9, no. 4, pp. 325-352, 1992.

[201] Herrmann, S., S. Kleinsteuber, T.R. Neu, H.H. Richnow, and C. Vogt, "Enrichment of anaerobic benzene-degrading microorganisms by in situ microcosms," *FEMS Microbiology Ecology,* vol. 63, no. 1, pp. 94-106, 2008.

[202] Luz, A.D., S.M.A.G.U. de Souza, C. da Luz, R.V. de Paula Rezende, and A.A.U. de Souza, "Multicomponent adsorption and desorption of BTX compounds using coconut shell activated carbon: Experiments, mathematical modeling, and numerical simulation," *Industrial & Engineering Chemistry Research,* vol. 52, no. 23, pp. 7896-7911, 2013.

[203] Haag, F., M. Reinhard, and P.L. McCarty, "Degradation of toluene and p-xylene in anaerobic microcosms: Evidence for sulfate as a terminal electron acceptor," *Environmentol Toxicology and Chemistry,* vol. 10, no. 11, pp. 1379-1389, 1991.

[204] Kampbell, D.H., T.H. Wiedemeier, and J.E. Hansen, "Intrinsic bioremediation of fuel contamination in ground water at a field site," *Journal of Hazardous Materials,* vol. 49, no. 2-3, pp. 197-204, 1996.

[205] Hunkeler, D., D. Jorger, K. Haberli, P. Hohener, and J. Zeyer, "Petroleum hydrocarbon mineralization in anaerobic laboratory aquifer columns," *Journal of Contaminant Hydrology,* vol. 32, no. 1-2, pp. 41-61, 1998.

[206] Da Silva, M.L.B., and P.J.J. Alvarez, "Effects of ethanol versus MTBE on benzene, toluene, ethylbenzene, and xylene natural attenuation in aquifer columns," *Journal of Environmental Engineering,* vol. 128, no. 9, pp. 862-867, 2002.

[207] Losey, N.A., B.S. Stevenson, H-J. Busse, J.S. Sinninghe Damste, W.I.C. Rijpstra, S. Rudd, and P.A. Lawson, "Thermoanaerobaculum aquaticum gen. nov., sp. nov., the first cultivated member of Acidobacteria subdivision 23, isolated from a hot spring," *International Journal of Systematic and Evolutionary Microbiology,* vol. 63, pp. 4149-4157, 2013.

[208] Zhang, W., Q. Mo, Z. Huang, M.A. Sabar, G. Medunic, T. Ivoševic, H. He, M. Urynowicz, F-J Liu, H. Guo, R. Haider, M.I. Ali, and A. Jamal, "Contaminants from a former Croatian coal sludge dictate the sturcture of microbiota in the estuarine (Rasa Bay) sediment and soil," *Frontiers in Microbiology,* vol. 14, p. 1126612, 2023.

[209] Aburto-Medina, A., and A.S. Ball, "Microorganisms involved in anaerobic benzene degradation," *Annals of Microbiology,* vol. 65, pp. 1201-1213, 2015.

[210] Sarkar, J., A. Saha, A. Roy, H. Bose, S. Pal, P. Sar, and S.K. Kazy, "Development of nitrate stimulated hydrocarbon degrading microbial consortia from refinery sludge as potent bioaugmenting agent for enhanced bioremediation of petroleum contaminated waste," *World Journal of Microbiology and Biotechnology,* vol. 36, no. 10, p. 156, 2020.

[211] Hosokawa, S., K. Kuroda, T. Narihiro, Y. Aoi, N. Ozaki, A. Ohashi, and T. Kindaichi, "Cometabolism of the superphylum Patescibacteria with anammox bacteria in a long-term freshwater anammox column reactor," *Water,* vol. 13, no. 2, p. 208, 2021.

[212] Kuroda, K., K. Yamamoto, R. Nakai, Y. Hirakata, K. Kubota, M.K. Nobu, and T. Narihiro, "Symbiosis between Candidatus Patescibacteria and Archaea Discovered in Wastewater-Treating Bioreactors," *American Society for Microbiology,* vol. 13, no. 5, p. e0171122, 2022.

[213] D'Ugo, E., M. Bruno, A. Mukherjee, D. Chattopadhyay, R. Giuseppetti, R. De Pace, and F. Magurano, "Characterization of microbial response to petroleum hydrocarbon contamination in a lacustrine ecosystem," *Environmental Science and Pollution Research,* vol. 28, no. 20, pp. 26187-26196, 2021.

[214] Wu, Z., G. Liu, Y. Ji, P. Li, X. Yu, W. Qiao, B. Wang, K. Shi, W. Liu, Bin Liang, D. Wang, K. Yanuka-Golub, S. Freilich, and J. Jiang, "Electron acceptors determine the BTEX degradation capacity of anaerobic microbiota via regulating the microbial community," *Environmental Research,* vol. 215, no. 3, p. 114420, 2022.

[215] Meckenstock, R.U., "Fermentative toluene degradation in anaerobic defined syntrophic cocultures," *FEMS Microbiology Letters,* vol. 177, no. 1, pp. 67-73, 1999.

[216] Yamada, T., Y. Sekiguchi, S. Hanada, H. Imachi, A. Ohashi, H. Harada, and Y. Kamagata, "Anaerolinea thermolimosa sp. nov., Levilinea saccharolytica gen. nov., sp. nov. and Leptolinea tardivitalis gen. nov., sp. nov., novel filamentous anaerobes, and description of the new classes Anaerolineae classis nov. and Caldilineae classis nov. in the," *International Journal of Systematic and Evolutionary Microbiology,* vol. 56, no. 6, pp. 1331-1340, 2006.

[217] Watanabe, T., H. Kojima, K. Umezawa, C. Hori, T.E. Takasuka, Y. Kato, and M. Fukui, "Genomes of neutrophilic sulfur-oxidizing chemolithoautotrophs representing 9 Proteobacterial species from 8 genera," *Frontiers in Microbiology,* vol. 10, p. 316, 2019.

[218] Ficker, M., K. Krastel, S. Orlicky, and E. Edwards, "Molecular characterization of a toluene-degrading methanogenic consortium," *Applied and Environmental Microbiology,* vol. 65, no. 12, pp. 5576-5585, 1999.

[219] Gieg, L.M., I.A. Davidova, K.E. Duncan, and J.M. Suflita, "Methanogenesis, sulfate reduction and crude oil biodegradation in hot Alaskan oilfields," *Environmental Microbiology,* vol. 12, no. 11, pp. 3074-3086, 2010.

[220] Liu, Y., and W.B. Whitman, "Metabolic, phylogenetic, and ecological diversity of the methanogenic archaea," *Annals of the New York Academy of Sciences,* vol. 1125, no. 1, pp. 171-189, 2008.

[221] Oren, A., The Prokaryotes Other Major Lineages of Bacteria and the Archaea: 10 The Family Methanocalculaceae, Springer-Verlag Berlin Heidelberg, 2014.

[222] Jiménez, N., H.H. Richnow, C. Vogt, T. Treude, and M. Krüger, "Methanogenic hydrocarbon degradation: Evidence from field and laboratory studies," *Journal of Molecular Microbiology and Biotechnology,* vol. 26, no. 1-3, pp. 227-242, 2016.

[223] Guo, S., C.R.A. Toth, F. Luo, X. Chen, J. Xiao, and E.A. Edwards, "Transient oxygen exposure causes profound and lasting changes to a benzene-degrading methanogenic community," *Environmental Science and Technology,* vol. 56, no. 18, pp. 13036-13045, 2022.

[224] Sakai, S., R. Conrad, and H. Imachi, The Prokaryotes Other Major Lineages of Bacteria and the Archaea: 12 The Family Methanocellaceae, Springer-Verlag Berlin Heidelberg, 2014.

[225] Fowler, S.J., X. Dong, C.W. Sensen, J.M. Suflita, and L.M. Gieg, "Methanogenic toluene metabolism: community structure and intermediates," *Environmental Microbiology,* vol. 14, no. 3, pp. 754-764, 2012.

[226] Barker, J.F., and P. Fritz, "The occurrence and origin of methane in some groundwater flow systems," *Canadian Journal of Earth Sciences,* vol. 18, no. 12, pp. 1802-1816, 1981.

[227] Baedecker, M.J., I.M. Cozzarelli, and R.P. Eganhouse, "Crude oil in a shallow sand and gravel aquifer-Ill. Biogeochemical reactions and mass balance modeling in anoxic groundwater," *Applied Geochemistry,* vol. 8, no. 6, pp. 569-586, 1993.

[228] Landmeyer, J.E., D.A. Vroblesky, and F.H. Chapelle, "Stable carbon isotope evidence of biodegradation zonation in a shallow jet-fuel contaminated aquifer," *Environmental Science & Technology,* vol. 30, no. 4, pp. 1120-1128, 1996.

[229] Su, X., H. Lv, W. Zhang, Y. Zhang, and X. Jiao, "Evaluation of petroleum hydrocarbon biodegradation in shallow groundwater by hydrogeochemical indicators and C, S-isotopes," *Environmental Earth Sciences,* vol. 69, pp. 2091-2101, 2013.

[230] Abadikhah, M., M.C. Rodriguez, F. Persson, B-M. Wilen, A. Farewell, and O. Modin, "Evidence of competition between electrogens shaping electroactive microbial communities in microbial electrolysis cells," *Frontiers in Microbiology,* vol. 13, p. 959211, 2022.

[231] Griffith, D.R., M. Carolan, M.M. Gutierrez, A. Romig, N. Garcia-Diaz, C.P. Hutchinson, and R.L. Zayas, "Microbial degradation of free and halogenated estrogens in river water-sediment microcosms," *Environmental Science and Technology,* vol. 57, no. 29, pp. 10782-10791, 2023.

[232] Vigneron, A., P. Cruaud, C. Lovejoy, and W.F. Vincent, "Genomic insights into cryptic cycles of microbial hydrocarbon production and degradation in contiguous freshwater and marine microbiomes," *Microbiome,* vol. 11, p. 104, 2023.

[233] Dojka, M.A., P. Hugenholtz, S.K. Haack, and N.R. Pace, "Microbial diversity in a hydrocarbon- and chlorinated-solvent-contaminated aquifer undergoing intrinsic bioremediation," *Applied and Environmental Microbiology,* vol. 64, no. 10, pp. 3869-3877, 1998.

[234] Elshahed, M.S., and M.J. McInerney, "Benzoate fermentation by the anaerobic bacterium Syntrophus aciditrophicus in the absence of hydrogen-using microorganisms," *Applied and Environmental Microbiology,* vol. 67, no. 12, pp. 5520-5525, 2001.

[235] Rochman, F.F., A. Sheremet, I. Tamas, A. Saidi-Mehrabad, J-J. Kim, X. Dong, C.W. Sensen, L.M. Gieg, and P.F. Dunfield, "Benzene and naphthalene degrading bacterial communities in an oil sands tailings pond," *Frontiers in Microbiology,* vol. 8, p. 1845, 2017.

[236] Trutschel, L.R., G.L. Chadwick, B. Kruger, J.G. BLank, W.J. Brazelton, E.R. Dart, and A.R. Rowe, "Investigation of microbial metabolisms in an extremely high pH marine-like terrestrial serpentinizing system: Ney Springs," *Science of the Total Environment,* vol. 836, p. 155492, 2022.

[237] Schirmer, M., B.J. Butler, C.D. Church, J.F. Barker, and N. Nadarajah, "Laboratory evidence of MTBE biodegradation in Borden aquifer material," *Journal of Contaminant Hydrology,* vol. 60, no. 3-4, pp. 229-249, 2003.

[238] Frind, E.O., J.W. Molson, M. Schirmer, and N. Guiguer, "Dissolution and mass transfer of multiple organics under field conditions: The Borden emplaced source," *Water Resources Research,* vol. 35, no. 3, pp. 683-694, 1999.

[239] Sudicky, E.A., J.A. Cherry, and E.O. Frind, "Migration of contaminants in groundwater at a landfill: A case study 4. A natural-gradient dispersion test," *Journal of Hydrology,* vol. 63, no. 1-2, pp. 81-108, 1983.

[240] Freyberg, D.L. , "A natural gradient experiment on solute transport in a sand aquifer 2. Spatial moments and the advection and dispersion of nonreactive tracers," *Water Resources Research,* vol. 22, no. 13, pp. 2031-2046, 1986.

[241] Dance, J.T., "Evaluation of reactive solute transport in a shallow unconfined sandy aquifer," M.S. Thesis, University of Waterloo. Waterloo, Ontario, Canada, 1980.

[242] Nicholson, R.V., J.A. Cherry, and E.J. Reardon, "Migration of contaminants in groundwater at a landfill: A case study," *Journal of Hydrology,* vol. 63, no. 1-2, pp. 131-176, 1983.

[243] Ferris, M.J., G. Muyzer, and D.M. Ward, "Denaturing gradient gel electrophoresis profiles of 16S rRNA-defined populations inhabiting a hot spring microbial mat community," *Applied and Environmental Microbiology,* vol. 62, no. 2, pp. 340-346, 1996.

[244] Engelbrektson, A., V. Kunin, K.C. Wrighton, N. Zvenigorodsky, F. Chen, H. Ochman, and P. Hugenholtz, "Experimental factors affecting PCR-based estimates of microbial species richness and evenness," *ISME Journal,* vol. 4, no. 5, pp. 642-647, 2010.

[245] Amann, R.I., W. Ludwig, and K.H. Schleifer, "Phylogenetic identification and in situ detection of individual microbial cells without cultivation," *Microbiological Reviews,* vol. 59, no. 1, pp. 143-169, 1995.

[246] Yu, Y., C. Lee, J. Kim, and S. Hwang, "Group-specific primer and probe sets to detect methanogenic communities using quantitative real-time polymerase chain reaction," *Biotechnology and Bioengineering,* vol. 89, no. 6, pp. 670-679, 2005.

[247] Qiao, W., F. Luo, L. Lomheim, E. Erin Mack, S. Ye, J. Wu, and E.A. Edwards, "Natural attenuation and anaerobic benzene detoxification processes at a chlorobenzene-contaminated industrial site inferred from field investigations and microcosm studies," *Environmental Science & Technology,* vol. 52, no. 1, pp. 22-31, 2018.

[248] Toth, C.R.A., N. Bawa, S. Guo, E.A. Edwards, J. Webb, C. Scales, K. Finney, and S. Dworatzek, "Laboratory demonstration of successful anaerobic benzene, toluene, and o-xylene bioremediation using mixed bioaugmentation cultures," in *Twelfth International Conference on the Remediation of Chlorinated and Recalcitrant Compounds*, Palm Springs, California, 2022.

[249] Ulrich, A.C., and E.A. Edwards, "Physiological and molecular characterization of anaerobic benzene-degrading mixed cultures," *Environmental Microbiology,* vol. 5, no. 2, pp. 92-102, 2003.

[250] Wood, G.O., "A review of the effects of covapors on adsorption rate coefficients of organic vapors adsorbed onto activated carbon from flowing gases," *Carbon,* vol. 40, no. 5, pp. 685-694, 2002.

[251] Lodewyckx, P., G.O. Wood, and S.K. Ryu, "The Wheeler–Jonas equation: a versatile tool for the prediction of carbon bed breakthrough times," *Carbon,* vol. 42, no. 7, pp. 1351-1355, 2004.

Appendix A: Supplementary material for Chapter 2

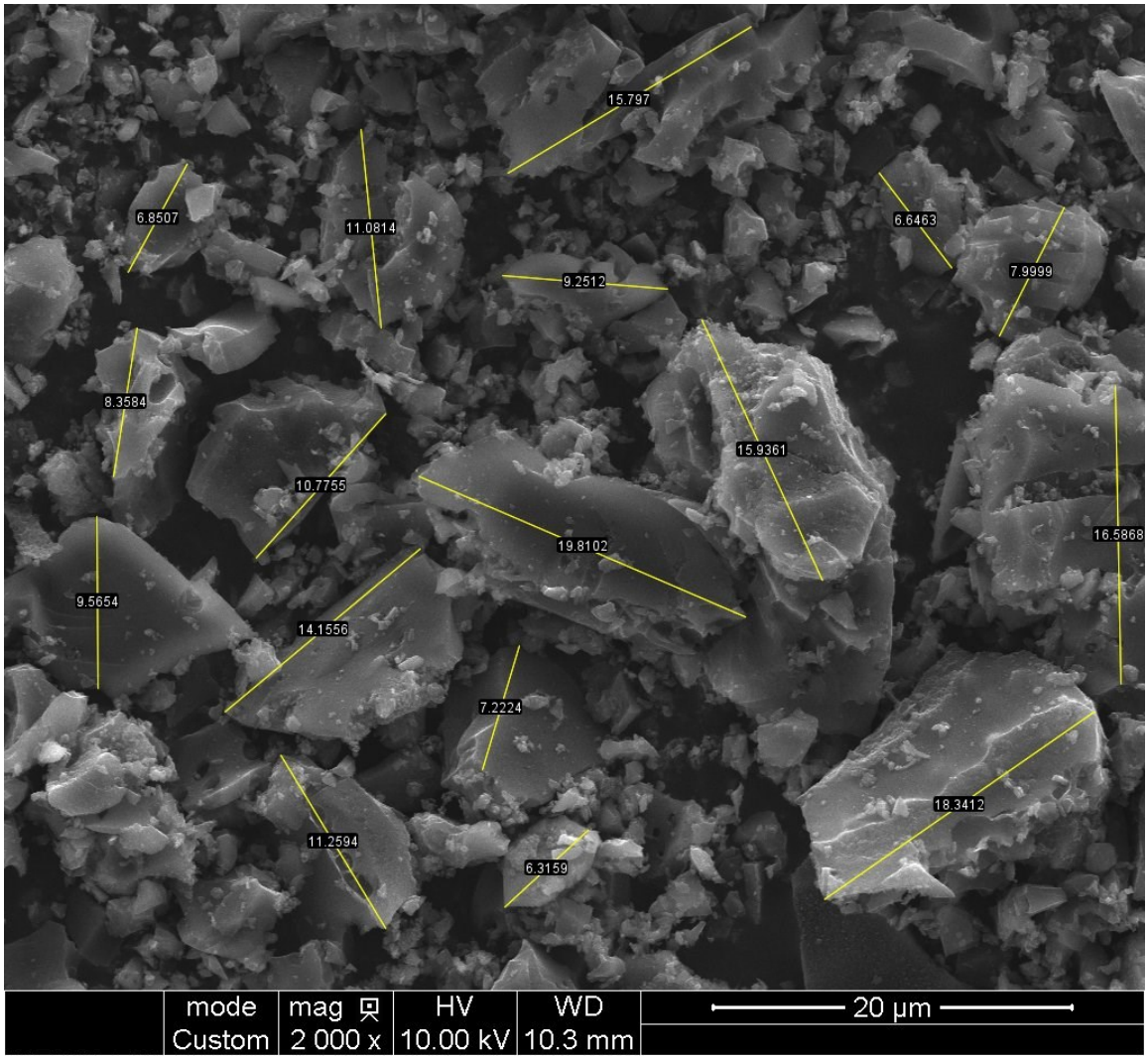

Figure A.1: WPC powdered activated carbon (PAC) particle size measurements (n = 17) carried out in ImageJ using the Measure and Label macro.

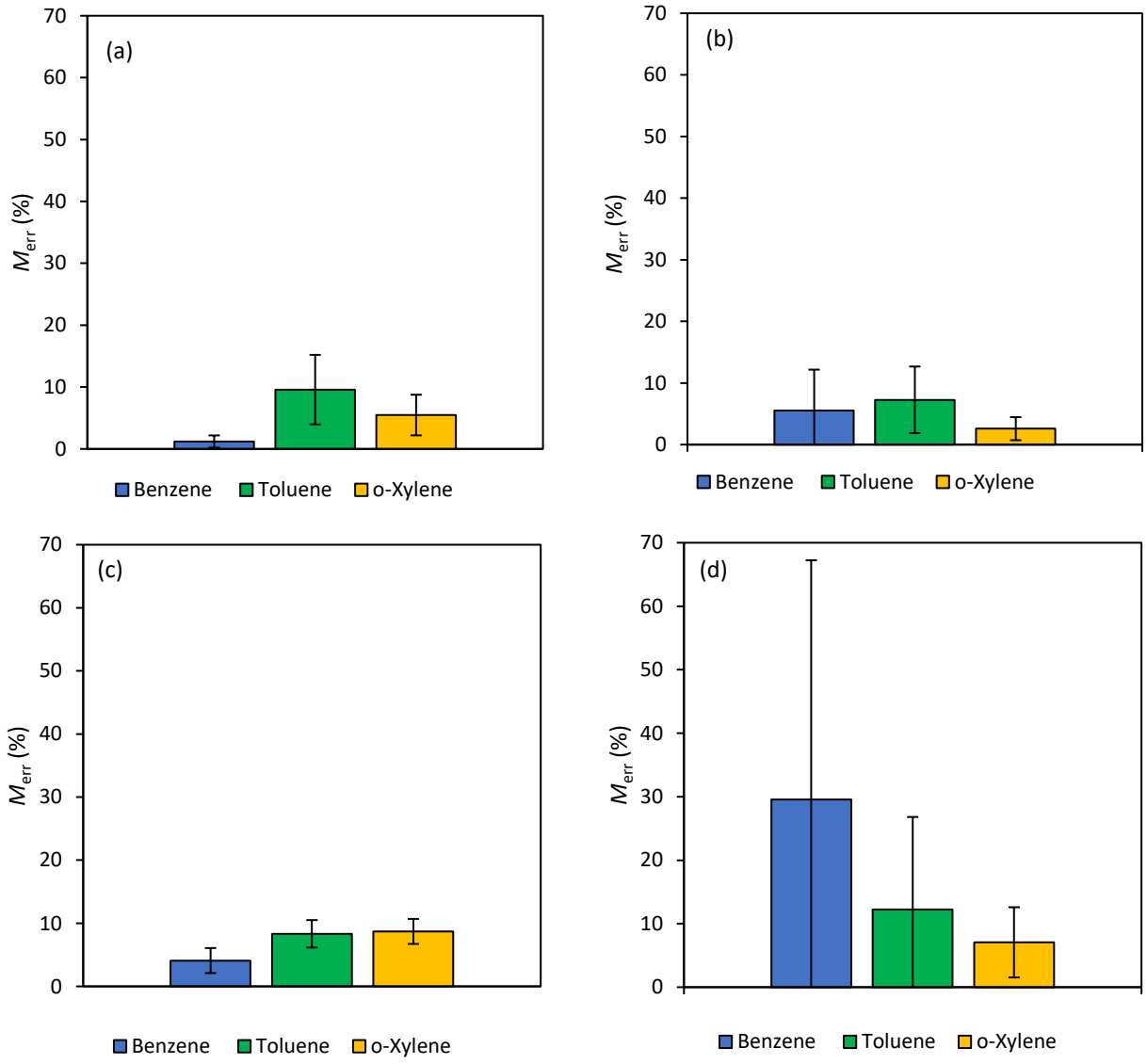

Figure A.2: Absolute mass lost or gained (M_{err}) for benzene, toluene and *o*-xylene (BTX) from single-solute (a) sorption and (b) desorption equilibrium data, and multi-solute (c) sorption and (d) desorption equilibrium data. The standard deviation of 6 estimates (pertaining to the 6 initial aqueous concentrations) are shown as ± error bars.

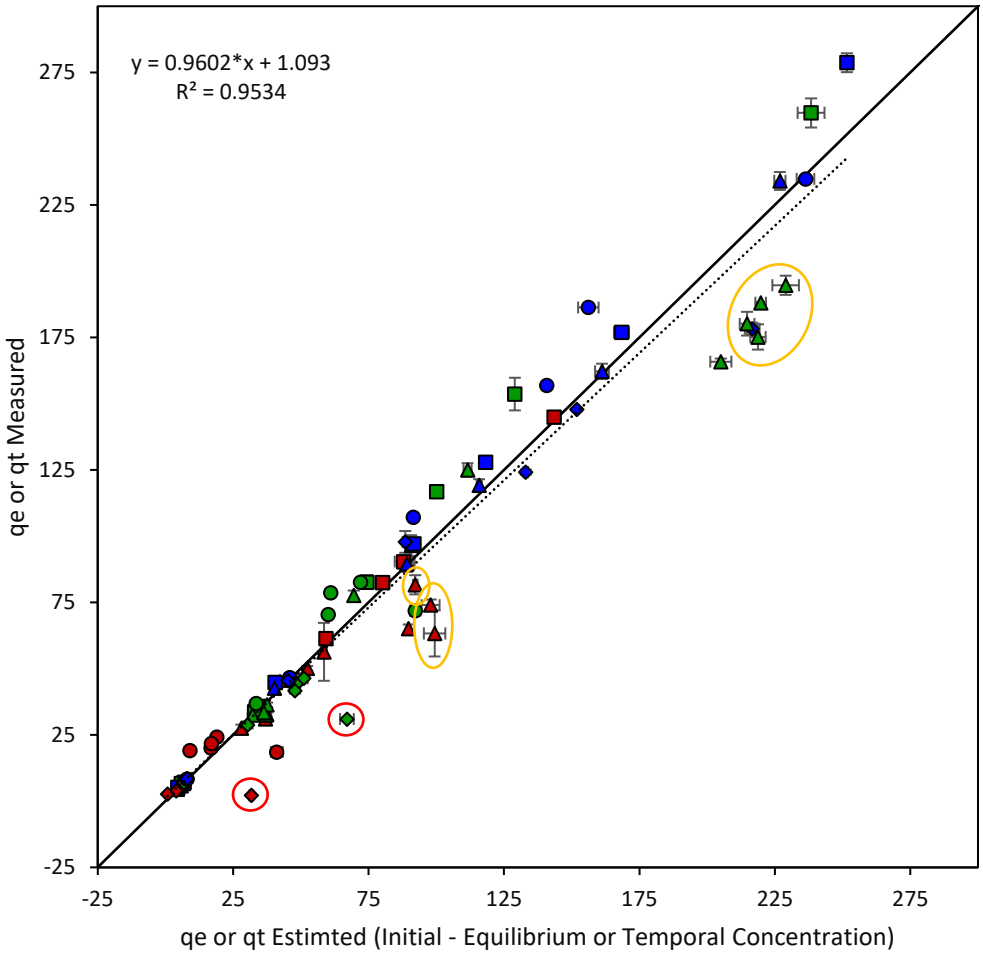

Figure A.3: Single- and multi-solute sorption and desorption equilibrium solid phase sorbed mass of benzene, toluene or *o*-xylene per gram of powdered activated carbon [PAC] (q_e) or temporal solid phase sorbed mass of benzene, toluene or *o*-xylene per gram of PAC (q_t) estimated indirectly using mass balance between the initial aqueous phase concentration and the equilibrium or temporal aqueous phase concentration (Equation 2.1 or 2.2) (x axis) relative to the directly measured q_e or q_t (y axis). Data for benzene, toluene and *o*-xylene are coloured red, green and blue, respectively. Single-solute sorption and desorption data are represented as squares and triangles, respectively, and multi-solute sorption and desorption data are represented as circles and diamonds, respectively. The red outlines represent data associated with elevated M_{err} for benzene and toluene from the multi-solute desorption equilibrium data, and the yellow outlines represent data associated with the elevated M_{err} for benzene and toluene from single-solute temporal data. The standard deviation of triplicate measurements is represented as ± error bars on each data point. The linear fit to the data and a 1:1 line are represented as a black dotted and solid line, respectively.

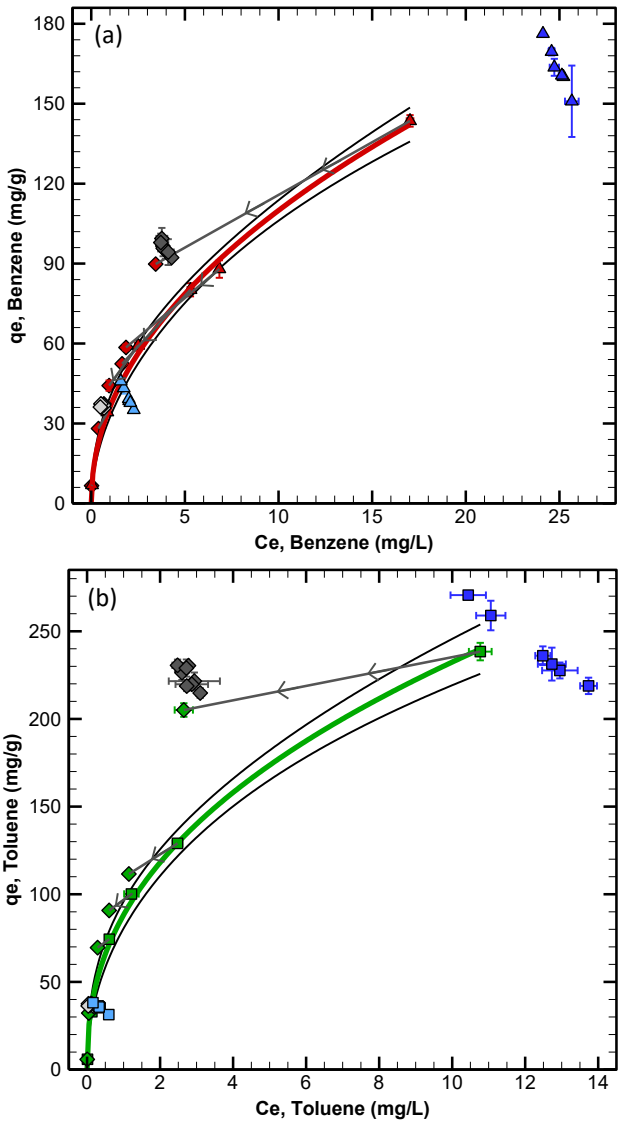

Figure A.4: Single-solute sorption ($C_{e_i}^{s}$ and $q_{e_i}^{s}$) and single-step desorption ($C_{e_i}^{d}$ and $q_{e_i}^{d}$) equilibrium capacity and temporal data for (a) benzene and (b) toluene in single-solute systems in contact with WPC powdered activated carbon (PAC) (C_e on the x axis represents the sorption or desorption equilibrium aqueous phase concentration (mg/L), and q_e on the y axis represents the sorption or desorption equilibrium solid phase concentration (mg/g)). The sorption equilibrium data are represented as filled (a) red triangles for benzene and (b) green squares for toluene, and the single-step desorption equilibrium data are represented as filled diamonds with the same colours used to represent the sorption capacities for each solute. Solid lines connect the sorption and desorption equilibrium data, and arrows represents the direction of concentration change between processes. The standard deviation of triplicate measurements is represented as ± error bars. The single-solute Freundlich isotherms with 95% confidence envelopes (black solid bands) are represented as solid-coloured lines, including (a) red for benzene and (b) green for toluene. The temporal sorption data are represented as the same shapes as the equilibrium sorption data for each solute, and filled with light blue for the C_{o_i} of 3 mg/L and dark blue for the C_{o_i} of 30 mg/L. The temporal desorption data are represented as the same shapes as the equilibrium desorption data, and filled with light grey for the C_{o_i} of 3 mg/L and dark grey for the C_{o_i} of 30 mg/L.

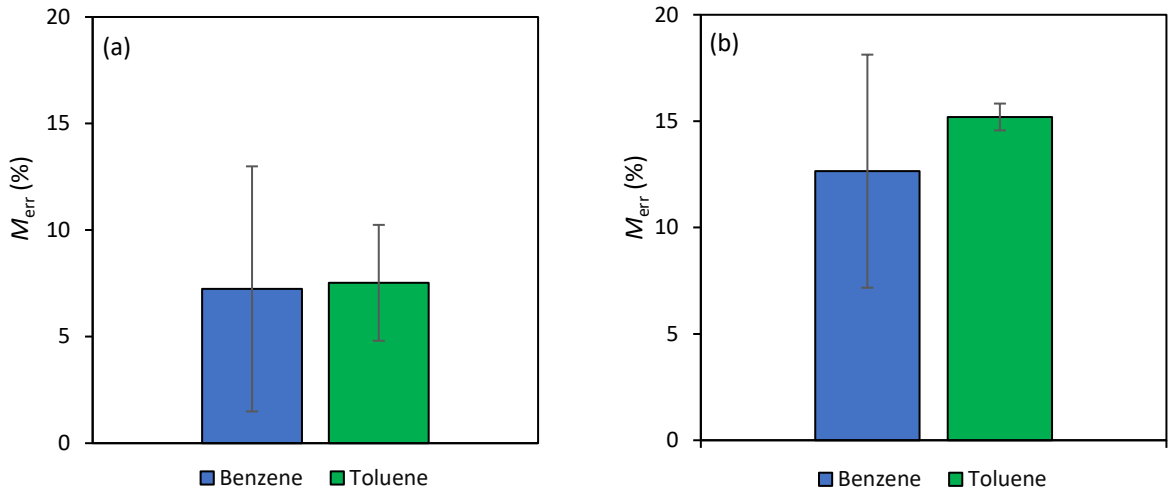

Figure A.5: Absolute mass lost or gained (M_{err}) for benzene and toluene from single-solute temporal desorption data, corresponding to initial aqueous concentrations of (a) 3 mg/L and (b) 30 mg/L. The standard deviation of 3 estimates for benzene and 4 estimates for toluene (pertaining to sampling times, including 24, 72 and 216 hours for benzene, and 24, 72, 216 and 720 hours for toluene) are shown as ± error bars.

Table A.1: Artificial groundwater (AGW) recipe used for sorption and desorption equilibrium and temporal experiments.

Chemical formula[1]	Chemical name	Molecular weight (g/mol)	Concentration (mg/L)
NH_4Cl	Ammonium chloride	53.49	49.7
$MgCl_2$	Magnesium chloride	95.21	4.8
$MnCl_2 \cdot 4H_2O$	Manganese (II) chloride	197.90	4
NaCl	Sodium chloride	58.44	7
$CaCl_2 \cdot 2H_2O$	Calcium chloride	147.01	147
$NaH_2PO_4 \cdot H_2O$	Monosodium phosphate	137.99	27.6
KH_2PO_4	Potassium dihydrogen phosphate	136.09	69.4
Na_2SO_4	Sodium sulfate	142.04	8.5

Notes:
1. All chemical components were dissolved into Milli-Q water.

Table A.2: Sorption and desorption equilibrium and temporal experimental design for WPC powdered activated carbon (PAC) in the presence of benzene, toluene and *o*-xylene (BTX) alone (single-solute) or combined (multi-solute).

Series [1]	Artificial groundwater (AGW) volume (mL)	Powdered activated carbon (PAC) mass (mg)	Single solute [2]	Multi-solute [3]	Sampling time (hr) [4]
			Benzene, toluene or *o*-xylene concentration (mg/L)	Benzene, toluene and *o*-xylene (BTX) concentration (mg/L)	
Sorption equilibrium capacity					
Control (without PAC)	160	-	0.5, 3, 6, 10, 12, 25	1:1:1	48
PAC	160	10	0.5, 3, 6, 10, 12, 25	1:1:1	48
Desorption equilibrium capacity					
Control (without PAC)	160	-	0.5, 3, 6, 10, 12, 25	1:1:1	48
PAC	160	10	0.5, 3, 6, 10, 12, 25	1:1:1	48
Sorption equilibrium time					
Control (without PAC)	160	-	3, 30	-	0.5, 2, 4, 8, 24, 48
PAC	160	10	3, 30	-	0.5, 2, 4, 8, 24, 48
Desorption equilibrium time					
Control (without PAC)	160	-	3, 30	-	0.5, 2, 4, 8, 24, 72, 216, 720
PAC	160	10	3, 30	-	0.5, 2, 4, 8, 24, 72, 216, 720

Notes:
1. Each series was prepared in triplicate.
2. Only benzene and toluene were used in single-solute temporal experiments.
3. Equal concentrations of each solute, using the same concentrations as the single-solute system.
4. For temporal desorption experiments, solid phase samples were only collected at sampling times of 24, 72 and 216 hours for benzene, and at sampling times of 24, 72, 216 and 720 hours for toluene.

Table A.3: Chemical properties of benzene, toluene and *o*-xylene (BTX).

Solute	Chemical formula	Molecular weight [1]	Density [1]	Solubility [1]	Vapour pressure [1]	Hydrophobicity ($\log K_{\mathrm{ow}_i}$) [2]	Henry's constant (K_{h_i}) [3]
		g/mol	g/mL (20ºC)	mg/L (20ºC)	kPa (20ºC)	(25ºC)	
Benzene	C_6H_6	78.1	0.878	1780	10.1	2.13	0.225
Toluene	C_7H_8	92.1	0.867	515	2.9	2.73	0.274
o-Xylene	C_8H_{10}	106.2	0.880	175	0.7	3.12	0.221

Notes: 1. [190], 2. [159], 3. [151].

Table A.4: Absolute mass of single- or multi-solute benzene, toluene and *o*-xylene lost or gained (M_{err}) from the sorption and desorption equilibrium capacity and temporal data.

	C_{o_i} (mg/L)	M_{o_i} (mg)	$M^{\text{s}}_{\text{aq}_i}$ (mg)	$M^{\text{s}}_{\text{s}_i}$ (mg)	$M^{\text{s}}_{\text{err}_i}$ (%)		C_{o_i} (mg/L)	$M_{\text{o}_i} - M^{\text{s}}_{\text{aq}_i}$ (mg)	$M^{\text{d}}_{\text{aq}_i}$ (mg)	$M^{\text{d}}_{\text{s}_i}$ (mg)	$M^{\text{d}}_{\text{err}_i}$ (%)
Single-solute benzene sorption capacity	0.47	0.08	0.01	0.07	2.92	Single-solute benzene desorption capacity	0.47	0.07	0.00	0.07	0.44
	3.00	0.48	0.14	0.35	1.47		3.00	0.34	0.06	0.27	4.31
	6.27	1.00	0.40	0.59	1.06		6.27	0.60	0.15	0.47	3.15
	10.22	1.64	0.85	0.79	0.27		10.22	0.79	0.26	0.49	4.14
	12.39	1.98	1.09	0.88	0.26		12.39	0.89	0.30	0.57	2.43
	26.21	4.19	2.72	1.52	1.21		26.21	1.47	0.55	0.64	18.76
M_{err_i} ± Standard deviation (%)					**1.20 ± 0.98**						**5.54 ± 6.63**
Single-solute toluene sorption capacity	0.38	0.06	0.00	0.07	11.45	Single-solute toluene desorption capacity	0.38	0.06	0.00	0.06	1.52
	2.19	0.35	0.02	0.33	0.30		2.19	0.33	0.01	0.32	0.78
	5.07	0.81	0.10	0.82	12.89		5.07	0.71	0.05	0.76	12.71
	7.69	1.23	0.19	1.20	13.03		7.69	1.04	0.10	1.00	5.60
	10.94	1.75	0.40	1.61	14.66		10.94	1.35	0.18	1.31	10.36
	25.67	4.11	1.72	2.60	5.15		25.67	2.38	0.42	1.66	12.64
M_{err_i} ± Standard deviation (%)					**9.58 ± 5.62**						**7.27 ± 5.40**
Single-solute *o*-xylene sorption capacity	0.30	0.05	0.00	0.05	10.14	Single-solute *o*-xylene desorption capacity	0.30	0.05	0.00	0.05	2.15
	2.74	0.44	0.01	0.44	4.19		2.74	0.42	0.00	0.45	5.90
	6.03	0.96	0.06	0.93	1.92		6.03	0.91	0.01	0.90	0.43
	8.39	1.34	0.09	1.28	2.34		8.39	1.25	0.03	1.26	2.85
	11.61	1.86	0.25	1.72	6.01		11.61	1.61	0.07	1.56	1.33
	22.09	3.53	0.99	2.83	8.26		22.09	2.54	0.25	2.36	2.85
M_{err_i} ± Standard deviation (%)					**5.48 ± 3.28**						**2.58 ± 1.87**
Multi-solute benzene sorption capacity	0.53	0.08	0.02	0.06	1.07	Multi-solute benzene desorption capacity	0.53	0.07	0.01	0.05	15.82
	2.96	0.47	0.31	0.20	7.09		2.96	0.17	0.09	0.07	3.92
	6.56	1.05	0.85	0.24	3.94		6.56	0.20	0.14	0.06	2.09
	11.01	1.76	1.59	0.23	3.16		11.01	0.17	0.13	0.04	0.58
	14.03	2.24	2.15	0.19	4.41		14.03	0.09	0.14	0.03	83.05
	27.47	4.39	4.00	0.18	4.87		27.47	0.40	0.09	0.02	71.92
M_{err_i} ± Standard deviation (%)					**4.09 ± 1.98**						**29.56 ± 37.67**

	C_{o_i} (mg/L)	M_{o_i} (mg)	$M^{s}_{aq_i}$ (mg)	$M^{s}_{s_i}$ (mg)	$M^{s}_{err_i}$ (%)		C_{o_i} (mg/L)	$M_{o_i} - M^{s}_{aq_i}$ (mg)	$M^{d}_{aq_i}$ (mg)	$M^{d}_{s_i}$ (mg)	$M^{d}_{err_i}$ (%)
Multi-solute toluene sorption capacity	0.46	0.07	0.00	0.07	7.48	Multi-solute toluene desorption capacity	0.46	0.07	0.00	0.07	2.67
	2.61	0.42	0.09	0.38	10.84		2.61	0.33	0.03	0.28	4.76
	5.80	0.93	0.31	0.70	9.19		5.80	0.62	0.12	0.46	7.29
	9.68	1.55	0.83	0.86	9.24		9.68	0.72	0.21	0.46	6.50
	12.22	1.96	1.35	0.78	8.78		12.22	0.60	0.26	0.41	10.68
	24.27	3.88	2.99	0.72	4.47		24.27	0.89	0.22	0.30	41.49
M_{err_i} ± Standard deviation (%)					**8.33 ± 2.18**						**12.23 ± 14.58**
Multi-solute *o*-xylene sorption capacity	0.51	0.08	0.00	0.08	6.87	Multi-solute *o*-xylene desorption capacity	0.51	0.08	0.00	0.08	6.67
	3.00	0.48	0.03	0.49	7.86		3.00	0.45	0.01	0.45	1.27
	6.60	1.06	0.11	1.06	11.22		6.60	0.94	0.03	1.01	10.14
	10.98	1.76	0.35	1.62	12.18		10.98	1.41	0.08	1.25	5.44
	13.90	2.22	0.68	1.84	13.19		13.90	1.54	0.12	1.46	2.53
	26.98	4.32	2.03	2.32	0.94		26.98	2.28	0.19	1.72	16.36
M_{err_i} ± Standard deviation (%)					**8.71 ± 4.54**						**7.07 ± 5.53**
						Singel-solute benzene desorption time (C_{o_i}, 3 mg/L)	4.43 ± 0.086	0.43	0.11	0.32	0.82
								0.46	0.11	0.31	8.99
								0.46	0.08	0.32	11.91
M_{err_i} ± Standard deviation (%)											**7.24 ± 5.75**
						Singel-solute benzene desorption time (C_{o_i}, 30 mg/L)	35.02 ± 0.95	1.73	0.69	0.79	14.28
								1.62	0.67	0.85	6.54
								1.62	0.59	0.75	17.12
M_{err_i} ± Standard deviation (%)											**12.65 ± 5.48**
						Singel-solute toluene desorption time (C_{o_i}, 3 mg/L)	2.57 ± 0.14	0.36	0.02	0.32	5.11
								0.39	0.01	0.34	9.69
								0.39	0.01	0.36	5.24
								0.39	0.01	0.34	10.07
M_{err_i} ± Standard deviation (%)											**7.53 ± 2.72**
						Singel-solute toluene desorption time (C_{o_i}, 30 mg/L)	27.18 ± 1.92	2.58	0.50	1.72	14.31
								2.70	0.46	1.82	15.55
								2.70	0.42	1.86	15.71
								2.70	0.44	1.86	15.21
M_{err_i} ± Standard deviation (%)											**15.20 ± 0.63**

Notes: For each solute *i* the M_{err_i} is the percentage of absolute mass lost or gained from sorption ($M^{s}_{err_i}$) or desorption ($M^{d}_{err_i}$), $M^{s}_{aq_i}$ and $M^{d}_{aq_i}$ are the sorption and desorption equilibrium or temporal masses in the aqueous phase, respectively, $M^{s}_{s_i}$ and $M^{d}_{s_i}$ are the sorption and desorption equilibrium or temporal masses in the solid phase, respectively, and M_{o_i} and C_{o_i} are the initial mass and concentration, respectively.

Appendix B: Supplementary material for Chapter 3

Appendix B.1: Anaerobic Artificial Groundwater Recipe – Microcosms

The following anaerobic artificial groundwater (AGW) recipe was adapted from Edwards and Grbić-Galić (1994) [159].

1. Prepare a phosphate buffer (2 mM) by adding 27.2 g of KH_2PO_4 and 34.8 g of K_2HPO_4 to 1 L of Milli-Q water.
2. Prepare a trace mineral stock solution by adding 0.1 g of ZnCl, 0.75 g of $NiCl_2 \cdot 6H_2O$, 0.1 g of $CuCl_2 \cdot 2H_2O$, 0.02 g of Na_2SeO_3, 0.3 g of H_3BO_3, 0.1 g of $Na_2MoO_4 \cdot 2H_2O$, 1.0 g of $MnCl_2 \cdot 4H_2O$, 1.5 g of $CoCl_2 \cdot 6H_2O$, 0.1 g of $Al_2(SO_4)_3 \cdot 18h_2O$ and 1 mL of H_2SO_4 (to dissolved compounds) to 1 L of Milli-Q water.
3. Prepare a sodium sulfate stock solution by adding 62.5 g of Na_2SO_4 to 1 L of Milli-Q water.
4. Prepare a sodium bicarbonate stock solution by adding 20 g of $NaHCO_3$ to 100 mL Milli-Q water.
5. Prepare an amorphous ferrous sulfide (FeS) stock solution (2 g/L, sulfide). Pre-weigh 6.5 g of $(NH_4)2Fe(SO_4)2 \cdot 6H_2O$ and 4 g of $Na_2S \cdot 9H_2O$, and transfer each chemical into separate falcon tubes and cap. Repeat twice more. Autoclave 1.5 L of Milli-Q water at 121ºC for 40 minutes to deoxygenate the water, then purge with N_2 gas at low pressure through a sterile in-line filter while cooling in an ice bath to ensure the water remains anaerobic. Transport the sealed falcon tubes and deoxygenated water directly into a glove box (N_2/H_2 atmosphere), in addition to three 200 mL centrifuge bottles. Add 167 mL of anaerobic Milli-Q water to one centrifuge bottle, followed by the contents of one falcon tube containing the $(NH_4)2Fe(SO_4)$, then add the contents of one falcon tube containing the Na_2S (a black precipitate [FeS] will immediately form). Repeat twice more. Tightly cap and shake the solutions vigorously by hand for at least 5 minutes. Remove the centrifuge bottles from the glove box and centrifuge each bottle for 10 minutes at 8,000 × g_{av}. Transport the centrifuge bottles back into the glove box and remove the supernatant as waste. Refill the centrifuge bottles with 167 mL of anaerobic Milli-Q water and repeat the rinse process 2-3 more times, or until the FeS does not form a pellet after centrifuging but instead remains suspended in solution.
6. Prepare the resazurin redox indicator by adding 1 g of resazurin to 1 L of Milli-Q water.

   Dispense 100 mL aliquots of each stock solution into separate 160 mL serum bottles and seal with butyl rubber stoppers and crimp caps. Wrap the exterior of the serum bottles containing the mineral medium in tin foil to limit direct light exposure and potential photodegradation over time. Autoclave the serum bottles containing contents from step 1-4 at 121ºC for 20 to 30 minutes, then purge with N_2 gas for 15 minutes at low pressure through a sterile in-line filter while cooling in an ice bath. Store the anaerobic stock solutions at 4 ºC.

   All stock solutions are to be maintained under positive pressure; if large aqueous volumes are removed equal volumes of the sterile glove box atmosphere should be passively added back by inserting a sterile needle connected to a 0.2 µM syringe filter into the stock bottle septa while inside a glove box.

7. Prepare a salt solution by adding 49.75 mg of NH_4Cl, 7.01 mg of NaCl, 4.76 mg of $MgCl_2$, 3.96 mg of $MnCl_2 \cdot 4H_2O$, 8.52 mg of Na_2SO_4 and 147.02 mg of $CaCl_2 \cdot 2H_2O$ to 1 L of Milli-Q water.
8. Autoclave the salt solution at 121ºC for 0.75 to 1 hour to deoxygenate the water, then purge the solution in a sealed vessel with N_2 gas at low pressure through a sterile in-line filter while cooling in

an ice bath for 0.5 to 1 hour to ensure the water remains anaerobic (autoclave and purging time is dependent on the solution volume).

9. Once the salt solution is cooled, add 10 mL of the phosphate buffer, 1 mL of the trace mineral solution and 0.5 mL of the supernatant from the sodium bicarbonate stock solution (per liter of salt solution). Continue purging the AGW solution at a slightly elevated pressure for 5 to 10 minutes.
10. Following purging, clamp the inlet and outlet purging lines of the vessel, detach from the gas lines, and directly transfer the solution into a deoxygenated glove bag or box.
11. Add 3 mL of the FeS stock solution (per L of AGW) to the deoxygenated AGW solution using a sterilized syringe. Leave the vessel undisturbed and covered in the glove bag or box for 2 days to fully reduce the AGW solution.
12. Measure the AGW pH and DO, ensuring the AGW medium pH is neutral and DO is ≤ 0.3 mg/L.

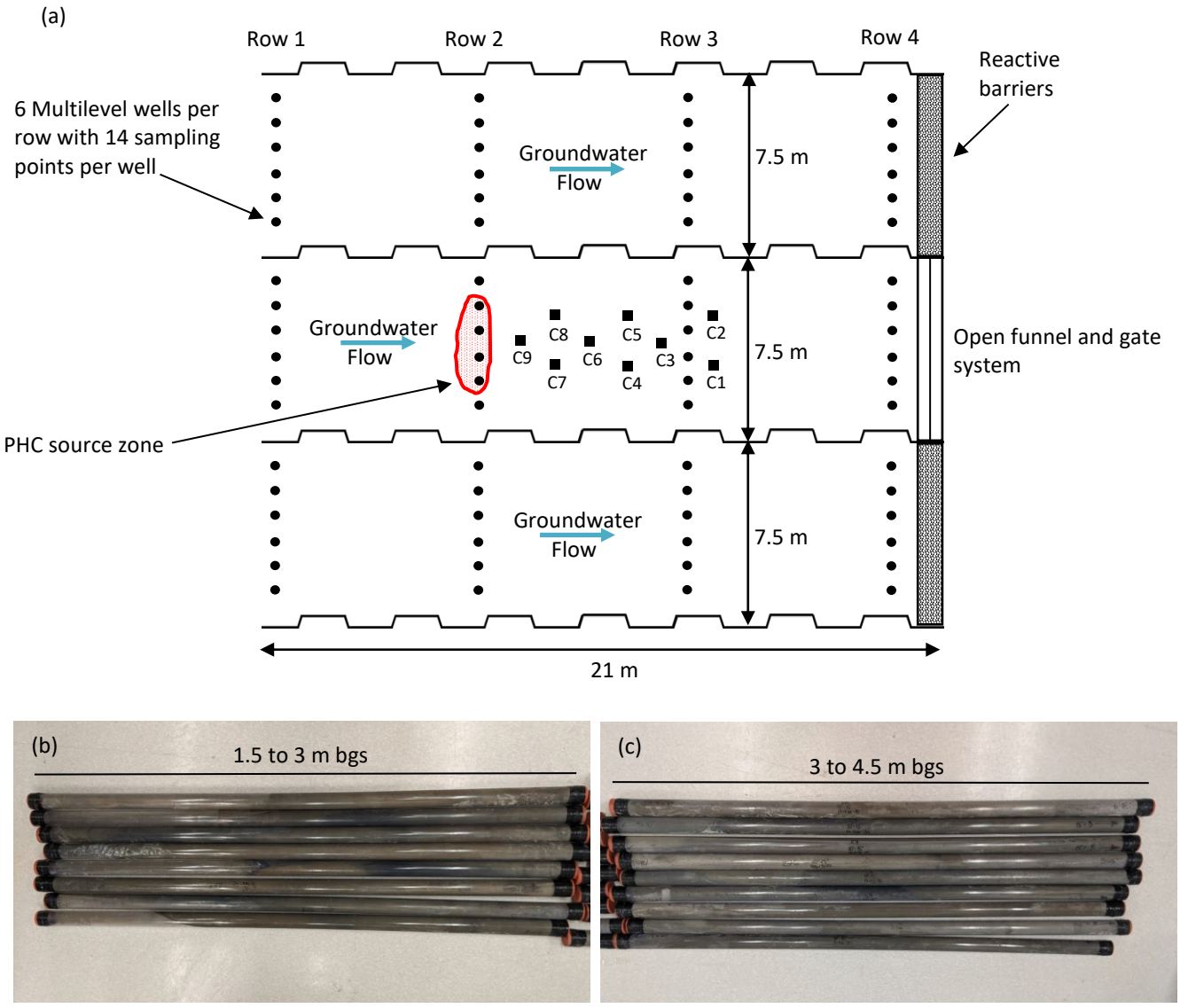

Figure B.1: Details for the Borden sand (BS) collected from CFB Borden Ontario, Canada at the sandpit research area and within the (a) middle of three hydraulically isolated sheet piled experimental research gates. Each experimental gate contains 4 rows of multilevel monitoring wells for groundwater monitoring (6 wells per row and per gate, and 14 depths per well). The upgradient ends of each gate are open to groundwater flow, whereas the downgradient ends adjoin to an open funnel and gate system for groundwater treatment prior to groundwater exiting the gates. The middle experimental gate shows the location of the injected petroleum hydrocarbons (PHCs) within the PHC source zone, and the 9 core extraction locations downgradient of the PHC source zone (core extraction locations are labelled C1 [i.e., core extraction location 1] to C9). Images of the 17 anaerobic cores collected (i.e., 1-2 cores collected per core extraction location) from the middle experimental research gate are shown from (b) 1.5 to 3 m below ground surface (bgs), and (c) 3 to 4.5 m bgs.

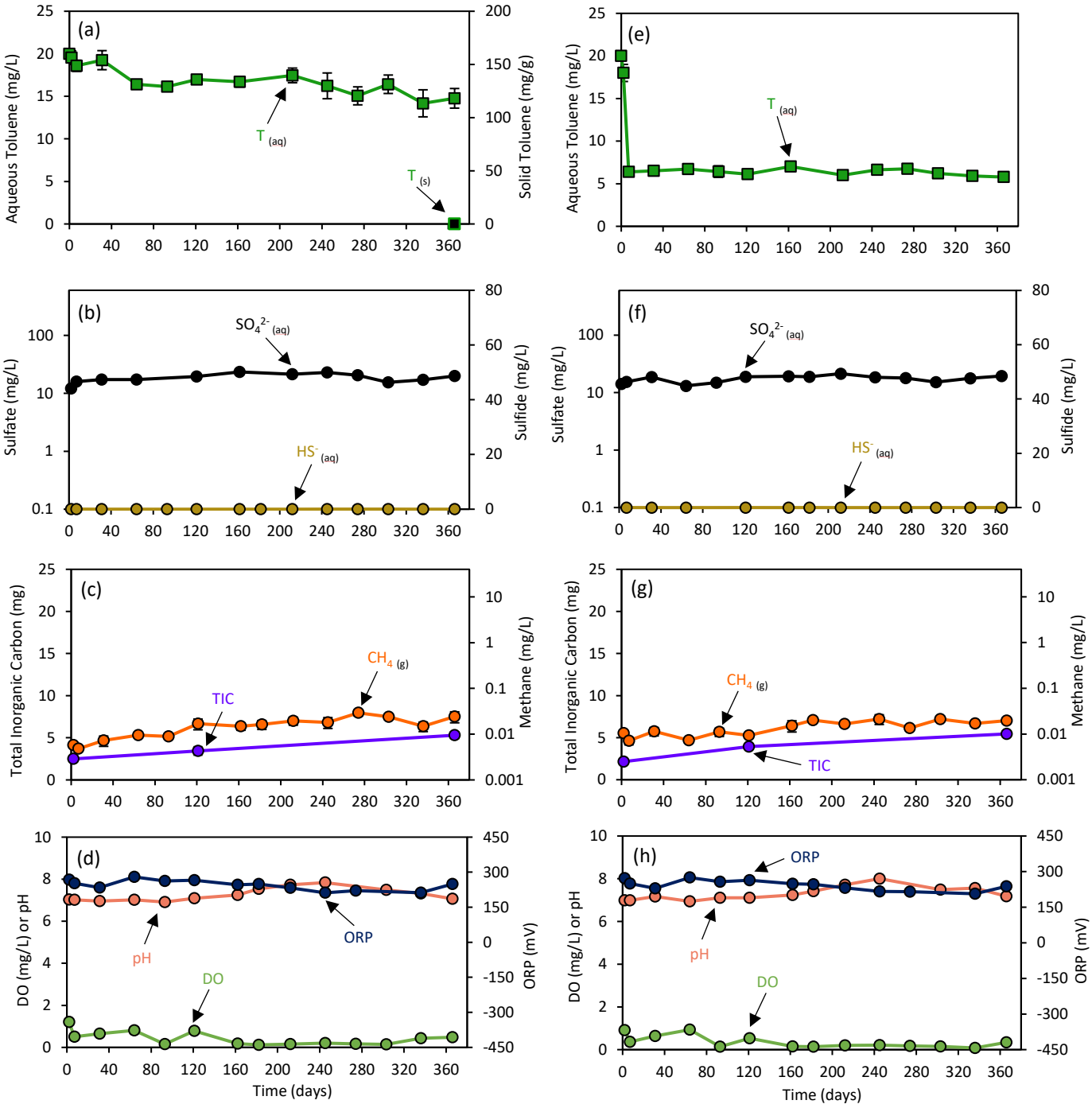

Figure B.2: Temporal changes in the (a, e) aqueous and solid phase toluene concentrations ($T_{(aq)}$ and $T_{(s)}$) (green and black filled squares, respectively); (b, f) aqueous sulfate ($SO_4^{2-}{}_{(aq)}$) (black filled circles) and sulfide ($HS^-_{(aq)}$) (yellow filled circles) concentrations; (c, g) total inorganic carbon (TIC) (purple filled circles) and gaseous methane concentration ($CH_{4(g)}$) (orange filled circles); and (d, h) dissolved oxygen (DO) (light green filled circles), pH (pink filled circles) and the oxidation reduction potential (ORP) (dark blue filled circles) for the single-solute (toluene-only) (a-d) KC and (e-h) KC+PAC microcosms. Each timepoint represents the average of three values and the error bars are ± 1 standard deviation.

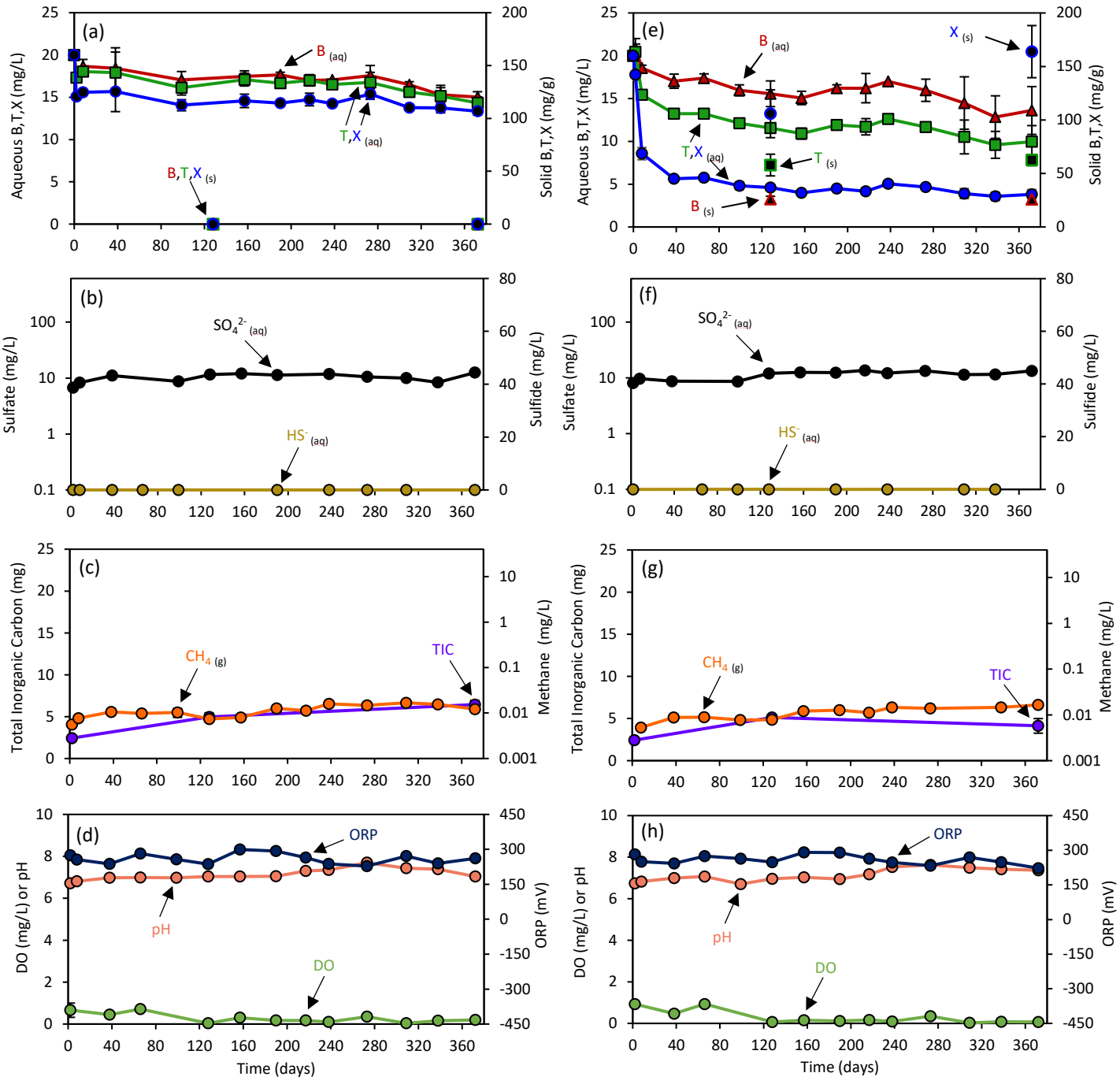

Figure B.3: Temporal changes in the (a, e) aqueous phase benzene, toluene and *o*-xylene (BTX) ($B,T,X_{(aq)}$) (red filled triangles [B], green filled squares [T] and blue filled circles [X]) and solid phase BTX ($B,T,X_{(s)}$) (black filled triangles [B], squares [T] and circles [X]) concentrations; (b, f) aqueous sulfate ($SO_4^{2-}{}_{(aq)}$) (black filled circles) and sulfide ($HS^-_{(aq)}$) (yellow filled circles) concentrations; (c, g) total inorganic carbon (TIC) (purple filled circles) and gaseous methane concentration ($CH_{4(g)}$) (orange filled circles); and (d, h) dissolved oxygen (DO) (light green filled circles), pH (pink filled circles) and the oxidation reduction potential (ORP) (dark blue filled circles) for the multi-solute (BTX) (a-d) KC and (e-h) KC+PAC microcosms. Each timepoint represents the average of three values and the error bars are ± 1 standard deviation.

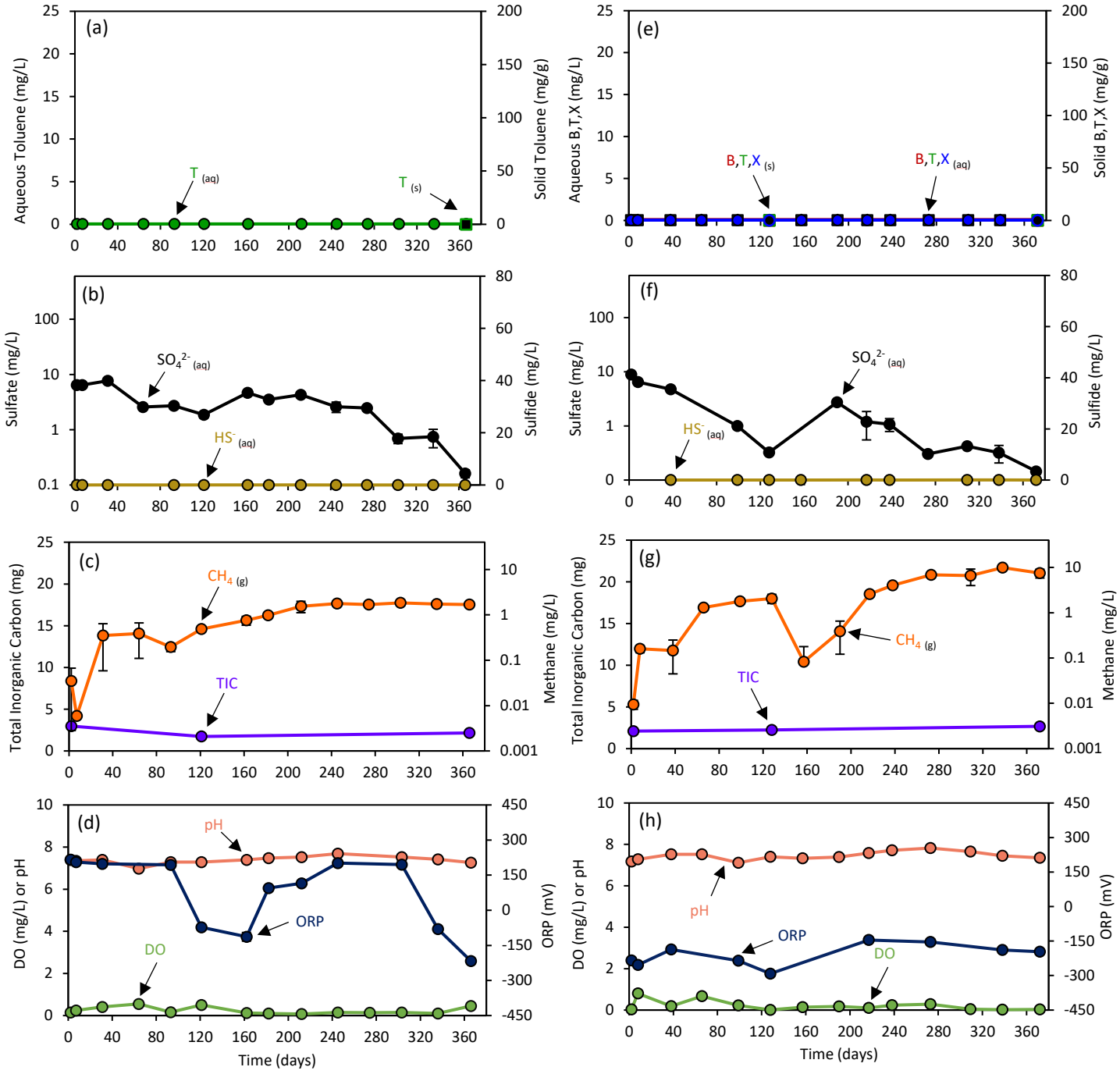

Figure B.4: Temporal changes in the (a) aqueous and solid phase toluene ($T_{(aq)}$ and $T_{(s)}$) (green and black filled squares, respectively), and (e) aqueous phase benzene, toluene and *o*-xylene (BTX) ($B,T,X_{(aq)}$) (red filled triangles [B], green filled squares [T] and blue filled circles [X]) and solid phase BTX ($B,T,X_{(s)}$) (black filled triangles [B], squares [T] and circles [X]) concentrations; (b, f) aqueous sulfate ($SO_4^{2-}{}_{(aq)}$) (black filled circles) and sulfide ($HS^-_{(aq)}$) (yellow filled circles) concentrations; (c, g) total inorganic carbon (TIC) (purple filled circles) and gaseous methane concentration ($CH_{4(g)}$) (orange filled circles); and (d, h) dissolved oxygen (DO) (light green filled circles), pH (pink filled circles) and the oxidation reduction potential (ORP) (dark blue filled circles) for the multi-solute (BTX) (a-d) KC and (e-h) KC+PAC microcosms. Each timepoint represents the average of three values and the error bars are ± 1 standard deviation.

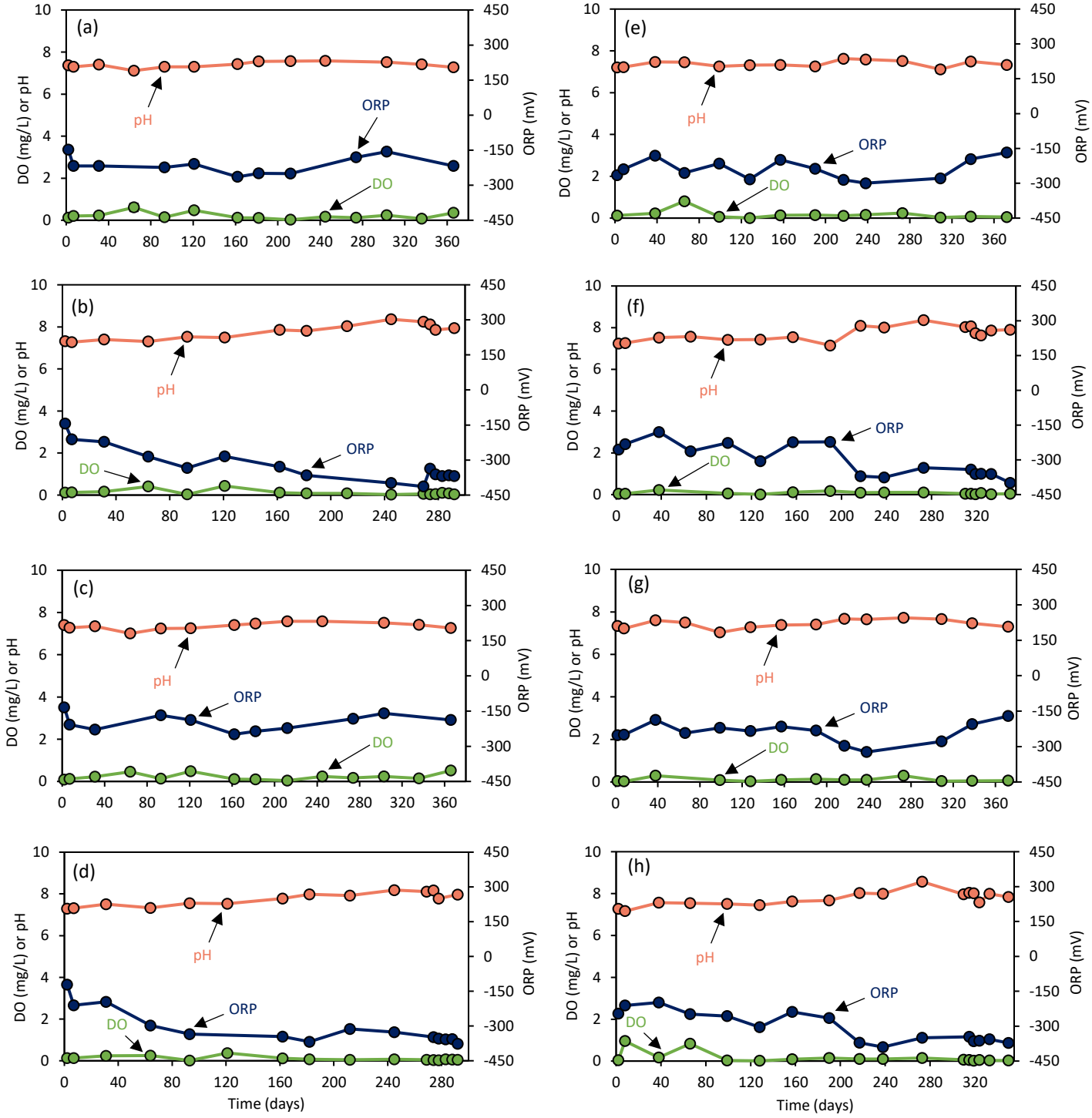

Figure B.5: Temporal changes in dissolved oxygen (DO) (light green filled circles), pH (pink filled circles) and the oxidation reduction potential (ORP) (dark blue filled circles) for the single-solute (toluene-only) (a) BA-PC, (b) BA+PAC, (c) BA-PC+EA and (d) BA+PAC+EA microcosms; and the multi-solute (benzene, toluene and *o*-xylene [BTX]) (e) BA-PC, (f) BA+PAC, (g) BA-PC+EA and (h) BA+PAC+EA microcosms. Each timepoint represents the average of three values and the error bars are ± 1 standard deviation.

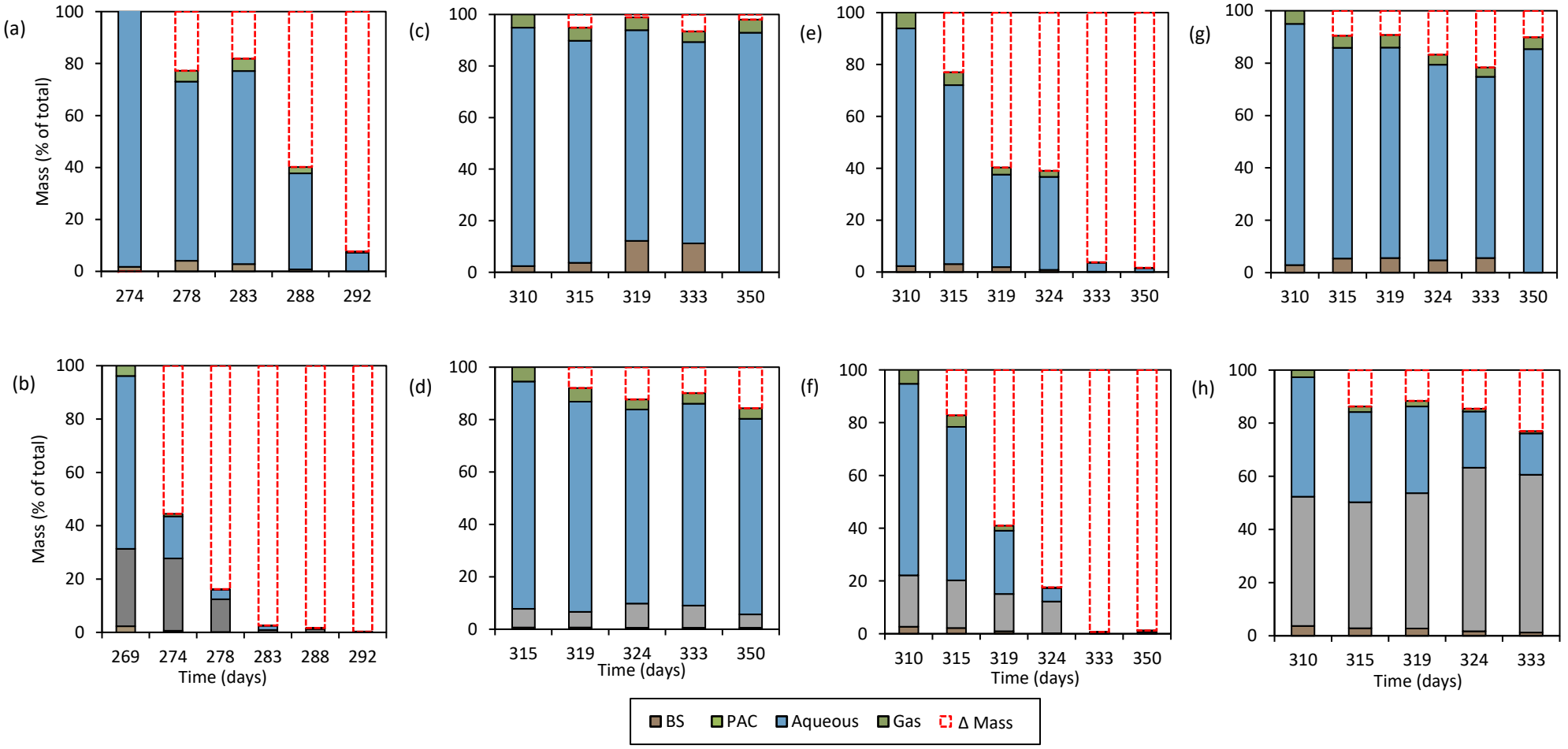

Figure B.6: Total mass during high-resolution monitoring for single-solute (a-b) toluene, and multi-solute (c-d) benzene, (e-f) toluene and (g-h) *o*-xylene in the BA-PC+EA (top panel) and BA+PAC+EA (bottom panel) microcosms.

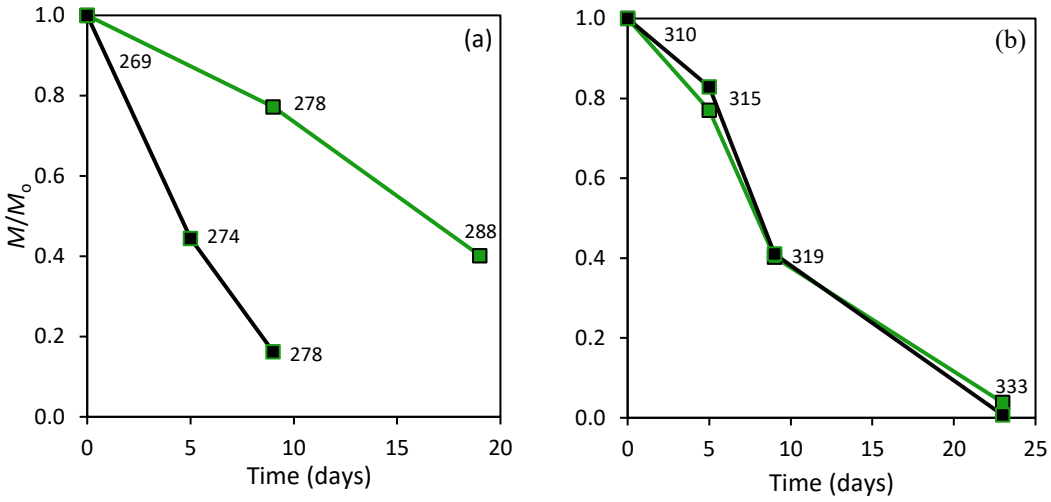

Figure B.7: Change in total mass of toluene within the (a) single-solute (toluene-only) and (b) multi-solute solute (benzene, toluene and *o*-xylene [BTX]) BA-PC+EA (green lines and filled symbols) and BA+PAC+EA (black lines and filled symbols) microcosms. The sampling day corresponding to each data point are shown as labels. Data were fit with a straight line to estimate zero-order rate constants (see Table B.10) from the slope (K = - slope).

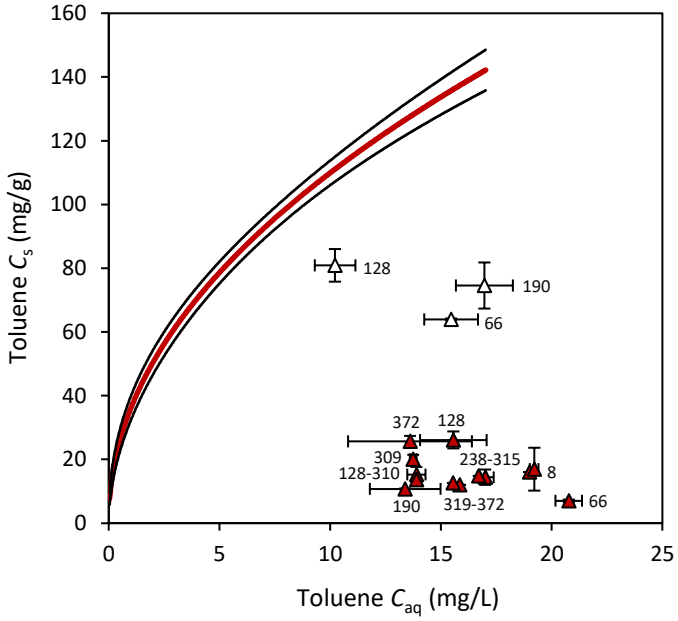

Figure B.8: Aqueous (C_{aq}) and solid (C_s) phase benzene concentrations from the KC+PAC, BA+PAC and BA+PAC+EA multi-solute microcosms with the sampling day (or range in days) corresponding to each datapoint (or cluster of data points). All data are represented as red filled triangles, neglecting three data points that are more representative of single-solute conditions and shown as unfilled triangles. The standard deviation of triplicate measurements is represented as ± error bars on each data point. The Freundlich sorption equilibrium isotherm for single-solute benzene is shown as a solid red line with a 95% confidence envelope represented as black solid bands.

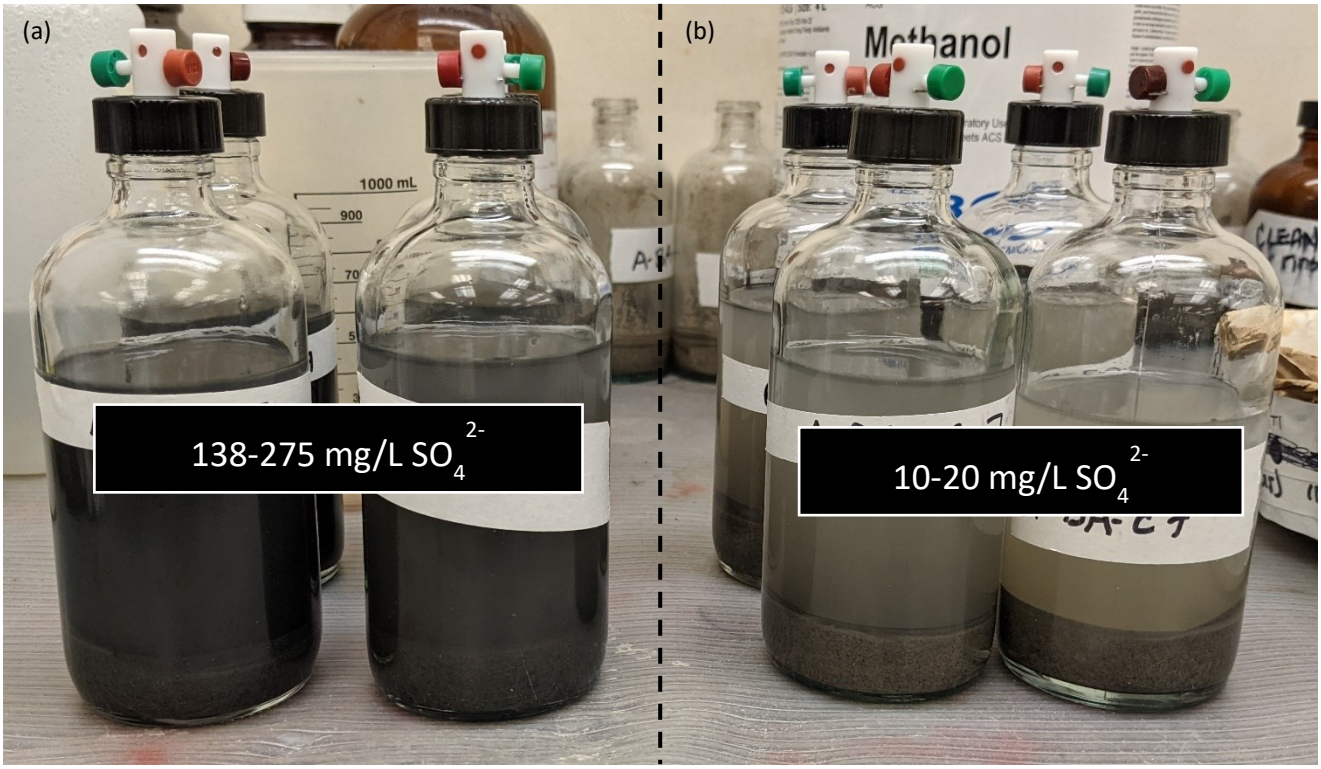

Figure B.9: Presumed ferrous sulfide (FeS) precipitation in the (a) BA-PC+EA microcosms (i.e., 138-275 mg/L SO_4^{2-}) on Day 278 and 319 for single- or multi-solute microcosms, respectively, relative to (b) microcosms without electron acceptor (EA) amendments (i.e., 10-20 mg/L SO_4^{2-}).

Table B.1: Hydrogeologic and geochemical characteristics at CFB Borden (Ontario, Canada).

Parameter	Value(s)	Reference(s)
Groundwater flow direction	North to northeast with seasonal oscillations up to 39º in direction	[139]
	N40ºE to N53ºE	[135]
Depth to water table	≥ 1 m bgs (fluctuates seasonally)	[137]
	Ground surface to 1.5 m bgs (varies with time)	[138]
Groundwater temperature	10ºC (varies from 6 to 15ºC seasonally)	[135, 237]
Porosity	0.38	[137]
	0.33	[135]
Specific storage	0.001 m^{-1}	[238]
Hydraulic gradient	0.003	[137]
	0.0043	[136]
Aquifer depth	9 m bgs	[135, 136]
Aquifer groundwater velocity	0.091 m/day	[135]
Aquifer hydraulic conductivity	3×10^{-5} to 5×10^{-5} m/s	[137]
	6×10^{-6} to 2×10^{-4} m/s (mean 9.75×10^{-5} m/s)	[136]
	5×10^{-5} to 1×10^{-4} m/s (mean 7×10^{-5} m/s)	[135, 238]
Aquitard depth	9 to 17 m bgs	[237]
Aquitard hydraulic conductivity	1.12×10^{-10} to 5.39×10^{-10} m/s (mean of 2.4×10^{10} m/s)	[237]
Aquitard Darcy flux	3.3 mm/year	[237]
Longitudinal dispersivity	0.08 m	[239]
	0.06 to 0.43 m (mean 0.36 m)	[240]
Traverse horizontal dispersivity	0.03 m	[239]
	0.039 m	[240]
Vertical dispersion coefficient	10×10^{-10} m^2/s	[239]
Grain size	0.070 to 0.69 mm	[135]
Median grain size (d_{50})	0.15 mm	[238]
Dry bulk density	1.76 g/cm^3	[137]
	1.81 g/cm^3	[135]
Solid density	2.71 g/cm^3	[135]
Specific surface area	0.6 to 1.6 m^2/g (mean 0.8 m^2/g)	[135]
Organic carbon content	0.01 to 0.09% (mean 0.02%)	[135]
Cation exchange capacity	0.52 ± 0.09 meq/100g	[241]
Minerology	58% quartz, 19% feldspars, 14% carbonates, 7% amphiboles, 2% chlorite	[135]
Dissolved organic carbon	2.4 to 6.4 mg/L	[140]
	< 0.7 mg/L	[135]
pH	7.3 to 7.9	[135]
Calcium (Ca^{2+})	50 to 110 mg/L	[242, 135, 138]
Magnesium (Mg^{2+})	2.4 to 6.1 mg/L	[242, 135, 138]
Sodium (Na^{+})	0.9 to 2.0 mg/L	[242, 135, 138]
Potassium (K^{+})	0.1 to 1.2 mg/L	[242, 135, 138]
Calcium carbonate ($CaCO_3$)	100 to 250 mg/L	[242, 135, 138]
Chloride (Cl^{-})	1 to 3 mg/L	[242, 135, 138]
Sulfate ($SO4^{-}$)	10 to 30 mg/L	[242, 135, 138]
Nitrate ($NO3^{-}$)	< 0.6 to 6 mg/L	[242, 135, 138]
Iron (Fe^{2+})	< 0.004 to 2.8 mg/L	[242]
Manganese (Mn)	< 0.04 to 0.3 < mg/L	[242]
Total dissolved solids (TDS)	380 to 500 mg/L	[242, 135, 138]
Dissolved oxygen (DO)	0 to 8.5 mg/L	[135, 138]

Table B.2: Details of the single-solute (toluene-only) and multi-solute (benzene, toluene and *o*-xylene [BTX]) microcosm experiments.

Microcosm type	Acronym	Artificial groundwater (AGW) volume (mL)	Biocide and sterilization [1]	Borden sand (BS) (mL [g]) [2]	Powdered activated carbon (PAC) mass (mg) [3]	Sulfate stock concentration (mg/L) [4]	Toluene or benzene, toluene and *o*-xylene (BTX) concentration (mg/L)	Number of triplicate bottle sets (number of microcosm bottles)
Single-solute (toluene-only)								
Killed control	KC	175	✓	45 (81.5)	-	10-20	20	2 (6)
Killed control + powdered activated carbon	KC+PAC	175	✓	45 (81.5)	15	10-20	20	2 (6)
Starved control	SC	175	-	45 (81.5)	-	10-20	-	2 (6)
Bioactive-positive control	BA-PC	175	-	45 (81.5)	-	10-20	20	8 (24)
Bioactive-positive control + electron acceptor	BA-PC+EA	175	-	45 (81.5)	-	138-275 [5]	20	8 (24)
Bioactive + powdered activated carbon	BA+PAC	175	-	45 (81.5)	15	10-20	20	8 (24)
Bioactive + powdered activated carbon + electron acceptor	BA+PAC+EA	175	-	45 (81.5)	15	138-275 [5]	20	8 (24)
Multi-solute (benzene, toluene and *o*-xylene [BTX])								
Killed control	KC	175	✓	45 (81.5)	-	10-20	20:20:20	2 (6)
Killed control + powdered activated carbon	KC+PAC	175	✓	45 (81.5)	15	10-20	20:20:20	2 (6)
Starved control	SC	175	-	45 (81.5)	-	10-20	-	2 (6)
Bioactive-positive control	BA-PC	175	-	45 (81.5)	-	10-20	20:20:20	8 (24)
Bioactive-positive control + electron acceptor	BA-PC+EA	175	-	45 (81.5)	-	138-275 [5]	20:20:20	8 (24)
Bioactive + powdered activated carbon	BA+PAC	175	-	45 (81.5)	15	10-20	20:20:20	8 (24)
Bioactive + powdered activated carbon + electron acceptor	BA+PAC+EA	175	-	45 (81.5)	15	138-275 [5]	20:20:20	8 (24)

Notes:

1. BS was autoclaved three times on three consecutive days (121ºC) and amended with 2.5 mL (2.71 g/100 mL) of mercuric chloride and 0.45 mL (5g/100 mL) of sodium azide.
2. Anaerobic BS was sourced from the Borden aquifer.
3. Calgon Carbon WPC PAC.
4. The target sulfate concentration in the KC, KC+PAC, SC, BA-PC and BA+PAC microcosms was representative of background sulfate concentration within the Borden aquifer (Table B.1), and the target sulfate concentration in BA-PC+EA and BA+PAC+EA microcosms was representative of electron acceptor (EA) amended conditions.
5. The higher target sulfate concentration of 275 mg/L was used during all dosing events, with the expectation of the dosing event at the start of the high-resolution sampling period which was reduced by half to a target sulfate concentration of 138 mg/L.

Table B.3: Predicted partitioning of toluene (single-solute) or benzene, toluene and *o*-xylene (BTX) (multi-solute) in PAC amended microcosms dosed with 4 µL or 12 µL of pure phase toluene or BTX (4 µL per solute), respectively.

Chemical properties (sorbate and sorbent):	**Toluene (single-solute)**	**Benzene (multi-solute)**	**Toluene (multi-solute)**	***o*-xylene (multi-solute)**
Henry's constant (K_{h_i}) [-] [1]	0.274	0.225	0.274	0.221
Density (ρ) [$\frac{mg}{\mu L}$] [2]	0.867	0.878	0.867	0.88
Soil-water partitioning coefficient (K_{d_i}) [mL/g] [3]	0.09125	0.01996	0.09125	0.1996
Freundlich constant (K_{f_i}) [$(\frac{mg}{g}\frac{L}{mg})^n$]	88.19	36.10	88.19	131.76
Freundlich constant (n_{f_i}) [-]	0.42	0.48	0.42	0.37
Improved simplified ideal adsorption solution (ISIAS) constant (a_i)	-	1.42	1.43	1.08
Equilibrated aqueous concentration:				
$C_{e_i}^s$ [$\frac{mg}{L}$] [4]	4.9	17.2	11.5	5.2
Equilibrated solid concentration:				
Single-solute sorption capacity, $q_{e_i}^s$ [$\frac{mg}{g}$] $= (K_{f_i} \times C_{e_i}^s)^{n_{f_i}}$	171.91	-	-	-
Multi-solute sorption capacity, $q_{e_i}^s$ [$\frac{mg}{g}$] $= [(\frac{\sum(\frac{K_{f_i}}{a_i})}{N})^{(\frac{\sum n_{f_i}}{N})-1}{}^{(\frac{\sum n_{f_i}}{N})} [\frac{K_{f_i}}{a_i} C_{e_i}^{n_{f_i}}]^{\frac{1}{(\frac{\sum n_{f_i}}{N})}} [\sum_i^N (\frac{\frac{K_{f_i}}{a_i} C_{e_i}^{n_{f_i}}}{(\frac{\sum(\frac{K_{f_i}}{a_i})}{N})})^{\frac{1}{(\frac{\sum n_{f_i}}{N})}}]^{((\frac{\sum n_{f_i}}{N})-1)}]$	-	24.79	88.73	166.55
Microcosm material volume or mass:				
$V_{(g)}$ [mL]	30	30	30	30
$V_{(aq)}$ [mL]	175	175	175	175
m_{BS} [g]	68.5	68.5	68.5	68.5
m_{PAC} [mg]	15	15	15	15
Equilibrium mass partitioned to each phase:				
M_{g_i}[mg] $= C_{e_i}^s \frac{V_{(g)}}{1000} K_{h_i}$	0.040	0.12	0.095	0.034
M_{aq_i} [mg] $= C_{e_i}^s \frac{V_{(aq)}}{1000}$	0.86	3.01	2.01	0.91
M_{BS_i} [mg] $= m_{BS} \frac{C_{e_i}^s}{1000} K_{d_i}$	0.031	0.024	0.072	0.071
M_{PAC_i} [mg] $= q_{e_i}^s \frac{m_{PAC}}{1000}$	2.58	0.37	1.33	2.50
M_{T_i} [mg] $= M_{g_i} + M_{aq_i} + M_{BS_i} + M_{PAC_i}$	3.51	3.52	3.51	3.51
Initial aqueous concentration (before PAC addition):				
C_{o_i} [$\frac{mg}{L}$] $= \frac{M_{T_i}}{\frac{V_{(aq)}}{1000}}$	20.04	20.12	20.06	20.08
Pure phase addition:				
V_p [µL] $= \frac{M_{i_T}}{\rho}$	4.05	4.01	4.05	3.99

Notes: 1. [151], 2. [190], 3. [152] and 4. value adjusted to achieve ~20 mg/L.

Table B.4: Quantitative polymerase chain reaction (qPCR) primers for DNA analysis.

Primer name	Target 16S rRNA sequence	Primer Sequence 5'-3'	Expected amplicon size (bp)	Annealing temperature (°C)	Reference(s)
926f_modified	Bacteria, Archaea and some Eukarya	AAACTYAAAKGAATWGRCGG	467	54	[243, 244]
1392r_modified		ACGGGCGGTGWGTRC			
Bac_1055f	General Bacteria	ATGGCTGTCGTCAGCT	338	55	[245, 243]
Bac_1392r		ACGGGCGGTGTGTAC			
Arch_787f	General Archaea	ATTAGATACCCGBGTAGTCC	273	59	[246]
Arch_1059r		GCCATGCACCWCCTCT			
ORM2_168f	Deltaproteobacteria ORM2	GAGGGAATAGCCAAAGGTGA	255	59	[247, 154]
ORM2_422r		GAGCTTTACGACCCGAAGAC			
Dsp_1304f	Desulfosporosinus sp. DGG-T	GGGGAGCAAATCCGAGAAAG	191	59	[248]
Dsp_1494r		GAATCTCGAGTCGGTTACCTC			
Pep_87f	Peptococcaceae sp. DGG-X	TTGGATGTCAGATAGTGGCG	142	65	[248]
Pep_228r		GCGATTTGCATCGCCTTTCTAC			

Table B.5: Sampling (long-term repetitive sampling [LT-RS], long-term sacrificial sampling [LT-SS] or high-resolution sacrificial sampling [HR-SS]) or amendment (i.e., powdered activated carbon [PAC]; toluene [T]; benzene, toluene and *o*-xylene [BTX]; toluene and *o*-xylene [TX]; or sulfate [SO_4^{2-}]) days for the single-solute (toluene-only) or multi-solute (BTX) microcosms.

Day	Toluene	Day	Benzene, toluene and *o*-xylene (BTX)
0	T: All microcosms except SC SO_4^{2-}: BA-PC+EA and BA+PAC+EA microcosms	0	BTX: All microcosms except SC
2	LT-SS: Triplicate bottle set 1 (timepoint 1) PAC: KC+PAC, BA+PAC and BA+PAC+EA microcosms	2	LT-SS: Triplicate bottle set 1 (timepoint 1) PAC: KC+PAC, BA+PAC and BA+PAC+EA microcosms
7	LT-SS: Triplicate bottle set 2 (timepoint 2)		
		8	SO_4^{2-}: BA-PC+EA and BA+PAC+EA microcosms LT-SS: Triplicate bottle set 2 (timepoint 2)
31	LT-RS: Triplicate bottle set 3 (timepoint 3)		
		38	LT-RS: Triplicate bottle set 3 (timepoint 3)
64	LT-SS: Triplicate bottle set 3 (timepoint 4)		
		66	LT-SS: Triplicate bottle set 3 (timepoint 4)
77	T: BA-PC+EA and BA+PAC+EA microcosms		
93	LT-RS: Triplicate bottle set 4 (timepoint 5)		
		99	LT-RS: Triplicate bottle set 4 (timepoint 5)
105	T: BA-PC+EA and BA+PAC+EA microcosms		
		112	SO_4^{2-}: BA+PAC+EA microcosms only
121	LT-SS: Triplicate bottle set 4 (timepoint 6)		
128	SO_4^{2-}: BA-PC+EA and BA+PAC+EA microcosms	128	LT-SS: Triplicate bottle set 4 (timepoint 6)
149	SO_4^{2-}: BA-PC+EA and BA+PAC+EA microcosms		
		157	LT-RS: Triplicate bottle set 5 (timepoint 7)
162	LT-RS: Triplicate bottle set 5 (timepoint 7)		
170	T: BA-PC+EA and BA+PAC+EA microcosms		
182	LT-SS: Triplicate bottle set 5 (timepoint 8)		
		190	LT-SS: Triplicate bottle set 5 (timepoint 8)
		193	TX: BA-PC+EA and BA+PAC+EA microcosms SO_4^{2-}: BA-PC+EA microcosms only
199	T: BA+PAC+EA microcosms only		
205	T: BA-PC+EA microcosms only		
212	LT-RS: Triplicate bottle set 6 (timepoint 9)		
		217	LT-RS: Triplicate bottle set 6 (timepoint 9)
221	BA+PAC+EA microcosms only		
		238	LT-SS: Triplicate bottle set 6 (timepoint 10)
245	LT-SS: Triplicate bottle set 6 (timepoint 10)		
269	T: BA-PC+EA and BA+PAC+EA microcosms SO_4^{2-}: BA-PC+EA and BA+PAC+EA microcosms HR-SS: Triplicate bottle set 7 (BA-PC+EA and BA+PAC+EA microcosms only) (timepoint 11)		

Day	Toluene	Day	Benzene, toluene and *o*-xylene (BTX)
		273	LT-RS: Triplicate bottle set 7 (KC, KC+PAC, SC, BA-PC and BA+PAC microcosms only) (timepoint 11)
274	LT-RS: Triplicate bottle set 7 (KC, KC+PAC, SC, BA-PC and BA+PAC microcosms only) (timepoint 11)		
	HR-SS: Triplicate bottle set 7 (BA-PC+EA and BA+PAC+EA microcosms only) (timepoint 12		
278	HR-SS: Triplicate bottle set 7 (BA-PC+EA and BA+PAC+EA microcosms only) (timepoint 13)		
283	HR-SS: Triplicate bottle set 8 (BA-PC+EA and BA+PAC+EA microcosms only) (timepoint 14)		
288	HR-SS: Triplicate bottle set 8 (BA-PC+EA and BA+PAC+EA microcosms only) (timepoint 15)		
292	HR-SS: Triplicate bottle set 8 (BA-PC+EA and BA+PAC+EA microcosms only) (timepoint 16)		
303	LT-SS: Triplicate bottle set 7 (KC, KC+PAC, SC, BA-PC and BA+PAC microcosms only) (timepoint 12)		
		309	LT-SS: Triplicate bottle set 7 (KC, KC+PAC, SC, BA-PC and BA+PAC microcosms only) (timepoint 12)
		310	TX: BA-PC+EA and BA+PAC+EA microcosms
			SO_4^{2-}: BA-PC+EA and BA+PAC+EA microcosms
			HR-SS: Triplicate bottle set 7 (BA-PC+EA and BA+PAC+EA microcosms only) (timepoint 11)
		315	HR-SS: Triplicate bottle set 7 (BA-PC+EA and BA+PAC+EA microcosms only) (timepoint 12)
		319	HR-SS: Triplicate bottle set 7 (BA-PC+EA and BA+PAC+EA microcosms only) (timepoint 13)
		324	HR-SS: Triplicate bottle set 8 (BA-PC+EA and BA+PAC+EA microcosms only) (timepoint 14)
		333	HR-SS: Triplicate bottle set 8 (BA-PC+EA and BA+PAC+EA microcosms only) (timepoint 15)
336	LT-RS: Triplicate bottle set 8 (KC, KC+PAC, SC, BA-PC and BA+PAC microcosms only) (timepoint 13)		
		338	LT-RS: Triplicate bottle set 8 (KC, KC+PAC, SC, BA-PC and BA+PAC microcosms only) (timepoint 13)
		350	HR-SS: Triplicate bottle set 8 (BA-PC+EA and BA+PAC+EA microcosms only) (timepoint 16)
366	LT-SS: Triplicate bottle set 8 (KC, KC+PAC, SC, BA-PC and BA+PAC microcosms only) (timepoint 14)		
		372	LT-SS: Triplicate bottle set 8 (KC, KC+PAC, SC, BA-PC and BA+PAC microcosms only) (timepoint 14)

Table B.6: Average abundance of total bacteria, total archaea, Deltaproteobacteria, *Desulfosporosinus* sp.and Peptococcaceae sp. (± standard error) generated from quantitative polymerase chain reaction (qPCR) analysis for the single-solute (toluene-only) and multi-solute (benzene, toluene and *o*-xylene [BTX]) KC, KC+PAC, SC, BA-PC, BA+PAC, BA-PC+EA and BA+PAC+EA microcosms after 1 year relative to background conditions.

	Abundance (copies/g)									
	Total Bacteria		Total Archaea		Deltaproteobacteria		*Desulfosporosinus* sp.		Peptococcaceae sp.	
Microcosm type	Average	Standard error	Average	Standard error	Average	Standard error	Average	Standard error	Average	Standard error
Single-solute (toluene-only)										
Background	$7.20 \times 10^{+6}$		$4.47 \times 10^{+4}$		$9.59 \times 10^{+1}$		$7.20 \times 10^{+4}$		$9.36 \times 10^{+2}$	
KC	$1.39 \times 10^{+5}$	$1.48 \times 10^{+4}$	$3.45 \times 10^{+3}$	$8.74 \times 10^{+2}$			$8.03 \times 10^{+2}$	$4.02 \times 10^{+2}$		
KC+PAC	$1.54 \times 10^{+5}$	$1.39 \times 10^{+4}$	$4.04 \times 10^{+3}$	$8.36 \times 10^{+2}$			$8.94 \times 10^{+2}$	$4.48 \times 10^{+2}$		
SC	$2.44 \times 10^{+6}$	$3.35 \times 10^{+5}$	$1.70 \times 10^{+6}$	$6.33 \times 10^{+5}$			$2.08 \times 10^{+3}$	$7.00 \times 10^{+2}$		
BA-PC	$1.11 \times 10^{+5}$	$1.95 \times 10^{+4}$	$1.60 \times 10^{+3}$	$1.60 \times 10^{+3}$			$6.93 \times 10^{+2}$	$3.99 \times 10^{+2}$		
BA+PAC	$6.36 \times 10^{+6}$	$1.11 \times 10^{+6}$	$2.67 \times 10^{+6}$	$1.36 \times 10^{+6}$			$3.53 \times 10^{+3}$	$1.87 \times 10^{+3}$		
BA-PC+EA	$1.15 \times 10^{+7}$		$4.09 \times 10^{+5}$				$1.08 \times 10^{+4}$			
BA+PAC+EA	$6.00 \times 10^{+6}$		$5.02 \times 10^{+5}$				$8.76 \times 10^{+3}$			
Multi-solute (benzene, toluene and *o*-xylene [BTX])										
Background	$3.12 \times 10^{+6}$		$3.38 \times 10^{+4}$		$4.70 \times 10^{+1}$		$2.60 \times 10^{+4}$			
KC	$1.22 \times 10^{+5}$	$3.05 \times 10^{+4}$	$4.74 \times 10^{+3}$	$1.26 \times 10^{+3}$	$9.80 \times 10^{+2}$	$5.72 \times 10^{+2}$	$0.00 \times 10^{+0}$	$0.00 \times 10^{+0}$	$1.55 \times 10^{+3}$	$1.11 \times 10^{+2}$
KC+PAC	$1.52 \times 10^{+5}$	$1.40 \times 10^{+3}$	$2.53 \times 10^{+3}$	$1.24 \times 10^{+3}$	$0.00 \times 10^{+0}$	$0.00 \times 10^{+0}$	$4.80 \times 10^{+2}$	$3.53 \times 10^{+2}$	$3.96 \times 10^{+3}$	$2.11 \times 10^{+3}$
SC	$3.42 \times 10^{+6}$	$1.26 \times 10^{+6}$	$2.05 \times 10^{+6}$	$9.43 \times 10^{+5}$	$1.85 \times 10^{+3}$	$9.47 \times 10^{+2}$	$1.05 \times 10^{+4}$	$4.95 \times 10^{+3}$	$9.74 \times 10^{+3}$	$4.65 \times 10^{+3}$
BA-PC	$1.31 \times 10^{+5}$	$3.14 \times 10^{+4}$	$7.83 \times 10^{+3}$	$2.79 \times 10^{+3}$	$6.46 \times 10^{+1}$	$5.80 \times 10^{+1}$	$2.82 \times 10^{+1}$	$2.82 \times 10^{+1}$	$3.20 \times 10^{+3}$	$1.06 \times 10^{+3}$
BA+PAC	$3.17 \times 10^{+6}$	$1.25 \times 10^{+6}$	$1.79 \times 10^{+6}$	$8.76 \times 10^{+5}$	$7.49 \times 10^{+2}$	$6.06 \times 10^{+2}$	$1.04 \times 10^{+4}$	$1.72 \times 10^{+3}$	$1.37 \times 10^{+4}$	$1.18 \times 10^{+4}$
BA-PC+EA	$2.71 \times 10^{+7}$		$4.30 \times 10^{+5}$		$2.11 \times 10^{+3}$		$6.11 \times 10^{+6}$		$2.49 \times 10^{+3}$	
BA+PAC+EA	$2.28 \times 10^{+7}$		$1.86 \times 10^{+6}$		$7.33 \times 10^{+2}$		$3.58 \times 10^{+6}$		$1.72 \times 10^{+3}$	

Table B.7: Electron donors, electron acceptors and chemical reactions associated with sulfate reduction coupled to benzene, toluene or *o*-xylene (BTX) oxidation.

Electron donor	**Electron acceptor**	**Chemical reaction**	**Δ G (kJ/ mol)**
Benzene	Sulfate	$C_6H_6 + 3\ H_2O + 3.75\ SO_4^{2-} \rightarrow 6\ HCO_3 + 1.88\ H_2S + 1.88\ HS + 0.38\ H^+$	-200 [1]
Toluene	Sulfate	$C_7H_8 + 4.5\ SO_4^{2-} + 3\ H_2O \rightarrow 7\ HCO_3^- + 2.25\ HS^- + 2.25\ H_2S + 0.25\ H^+$	-54.7 [2]
Xylene	Sulfate	$C_8H_{10} + 5.25\ SO_4^{2-} + 3\ H_2O \rightarrow 8\ HCO_3^- + 2.625\ HS^- + 2.625\ H_2S + 0.125\ H^+$	-63.8 [2]

Notes: 1. [249] and 2. [54].

Table B.8: Mass of benzene, toluene or *o*-xylene in the aqueous ($M_{i_{(aq)}}$), gas ($M_{i_{(g)}}$) and solid ($M_{i_{(s)}}$) phases, and the total mass (M_{i_T}) of each solute from the the sum of the mass in each phase for all microcosm types and sampling times.

		Mass (mg)											
		Benzene				**Toluene**				***o*-Xylene**			
	Sample Day	Aqueous ($M_{\mathrm{Ben}_{(aq)}}$)	Gas ($M_{\mathrm{Ben}_{(g)}}$)	Solid ($M_{\mathrm{Ben}_{(s)}}$)	Total (M_{Ben_T})	Aqueous ($M_{\mathrm{Tol}_{(aq)}}$)	Gas ($M_{\mathrm{Tol}_{(g)}}$)	Solid ($M_{\mathrm{Tol}_{(s)}}$)	Total (M_{Tol_T})	Aqueous ($M_{\mathrm{Xyl}_{(aq)}}$)	Gas ($M_{\mathrm{Xyl}_{(g)}}$)	Solid ($M_{\mathrm{Xyl}_{(s)}}$)	Total (M_{Xyl_T})
KC-toluene	2					3.41	0.20						
	7					3.11	0.23						
	31					3.14	0.26						
	64					2.61	0.24						
	93					2.48	0.26						
	121					2.54	0.29	0.14	2.97				
	162					2.92	0.17						
	212					2.75	0.26						
	245					2.49	0.26						
	274					2.25	0.26						
	303					2.39	0.30						
	336					2.01	0.27						
	366					2.03	0.30	0.01	2.35				
KC+PAC-toluene	2					2.78	0.28						
	7					1.07	0.079						
	31					1.06	0.087						
	64					1.07	0.098						
	93					0.99	0.10						
	121					0.92	0.10	2.76	3.79				
	162					1.22	0.072						
	212					1.00	0.075						
	245					1.08	0.090						
	274					1.07	0.099						
	303					0.96	0.099						
	336					0.89	0.10						
	366					0.85	0.10	1.46	2.41				

		Mass (mg)											
		Benzene				**Toluene**				***o*-Xylene**			
	Sample Day	Aqueous ($M_{\mathrm{Ben}_{(aq)}}$)	Gas ($M_{\mathrm{Ben}_{(g)}}$)	Solid ($M_{\mathrm{Ben}_{(s)}}$)	Total ($M_{\mathrm{Ben}_{T}}$)	Aqueous ($M_{\mathrm{Tol}_{(aq)}}$)	Gas ($M_{\mathrm{Tol}_{(g)}}$)	Solid ($M_{\mathrm{Tol}_{(s)}}$)	Total ($M_{\mathrm{Tol}_{T}}$)	Aqueous ($M_{\mathrm{Xyl}_{(aq)}}$)	Gas ($M_{\mathrm{Xyl}_{(g)}}$)	Solid ($M_{\mathrm{Xyl}_{(s)}}$)	Total ($M_{\mathrm{Xyl}_{T}}$)
BA-PC-toluene	2					3.28	0.19	0.029	3.50				
	7					3.20	0.19	0.033	3.42				
	31					2.97	0.17						
	64					2.66	0.18	0.0082	2.84				
	93					2.61	0.16						
	121					2.55	0.17	0.11	2.83				
	162					2.70	0.16						
	182							0.19					
	212					2.57	0.15						
	245					2.68	0.18	0.11	2.96				
	274					2.63	0.16						
	303					2.52	0.17	0.029	2.72				
	336					2.73	0.16						
	366					2.55	0.17	0.0014	2.73				
BA+PAC-toluene	2					3.16	0.32	0.001	3.48				
	7					1.42	0.083	1.40	2.90				
	31					0.89	0.053						
	64					0.83	0.057	2.11	3.00				
	93					0.89	0.052						
	121					0.76	0.050	3.19	4.00				
	162					0.87	0.052						
	182							2.34					
	212					1.02	0.059						
	245					0.87	0.057	2.17	3.09				
	274					0.90	0.053						
	303					0.97	0.065	2.10	3.14				
	336					0.94	0.055						
	366					0.88	0.058	2.14	3.08				

		Mass (mg)											
		Benzene				**Toluene**				***o*-Xylene**			
	Sample Day	Aqueous ($M_{\mathrm{Ben_{(aq)}}}$)	Gas ($M_{\mathrm{Ben_{(g)}}}$)	Solid ($M_{\mathrm{Ben_{(s)}}}$)	Total ($M_{\mathrm{Ben_T}}$)	Aqueous ($M_{\mathrm{Tol_{(aq)}}}$)	Gas ($M_{\mathrm{Tol_{(g)}}}$)	Solid ($M_{\mathrm{Tol_{(s)}}}$)	Total ($M_{\mathrm{Tol_T}}$)	Aqueous ($M_{\mathrm{Xyl_{(aq)}}}$)	Gas ($M_{\mathrm{Xyl_{(g)}}}$)	Solid ($M_{\mathrm{Xyl_{(s)}}}$)	Total ($M_{\mathrm{Xyl_T}}$)
BA-PC+EA-toluene	2					3.05	0.17	0.011	3.24				
	7					3.29	0.19	0.067	3.54				
	31					2.63	0.15						
	64					0.0083	0.00055	0.0036	0.012				
	93					0.0085	0.00049						
	121					1.56	0.11	0.17	1.84				
	162					0.0086	0.00047						
	182							0.0016	0.0016				
	212					2.84	0.17						
	245					0.0083	0.00055	0.0014	0.010				
	269					2.96	0.16	0.090	3.22				
	274					3.32	0.19	0.055	3.57				
	278					2.22	0.13	0.13	2.48				
	283					2.39	0.15	0.091	2.63				
	288					1.19	0.078	0.026	1.29				
	292					0.23	0.016		0.25				
BA+PAC+EA-toluene	2					3.13	0.31	0.014	3.46				
	7					1.17	0.066	1.28	2.52				
	31					1.00	0.057						
	64					0.0083	0.00055	0.056	0.065				
	93					0.0085	0.00049						
	121					0.75	0.052	2.81	3.61				
	162					0.0086	0.00047						
	182							0.065	0.065				
	212					0.015	0.00083						
	245					0.0083	0.00055	0.056	0.065				
	269					3.52	0.21	1.70	5.42				
	274					0.86	0.05	1.50	2.41				
	278					0.19	0.012	0.67	0.88				
	283					0.085	0.0055	0.049	0.14				
	288					0.018	0.0012	0.067	0.087				
	292					0.0082	0.00056	0.0014	0.010				

		Mass (mg)											
		Benzene				**Toluene**				***o*-Xylene**			
	Sample Day	Aqueous ($M_{\mathrm{Ben}_{(aq)}}$)	Gas ($M_{\mathrm{Ben}_{(g)}}$)	Solid ($M_{\mathrm{Ben}_{(s)}}$)	Total ($M_{\mathrm{Ben}_{T}}$)	Aqueous ($M_{\mathrm{Tol}_{(aq)}}$)	Gas ($M_{\mathrm{Tol}_{(g)}}$)	Solid ($M_{\mathrm{Tol}_{(s)}}$)	Total ($M_{\mathrm{Tol}_{T}}$)	Aqueous ($M_{\mathrm{Xyl}_{(aq)}}$)	Gas ($M_{\mathrm{Xyl}_{(g)}}$)	Solid ($M_{\mathrm{Xyl}_{(s)}}$)	Total ($M_{\mathrm{Xyl}_{T}}$)
KC-BTX	2	3.10	0.15			3.03	0.18			2.64	0.13		
	8	3.13	0.19			3.02	0.22			2.61	0.16		
	38	3.01	0.20			2.93	0.24			2.56	0.17		
	66												
	99	2.65	0.22			2.51	0.25			2.18	0.18		
	128			0.073				0.094				0.12	
	157	3.05	0.15			2.99	0.18			2.55	0.12		
	190	3.01	0.16			2.84	0.19			2.44	0.13		
	217	2.83	0.17			2.83	0.21			2.46	0.15		
	238	2.77	0.19			2.69	0.22			2.32	0.16		
	273	2.78	0.21			2.66	0.25			2.44	0.19		
	309	2.55	0.21			2.42	0.25			2.13	0.18		
	338	2.31	0.21			2.29	0.25			2.08	0.19		
	372	2.20	0.22	0.047	2.47	2.10	0.21	0.027	2.34	1.96	0.20	0.11	2.26
KC+PAC-BTX	2	3.23	0.27			3.16	0.32			2.75	0.23		
	8	3.10	0.19			2.58	0.19			1.43	0.087		
	38	2.78	0.19			2.16	0.18			0.92	0.062		
	66	2.77	0.21			2.11	0.19			0.92	0.069		
	99	2.47	0.21			1.88	0.19			0.75	0.062		
	128	2.35	0.21	0.18	2.74	1.74	0.19	0.77	2.71	0.70	0.064	1.58	2.35
	157	2.64	0.13			1.91	0.11			0.70	0.033		
	190	2.77	0.15			2.03	0.13			0.77	0.042		
	217	2.71	0.16			1.96	0.14			0.70	0.042		
	238	2.77	0.19			2.06	0.17			0.82	0.056		
	273	2.54	0.19			1.85	0.17			0.74	0.056		
	309	2.24	0.18			1.63	0.16			0.61	0.050		
	338	1.94	0.18			1.45	0.16			0.54	0.049		
	372	2.00	0.20	0.20	2.40	1.47	0.18	0.86	2.50	0.56	0.056	2.48	3.10

		Mass (mg)											
		Benzene				**Toluene**				***o*-Xylene**			
	Sample Day	Aqueous ($M_{\mathrm{Ben}_{(aq)}}$)	Gas ($M_{\mathrm{Ben}_{(g)}}$)	Solid ($M_{\mathrm{Ben}_{(s)}}$)	Total ($M_{\mathrm{Ben}_{T}}$)	Aqueous ($M_{\mathrm{Tol}_{(aq)}}$)	Gas ($M_{\mathrm{Tol}_{(g)}}$)	Solid ($M_{\mathrm{Tol}_{(s)}}$)	Total ($M_{\mathrm{Tol}_{T}}$)	Aqueous ($M_{\mathrm{Xyl}_{(aq)}}$)	Gas ($M_{\mathrm{Xyl}_{(g)}}$)	Solid ($M_{\mathrm{Xyl}_{(s)}}$)	Total ($M_{\mathrm{Xyl}_{T}}$)
BA-PC-BTX	2	3.55	0.17	0.16	3.89	3.49	0.21	0.17	3.86	3.01	0.14	0.15	3.31
	8	3.53	0.17	0.096	3.79	3.47	0.20	0.10	3.77	3.02	0.14	0.090	3.25
	38												
	66	3.47	0.19	0.011	3.67	3.16	0.21	0.023	3.39	2.87	0.15	0.047	3.07
	99	3.31	0.16			3.01	0.18			2.66	0.13		
	128			0.039				0.11				0.15	
	157	3.42	0.16			3.10	0.18			2.79	0.13		
	190					3.03	0.20			2.77	0.15		
	217	3.30	0.16			2.89	0.17			2.67	0.13		
	238	3.14	0.17	0.030	3.35	2.78	0.19	0.048	3.01	2.55	0.14	0.087	2.77
	273	3.20	0.15			2.91	0.17			2.58	0.12		
	309	2.72	0.15	0.024	2.89	2.25	0.15	0.094	2.49	2.10	0.11	0.16	2.37
	338	2.78	0.13			2.43	0.14			2.38	0.11		
	372	2.85	0.16	0.029	3.04	2.39	0.16	0.010	2.55	2.47	0.13	0.11	2.71
BA+PAC-BTX	2	3.34	0.28	0.21	3.83	3.27	0.33	0.22	3.83	2.84	0.23	0.20	3.27
	8	3.33	0.16	0.27	3.75	2.60	0.15	0.66	3.41	1.27	0.060	0.82	2.15
	38	3.59	0.17			2.81	0.17			1.35	0.064		
	66	3.55	0.19	0.14	3.88	2.68	0.18	0.71	3.56	1.13	0.061	1.25	2.44
	99	2.82	0.13			1.95	0.11			0.71	0.033		
	128	2.36	0.13	0.25	2.74	1.62	0.11	0.97	2.69	0.57	0.032	1.70	2.30
	157	2.45	0.12			1.72	0.10			0.59	0.028		
	190	2.27	0.13	0.18	2.58	1.52	0.10	0.78	2.41	0.57	0.031	1.59	2.19
	217	2.63	0.13			1.72	0.10			0.62	0.029		
	238			0.24				1.06				1.93	
	273	2.27	0.11			1.68	0.099			0.58	0.027		
	309	2.35	0.13	0.32	2.80	1.57	0.10	1.15	2.83	0.59	0.032	2.24	2.87
	338	2.74	0.13			1.87	0.11			0.67	0.031		
	372	2.71	0.15	0.20	3.06	1.76	0.12	0.76	2.63	0.64	0.034	2.06	2.74

		Mass (mg)											
		Benzene				**Toluene**				***o*-Xylene**			
	Sample Day	Aqueous ($M_{\mathrm{Ben_{(aq)}}}$)	Gas ($M_{\mathrm{Ben_{(g)}}}$)	Solid ($M_{\mathrm{Ben_{(s)}}}$)	Total ($M_{\mathrm{Ben_T}}$)	Aqueous ($M_{\mathrm{Tol_{(aq)}}}$)	Gas ($M_{\mathrm{Tol_{(g)}}}$)	Solid ($M_{\mathrm{Tol_{(s)}}}$)	Total ($M_{\mathrm{Tol_T}}$)	Aqueous ($M_{\mathrm{Xyl_{(aq)}}}$)	Gas ($M_{\mathrm{Xyl_{(g)}}}$)	Solid ($M_{\mathrm{Xyl_{(s)}}}$)	Total ($M_{\mathrm{Xyl_T}}$)
BA-PC+EA-BTX	2	3.24	0.15	0.17	3.56	3.20	0.19	0.18	3.56	2.77	0.13	0.16	3.06
	8	3.34	0.16	0.11	3.61	3.26	0.19	0.093	3.54	2.81	0.13	0.095	3.04
	38	3.30	0.15			2.91	0.16			2.72	0.12		
	66	3.38	0.18	0.013	3.57	0.0083	0.00054	0.0013	0.010	0.072	0.0038	0.0018	0.078
	99	3.35	0.16			0.0085	0.00049			0.0078	0.00036		
	128	2.96	0.16	0.048	3.17	0.0083	0.00055	0.0013	0.010	0.0076	0.00041	0.0034	0.011
	157	2.92	0.14			0.0085	0.00048			0.0079	0.00036		
	190	3.07	0.16	0.0052	3.24	0.0083	0.00054	0.0013	0.010	0.0077	0.00040	0.0013	0.0094
	217	3.04	0.14			0.029	0.0016			2.75	0.12		
	238	3.17	0.17	0.066	3.41	0.0083	0.00053	0.0014	0.010	2.59	0.13	0.10	2.82
	273	3.30	0.15			0.0086	0.00047		64.2	0.78	0.035		
	310	2.91	0.16	0.076	3.15	3.16	0.21	0.081	3.45	3.17	0.17	0.099	3.44
	315	2.71	0.16	0.12	2.98	2.38	0.17	0.11	2.65	2.77	0.16	0.19	3.11
	319	2.57	0.16	0.15	2.88	1.23	0.091	0.067	1.39	2.76	0.17	0.19	3.12
	324	2.69	0.14	0.10	2.94	1.24	0.079	0.029	1.35	2.57	0.13	0.16	2.87
	333	2.46	0.13	0.14	2.72	0.12	0.0076	0.0041	0.13	2.38	0.12	0.19	2.70
	350	2.92	0.16		3.08	0.054	0.0036		0.057	2.94	0.16		3.09
BA+PAC+EA-BTX	2	3.28	0.27	0.19	3.74	3.22	0.33	0.20	3.74	2.79	0.23	0.18	3.20
	8	3.36	0.16	0.28	3.81	2.64	0.15	0.75	3.54	1.35	0.063	0.94	2.34
	38	3.27	0.15			2.31	0.13			1.18	0.054		
	66	2.65	0.14	0.99	3.79	0.0083	0.00054	0.021	0.030	0.058	0.0031	0.86	0.92
	99	2.05	0.096			0.0085	0.00048			0.0079	0.00036		
	128	1.76	0.091	1.25	3.10	0.0084	0.00053	0.0071	0.016	0.0077	0.00039	0.029	0.037
	157	1.77	0.081			0.0085	0.00048			0.0079	0.00035		
	190	2.92	0.15	1.16	4.23	0.0083	0.00053	0.0040	0.013	0.0077	0.00039	0.023	0.031
	217	2.49	0.11			0.51	0.028			0.62	0.028		
	238	2.94	0.15	0.44	3.54	0.0084	0.00053	0.019	0.028	0.41	0.021	2.04	2.47
	273	2.71	0.13			0.0084	0.00050			0.35	0.017		
	310	2.33	0.14	0.23	2.70	2.38	0.17	0.73	3.28	2.03	0.12	2.36	4.50
	315	2.77	0.17	0.25	3.20	1.91	0.15	0.67	2.72	1.53	0.094	2.26	3.89
	319	2.56	0.17	0.21	2.94	0.79	0.062	0.49	1.35	1.47	0.093	2.42	3.98
	324	2.37	0.12	0.31	2.80	0.17	0.010	0.40	0.58	0.95	0.048	2.85	3.85
	333	2.46	0.13	0.29	2.88	0.0083	0.00053	0.013	0.022	0.70	0.036	2.73	3.47
	350	2.38	0.13	0.18	2.69	0.022	0.0015	0.017	0.040	1.16	0.062		1.22

Table B.9: Relative abundance of bacteria and archaea (≥ 4% for any amplicon sequencing variant [ASV] detected) generated from 16S ribosomal ribonucleic acid (rRNA) next generation sequencing (NGS) for the single-solute (toluene-only) and multi-solute (benzene, toluene and *o*-xylene [BTX]) SC, BA-PC, BA+PAC, BA-PC+EA and BA+PAC+EA microcosms (data shown for bottle replicates A, B and/or C) after 1 year relative to background conditions.

Taxonomic designation						Relative abundance (%)											
						Background	SC			BA-PC			BA+PAC			BA-PC+EA	BA+PAC+EA
Domain	Phylum	Class	Order	Family	Genus		A	B	C	A	B	C	A	B	C	C	C
Single-solute (toluene-only)																	
Bacteria	Actinobacteriota	Coriobacteriia				9.45	11.15	5.63	8.94	12.32	11.23	12.42	9.52	8.91	8.89	7.53	4.18
Bacteria	Campilobacterota	Campylobacteria	Campylobacterales	Sulfurimonadaceae	*Sulfuricurvum*	0.00	1.93	34.74	3.46	0.00	0.00	0.00	0.30	0.00	0.00	0.00	0.00
Bacteria	Deferrisomatota	Defferrisomatia	Defferrisomatales	Defferrisomataceae	*Deferrisoma*	0.00	0.72	0.77	0.81	3.62	5.46	2.15	3.05	3.00	4.05	0.00	0.00
Bacteria	Desulfobacterota	Desulfobulbia	Desulfobulbales	Desulfocapsaceae	*Desulfoprunum*	0.03	0.04	0.00	0.00	0.41	0.23	0.14	0.00	0.00	0.07	26.13	34.51
Bacteria	Desulfobacterota	Desulfobacteria	Desulfobacterales	Desulfosarcinaceae	*Desulfatirhabdium*	0.05	0.00	0.12	0.00	0.00	0.00	0.00	0.00	0.05	0.05	4.67	1.24
Bacteria	Desulfobacterota	Desulfobulbia	Desulfobulbales	Desulfocapsaceae		0.00	1.37	1.45	1.39	1.62	1.57	0.30	0.62	2.25	2.70	1.45	5.24
Bacteria	Desulfobacterota	Desulfobacteria	Desulfobacterales	Desulfobacteraceae		0.00	0.00	0.00	0.00	0.00	0.00	0.00	0.00	0.00	0.00	16.03	8.69
Bacteria	Desulfobacterota	Desulfobacteria	Desulfobacterales	Desulfosarcinaceae		0.00	0.00	0.00	0.00	0.00	0.00	0.00	0.00	0.00	0.00	0.00	4.14
Bacteria	Edwardsbacteria	Edwardsbacteria	Edwardsbacteria	Edwardsbacteria	*Edwardsbacteria*	0.00	1.97	1.96	4.34	2.63	3.74	2.97	1.98	1.45	1.19	0.65	0.59
Archaea	Euryarchaeota	Methanobacteria	Methanobacteriales	Methanobacteriaceae	*Methanobacterium*	0.00	4.08	2.51	1.02	2.00	0.90	1.10	2.30	0.79	1.42	0.00	0.18
Bacteria	Firmicutes	Clostridia	Peptococcales	Peptococcaceae		0.00	6.39	0.10	13.22	0.56	0.11	0.30	6.80	7.51	5.49	0.02	1.12
Archaea	Halobacterota	Methanosarcinia	Methanosarciniales	Methanosarcinaceae	*Methanomethylovorans*	0.00	7.12	4.11	2.89	3.80	2.59	2.36	4.54	5.23	6.72	1.51	3.74
Archaea	Halobacterota	Methanosarcinia	Methanosarciniales	Methanosaetaceae	*Methanosaeta*	0.00	0.00	0.00	0.00	0.15	0.73	1.01	4.99	2.65	3.76	0.00	0.00
Bacteria	Proteobacteria	Gammaproteobacteria	Xanthomonadales	Xanthomonadaceae	*Lysobacter*	3.55	0.46	0.54	1.02	5.37	5.66	5.09	2.52	3.50	1.91	0.63	0.72
Bacteria	Proteobacteria	Gammaproteobacteria	Burkholderiales	Comamonadaceae	*Hydrogenophaga*	1.78	0.22	0.08	0.27	1.05	1.23	2.22	0.46	0.91	6.11	0.30	0.13
Multi-solute (benzene, toluene and *o*-xylene [BTX])																	
Bacteria	Actinobacteriota	Coriobacteriia				5.65	7.49	5.34	4.33	6.05	6.06	5.57	4.35	4.25	3.22	3.11	3.82
Bacteria	Chloroflexi	Anaerolineae	Anaerolineales	Anaerolineaceae		0.87	0.99	1.78	0.80	7.64	0.93	1.76	0.91	0.96	0.92	1.86	0.73
Bacteria	Deferrisomatota	Defferrisomatia	Defferrisomatales	Defferrisomataceae	*Deferrisoma*	0.34	8.98	6.71	7.94	7.65	10.24	13.14	5.47	2.7	0.22	0.18	0.22
Bacteria	Desulfobacterota	Desulfobulbia	Desulfobulbales	Desulfocapsaceae	*Desulfoprunum*	0.00	0.00	0.11	0.35	0.00	0.13	0.00	0.30	0.00	0.00	22.09	18.76
Bacteria	Desulfobacterota	Desulfuromonadia	Geobacterales	Geobacteraceae		0.00	11.45	9.08	7.45	1.91	2.29	1.15	6.55	3.89	1.78	0.36	2.35
Bacteria	Desulfobacterota	Desulfobacteria	Desulfobacterales	Desulfosarcinaceae	*Desulfatirhabdium*	0.00	0.00	0.00	0.17	0.00	0.00	0.00	0.00	0.00	0.00	6.45	5.41
Bacteria	Desulfobacterota	Desulfuromonadia	Geobacterales	Geobacteraceae	*Geobacter*	0.11	0.00	0.00	0.00	5.25	0.10	0.40	0.00	0.00	0.00	0.00	0.00
Bacteria	Desulfobacterota	Desulfuromonadia	Geobacterales	Geobacteraceae		0.00	0.92	0.41	1.39	2.55	1.23	1.03	3.05	1.26	6.94	0.00	0.19
Bacteria	Edwardsbacteria	Edwardsbacteria	Edwardsbacteria	Edwardsbacteria	*Edwardsbacteria*	0.00	1.55	1.10	0.16	3.18	4.05	1.86	2.34	1.46	1.43	0.98	0.86
Archaea	Euryarchaeota	Methanobacteria	Methanobacteriales	Methanobacteriaceae	*Methanobacterium*	0.00	5.16	8.51	4.13	1.27	0.42	0.5	0.69	2.10	10.03	0.09	2.35
Bacteria	Firmicutes	Desulfitobacteriia	Desulfitobacteriales	Desulfitobacteriaceae	*Desulfosporosinus*	0.06	0.00	0.00	0.00	0.00	0.21	0.00	0.00	0.00	0.00	12.72	6.68
Archaea	Halobacterota	Methanosarcinia	Methanosarciniales	Methanosarcinaceae	*Methanomethylovorans*	0.00	0.63	0.51	14.60	0.00	0.61	0.20	4.45	4.60	6.40	0.33	3.42
Archaea	Halobacterota	Methanosarcinia	Methanosarciniales	Methanosaetaceae	*Methanosaeta*	0.00	2.56	2.36	2.40	0.00	0.80	0.08	5.39	6.25	11.69	0.03	0.03
Bacteria	Proteobacteria	Gammaproteobacteria	Burkholderiales	Comamonadaceae		7.53	0.93	0.65	0.30	5.73	1.30	0.58	0.38	1.16	0.54	0.24	0.13
Bacteria	Proteobacteria	Gammaproteobacteria	Pseudomonadales	Moraxellaceae	*Acinetobacter*	0.28	0.23	0.92	0.00	0.00	0.91	1.21	6.92	9.18	8.15	0.00	0.01

Table B.10: Zero-order biodegradation rate constants for toluene in the single-solute (toluene-only) and multi-solute (benzene, toluene and *o*-xylene [BTX]) BA-PC+EA and BA+PAC+EA microcosms during high-resolution monitoring.

Rate constant (mg/day) ± Confidence interval		
Single-solute (toluene)	BA-PC+EA	0.10 ± 0.14
	BA+PAC+EA	0.51 ± 0.79
Multi-solute (BTX)	BA-PC+EA	0.14 ± 0.11
	BA+PAC+EA	0.14 ± 0.11

Table B.11: Theoretical and measured mole ratios between toluene and sulfate, and sulfate and sulfide during high-resolution monitoring.

		C_7H_8:SO_4^{2-}		SO_4^{2-}:H_2S and HS^-	
		Theoretical	Measured	Theoretical	Measured
Single-solute (toluene)	BA-PC+EA	4.5	4.47	1	0.88
	BA+PAC+EA	4.5	4.14	1	1.08
Multi-solute (toluene)	BA-PC+EA	4.5	4.74	1	1.08
	BA+PAC+EA	4.5	4.58	1	1.5

Appendix C: Supplementary material for Chapter 4

Appendix C.1: Ideal breakthrough time estimation

To estimate the ideal breakthrough time for solute *i*, t_{b_i} (days), (i.e., 50% PAC saturation) for columns with PAC zones, Equation C.1 [250, 251] was used as defined below

$$t_{b_i} = \frac{q_{e_i} \times f_{PAC} \times \rho_{BS} \times V_{PAC_Z}}{C_{o_i} \times Q} \quad \text{(Equation C.1)}$$

where

q_{e_i} = equilibrium solid phase sorption capacity of the PAC for solute *i* (mg/g)

f_{PAC} = fraction of PAC (-)

ρ_{BS} = bulk density of Borden sand (g/cm^3)

V_{PAC_Z} = volume of the PAC zone (cm^3)

C_{o_i} = initial aqueous phase concentration of a solute *i* (mg/L)

Q = flow rate (L/day)

The q_{e_i} was estimated using the single-solute Freundlich model parameters or multi-solute improved simplified ideal adsorption solution (ISIAS) competition factors listed in Table 2.2, the f_{PAC} is listed in Table C.1 for each column, the V_{PAC_Z} and Q are listed in Table C.2 for each column, and the ρ_{BS} is listed in Table B.1 [135].

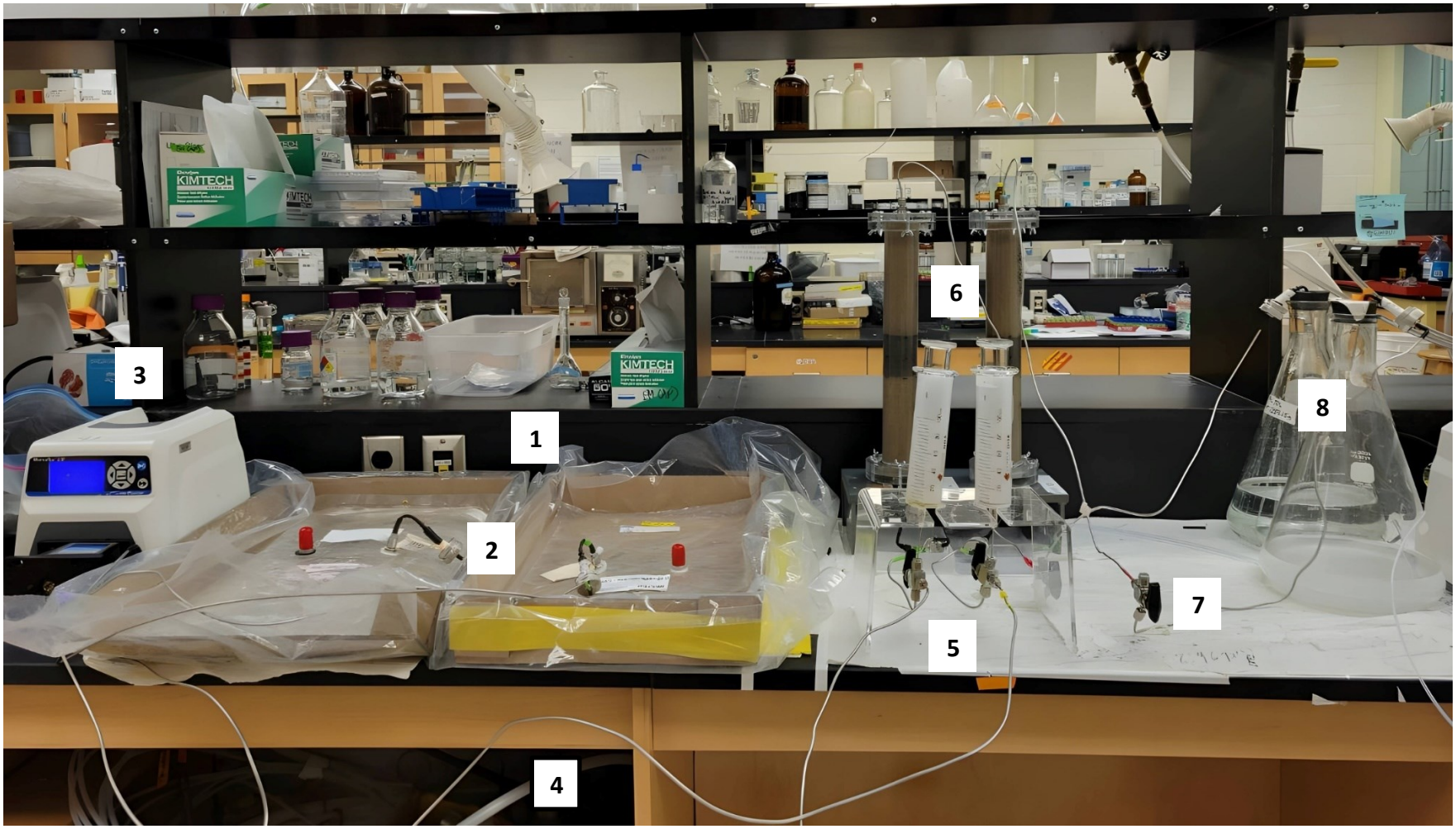

Figure C.1: Image of the column benchtop experimental set-up, including: (1) 10 L Tedlar bags with anaerobic artificial groundwater (AGW); (2) 25 mm stainless steel (SS) filter folder; (3) peristaltic pump; (4) 1.6 mm SS tubing; (5) 100 mL glass sampling syringes attached to 2-way nylon stopcocks and 17-gauge stainless steel needles inserted into the influent sampling ports of 3-way SS ball valves, and positioned vertically on a plexiglass stand (temporary set-up for influent sample collection; syringe removal and ball valve readjustment redirects AGW flow into the column); (6) packed columns (37 cm length, 3.75 cm inner diameter) with Borden sand (BS) and a homogenized PAC zone (0.5% w/w); (7) 3-way SS ball valve for effluent sample collection (requiring the same temporary set-up as shown for influent sample collection, described in [5]); and (8) 1 L Erlenmeyer flask for effluent waste collection.

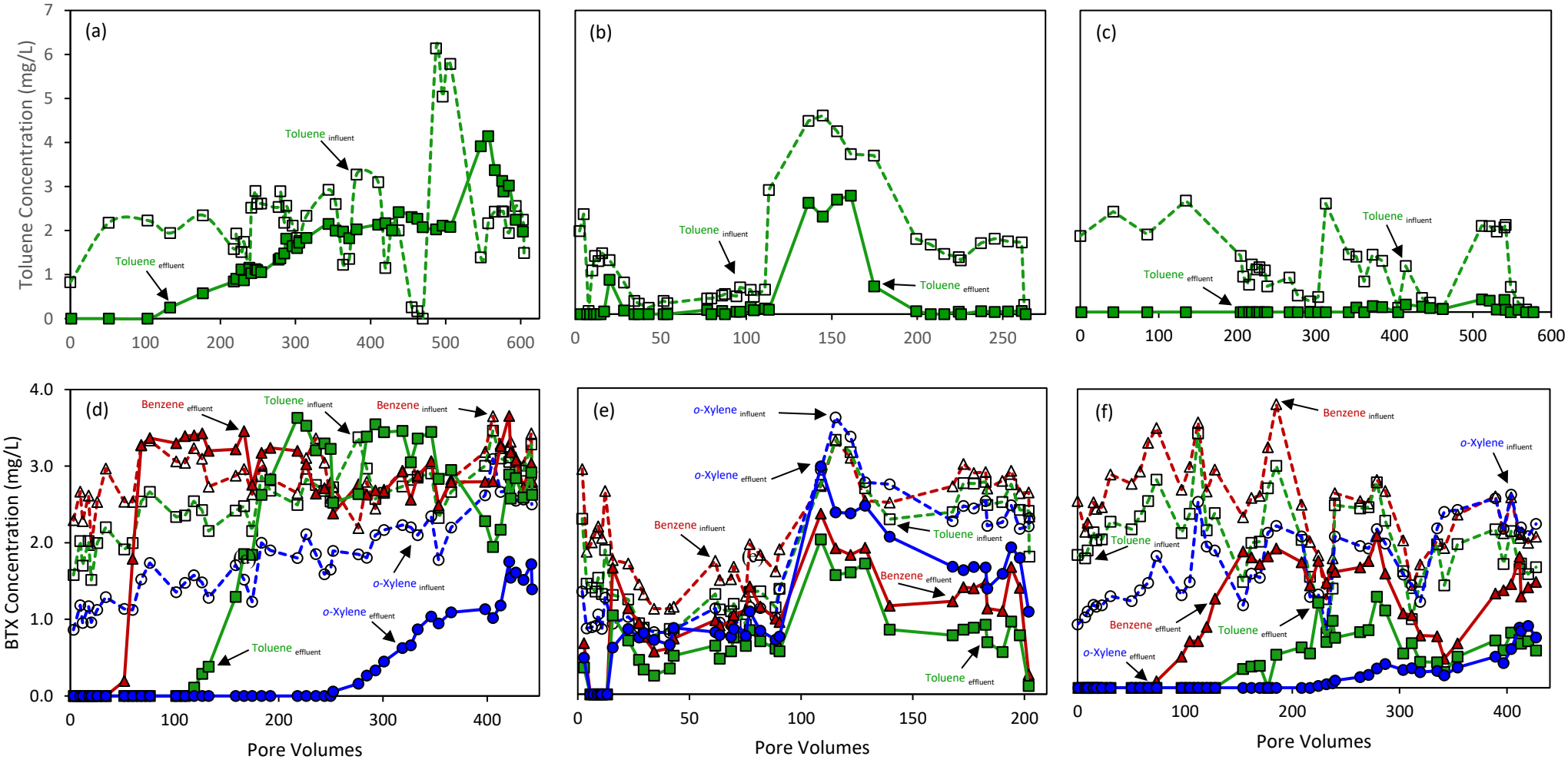

Figure C.2: Year-1 influent (dashed lines with open symbols) and effluent (solid lines with closed symbols) aqueous concentrations of toluene-only (single-solute) (top panel) and benzene, toluene and *o*-xylene (BTX) (multi-solute) (bottom panel) aqueous concentrations from the (a, d) KC+PACz, (b, e) PC-BA and (c, f) PAC+BA columns.

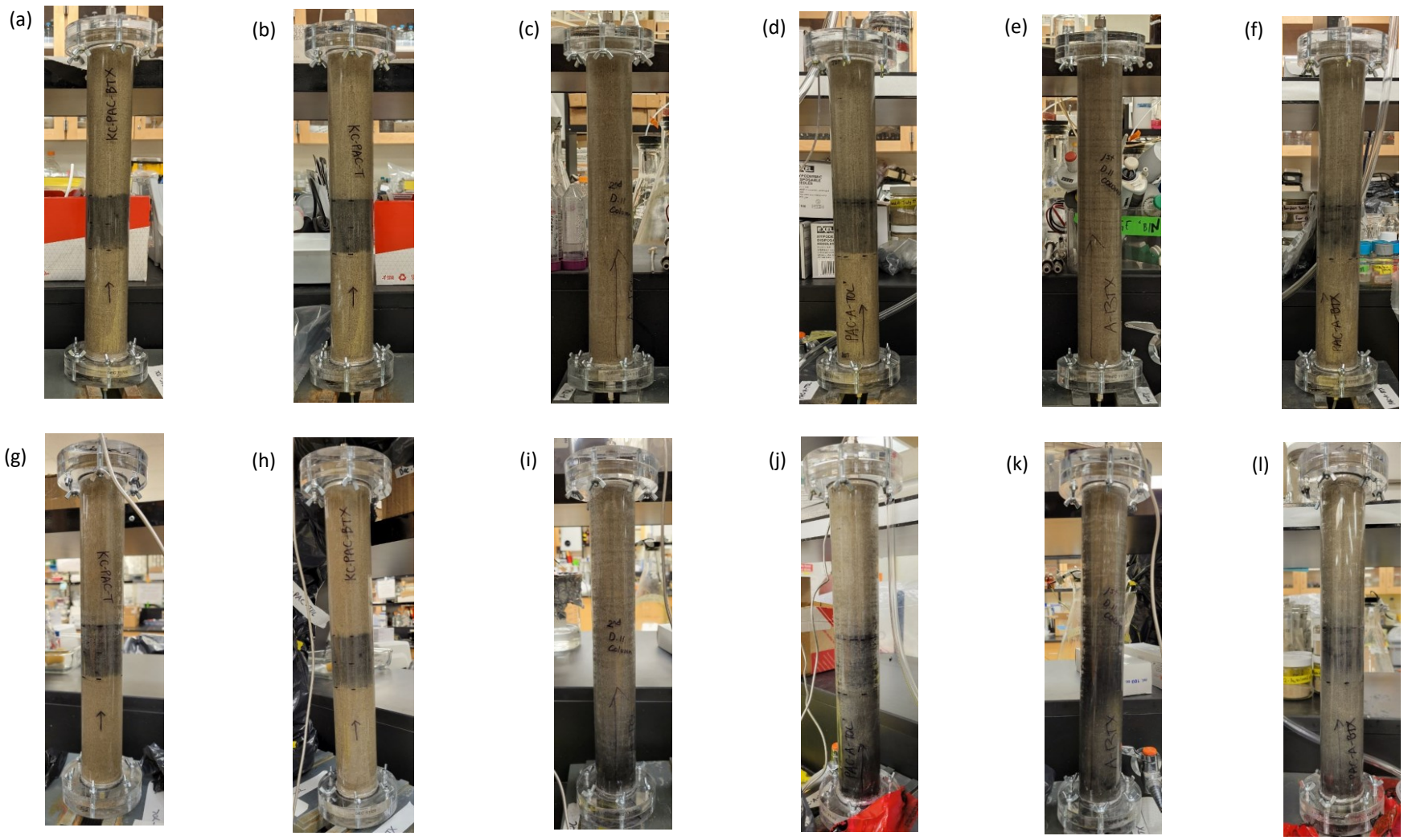

Figure C.3: Column conditions prior to operation (top panel) and after 1.6 years of operation (bottom panel) for the (a, g) KC+PACz-toluene; (b, h) KC+PACz-benzene, toluene and *o*-xylene (BTX); (c, i) BA-PC-toluene; (d, j) BA+PACz-toluene; (e, k) BA-PC-BTX; and (f, l) BA+PACz-BTX columns.

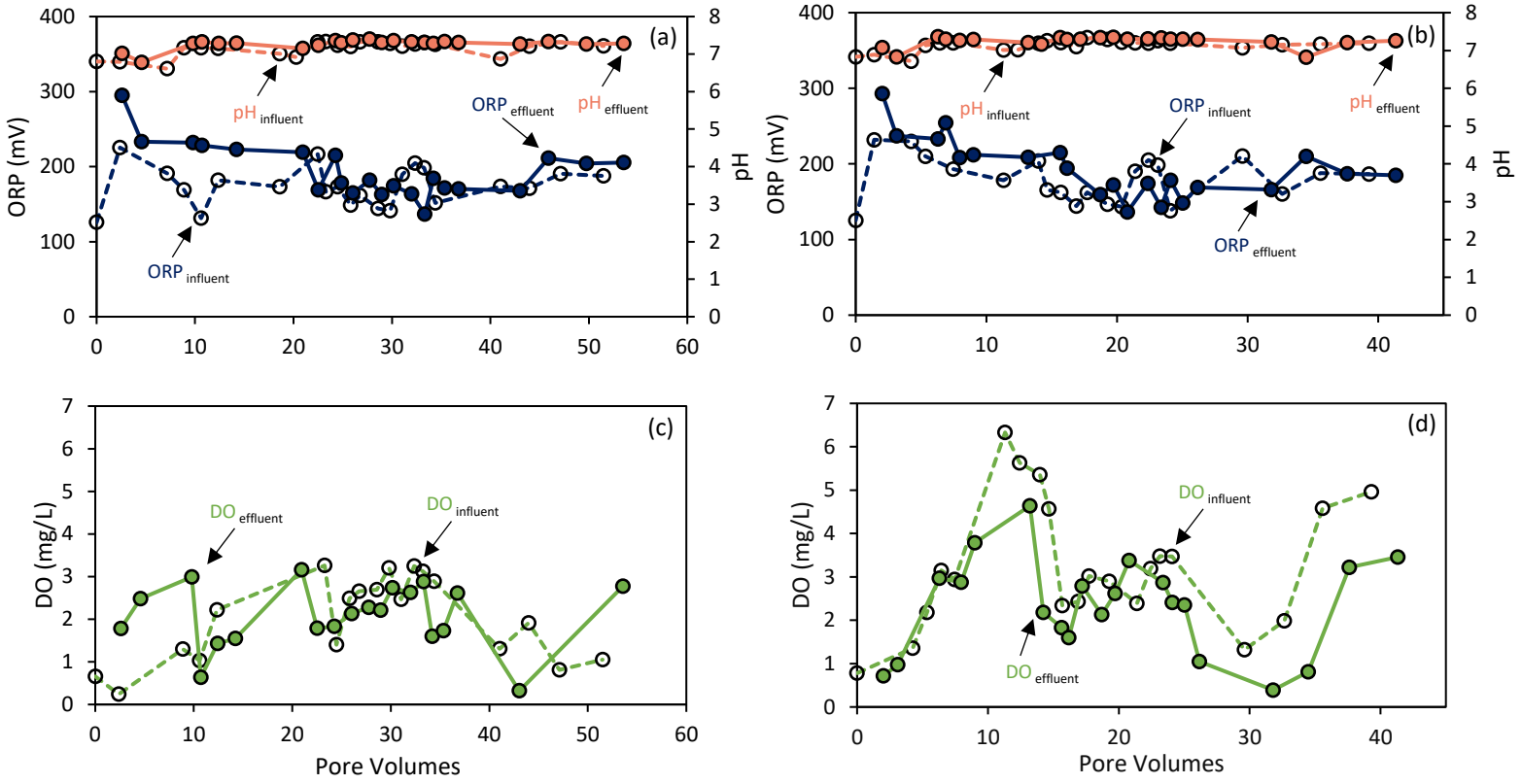

Figure C.4: Influent (dashed lines with open symbols) and effluent (solid lines with closed symbols) data from the toluene-only (left panel) and benzene, toluene and *o*-xylene (BTX) (right panel) KC+PACz columns, including (a, b) the oxidation reduction potential (ORP) (dark blue filled circles) and pH (pink filled circles), and (c, d) dissolved oxygen (DO) (light green filled circles).

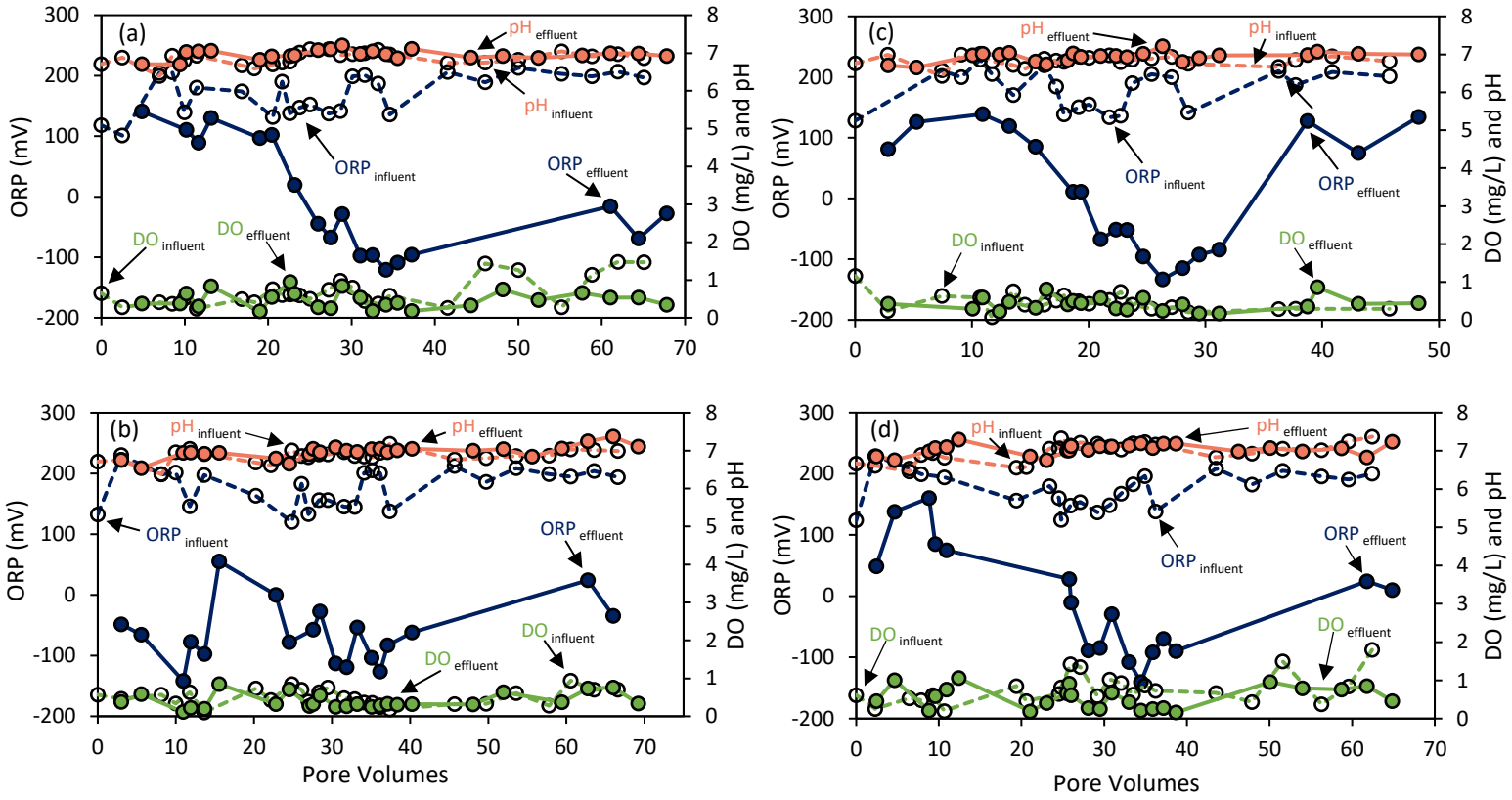

Figure C.5: Influent (dashed lines with open symbols) and effluent (solid lines with closed symbols) data for the toluene-only (left panel) and benzene, toluene and *o*-xylene (BTX) (right panel) (a, c) BA-PC and (b, d) BA+PACz columns, showing dissolved oxygen (DO), pH and the oxidation reduction potential (ORP).

Table C.1: Details of single-solute (toluene-only) and multi-solute (benzene, toluene and *o*-xylene) column experiments.

Column type	Acronym	Dry (wet) mass of BS (g)	Fraction of PAC (% PAC) [1]	Sulfate concentration (mg/L) [2]	Biocide [3]	Toluene-only concentration (mg/L) [4]	BTX concentration (mg/L) [4]
Single-solute (toluene-only)							
Killed control + powdered activated carbon zone	KC+PACz	732 (872)	0.005 (0.5)	5 → ↑ 20	✓	5 → ↑ 10 → ↑ 20	-
Bioactive-positive control	BA-PC	718 (854)	-	5 → ↑ 20 → ↑ 30	-	5 → ↑ 20	-
Bioactive + powdered activated carbon zone	BA+PACz	704 (837)	0.005 (0.5)	5 → ↑ 20 → ↑ 30	-	5 → ↑ 10 → ↑ 20	-
Multi-solute (benzene, toluene and *o*-xylene [BTX])							
Killed control + powdered activated carbon zone	KC+PACz	717 (854)	0.005 (0.5)	5 → ↑ 20 → ↑ 30	✓	-	1:1:1
Bioactive-positive control	BA-PC	754 (896)	-	5 → ↑ 20 → ↑ 30	-	-	1:1:1
Bioactive + powdered activated carbon zone	BA+PACz	768 (914)	0.005 (0.5)	5 → ↑ 20 → ↑ 30	-	-	1:1:1

Notes:

1. Mass of powdered activated carbon (PAC) divided by the total mass of solids (Borden sand [BS] and PAC).
2. The sulfate concentration was increased in a stepwise manner between columns from a target concentration of 5 mg/L over pore volume (PV) 0 to 4.7 ± 0.9 to 20 mg/L over PV 9.2 ± 1.6 to 11.7 ± 5.3 to 30 mg/L over PV 27.9 ± 4.8 to 58.8 ± 10.
3. Sodium azide was used as the biocide (0.5 mL/ 200 mL AGW).
4. The toluene and benzene, toluene and *o*-xylene (BTX) (1:1:1) concentrations were increased in a stepwise manner between the single-solute (toluene-only) and multi-solute (BTX) columns, respectively, from a target concentration of 5 mg/L per solute over PV 0 to 20.2 ± 4.1 to 10 mg/L per solute over PV 22.2 ± 4.4 to 26.6 ± 4.6 to 20 mg/L per solute over PV 27.9 ± 4.8 to 58.8 ± 10.

Table C.2: Specifications and flow conditions for the single-solute (toluene-only) and multi-solute (benzene, toluene and *o*-xylene [BTX]) columns.

	Single-solute (toluene-only)			Multi-solute (benzene, toluene and *o*-xylene [BTX])		
Parameter	**KC+PACz**	**BA-PC**	**BA+PACz**	**KC+PACz**	**BA-PC**	**BA+PACz**
Packed length (cm)	37.1	36.9	36.3	37.1	36.9	36.8
Inner diameter (cm)	3.75	3.75	3.75	3.75	3.75	3.75
Area (cm^2)	11	11	11	11	11	11
Volume (mL)	410	407	401	410	407	406
Dry soil mass (g)	732	718	704	717	754	768
Pore volume (mL)	118	109	104	139	127	122
Porosity [1]	0.288	0.268	0.26	0.339	0.311	0.299
Dispersivity (m) [1]	0.0034	0.0020	0.0020	0.0023	0.0055	0.0094
Measured flow rate (mL/min)	0.02 ± 0.0045	0.019 ± 0.003	0.018 ± 0.006	0.017 ± 0.0029	0.019 ± 0.0069	0.025 ± 0.019
Specific discharge (cm/min)	0.00181	0.00181	0.00181	0.00181	0.00181	0.00181
Average linear velocity (cm/min)	0.00629	0.00676	0.00697	0.00534	0.00582	0.00608
Residence time (days)	4.1	3.79	3.62	4.82	4.39	4.22
PAC zone length (cm)	6		6	6		6
PAC zone volume (mL)	66.3		66.3	66.3		66.3
PAC zone soil mass (g)	120		120	120		120
PAC zone residence time (days)	0.6		0.598	0.78		0.688

Notes: 1. Parameters generated from a bromide tracer test (Bill McClaren, MASc).

Table C.3: Relative abundance (generated using 16S ribosomal ribonucleic acid [rRNA] next generation sequencing [NGS]) of amplicon sequencing variants (ASVs) from the extraction black (Eblank) samples that were removed from the single-solute (toluene-only) and multi-solute (benzene, toluene and *o*-xylene [BTX]) BA-PC and BA+PACz column samples due to sample contamination.

Taxonomic designation						**Relative abundance (%)**				
Domain	Phylum	Class	Order	Family	Genus					
						BA-PC-toluene				
						4 cm	**10 cm**	**14 cm**	**24 cm**	**30 cm**
Bacteria	Proteobacteria	Gammaproteobacteria	Burkholderiales	Alcaligenaceae		36.08	66.01	84.67	89.62	92.24
Bacteria	Bacteroidota	Bacteroidia	Sphingobacteriales	Sphingobacteriaceae	Pedobacter	0.63	1.21	2.29	1.89	1.92
Bacteria	Actinobacteriota	Actinobacteria	Micrococcales	Microbacteriaceae	Leifsonia	0.60	0.72	1.52	1.23	1.63
Bacteria	Proteobacteria	Gammaproteobacteria	Burkholderiales	Comamonadaceae	Delftia	0.18	0.51	0.14	0.70	0.24
Bacteria	Proteobacteria	Gammaproteobacteria	Enterobacterales	Enterobacteriaceae	Escherichia-Shigella	0.08	0.00	0.16	0.22	0.00
Bacteria	Firmicutes	Clostridia	Eubacteriales	Eubacteriaceae	Pseudoramibacter	0.00	0.00	0.00	0.00	0.00
Bacteria	Proteobacteria	Gammaproteobacteria	Burkholderiales	Comamonadaceae	Delftia	0.15	0.00	0.09	0.32	0.00
Bacteria	Actinobacteriota	Actinobacteria	Propionibacteriales	Propionibacteriaceae	Cutibacterium	0.00	0.00	0.00	0.18	0.00
Bacteria	Proteobacteria	Alphaproteobacteria	Sphingomonadales	Sphingomonadaceae	Sphingomonas	0.00	0.00	0.07	0.04	0.15
Eukaryota	Phragmoplastophyta	Embryophyta	Magnoliophyta	Magnoliophyta	Magnoliophyta	0.00	0.00	0.00	0.00	0.00
Bacteria	Firmicutes	Desulfotomaculia	Desulfotomaculales			0.00	0.00	0.00	0.00	0.00
Bacteria	Proteobacteria	Gammaproteobacteria	Pseudomonadales	Moraxellaceae		0.00	0.00	0.00	0.00	0.00
Bacteria	Firmicutes	Bacilli	Bacillales	Bacillaceae	Bacillus	0.00	0.00	0.00	0.00	0.00
Bacteria	Proteobacteria	Gammaproteobacteria	Enterobacterales	Enterobacteriaceae		0.00	0.00	0.00	0.00	0.00
Bacteria	Proteobacteria	Gammaproteobacteria	Burkholderiales	Alcaligenaceae		0.00	0.00	0.00	0.00	0.00
Bacteria	Proteobacteria	Gammaproteobacteria	Burkholderiales	Alcaligenaceae		0.00	0.00	0.00	0.00	0.00
Bacteria	Proteobacteria	Gammaproteobacteria	Burkholderiales	Alcaligenaceae		0.00	0.00	0.00	0.00	0.00
Bacteria	Proteobacteria	Gammaproteobacteria	Burkholderiales	Alcaligenaceae		0.00	0.00	0.00	0.00	0.00
Bacteria	Proteobacteria	Gammaproteobacteria	Burkholderiales	Alcaligenaceae		0.00	0.00	0.00	0.00	0.00
Bacteria	Actinobacteriota	Actinobacteria	Propionibacteriales	Propionibacteriaceae	Cutibacterium	0.00	0.00	0.00	0.00	0.00
Bacteria	Proteobacteria	Gammaproteobacteria	Burkholderiales	Alcaligenaceae		0.00	0.00	0.00	0.00	0.00
Bacteria	Firmicutes	Bacilli	Staphylococcales	Staphylococcaceae	Staphylococcus	0.00	0.00	0.00	0.00	0.00
Bacteria	Actinobacteriota	Actinobacteria	Corynebacteriales	Corynebacteriaceae	Corynebacterium	0.00	0.00	0.00	0.00	0.00
Bacteria	Proteobacteria	Gammaproteobacteria	Burkholderiales	Alcaligenaceae		0.00	0.00	0.00	0.00	0.00
Bacteria	Proteobacteria	Gammaproteobacteria	Pseudomonadales	Moraxellaceae	Acinetobacter	0.00	0.00	0.00	0.00	0.00
Bacteria	Proteobacteria	Gammaproteobacteria	Burkholderiales	Alcaligenaceae		0.00	0.00	0.00	0.00	0.00
Bacteria	Firmicutes	Bacilli	Staphylococcales	Gemellaceae	Gemella	0.00	0.00	0.00	0.00	0.00
Bacteria	Proteobacteria	Gammaproteobacteria	Enterobacterales	Morganellaceae	Proteus	0.00	0.00	0.00	0.00	0.00
Bacteria	Proteobacteria	Gammaproteobacteria	Burkholderiales	Alcaligenaceae		0.00	0.00	0.00	0.00	0.00
Eukaryota	Vertebrata	Mammalia	Mammalia	Mammalia	Mammalia	0.00	0.00	0.00	0.00	0.00

						BA+PACz-toluene												
Domain	Phylum	Class	Order	Family	Genus	**2.5 cm**	**6 cm**	**9 cm**	**13.5 cm**	**14.5 cm**	**15.5 cm**	**16.5 cm**	**18.5 cm**	**20.5 cm**	**22 cm**	**25 cm**	**28 cm**	**34.5 cm**
Bacteria	Proteobacteria	Gammaproteobacteria	Burkholderiales	Alcaligenaceae		71.27	88.19	85.77	89.15	72.09	85.33	76.18	79.90	87.00	91.15	93.32	90.36	91.16
Bacteria	Bacteroidota	Bacteroidia	Sphingobacteriales	Sphingobacteriaceae	Pedobacter	0.22	1.56	0.30	0.27	0.33	1.23	0.20	0.36	0.17	0.46	0.25	0.16	0.11
Bacteria	Actinobacteriota	Actinobacteria	Micrococcales	Microbacteriaceae	Leifsonia	1.02	1.31	0.90	1.13	0.78	1.29	0.88	1.07	1.39	1.28	0.71	1.31	1.19
Bacteria	Proteobacteria	Gammaproteobacteria	Burkholderiales	Comamonadaceae	Delftia	0.33	0.79	0.46	0.75	0.52	0.73	0.24	1.40	0.26	0.20	0.54	1.44	0.99
Bacteria	Proteobacteria	Gammaproteobacteria	Enterobacterales	Enterobacteriaceae	Escherichia-Shigella	0.00	0.02	0.00	0.04	0.00	0.01	0.05	0.21	0.00	0.01	0.07	0.03	0.00
Bacteria	Firmicutes	Clostridia	Eubacteriales	Eubacteriaceae	Pseudoramibacter	0.06	0.00	0.00	0.00	0.00	0.00	0.03	0.09	0.00	0.00	0.00	0.00	0.00
Bacteria	Proteobacteria	Gammaproteobacteria	Burkholderiales	Comamonadaceae	Delftia	0.09	0.14	0.00	0.00	0.00	0.18	0.00	0.00	0.25	0.00	0.00	0.00	0.17
Bacteria	Actinobacteriota	Actinobacteria	Propionibacteriales	Propionibacteriaceae	Cutibacterium	0.00	0.00	0.00	0.05	0.00	0.00	0.00	0.00	0.00	0.00	0.00	0.03	0.00
Bacteria	Proteobacteria	Alphaproteobacteria	Sphingomonadales	Sphingomonadaceae	Sphingomonas	0.00	0.00	0.00	0.00	0.00	0.05	0.00	0.04	0.00	0.00	0.00	0.01	0.00
Eukaryota	Phragmoplastophyta	Embryophyta	Magnoliophyta	Magnoliophyta	Magnoliophyta	0.00	0.00	0.00	0.00	0.00	0.00	0.00	0.00	0.00	0.00	0.00	0.00	0.00
Bacteria	Firmicutes	Desulfotomaculia	Desulfotomaculales			0.00	0.00	0.00	0.00	0.00	0.00	0.00	0.00	0.00	0.00	0.00	0.00	0.00
Bacteria	Proteobacteria	Gammaproteobacteria	Pseudomonadales	Moraxellaceae		0.00	0.02	0.00	0.00	0.00	0.00	0.00	0.00	0.00	0.00	0.00	0.00	0.00
Bacteria	Firmicutes	Bacilli	Bacillales	Bacillaceae	Bacillus	0.00	0.00	0.00	0.00	0.00	0.00	0.00	0.01	0.00	0.00	0.00	0.00	0.00
Bacteria	Proteobacteria	Gammaproteobacteria	Enterobacterales	Enterobacteriaceae		0.00	0.00	0.00	0.00	0.00	0.00	0.00	0.00	0.00	0.00	0.03	0.02	0.00
Bacteria	Proteobacteria	Gammaproteobacteria	Burkholderiales	Alcaligenaceae		0.00	0.00	0.00	0.00	0.00	0.00	0.00	0.00	0.00	0.00	0.00	0.00	0.00
Bacteria	Proteobacteria	Gammaproteobacteria	Burkholderiales	Alcaligenaceae		0.00	0.00	0.00	0.00	0.00	0.00	0.00	0.00	0.00	0.00	0.00	0.00	0.00
Bacteria	Proteobacteria	Gammaproteobacteria	Burkholderiales	Alcaligenaceae		0.00	0.00	0.00	0.00	0.00	0.00	0.00	0.00	0.00	0.00	0.00	0.00	0.00
Bacteria	Proteobacteria	Gammaproteobacteria	Burkholderiales	Alcaligenaceae		0.00	0.00	0.00	0.00	0.00	0.00	0.00	0.00	0.00	0.00	0.00	0.00	0.00
Bacteria	Proteobacteria	Gammaproteobacteria	Burkholderiales	Alcaligenaceae		0.00	0.00	0.00	0.00	0.00	0.00	0.00	0.00	0.00	0.00	0.00	0.00	0.00
Bacteria	Actinobacteriota	Actinobacteria	Propionibacteriales	Propionibacteriaceae	Cutibacterium	0.00	0.00	0.00	0.00	0.00	0.00	0.00	0.00	0.00	0.00	0.00	0.00	0.00
Bacteria	Proteobacteria	Gammaproteobacteria	Burkholderiales	Alcaligenaceae		0.00	0.00	0.00	0.00	0.00	0.00	0.00	0.00	0.00	0.00	0.00	0.00	0.00
Bacteria	Firmicutes	Bacilli	Staphylococcales	Staphylococcaceae	Staphylococcus	0.00	0.00	0.00	0.00	0.00	0.00	0.00	0.00	0.00	0.00	0.00	0.00	0.00
Bacteria	Actinobacteriota	Actinobacteria	Corynebacteriales	Corynebacteriaceae	Corynebacterium	0.00	0.00	0.00	0.00	0.00	0.00	0.00	0.00	0.00	0.00	0.00	0.00	0.00
Bacteria	Proteobacteria	Gammaproteobacteria	Burkholderiales	Alcaligenaceae		0.00	0.00	0.00	0.00	0.00	0.00	0.00	0.00	0.00	0.00	0.00	0.00	0.00
Bacteria	Proteobacteria	Gammaproteobacteria	Pseudomonadales	Moraxellaceae	Acinetobacter	0.00	0.00	0.00	0.00	0.00	0.00	0.00	0.00	0.00	0.00	0.00	0.00	0.00
Bacteria	Proteobacteria	Gammaproteobacteria	Burkholderiales	Alcaligenaceae		0.00	0.00	0.00	0.00	0.00	0.00	0.00	0.00	0.00	0.00	0.00	0.00	0.00
Bacteria	Firmicutes	Bacilli	Staphylococcales	Gemellaceae	Gemella	0.00	0.00	0.00	0.00	0.00	0.00	0.00	0.00	0.00	0.00	0.00	0.00	0.00
Bacteria	Proteobacteria	Gammaproteobacteria	Enterobacterales	Morganellaceae	Proteus	0.00	0.00	0.00	0.00	0.00	0.00	0.00	0.00	0.00	0.00	0.00	0.00	0.00
Bacteria	Proteobacteria	Gammaproteobacteria	Burkholderiales	Alcaligenaceae		0.00	0.00	0.00	0.00	0.00	0.00	0.00	0.00	0.00	0.00	0.00	0.00	0.00
Eukaryota	Vertebrata	Mammalia	Mammalia	Mammalia	Mammalia	0.00	0.00	0.00	0.00	0.00	0.00	0.00	0.00	0.00	0.00	0.00	0.00	0.00

Taxonomic designation						Relative abundance (%)									
Domain	Phylum	Class	Order	Family	Genus										
						BA-PC-BTX									
						4 cm	**10 cm**	**14 cm**	**24 cm**	**30 cm**					
Bacteria	Proteobacteria	Gammaproteobacteria	Burkholderiales	Alcaligenaceae		38.86	49.46	80.40	76.78	85.59					
Bacteria	Bacteroidota	Bacteroidia	Sphingobacteriales	Sphingobacteriaceae	Pedobacter	0.33	0.38	0.64	0.29	0.38					
Bacteria	Actinobacteriota	Actinobacteria	Micrococcales	Microbacteriaceae	Leifsonia	0.32	0.44	1.09	0.85	1.16					
Bacteria	Proteobacteria	Gammaproteobacteria	Burkholderiales	Comamonadaceae	Delftia	0.22	0.52	1.13	0.65	0.96					
Bacteria	Proteobacteria	Gammaproteobacteria	Enterobacterales	Enterobacteriaceae	Escherichia-Shigella	0.03	0.13	0.00	0.00	0.00					
Bacteria	Firmicutes	Clostridia	Eubacteriales	Eubacteriaceae	Pseudoramibacter	0.01	0.00	0.00	0.10	0.27					
Bacteria	Proteobacteria	Gammaproteobacteria	Burkholderiales	Comamonadaceae	Delftia	0.00	0.07	0.17	0.00	0.18					
Bacteria	Actinobacteriota	Actinobacteria	Propionibacteriales	Propionibacteriaceae	Cutibacterium	0.00	0.00	0.00	0.00	0.00					
Bacteria	Proteobacteria	Alphaproteobacteria	Sphingomonadales	Sphingomonadaceae	Sphingomonas	0.00	0.00	0.00	0.00	0.00					
Eukaryota	Phragmoplastophyta	Embryophyta	Magnoliophyta	Magnoliophyta	Magnoliophyta	0.00	0.00	0.00	0.00	0.00					
Bacteria	Firmicutes	Desulfotomaculia	Desulfotomaculales			0.00	0.00	0.00	0.00	0.00					
Bacteria	Proteobacteria	Gammaproteobacteria	Pseudomonadales	Moraxellaceae		0.00	0.00	0.00	0.00	0.00					
Bacteria	Firmicutes	Bacilli	Bacillales	Bacillaceae	Bacillus	0.00	0.00	0.00	0.00	0.00					
Bacteria	Proteobacteria	Gammaproteobacteria	Enterobacterales	Enterobacteriaceae		0.00	0.00	0.00	0.00	0.00					
Bacteria	Proteobacteria	Gammaproteobacteria	Burkholderiales	Alcaligenaceae		0.00	0.00	0.00	0.00	0.00					
Bacteria	Proteobacteria	Gammaproteobacteria	Burkholderiales	Alcaligenaceae		0.00	0.00	0.00	0.00	0.00					
Bacteria	Proteobacteria	Gammaproteobacteria	Burkholderiales	Alcaligenaceae		0.00	0.00	0.00	0.00	0.00					
Bacteria	Proteobacteria	Gammaproteobacteria	Burkholderiales	Alcaligenaceae		0.00	0.00	0.00	0.00	0.00					
Bacteria	Proteobacteria	Gammaproteobacteria	Burkholderiales	Alcaligenaceae		0.00	0.00	0.00	0.00	0.00					
Bacteria	Actinobacteriota	Actinobacteria	Propionibacteriales	Propionibacteriaceae	Cutibacterium	0.00	0.00	0.00	0.00	0.00					
Bacteria	Proteobacteria	Gammaproteobacteria	Burkholderiales	Alcaligenaceae		0.00	0.00	0.00	0.00	0.00					
Bacteria	Firmicutes	Bacilli	Staphylococcales	Staphylococcaceae	Staphylococcus	0.00	0.00	0.00	0.00	0.00					
Bacteria	Actinobacteriota	Actinobacteria	Corynebacteriales	Corynebacteriaceae	Corynebacterium	0.00	0.00	0.00	0.00	0.00					
Bacteria	Proteobacteria	Gammaproteobacteria	Burkholderiales	Alcaligenaceae		0.00	0.00	0.00	0.00	0.00					
Bacteria	Proteobacteria	Gammaproteobacteria	Pseudomonadales	Moraxellaceae	Acinetobacter	0.00	0.00	0.00	0.00	0.00					
Bacteria	Proteobacteria	Gammaproteobacteria	Burkholderiales	Alcaligenaceae		0.00	0.00	0.00	0.00	0.00					
Bacteria	Firmicutes	Bacilli	Staphylococcales	Gemellaceae	Gemella	0.00	0.00	0.00	0.00	0.00					
Bacteria	Proteobacteria	Gammaproteobacteria	Enterobacterales	Morganellaceae	Proteus	0.00	0.00	0.00	0.00	0.00					
Bacteria	Proteobacteria	Gammaproteobacteria	Burkholderiales	Alcaligenaceae		0.00	0.00	0.00	0.00	0.00					
Eukaryota	Vertebrata	Mammalia	Mammalia	Mammalia	Mammalia	0.00	0.00	0.00	0.00	0.00					
						BA+PAC-BTX									
						2.5 cm	**13.5 cm**	**14.5 cm**	**15.5 cm**	**16.5 cm**	**17.5 cm**	**18.5 cm**	**20.5 cm**	**22 cm**	**25 cm**
Bacteria	Proteobacteria	Gammaproteobacteria	Burkholderiales	Alcaligenaceae		71.27	88.19	85.77	89.15	72.09	85.33	76.18	79.90	87.00	91.15
Bacteria	Bacteroidota	Bacteroidia	Sphingobacteriales	Sphingobacteriaceae	Pedobacter	0.22	1.56	0.30	0.27	0.33	1.23	0.20	0.36	0.17	0.46
Bacteria	Actinobacteriota	Actinobacteria	Micrococcales	Microbacteriaceae	Leifsonia	1.02	1.31	0.90	1.13	0.78	1.29	0.88	1.07	1.39	1.28
Bacteria	Proteobacteria	Gammaproteobacteria	Burkholderiales	Comamonadaceae	Delftia	0.33	0.79	0.46	0.75	0.52	0.73	0.24	1.40	0.26	0.20
Bacteria	Proteobacteria	Gammaproteobacteria	Enterobacterales	Enterobacteriaceae	Escherichia-Shigella	0.00	0.02	0.00	0.04	0.00	0.01	0.05	0.21	0.00	0.01
Bacteria	Firmicutes	Clostridia	Eubacteriales	Eubacteriaceae	Pseudoramibacter	0.06	0.00	0.00	0.00	0.00	0.00	0.03	0.09	0.00	0.00
Bacteria	Proteobacteria	Gammaproteobacteria	Burkholderiales	Comamonadaceae	Delftia	0.09	0.14	0.00	0.00	0.00	0.18	0.00	0.00	0.25	0.00
Bacteria	Actinobacteriota	Actinobacteria	Propionibacteriales	Propionibacteriaceae	Cutibacterium	0.00	0.00	0.00	0.05	0.00	0.00	0.00	0.00	0.00	0.00
Bacteria	Proteobacteria	Alphaproteobacteria	Sphingomonadales	Sphingomonadaceae	Sphingomonas	0.00	0.00	0.00	0.00	0.00	0.05	0.00	0.04	0.00	0.00
Eukaryota	Phragmoplastophyta	Embryophyta	Magnoliophyta	Magnoliophyta	Magnoliophyta	0.00	0.00	0.00	0.00	0.00	0.00	0.00	0.00	0.00	0.00
Bacteria	Firmicutes	Desulfotomaculia	Desulfotomaculales			0.00	0.00	0.00	0.00	0.00	0.00	0.00	0.00	0.00	0.00
Bacteria	Proteobacteria	Gammaproteobacteria	Pseudomonadales	Moraxellaceae		0.00	0.02	0.00	0.00	0.00	0.00	0.00	0.00	0.00	0.00
Bacteria	Firmicutes	Bacilli	Bacillales	Bacillaceae	Bacillus	0.00	0.00	0.00	0.00	0.00	0.00	0.00	0.01	0.00	0.00
Bacteria	Proteobacteria	Gammaproteobacteria	Enterobacterales	Enterobacteriaceae		0.00	0.00	0.00	0.00	0.00	0.00	0.00	0.00	0.00	0.00
Bacteria	Proteobacteria	Gammaproteobacteria	Burkholderiales	Alcaligenaceae		0.00	0.00	0.00	0.00	0.00	0.00	0.00	0.00	0.00	0.00
Bacteria	Proteobacteria	Gammaproteobacteria	Burkholderiales	Alcaligenaceae		0.00	0.00	0.00	0.00	0.00	0.00	0.00	0.00	0.00	0.00
Bacteria	Proteobacteria	Gammaproteobacteria	Burkholderiales	Alcaligenaceae		0.00	0.00	0.00	0.00	0.00	0.00	0.00	0.00	0.00	0.00
Bacteria	Proteobacteria	Gammaproteobacteria	Burkholderiales	Alcaligenaceae		0.00	0.00	0.00	0.00	0.00	0.00	0.00	0.00	0.00	0.00
Bacteria	Proteobacteria	Gammaproteobacteria	Burkholderiales	Alcaligenaceae		0.00	0.00	0.00	0.00	0.00	0.00	0.00	0.00	0.00	0.00
Bacteria	Actinobacteriota	Actinobacteria	Propionibacteriales	Propionibacteriaceae	Cutibacterium	0.00	0.00	0.00	0.00	0.00	0.00	0.00	0.00	0.00	0.00
Bacteria	Proteobacteria	Gammaproteobacteria	Burkholderiales	Alcaligenaceae		0.00	0.00	0.00	0.00	0.00	0.00	0.00	0.00	0.00	0.00
Bacteria	Firmicutes	Bacilli	Staphylococcales	Staphylococcaceae	Staphylococcus	0.00	0.00	0.00	0.00	0.00	0.00	0.00	0.00	0.00	0.00
Bacteria	Actinobacteriota	Actinobacteria	Corynebacteriales	Corynebacteriaceae	Corynebacterium	0.00	0.00	0.00	0.00	0.00	0.00	0.00	0.00	0.00	0.00
Bacteria	Proteobacteria	Gammaproteobacteria	Burkholderiales	Alcaligenaceae		0.00	0.00	0.00	0.00	0.00	0.00	0.00	0.00	0.00	0.00
Bacteria	Proteobacteria	Gammaproteobacteria	Pseudomonadales	Moraxellaceae	Acinetobacter	0.00	0.00	0.00	0.00	0.00	0.00	0.00	0.00	0.00	0.00
Bacteria	Proteobacteria	Gammaproteobacteria	Burkholderiales	Alcaligenaceae		0.00	0.00	0.00	0.00	0.00	0.00	0.00	0.00	0.00	0.00
Bacteria	Firmicutes	Bacilli	Staphylococcales	Gemellaceae	Gemella	0.00	0.00	0.00	0.00	0.00	0.00	0.00	0.00	0.00	0.00
Bacteria	Proteobacteria	Gammaproteobacteria	Enterobacterales	Morganellaceae	Proteus	0.00	0.00	0.00	0.00	0.00	0.00	0.00	0.00	0.00	0.00
Bacteria	Proteobacteria	Gammaproteobacteria	Burkholderiales	Alcaligenaceae		0.00	0.00	0.00	0.00	0.00	0.00	0.00	0.00	0.00	0.00
Eukaryota	Vertebrata	Mammalia	Mammalia	Mammalia	Mammalia	0.00	0.00	0.00	0.00	0.00	0.00	0.00	0.00	0.00	0.00

Table C.4: Cumulative influent and effluent mass and the change in cumulative mass (ΔM) between the influent and effluent (with the percentage of mass reduction or increase) of benzene (B), toluene (T), *o*-xylene (X), sulfate (SO_4^{2-}), methane (CH_4) and dissolved inorganic carbon (DIC) during Year-1 and Year-2 of column operation.

	Mass (mg) (% Reduction or Increase)					
	Single-solute (toluene-only)			**Multi-solute (benzene, toluene and *o*-xylene [BTX])**		
Year-1	**KC+PACz**	**BA-PC**	**BA+PACz**	**KC+PACz**	**BA-PC**	**BA+PACz**
Pore Volumes	605.18	263.35	577.07	443.08	202.94	434.62
Influent B				176.76	55.7	131.62
Effluent B				160.18	29.91	53.33
ΔM of B				-16.58 (9.38%)	-25.79 (46.31%)	-78.29 (59.48%)
Influent T	165.13	55.52	90.55	159.07	48.27	107.06
Effluent T	103.89	16.1	3.19	117.52	20.67	19.44
ΔM of T	-61.23 (37.08%)	-39.42 (71%)	-87.36 (96.47%)	-41.54 (26.12%)	-27.61 (57.19%)	-87.62 (81.84%)
Influent X				112.86	46.73	91.92
Effluent X				22.39	35.01	7.62
ΔM of X				-90.47 (80.17%)	-11.72 (25.08%)	-84.31 (91.72%)
Year-2						
Pore Volumes	55.81	67.82	69.20	46.61	48.24	64.86
Influent B				89.29	72.42	99.51
Effluent B				84.66	66.44	85.18
ΔM of B				-4.62 (5.18%)	-5.98 (8.25%)	-14.32 (14.39%)
Influent T	73.55	87.45	68.41	84.24	64.72	90.26
Effluent T	18.69	48.61	0.35	62.81	26.4	1.37
ΔM of T	-54.86 (74.59%)	-38.84 (44.42%)	-68.06 (99.49%)	-21.42 (25.43%)	-38.33 (59.22%)	-88.89 (98.48%)
Influent X				76.21	67.1	87.65
Effluent X				44.02	55.76	13.01
ΔM of X				-32.19 (42.24%)	-11.34 (16.89%)	-74.65 (85.16%)
Influent SO_4^{2-}	141.69	161.13	170.29	145.17	137.77	197.78
Effluent SO_4^{2-}	134.93	12.85	1.13	142.98	1.3	1.72
ΔM of SO_4^{2-}	-6.76 (4.77%)	-148.28 (92.02%)	-169.16 (99.34%)	-2.2 (1.51%)	-136.47 (99.06%)	-196.06 (99.13%)
Influent CH_4	0.0	0.04	0.38	0.01	0.11	0.01
Effluent CH_4	0.0	113.15	102.84	0.01	110.54	65.34
ΔM of CH_4	0.0 (0.0%)	113.11 (99.97%)	102.46 (99.63%)	0.0 (0.0%)	110.43 (99.9%)	65.34 (99.99%)
Influent DIC	26.72	82.84	65.43	29.05	65.56	69.11
Effluent DIC	54.48	177.92	196.31	66.07	192.9	152.29
ΔM of DIC	27.77 (50.97%)	95.08 (53.44%)	130.88 (66.67%)	37.02 (56.03%)	127.34 (66.01%)	83.18 (54.62%)
∑(Year-1, Year-2)						
Pore Volumes	660.99	331.18	646.26	489.69	251.18	499.48
Influent B				266.05	128.12	231.13
Effluent B				244.84	96.35	138.52
ΔM of B				-21.20 (7.97%)	-31.77 (24.8%)	-92.61 (40.07%)
Influent T	238.68	142.97	158.96	243.3	113	197.32
Effluent T	122.58	64.71	3.55	180.34	47.06	20.81
ΔM of T	-116.09 (48.64%)	-78.26 (54.74%)	-155.42 (97.77%)	-62.97 (25.88%)	-65.94 (58.35%)	-176.51 (89.45%)
Influent X				189.07	113.83	179.58
Effluent X				66.41	90.77	20.62
ΔM of X				-122.66 (64.88%)	-23.06 (20.26%)	-158.96 (88.52%)

Table C.5: Stoichiometrically estimated mass of dissolved inorganic carbon (DIC) and toluene produced or consumed, respectively, during sulfate reduction or methanogenesis compared to the experimentally measured change in cumulative mass (ΔM) of DIC and toluene (from Table C.3) during Year-2 of column operation.

	Mass (mg) (% mass relative to ΔM)		
	ΔM – from Table C.3	Stoichiometric mass produced or consumed from biodegradation [1, 2]	Mass sorbed and/or error [3]
Single-solute (toluene-only)			
KC+PACz			
DIC produced from sulfate reduction		1.31	
DIC produced from methanogenesis		0.0	
∑ carbon produced	27.77	1.31 (4.74%)	
Toluene consumed from sulfate reduction	-54.86	1.44 (2.63%)	53.42 (97.37%)
BA-PC			
DIC produced from sulfate reduction		28.84	
DIC produced from methanogenesis		84.7	
∑ carbon produced	95.08	113.54 (119.41%)	
Toluene consumed from sulfate reduction	-38.84	31.61 (81.37%)	7.24 (18.63%)
BA+PACz			
DIC produced from sulfate reduction		32.9	
DIC produced from methanogenesis		76.72	
∑ carbon produced	130.88	109.62 (83.76%)	
Toluene consumed from sulfate reduction	-68.06	36.06 (52.98%)	32 (47.02%)
Multi-solute (benzene, toluene and *o*-xylene [BTX])			
KC+PACz			
DIC produced from sulfate reduction		0.43	
DIC produced from methanogenesis		0.0	
∑ carbon produced	37.02	0.43 (1.16%)	
Toluene consumed from sulfate reduction	-21.42	0.47 (2.18%)	20.96 (97.82%)
BA-PC			
DIC produced from sulfate reduction		26.54	
DIC produced from methanogenesis		82.69	
∑ carbon produced	127.34	109.24 (85.78%)	
Toluene consumed from sulfate reduction	-38.33	29.09 (75.9%)	9.24 (24.10%)
BA+PACz			
DIC produced from sulfate reduction		38.13	
DIC produced from methanogenesis		48.93	
∑ carbon produced	83.18	87.06 (104.66%)	
Toluene consumed from sulfate reduction	-88.89	41.79 (47.01%)	47.1 (52.99%)

Notes:

1. Mass of dissolved inorganic carbon (DIC) produced was determined using the ΔM of sulfate and the stoichiometric mass ratios between DIC (as carbon) and sulfate during sulfate reduction (0.19), or the ΔM of CH_4 and the stoichiometric mass ratio between DIC (as carbon) and CH_4 during methanogenesis (0.75).
2. Mass of toluene consumed was determined using the ΔM of toluene and the stoichiometric mass ratios between toluene and sulfate during sulfate reduction (0.21).
3. The mass of toluene sorbed to the solid phases (Borden sand [BS] or powdered activated carbon [PAC]) and/or the mass of toluene associated with error was estimated from the difference between the ΔM from Table C.3 and the stoichiometric mass consumed.

Table C.6: Isotope data and the change in isotopes relative to the signatures for the single-solute (toluene-only) and multi-solute (benzene, toluene and *o*-xylene [BTX]) KC+PACz, BA-PC and BA+PACz columns during Year-2.

	Pore Volume	δ^{13}C-DIC	δ^{13}C-Benzene	$\Delta\delta^{13}$C-Benzene	δ^{13}C-Toluene	$\Delta\delta^{13}$C-Toluene	δ^{13}C-*o*-Xylene	$\Delta\delta^{13}$C-*o*-Xylene	δ^{2}H-Benzene	$\Delta\delta^{2}$H-Benzene	δ^{2}H-Toluene	$\Delta\delta^{2}$H-Toluene	δ^{2}H-*o*-Xylene	$\Delta\delta^{2}$H-*o*-Xylene
Error		PDB ± 0.2‰	PDB ± 0.3‰		PDB ± 0.3‰		PDB ± 0.3‰		VSMOW ± 0.5‰		VSMOW ± 0.5‰		VSMOW ± 0.5‰	
Signature		-2.94	-25.61		-27.77		-29.90		-98.37		-82.07		-132.05	
Single-solute (toluene-only)														
KC-PAC	4.58	0.53			-27.90	-0.13					-69.18	12.89		
	24.27	1.52			-28.12	-0.35					-69.32	12.75		
	32.01	2.54			-27.64	0.13					-68.93	13.14		
	45.91	2.68			-27.49	0.28					-70.62	11.45		
	55.81	5.57			-27.70	0.07					-56.47	25.60		
BA-PC	4.87	-2.45			-27.27	0.50					-35.50	46.57		
	9.45	-8.37			-26.97	0.80					-20.55	61.52		
	27.51	-4.77			-25.38	2.39					-20.55	61.52		
	37.23	3.65			-27.18	0.59					-45.45	36.62		
	48.14	0.30			-27.46	0.31					-25.24	56.83		
	61.06	3.07			-27.50	0.27					-3.37	78.70		
BA+PACz	4.58	8.30												
	20.94	-1.57												
	34.20	-3.61												
	43.03	-2.57												
	49.75	-0.8												
	60.31	-12.45												
Multi-solute (benzene, toluene and *o*-xylene [BTX])														
KC-PAC	3.12	3.68	-23.84	1.76	-27.34	0.43	-30.13	-0.23	-62.60	35.77	-62.69	19.38	-69.41	62.64
	15.65	3.11	-24.84	0.76	-28.03	-0.26	-30.71	-0.81	-75.17	23.20	-61.49	20.58	-87.76	44.29
	26.18	2.43	-25.02	0.58	-28.50	-0.73	-31.06	-1.16	-81.85	16.51	-67.86	14.21	-77.20	54.85
	37.62	4.97	-24.69	0.92	-28.71	-0.94	-30.88	-0.98	-78.55	19.81	-67.56	14.51	-84.57	47.48
	44.13	4.33	BALL		-27.93	-0.16	BALL		BALL		-56.14	25.93	BALL	
BA-PC	5.25	12.28	-25.41	0.19	-27.75	0.02	-31.50	-1.60	-67.56	30.81	-48.49	33.58	-109.33	22.72
	31.18	3.84	-25.30	0.31	-28.00	-0.23	-33.02	-3.12	-65.47	32.89	-25.88	56.19	-107.85	24.20
	43.10	-6.54	-24.98	0.63	-28.60	-0.83	-32.61	-2.71	-77.71	20.66	-23.68	58.39	-60.55	71.50
	50.76	-5.40	-23.87	1.74	-28.71	-0.94	-31.23	-1.33	-79.40	18.96	BALL		-66.54	65.51
BA+PACz	4.63	-3.02	-24.58	1.02					-69.25	29.12				
	25.50	-4.15	BALL						BALL					
	29.47	-8.03	-24.87	0.74					-80.02	18.34				
	33.01	-3.91												
	37.17	-1.59	-23.91	1.70			-29.90	0.00	-82.98	15.39			-132.05	0.00
	38.70						-32.34	-2.44					-48.09	83.96
	46.25	-1.13	-26.29	-0.68			-30.53	-0.63	-84.56	13.81			-42.09	89.96
	53.98	-0.92	-25.45	0.15			-30.73	-0.83	-85.39	12.97			-48.56	83.49
	58.71	-1.15					-35.50	-5.60					-47.42	84.63
	61.78	-2.53	-26.57	-0.96			-33.65	-3.75	-81.81	16.55			-45.48	86.57

Table C.7: Average abundance of total bacteria, total archaea, Deltaproteobacteria, *Desulfosporosinus* sp.and *Peptococcaceae* sp. (± standard error) generated from quantitative polymerase chain reaction (qPCR) analysis for the single-solute (toluene-only) and multi-solute (benzene, toluene and *o*-xylene [BTX]) BA-PC and BA+PACz column after 2 years of operation.

		Abundance (copies/g)									
		Total Bacteria		Total Archaea		Deltaproteobacteria		Desulfosporosinus sp.		Peptococcaceae sp.	
Column	Distance from influent (cm)	Average	Standard deviation	Average	Standard deviation	Average	Standard deviation	Average	Standard deviation	Average	Standard deviation
Background		$5.2\times10^{+6}$	$2.9\times10^{+6}$	$3.9\times10^{+4}$	$7.7\times10^{+3}$	$7.1\times10^{+1}$	$3.5\times10^{+1}$	$4.9\times10^{+4}$	$3.3\times10^{+4}$	$9.4\times10^{+2}$	$5.2\times10^{+6}$
Single-solute (toluene-only)											
BA-PC	4	$2.8\times10^{+6}$	$1.4\times10^{+5}$	$3.3\times10^{+6}$	$6.4\times10^{+4}$	$2\times10^{+1}$	0.0	$5.6\times10^{+4}$	$3\times10^{+2}$	$1.3\times10^{+3}$	0.0
	10	$3.2\times10^{+6}$	$6\times10^{+4}$	$5.7\times10^{+5}$	$6.4\times10^{+4}$			$3.1\times10^{+5}$	$2.4\times10^{+4}$		
	17	$2.4\times10^{+6}$	$2\times10^{+5}$	$1.8\times10^{+5}$	$2.4\times10^{+4}$			$5\times10^{+4}$	$4.7\times10^{+3}$		
	24	$1.9\times10^{+6}$	$9.8\times10^{+4}$	$3.3\times10^{+4}$	$7.4\times10^{+2}$			$2.3\times10^{+4}$	$5.6\times10^{+3}$		
	30	$1.6\times10^{+6}$	$3.0\times10^{+4}$	$1.4\times10^{+4}$	$9.5\times10^{+2}$			$1.2\times10^{+4}$	$4.8\times10^{+3}$		
BA+PACz	2.5	$2.2\times10^{+6}$	$9.1\times10^{+3}$	$4.1\times10^{+5}$	$3.2\times10^{+4}$			$4.9\times10^{+3}$	$6.5\times10^{+2}$		
	6	$1.8\times10^{+6}$	$1.6\times10^{+4}$	$2.1\times10^{+4}$	$2.5\times10^{+2}$			$1.1\times10^{+4}$	$2.7\times10^{+3}$		
	9	$1.4\times10^{+6}$	$3.0\times10^{+4}$	$1.9\times10^{+5}$	$4.1\times10^{+4}$	$1.9\times10^{+1}$	0.0	$5.0\times10^{+3}$	$1.2\times10^{+3}$	1.0×10^{-4}	0.0
	12	$1.6\times10^{+6}$	$3.8\times10^{+4}$	$7.2\times10^{+3}$	$1.8\times10^{+3}$			$8.4\times10^{+3}$	$9.1\times10^{+3}$		
	13.5	$1.5\times10^{+6}$	$1.6\times10^{+4}$	$1.0\times10^{+5}$	$2.3\times10^{+4}$			$5.0\times10^{+3}$	$5.3\times10^{+2}$		
	14.5	$2.3\times10^{+6}$	$2.3\times10^{+4}$	$4.0\times10^{+5}$	$1.8\times10^{+4}$	$1.4\times10^{+2}$	0.0	$3.3\times10^{+4}$	$7.6\times10^{+3}$	$1.5\times10^{+3}$	0.0
	15.5	$1.7\times10^{+6}$	$2.7\times10^{+4}$	$5.1\times10^{+4}$	$2.2\times10^{+3}$			$1.9\times10^{+4}$	$4.6\times10^{+3}$		
	16.5	$2.8\times10^{+6}$	$2.1\times10^{+4}$	$6.4\times10^{+5}$	$5.6\times10^{+4}$	$4.6\times10^{+1}$	0.0	$3.5\times10^{+4}$	$5.8\times10^{+3}$	1.0×10^{-4}	0.0
	17.5										
	18.5	$1.7\times10^{+6}$	$1.0\times10^{+5}$	$2.8\times10^{+5}$	$3.54\times10^{+3}$			$1.7\times10^{+4}$	$2.6\times10^{+3}$		
	19.5										
	20.5	$1.4\times10^{+6}$	$9.2\times10^{+3}$	$2.6\times10^{+5}$	$1.68\times10^{+4}$			$1.4\times10^{+3}$	$1.9\times10^{+3}$		
	22	$1.6\times10^{+6}$	$3.5\times10^{+4}$	$1.3\times10^{+5}$	$1.61\times10^{+4}$	$5.5\times10^{+1}$	0.0	$3.4\times10^{+3}$	$4.2\times10^{+2}$		
	25	$1.5\times10^{+6}$	$4.6\times10^{+4}$	$2.7\times10^{+4}$	$7.64\times10^{+3}$			$3.5\times10^{+3}$	0.0	1.0×10^{-4}	0.0
	28	$1.4\times10^{+6}$	$1.0\times10^{+4}$	$1.5\times10^{+4}$	$6.6\times10^{+3}$			$7.2\times10^{+2}$	$9.7\times10^{+2}$		
	31										
	34.5	$1.5\times10^{+6}$	$2.3\times10^{+4}$	$3.4\times10^{+4}$	$6.0\times10^{+2}$			$1.7\times10^{+3}$	$2.2\times10^{+3}$		
Multi-solute (benzene, toluene and *o*-xylene [BTX])											
BA-PC	4	$2.6\times10^{+6}$	$2.4\times10^{+5}$	$2.1\times10^{+6}$	$4.1\times10^{+5}$	$5.3\times10^{+1}$	$1.5\times10^{+1}$	$1.1\times10^{+5}$	$5.4\times10^{+2}$	1.0×10^{-4}	0.0
	10	$2.3\times10^{+6}$	$2.2\times10^{+5}$	$1.5\times10^{+6}$	$1.5\times10^{+5}$	1.0×10^{-4}	0.0	$5.1\times10^{+4}$	$4.4\times10^{+3}$	$5.8\times10^{+2}$	0.0
	17	$1.3\times10^{+6}$	$2.3\times10^{+4}$	$2\times10^{+5}$	$1.0\times10^{+2}$	1.0×10^{-4}	0.0	$2.1\times10^{+4}$	$3.2\times10^{+3}$	1.0×10^{-4}	0.0
	24	$1.5\times10^{+6}$	$1.6\times10^{+5}$	$2.9\times10^{+5}$	$5.5\times10^{+4}$	1.0×10^{-4}	0.0	$8.6\times10^{+3}$	$3.7\times10^{+3}$	1.0×10^{-4}	0.0
	30	$1.4\times10^{+6}$	$6.6\times10^{+4}$	$8.9\times10^{+4}$	$7.6\times10^{+3}$	$5.8\times10^{+1}$	$1.9\times10^{+1}$	$5.0\times10^{+3}$	$2.8\times10^{+3}$	1.0×10^{-4}	0.0
BA+PACz	2.5	$7.5\times10^{+6}$	$1.7\times10^{+6}$	$3.8\times10^{+2}$	$4.4\times10^{+2}$	$2.8\times10^{+1}$	$1.4\times^{+1}$	1.1×10+5	$2.7\times10^{+3}$	$1.9\times10^{+3}$	0.0
	6	$2.4\times10^{+6}$	$3.5\times10^{+4}$	$2.3\times10^{+3}$	$8.4\times10^{+2}$	1.0×10^{-4}	0.0	$2.5\times10^{+4}$	$3.1\times10^{+3}$	$1.9\times10^{+3}$	0.0
	9	$6.3\times10^{+6}$	$6.9\times10^{+5}$	$1.1\times10^{+4}$	$1.9\times10^{+3}$	$1.7\times10^{+1}$	0.0	$8.5\times10^{+3}$	$3.8\times10^{+3}$	$8.5\times10^{+2}$	$8.7\times^{+1}$
	12	$2.2\times10^{+6}$	$2.7\times10^{+4}$	$4.9\times10^{+2}$	$4.9\times10^{+2}$	1.0×10^{-4}	0.0	$1.1\times10^{+4}$	$7.5\times10^{+3}$	1.0×10^{-4}	0.0
	13.5	$7\times10^{+6}$	$7.6\times10^{+5}$	$5.8\times10^{+4}$	$1.4\times10^{+4}$	$2\times10^{+1}$	0.0	$4.7\times10^{+4}$	$4.5\times10^{+3}$	$1.8\times10^{+3}$	0.0
	14.5	$1.0\times^{+7}$	$2\times10^{+5}$	$9.4\times10^{+5}$	$1.8\times10^{+4}$	$1.8\times10^{+2}$	$8.3\times10^{+1}$	$2.3\times10^{+5}$	$7.7\times10^{+2}$	1.0×10^{-4}	0.0
	15.5	$1.8\times10^{+6}$	$1.7\times10^{+2}$	$5.6\times10^{+4}$	$2.5\times10^{+3}$	1.0×10^{-4}	0.0	$3.2\times10^{+4}$	$1.8\times10^{+3}$	1.0×10^{-4}	0.0
	16.5	$4.6\times10^{+6}$	$3.0\times10^{+4}$	$2.6\times10^{+5}$	$3.0\times10^{+2}$	$6.6\times10^{+1}$	$5.9\times10^{+1}$	$2.5\times10^{+4}$	$5.6\times10^{+2}$	$2\times10^{+4}$	$8.8\times^{+3}$
	17.5	$2.5\times10^{+6}$	$3.7\times10^{+4}$	$1.5\times10^{+5}$	$6.2\times10^{+3}$	1.0×10^{-4}	0.0	$5.5\times10^{+4}$	$1.6\times10^{+2}$	$1.0\times10^{+4}$	0.0
	18.5	$4.2\times10^{+6}$	$2.6\times10^{+4}$	$2.3\times10^{+5}$	$1.5\times10^{+4}$	1.0×10^{-4}	0.0	$2.1\times10^{+4}$	$2.7\times10^{+3}$	$8.2\times10^{+3}$	$1.9\times^{+03}$
	19.5										
	20.5	$3.6\times10^{+6}$	$3.5\times10^{+5}$	$8.4\times10^{+4}$	$6.0\times10^{+3}$	1.0×10^{-4}	0.0	$6.9\times10^{+3}$	$1.1\times10^{+3}$	$1.4\times10^{+4}$	$8.5\times^{+3}$
	22	$5\times10^{+6}$	$2.8\times10^{+5}$	$9.2\times10^{+4}$	$4.1\times10^{+4}$	$1.0\times10^{+1}$	0.0	$2.2\times10^{+4}$	$4.6\times10^{+3}$	1.0×10^{-4}	0.0
	25	$3.5\times10^{+6}$	$2.5\times10^{+5}$	$9.2\times10^{+4}$	$4.8\times10^{+3}$	1.0×10^{-4}	0.0	$1.2\times10^{+4}$	$2.7\times10^{+3}$	$8.2\times10^{+2}$	0.0
	28	$3.1\times10^{+6}$	$4.0\times10^{+4}$	$1.9\times10^{+4}$	$8.7\times10^{+3}$	1.0×10^{-4}	0.0	$1.6\times10^{+3}$	$8.1\times10^{+2}$	1.0×10^{-4}	0.0
	31										
	34.5	$2.8\times10^{+6}$	$4.9\times10^{+4}$	$1.2\times10^{+4}$	$2.9\times10^{+3}$	1.0×10^{-4}	0.0	$3.2\times10^{+3}$	0.0	$1.0\times10^{+3}$	0.0

Table C.8: Relative abundance of bacteria and archaea (≥ 4% of any amplicon sequencing variant [ASV] detected) generated from 16S ribosomal ribonucleic acid (rRNA) next generation sequencing (NGS) for the single-solute (toluene-only) and multi-solute (benzene, toluene and *o*-xylene [BTX]) BA-PC and BA+PACz columns after 2 years of operation.

Taxonomic designation						Relative abundance (%)												
Domain	Phylum	Class	Order	Family	Genus													
						BA-PC-toluene												
						4 cm	**10 cm**	**14 cm**	**24 cm**	**30 cm**								
Archaea	Halobacterota	Methanomicrobia	Methanomicrobiales	Methanoregulaceae	*Methanoregula*	0.00	0.29	1.30	2.34	4.01								
Archaea	Halobacterota	Methanosarcinia	Methanosarciniales	Methanosaetaceae	*Methanosaeta*	0.02	14.15	23.30	7.13	18.19								
Archaea	Halobacterota	Methanosarcinia	Methanosarciniales	Methanosarcinaceae	*Methanosarcina*	81.43	5.73	1.80	4.16	1.00								
Archaea	Halobacterota	Methanosarcinia	Methanosarciniales	Methanosarcinaceae	*Methanomethylovorans*	0.00	1.80	0.00	4.94	6.17								
Archaea	Euryarchaeota	Methanobacteria	Methanobacteriales	Methanobacteriaceae	*Methanobacterium*	0.54	8.93	8.79	6.30	14.87								
Archaea	Halobacterota	Methanocellia	Methanocellales	Methanocellaceae		0.07	4.72	2.95	0.00	0.00								
Archaea	Halobacterota	Methanomicrobia	Methanomicrobiales	Methanomicrobiales		0.00	0.00	0.00	0.00	5.32								
Bacteria	Firmicutes	Desulfitobacteriia	Desulfitobacteriales	Desulfitobacteriaceae	*Desulfosporosinus*	0.72	7.88	4.34	9.89	5.96								
Bacteria	Patescibacteria	Berkelbacteria	Berkelbacteria	Berkelbacteria	*Berkelbacteria*	0.00	0.00	0.00	0.00	0.00								
Bacteria	Desulfobacterota	Desulfovibrionia	Desulfovibrionales	Desulfovibrionaceae	*Desulfovibrio*	0.00	0.06	0.15	0.00	0.00								
Bacteria	Edwardsbacteria	Edwardsbacteria	Edwardsbacteria	Edwardsbacteria	*Edwardsbacteria*	0.00	0.00	0.00	0.00	4.64								
Bacteria	Proteobacteria	Gammaproteobacteria	Burkholderiales	Comamonadaceae		0.15	1.48	1.35	1.40	0.00								
Bacteria	Proteobacteria	Gammaproteobacteria	Burkholderiales	Comamonadaceae	*Hydrogenophaga*	0.03	1.96	0.75	0.00	0.00								
Bacteria	Chloroflexi	Anaerolineae	Anaerolineales	Anaerolineaceae	*Leptolinea*	0.14	0.21	0.32	1.30	0.00								
Bacteria	Nitrospinota	Nitrospinota	Nitrospinota			0.00	1.31	0.35	0.31	1.05								
Bacteria	Spirochaetota	Spirochaetia	Spirochaetales	Spirochaetaceae		0.00	0.00	0.00	0.00	0.00								
Bacteria	Proteobacteria	Gammaproteobacteria	Xanthomonadales	Xanthomonadaceae	*Lysobacter*	0.04	0.00	0.00	1.72	1.48								
Bacteria	Bacteroidota	Bacteroidia	Sphingobacteriales	Lentimicrobiaceae	*Lentimicrobiaceae*	0.13	0.00	0.00	0.00	0.00								
Bacteria	Deferrisomatota	Defferrisomatia	Defferrisomatales	Defferrisomataceae	*Deferrisoma*	0.00	0.00	0.00	0.00	0.00								
Bacteria	Desulfobacterota	Syntrophia	Syntrophales	Syntrophaceae	*Syntrophus*	0.00	0.00	0.00	0.00	0.00								
Bacteria	Acidobacteriota	Vicinamibacteria	Vicinamibacterales			0.00	0.49	0.75	0.00	0.11								
Bacteria	Actinobacteriota	Actinobacteria	Corynebacteriales	Nocardiaceae	*Rhodococcus*	0.00	0.00	0.60	0.31	0.00								
Bacteria	Proteobacteria	Alphaproteobacteria	Caulobacterales	Caulobacteraceae	*Brevundimonas*	0.00	0.00	0.00	0.00	0.00								
Bacteria	Proteobacteria	Alphaproteobacteria	Rhizobiales	Devosiaceae	*Devosia*	0.04	0.10	0.00	0.00	0.00								
Bacteria	Proteobacteria	Gammaproteobacteria	Burkholderiales	Sulfuricellaceae		0.00	0.00	0.00	0.00	0.00								
						BA+PACz-toluene												
						2.5 cm	**6 cm**	**9 cm**	**13.5 cm**	**14.5 cm**	**15.5 cm**	**16.5 cm**	**18.5 cm**	**20.5 cm**	**22 cm**	**25 cm**	**28 cm**	**34.5 cm**
Archaea	Halobacterota	Methanomicrobia	Methanomicrobiales	Methanoregulaceae	*Methanoregula*	0.00	0.00	0.00	0.00	0.00	0.00	0.00	0.00	0.00	0.00	0.00	0.00	0.00
Archaea	Halobacterota	Methanosarcinia	Methanosarciniales	Methanosaetaceae	*Methanosaeta*	0.00	8.02	31.87	16.67	22.29	12.78	23.57	5.81	0.45	1.23	0.00	0.35	1.95
Archaea	Halobacterota	Methanosarcinia	Methanosarciniales	Methanosarcinaceae	*Methanosarcina*	35.50	7.86	6.19	3.21	2.97	1.40	1.84	21.98	41.64	24.52	6.70	2.67	19.09
Archaea	Halobacterota	Methanosarcinia	Methanosarciniales	Methanosarcinaceae	*Methanomethylovorans*	0.00	0.61	2.52	2.43	3.97	3.64	3.88	0.89	9.74	4.30	0.97	0.00	2.21
Archaea	Euryarchaeota	Methanobacteria	Methanobacteriales	Methanobacteriaceae	*Methanobacterium*	0.00	3.38	4.52	2.56	8.61	21.88	26.43	13.16	7.06	10.35	1.44	13.96	2.10
Archaea	Halobacterota	Methanocellia	Methanocellales	Methanocellaceae		0.00	0.00	0.00	0.00	0.00	0.00	1.67	0.00	0.00	0.00	0.00	0.00	0.00
Archaea	Halobacterota	Methanomicrobia	Methanomicrobiales	Methanomicrobiales		0.00	0.00	0.00	0.00	0.00	0.00	0.00	0.00	0.00	0.00	0.00	0.00	0.00
Bacteria	Firmicutes	Desulfitobacteriia	Desulfitobacteriales	Desulfitobacteriaceae	*Desulfosporosinus*	2.03	2.71	1.57	1.89	4.15	2.12	4.61	5.09	0.24	1.41	3.92	9.89	1.99
Bacteria	Patescibacteria	Berkelbacteria	Berkelbacteria	Berkelbacteria	*Berkelbacteria*	0.00	29.53	11.09	7.93	5.77	15.23	3.11	12.22	4.65	11.04	42.17	38.29	20.38
Bacteria	Desulfobacterota	Desulfovibrionia	Desulfovibrionales	Desulfovibrionaceae	*Desulfovibrio*	0.00	0.00	0.00	0.00	2.59	0.70	0.38	0.68	0.00	0.00	0.00	0.00	0.00
Bacteria	Edwardsbacteria	Edwardsbacteria	Edwardsbacteria	Edwardsbacteria	*Edwardsbacteria*	0.00	0.00	0.00	0.00	0.05	0.00	2.05	6.36	3.75	5.10	3.86	4.55	1.18
Bacteria	Proteobacteria	Gammaproteobacteria	Burkholderiales	Comamonadaceae		0.00	1.45	0.00	0.00	2.80	5.83	0.19	0.22	0.00	1.23	0.00	1.44	0.37
Bacteria	Proteobacteria	Gammaproteobacteria	Burkholderiales	Comamonadaceae	*Hydrogenophaga*	0.27	5.15	0.00	1.18	1.39	1.33	0.35	0.60	0.00	4.76	5.23	2.23	4.08
Bacteria	Chloroflexi	Anaerolineae	Anaerolineales	Anaerolineaceae	*Leptolinea*	0.00	1.26	0.00	0.54	0.94	0.00	0.00	0.00	1.92	3.04	0.34	0.92	5.37
Bacteria	Nitrospinota	Nitrospinota	Nitrospinota			0.00	0.00	0.00	0.00	0.00	0.35	0.08	0.67	0.20	0.00	0.00	0.22	4.05
Bacteria	Spirochaetota	Spirochaetia	Spirochaetales	Spirochaetaceae		0.63	0.45	0.32	1.15	0.00	0.00	0.65	0.68	0.00	0.69	0.00	0.00	0.48
Bacteria	Proteobacteria	Gammaproteobacteria	Xanthomonadales	Xanthomonadaceae	*Lysobacter*	0.06	0.00	0.00	0.00	0.00	0.00	0.00	0.05	0.40	0.00	0.34	2.36	0.48
Bacteria	Bacteroidota	Bacteroidia	Sphingobacteriales	Lentimicrobiaceae	*Lentimicrobiaceae*	6.81	0.00	0.00	0.00	0.30	0.16	0.00	0.00	0.00	0.00	0.00	0.00	0.00
Bacteria	Deferrisomatota	Defferrisomatia	Defferrisomatales	Defferrisomataceae	*Deferrisoma*	0.00	0.00	0.00	0.00	0.00	0.00	0.00	0.00	0.00	1.06	0.30	0.00	0.33
Bacteria	Desulfobacterota	Syntrophia	Syntrophales	Syntrophaceae	*Syntrophus*	0.00	0.00	0.00	0.00	0.00	0.00	0.00	0.00	0.00	0.00	0.00	0.00	0.00
Bacteria	Acidobacteriota	Vicinamibacteria	Vicinamibacterales			0.00	0.00	0.00	1.05	0.08	0.00	0.00	0.00	0.00	0.00	0.00	0.00	0.00
Bacteria	Actinobacteriota	Actinobacteria	Corynebacteriales	Nocardiaceae	*Rhodococcus*	1.71	0.97	4.15	0.24	0.05	0.00	0.00	0.00	0.00	0.00	0.00	0.00	0.00
Bacteria	Proteobacteria	Alphaproteobacteria	Caulobacterales	Caulobacteraceae	*Brevundimonas*	0.00	0.00	0.00	0.00	0.00	0.15	0.00	0.06	1.03	0.00	0.00	0.44	0.00
Bacteria	Proteobacteria	Alphaproteobacteria	Rhizobiales	Devosiaceae	*Devosia*	0.00	0.00	0.12	0.00	0.24	0.00	0.00	0.00	0.00	0.32	0.00	0.00	0.00
Bacteria	Proteobacteria	Gammaproteobacteria	Burkholderiales	Sulfuricellaceae		0.00	0.00	0.00	0.00	0.00	0.00	0.00	0.00	0.00	0.00	4.36	0.13	0.00

Taxonomic designation						Relative abundance (%)											
Domain	Phylum	Class	Order	Family	Genus												
						BA-PC-BTX											
						4 cm	**10 cm**	**14 cm**	**24 cm**	**30 cm**							
Archaea	Halobacterota	Methanomicrobia	Methanomicrobiales	Methanoregulaceae	*Methanoregula*	0.00	0.00	0.00	0.00	0.00							
Archaea	Halobacterota	Methanosarcinia	Methanosarciniales	Methanosaetaceae	*Methanosaeta*	0.71	1.57	4.53	0.86	4.12							
Archaea	Halobacterota	Methanosarcinia	Methanosarciniales	Methanosarcinaceae	*Methanosarcina*	53.40	19.30	23.26	44.37	27.12							
Archaea	Halobacterota	Methanosarcinia	Methanosarciniales	Methanosarcinaceae	*Methanomethylovorans*	0.29	35.63	3.32	0.75	0.62							
Archaea	Euryarchaeota	Methanobacteria	Methanobacteriales	Methanobacteriaceae	*Methanobacterium*	2.22	1.96	4.74	4.09	3.95							
Archaea	Halobacterota	Methanomicrobia	Methanomicrobiales	Methanomicrobiales		0.00	0.00	0.00	0.00	0.00							
Bacteria	Firmicutes	Desulfitobacteriia	Desulfitobacteriales	Desulfitobacteriaceae	*Desulfosporosinus*	3.39	2.30	7.50	4.76	1.77							
Bacteria	Patescibacteria	Berkelbacteria	Berkelbacteria	Berkelbacteria	*Berkelbacteria*	0.27	1.08	7.12	0.40	0.87							
Bacteria	Desulfobacterota	Desulfovibrionia	Desulfovibrionales	Desulfovibrionaceae	*Desulfovibrio*	1.98	4.97	3.79	2.00	3.24							
Bacteria	Edwardsbacteria	Edwardsbacteria	Edwardsbacteria	Edwardsbacteria	*Edwardsbacteria*	0.00	1.09	0.65	3.05	6.67							
Bacteria	Proteobacteria	Gammaproteobacteria	Burkholderiales	Comamonadaceae		0.76	0.37	1.30	0.73	0.45							
Bacteria	Proteobacteria	Gammaproteobacteria	Burkholderiales	Comamonadaceae	*Hydrogenophaga*	0.23	0.29	1.42	0.42	3.42							
Bacteria	Acidobacteriota	Thermoanaerobaculia	Thermoanaerobaculales	Thermoanaerobaculaceae		1.45	2.20	2.01	5.32	1.42							
Bacteria	Chloroflexi	Anaerolineae	Anaerolineales	Anaerolineaceae	*Leptolinea*	1.22	0.80	0.42	1.31	2.40							
Bacteria	Nitrospinota	Nitrospinota	Nitrospinota			0.00	0.21	0.08	0.22	0.07							
Bacteria	Spirochaetota	Spirochaetia	Spirochaetales	Spirochaetaceae		0.94	0.47	0.86	0.11	1.65							
Bacteria	Proteobacteria	Gammaproteobacteria	Xanthomonadales	Xanthomonadaceae	*Lysobacter*	0.12	0.00	0.25	0.12	0.70							
Bacteria	Bacteroidota	Bacteroidia	Bacteroidales	Rikenellaceae		0.00	0.00	0.00	0.00	0.00							
Bacteria	Deferrisomatota	Defferrisomatia	Defferrisomatales	Defferrisomataceae	*Deferrisoma*	0.00	0.00	0.00	0.00	0.00							
Bacteria	Desulfobacterota	Syntrophia	Syntrophales	Syntrophaceae	*Syntrophus*	0.00	0.00	0.00	0.00	0.13							
Bacteria	Acidobacteriota	Vicinamibacteria	Vicinamibacterales			0.00	0.04	0.00	0.20	1.30							
Bacteria	Actinobacteriota	Actinobacteria	Corynebacteriales	Nocardiaceae	*Rhodococcus*	0.03	0.00	0.00	0.00	0.00							
Bacteria	Proteobacteria	Alphaproteobacteria	Caulobacterales	Caulobacteraceae	*Brevundimonas*	0.00	0.00	0.25	0.00	0.00							
Bacteria	Desulfobacterota	Desulfobulbia	Desulfobulbales	Desulfurivibrionaceae	*Desulfurivibrio*	0.00	0.01	1.02	0.00	0.00							
Bacteria	Proteobacteria	Alphaproteobacteria	Rhizobiales	Devosiaceae	*Devosia*	0.00	0.00	0.00	0.54	0.00							
Bacteria	Proteobacteria	Gammaproteobacteria	Burkholderiales	Alcaligenaceae		0.00	0.00	0.00	0.00	0.00							
						BA+PACz-BTX											
						2.5 cm	**13.5 cm**	**14.5 cm**	**15.5 cm**	**16.5 cm**	**17.5 cm**	**18.5 cm**	**20.5 cm**	**22 cm**	**25 cm**	**28 cm**	**34.5 cm**
Archaea	Halobacterota	Methanomicrobia	Methanomicrobiales	Methanoregulaceae	*Methanoregula*	0.00	0.00	0.23	0.00	0.10	4.60	2.69	3.03	4.83	8.95	2.33	0.00
Archaea	Halobacterota	Methanosarcinia	Methanosarciniales	Methanosaetaceae	*Methanosaeta*	0.00	7.05	21.05	23.48	23.62	23.18	30.70	23.02	28.44	15.39	7.69	15.61
Archaea	Halobacterota	Methanosarcinia	Methanosarciniales	Methanosarcinaceae	*Methanosarcina*	0.00	1.78	3.43	0.50	1.51	1.71	0.11	1.56	1.89	0.46	0.00	0.00
Archaea	Halobacterota	Methanosarcinia	Methanosarciniales	Methanosarcinaceae	*Methanomethylovorans*	0.00	0.04	1.57	0.15	0.66	0.00	0.32	0.00	0.58	0.00	0.00	0.00
Archaea	Euryarchaeota	Methanobacteria	Methanobacteriales	Methanobacteriaceae	*Methanobacterium*	0.45	1.98	20.61	32.93	24.33	23.57	20.74	13.02	12.31	10.61	11.29	4.48
Archaea	Halobacterota	Methanomicrobia	Methanomicrobiales	Methanomicrobiales		0.00	0.00	0.44	0.00	1.90	0.59	0.37	0.00	2.13	0.18	0.00	0.00
Bacteria	Firmicutes	Desulfitobacteriia	Desulfitobacteriales	Desulfitobacteriaceae	*Desulfosporosinus*	31.17	5.72	11.88	4.75	3.56	3.17	5.28	8.25	3.19	4.76	3.71	1.83
Bacteria	Patescibacteria	Berkelbacteria	Berkelbacteria	Berkelbacteria	*Berkelbacteria*	0.00	0.00	0.03	0.00	0.00	0.00	0.00	0.00	0.00	0.00	0.00	0.00
Bacteria	Desulfobacterota	Desulfovibrionia	Desulfovibrionales	Desulfovibrionaceae	*Desulfovibrio*	0.00	4.01	1.00	0.00	0.00	0.00	0.30	0.00	0.09	0.15	0.30	0.00
Bacteria	Edwardsbacteria	Edwardsbacteria	Edwardsbacteria	Edwardsbacteria	*Edwardsbacteria*	0.00	9.66	11.45	0.83	2.95	5.99	7.07	8.61	11.27	3.59	3.94	2.31
Bacteria	Proteobacteria	Gammaproteobacteria	Burkholderiales	Comamonadaceae		0.00	0.82	0.08	1.22	0.14	0.24	0.00	0.00	0.00	0.50	4.99	4.39
Bacteria	Proteobacteria	Gammaproteobacteria	Burkholderiales	Comamonadaceae	*Hydrogenophaga*	0.92	1.70	0.41	0.19	0.27	0.64	1.08	0.20	0.25	1.83	0.00	0.00
Bacteria	Acidobacteriota	Thermoanaerobaculia	Thermoanaerobaculales	Thermoanaerobaculaceae		0.00	3.31	1.36	0.77	1.28	0.29	0.21	0.00	0.00	0.00	0.00	0.00
Bacteria	Chloroflexi	Anaerolineae	Anaerolineales	Anaerolineaceae	*Leptolinea*	0.00	1.34	0.61	0.00	0.48	0.17	0.30	1.27	0.25	2.12	0.00	0.76
Bacteria	Nitrospinota	Nitrospinota	Nitrospinota			0.00	0.50	0.56	3.97	7.15	4.06	3.93	9.64	3.20	2.41	6.45	4.04
Bacteria	Spirochaetota	Spirochaetia	Spirochaetales	Spirochaetaceae		6.70	0.00	0.18	0.00	0.00	0.00	0.00	0.17	0.00	0.36	0.00	0.00
Bacteria	Proteobacteria	Gammaproteobacteria	Xanthomonadales	Xanthomonadaceae	*Lysobacter*	4.23	0.00	0.01	0.56	0.11	0.42	0.00	1.39	0.68	0.08	5.85	1.73
Bacteria	Bacteroidota	Bacteroidia	Bacteroidales	Rikenellaceae		2.47	0.09	0.19	0.39	1.74	7.67	2.13	2.26	0.00	0.19	0.53	0.21
Bacteria	Deferrisomatota	Defferrisomatia	Defferrisomatales	Defferrisomataceae	*Deferrisoma*	0.00	0.00	0.03	0.00	0.00	0.10	1.38	0.46	0.00	0.51	4.16	0.00
Bacteria	Desulfobacterota	Syntrophia	Syntrophales	Syntrophaceae	*Syntrophus*	0.00	0.00	0.00	0.00	0.00	0.00	0.00	0.00	1.37	7.28	0.00	0.00
Bacteria	Acidobacteriota	Vicinamibacteria	Vicinamibacterales			0.00	0.06	0.01	0.62	0.00	0.09	0.05	0.00	0.08	0.54	4.88	2.69
Bacteria	Actinobacteriota	Actinobacteria	Corynebacteriales	Nocardiaceae	*Rhodococcus*	1.04	0.55	0.11	0.00	0.00	0.00	0.00	0.00	0.00	0.00	0.00	0.00
Bacteria	Proteobacteria	Alphaproteobacteria	Caulobacterales	Caulobacteraceae	*Brevundimonas*	0.00	0.00	0.06	2.09	0.00	0.06	0.24	0.26	0.00	0.06	1.95	5.78
Bacteria	Desulfobacterota	Desulfobulbia	Desulfobulbales	Desulfurivibrionaceae	*Desulfurivibrio*	0.00	0.00	0.07	0.00	0.00	0.00	0.00	0.00	0.00	0.00	0.00	8.05
Bacteria	Proteobacteria	Alphaproteobacteria	Rhizobiales	Devosiaceae	*Devosia*	0.00	0.00	0.00	0.00	0.00	0.00	0.08	0.00	0.43	0.00	0.00	4.67
Bacteria	Proteobacteria	Gammaproteobacteria	Burkholderiales	Alcaligenaceae		6.62	0.00	0.00	0.00	0.00	0.00	0.00	6.93	0.00	0.00	0.00	0.00